

Efficiency analysis of innovative tuning methods for immunity testing in reverberation chamber and comparison to anechoic room

Application to civil and military testing in the RMA chamber

Christo TSIGROS

Supervisors:

Prof. Dr. Ir. Guy.A.E. Vandenbosch (KU Leuven)
Prof. Dr. Ir. Marc Piette (ERM-KMS)
Prof. Dr. Ir. Dirk Van Troyen (KU Leuven)

Dissertation presented in partial fulfilment of the requirements for the degree of Doctor in Engineering

Members of the Examination Committee:

Prof. Dr. Ir. Herman Neuckermans (KU Leuven)
Prof. Dr. Ir. Michiel Steyaert (KU Leuven)
Prof. Dr. Ing. Bernard Uguen (Université de Rennes 1, France)
Prof. Dr. Ir. Bart Scheers (ERM-KMS)
Prof. Dr. Ir. Gilles Thierry (ERM-KMS)
Prof. Dr. Ir. Davy Pissoort (KU Leuven)

July 2014

© 2014 Katholieke Universiteit Leuven, Groep Wetenschap & Technologie, Arenberg
Doctoraatsschool, W. de Croylaan 6, 3001 Heverlee, België

© 2014 Koninklijke Militaire School, Faculteit Polytechniek, Renaissancelaan 30, 1000
Brussel, België

Alle rechten voorbehouden. Niets uit deze uitgave mag worden vermenigvuldigd en/of
openbaar gemaakt worden door middel van druk, fotokopie, microfilm, elektronisch of op
welke andere wijze ook zonder voorafgaandelijke schriftelijke toestemming van de
uitgever.

All rights reserved. No part of the publication may be reproduced in any form by print,
photoprint, microfilm, electronic or any other means without written permission from the
publisher.

ISBN 978-94-6018-875-6
D/2014/7515/99

Nederlandse abstract

Reverberatie kamers zijn, elektrisch gesproken, hoge Q caviteiten die verschillen van volledig lege caviteiten door het feit dat ze een roterende tuner bevatten om een statistisch uniform elektromagnetisch veld te bekomen. Men kan dit vergelijken met het effect van de schoepen van een propeller van een schip in het water.

Deze kamers werden voor het eerst in 1968 vermeld. Sindsdien werd er heel wat onderzoek uitgevoerd om een theorie uit te werken voor een beter begrip van hun werking. Deze onderzoeken waren gericht op het gebruik van deze kamers als een alternatief voor de anechoïsche kamers voor het uitvoeren van immuniteits- en emissietesten. Waarschijnlijk was één van de allereerste gebruiken begin jaren zeventig, als immuniteitstestinstrument, toen een ingenieur van Boeing het briljante idee had om de zendantenne te plaatsen op verschillende locaties, toen hij zich afvroeg hoe men hun vliegtuigen in een grote metalen loods kon testen.

Praktisch gezien zullen twee soorten tuningsystemen voorgesteld worden. De eerste is een elektrische mode tuning met twee antennes die beiden opgesteld zijn op twee orthogonale rails. Het verschil met een conventioneel tuningsysteem ligt in dit geval in het feit dat de antennes bewegen. Het tweede tuningsysteem is volledig statisch. Een netwerk van acht antennes wordt zodanig gevoed dat een efficiëntietuning bekomen wordt. Deze twee soorten tuners verschillen fundamenteel van de conventionele systemen die gewoonlijk in de literatuur beschreven worden. Dit is de reden waarom we een groot aantal verificaties hebben uitgevoerd om hun performantie en de overeenstemming met de norm (IEC 61000-4-21) te bepalen.

Eén van de toepassingen van een reverberatiekamer (RK) is het opmeten van de antenne-efficiëntie.

We hebben een nieuwe methode ontwikkeld zonder gebruik te maken van een referentieantenne.

Om de vergelijking te maken tussen de RK en onze semi-anechoïsche kamer (SAK), hebben we een referentie, Canonical Equipment Under Test (CEUT), ontworpen, ontwikkeld en geproduceerd. Dit toestel was bedoeld om zowel in de RK als in de SAK geplaatst te worden en om, via optische vezel, verbonden te worden met een PC buiten de kamer. De werking ervan was dermate bevredigend dat het gebruikt werd voor interlabotesten gewijd aan de stralingsimmunitet tegen het elektrisch stralingsveld, wat nog nooit werd gedaan bij gebrek aan een dergelijke referentie.

Met onze CEUT hebben we de vergelijking gemaakt en de efficiëntie van onze innovatieve tuners bewezen. Bovendien werden de voorwaarden voorgesteld voor de equivalentie tussen RF stralingsimmunitetstesten uitgevoerd in de RK en in de SAK. Het feit is dat deze testen niet equivalent kunnen zijn wanneer veel tuner stappen gebruikt worden in de RK of wanneer meer of minder bloot gestelde kanten aanwezig waren in de SAK. Betreffende het gebruik van de RK voor militaire testen, zijn we tot onverwachte besluiten gekomen die haaks staan op wat algemeen geweten is over de RK. Dit komt door de testafstand opgelegd in de MIL-STD-461.

Tenslotte werd de ergodiciteit van het stochastisch proces voor het opwekken van het elektrisch veld in een RK experimenteel geëvalueerd. De ergodiciteit is belangrijk in die zin dat het een verband legt tussen het tijdsgemiddelde van een willekeurige waarde (bijvoorbeeld het elektrisch veld) en zijn ruimtelijk gemiddelde. Zo is het mogelijk om het ruimtelijk gemiddelde op een wel bepaald tijdstip te kennen (het meetproces hiervoor kan

veel tijd in beslag nemen) door deze willekeurige waarden op te meten in een vast punt binnen het volume van de RK voor een gegeven tijdsduur, bijvoorbeeld enkele minuten.

English abstract

Reverberation chambers are electrically large, high Q cavities that differ from empty ones in that they include a rotating tuner in order to obtain statistically uniform electromagnetic fields. Imagine the tuning like the blades propeller action of a ship perturbing the water.

These chambers were first mentioned in 1968. Since then, a lot of work has been done to develop a theory in order to better understand the functioning. The orientations of the research studies were to use them as alternatives to anechoic chambers, in immunity and emission testing. It was probably first used as an immunity testing tool in the early seventies when an engineer from Boeing wondering how to test their planes in a large metallic hangar, had the brilliant idea to move the transmitting antenna at different locations.

Practically, two types of tuning systems will be presented. The first is an electronic mode tuning with two antennas each mounted on two orthogonal rails. The difference with the conventional tuning system is that, in this case, the antennas were moving. The second tuning system is completely static. We use a network of eight antennas powered in such a manner to produce efficient tuning. These two types of tuner differ fundamentally from the conventional systems usually described in literature. That is why we have made a lot of verifications for the assessment of their performance and their compliance with the applicable standard (IEC 61000-4-21).

One of the applications of a Reverberation Chamber (RC) is the measurement of the antenna efficiency. We have developed a new method that uses no reference antenna.

In order to make the comparison of the RC with our semi-anechoic room (SAR), we have designed, developed and manufactured a reference, called Canonical Equipment Under Test (CEUT). This equipment was intended to be placed both in the RC and SAR environments and linked via optic fibre to a PC outside the room. Its functioning was so satisfactory that it has been used for interlaboratory testing devoted to the radiated immunity to the radiated Electric field, which has never been done before because of a lack of such reference.

Thanks to our CEUT, we perform the comparison and stated the efficiency of our innovative tuners. Moreover, the conditions for equivalence between RF radiated immunity tests, performed both in RC and in SAR, were presented. The fact is that these tests may not be equivalent if a lot of tuner steps are used in RC, or, more or less exposed faces are presented in SAR. Regarding the use of RC for military testing we come to unexpected conclusions that are opposite to the common knowledge when thinking of RC, this because of the testing distance required in the MIL-STD-461.

Finally, the ergodicity of the stochastic process of generation of Electric field in a RC has been experimentally assessed. The ergodicity is important in a way that it makes a link between the time average of a random value (the Electric field for example) and its spatial average. So, it can be possible to know the spatial average of the Electric field in the complete volume of an RC at a fixed time (measurement process that can be very long), by measuring this random value in a fixed point in the RC volume but for a given length of time, some minutes for example.

This PhD is jointly organized by:

KATHOLIEKE UNIVERSITEIT LEUVEN

Arenberg Doctoral School of Science, Engineering & Technology

Faculty of Engineering Science

Department of Electrical Engineering (ESAT)

ROYAL MILITARY ACADEMY

Polytechnical Faculty

Department of Communication, Information, Systems & Sensors

"Beauty will save the world" (Dostoevsky)

Table of Contents

INTRODUCTION	19
1. ELECTROMAGNETIC WAVE EQUATION AND INTRODUCTION TO REVERBERATION CHAMBER	28
1.1 MAXWELL'S AND HELMHOLTZ EQUATIONS	28
1.1.1 <i>Maxwell's equations.....</i>	28
1.1.2 <i>Helmholtz equation.....</i>	29
1.2 A ONE DIMENSIONAL CAVITY	30
1.2.1 <i>Graphical Solution for one dimension and n=1.....</i>	32
1.2.2 <i>Graphical Solution for one-dimension and n=2.....</i>	33
1.2.3 <i>Graphical Solution for one-dimension and n=3.....</i>	34
1.3 A «1D REVERBERATION CHAMBER»	35
1.4 THEORY OF RESONATING CAVITIES.....	38
1.4.1 <i>Generalities</i>	38
1.4.2 <i>The Helmotz equation in 3-D parallelepiped cavity.....</i>	45
1.4.3. <i>RC = Resonating cavity + tuner</i>	50
1.5 STATISTICAL CHARACTERIZATION OF ELECTRIC FIELD AND POWER IN A RC... 51	51
1.5.1 <i>Introduction.....</i>	51
1.5.2 <i>Definitions</i>	51
1.5.3 <i>PDF and CDF for the Electric field components</i>	53
1.5.4 <i>PDF and CDF for the total Electric field.....</i>	58
1.5.5 <i>PDF and CDF for the Power received on an antenna in a RC.....</i>	60
1.6 STATISTICAL PROPERTIES OF THE ELECTRIC FIELD IN RC	61
1.7 THE KOLMOGOROV-SMIRNOV (KS) HYPOTHESIS TEST.....	64
2. DYNAMIC SOURCE-MODE TUNING WITH TWO ORTHOGONAL LPDA ANTENNAS SCANNING SYSTEM	67
2.1 INTRODUCTION	67
2.2 SET-UP AND MEASUREMENT METHOD	68
2.3 TESTS RESULTS	72
2.3.1 <i>Field uniformity</i>	72
2.3.2 <i>Field strength obtained</i>	76
2.3.3 <i>PDF, CDF and KS test for the Electric field components</i>	78

2.3.4	<i>PDF, CDF and KS test for the total Electric field</i>	86
2.3.5	<i>PDF, CDF and KS test for the Power received on an antenna</i>	90
2.4	CONCLUSION	92
3.	STATIC SOURCE-MODE TUNING WITH AN ELECTRONICALLY SWITCHED ANTENNA NETWORK	94
3.1	INTRODUCTION	94
3.2	SET-UP AND MEASUREMENT METHOD	94
3.3	TESTS RESULTS	101
3.3.1	<i>Field Uniformity</i>	101
3.3.2	<i>Field strength obtained</i>	106
3.3.3	<i>PDF, CDF and KS test for the Electric field components</i>	108
3.3.4	<i>PDF, CDF and KS test for the total Electric field</i>	112
3.3.5	<i>PDF, CDF and KS test for the Power received on an antenna</i>	113
3.3.6	<i>Testing Time and Costs</i>	115
3.4	CONCLUSION	117
4.	APPLICATION OF RC NEW TUNING METHOD TO ANTENNA EFFICIENCY DETERMINATION	119
4.1	INTRODUCTION	119
4.2	THEORY	124
4.2.1	<i>Definition</i>	124
4.2.2	<i>Relative method (with Reference antenna)</i>	126
4.2.3	<i>E-field method (without Reference antenna)</i>	127
4.3	MEASUREMENT ON HOME-MADE AND TWO COMMERCIAL ANTENNAS	129
4.3.1	<i>Set-up description</i>	129
4.3.2	<i>General considerations</i>	131
4.3.3	<i>Procedure for Relative method</i>	132
4.3.4	<i>Procedure for E-field method</i>	135
4.3.5	<i>Results for the home-made Quarter-wave antenna</i>	135
4.3.6	<i>Results for the Double Ridged Horn antenna</i>	136
4.3.7	<i>Results for the Log periodic antenna</i>	137
4.4	MEASUREMENT ON PIFA ANTENNAS	138
4.4.1	<i>Set-up description</i>	138
4.4.2	<i>General considerations</i>	139
4.4.3	<i>Procedure for Relative method</i>	143
4.4.4	<i>Procedure for E-field method</i>	144
4.4.5	<i>Results for PIFA antennas</i>	144

4.5 MEASUREMENTS ON DUAL-BAND, DUAL-POLARIZED AND DUAL FED PERFORATED ARRAY PATCH ANTENNA PAIR	146
4.5.1 <i>Set-up description and procedure.....</i>	146
4.5.2 <i>Results for the Dual-Band, Dual-Polarized patch antenna.....</i>	148
4.6 REPEATABILITY TESTS	148
4.5 CONCLUSIONS.....	149
5. THE CANONICAL EQUIPMENT UNDER TEST (CEUT).....	151
5.1 INTRODUCTION	151
5.2 WORKING MECHANISM	151
5.3 ELECTRICAL AND MECHANICAL DESCRIPTION.....	153
5.4 POWER RECEIVED BY CEUT IN RC.....	154
5.5 USER'S QUICK REFERENCE GUIDE	162
5.6 CEUT MEASUREMENTS IN SAR THEN IN RC.....	164
5.7 INTERLABORATORY TESTING IN BELGIUM AND JAPAN	168
6. COMPARISON OF RADIATED IMMUNITY TESTING PERFORMED BOTH IN A REVERBERATION CHAMBER AND IN A SEMI-ANECHOIC ROOM.....	171
6.1 INTRODUCTION	171
6.2 MEASUREMENT SET-UP	172
6.2.1 <i>Semi-Anechoic Room (SAR).....</i>	172
6.2.2 <i>RC with the STATIC tuner.....</i>	173
6.2.3 <i>RC with the RAIL tuner.....</i>	176
6.2.4 <i>Data acquisition of E-field and others.....</i>	178
6.2.5 <i>Calibration of RC</i>	179
6.3 IMMUNITY TESTING RESULTS: SAR VERSUS RC.....	181
6.4 CONDITIONS FOR RADIATED IMMUNITY TESTING EQUIVALENCE SAR v RC ..	187
6.5 POWER MANAGEMENT	189
6.6 NEW PROPERTY IN A RC.....	194
6.7 CONCLUSIONS.....	198
7. ERGODICITY.....	200
7.1 INTRODUCTION	200
7.2 ERGODIC THEORY	203
7.3 ERGODICITY IN REVERBERATION CHAMBER	204
7.3.1 <i>Velocities and Fields.....</i>	205
7.3.2 <i>Probability Density Functions</i>	207

7.3.3	<i>Energies</i>	210
7.3.4	<i>Ergodicity of electric fields in reverberation chambers</i>	213
7.4	EXPERIMENTAL TEST OF ERGODICITY OF ELECTRIC FIELDS IN REVERBERATION CHAMBER	213
7.4.1	<i>Measurement set-up</i>	213
7.4.2	<i>Data acquisition of E-fields</i>	216
7.4.3	<i>Measurement results</i>	217
7.5	CONCLUSION	223
8.	GENERAL CONCLUSIONS	224
9.	LIST OF PUBLICATIONS	231
ANNEX 1:	BIBLIOGRAPHY	233
ANNEX 2:	LIST OF ACRONYMS AND ABBREVIATIONS	244
ANNEX 3:	LIST OF SYMBOLS	245
ANNEX 4:	MATHEMATICAL NOTATIONS	246
ANNEX 5:	INTERLABORATORY TESTING IN BELGIUM AND JAPAN	247

List of Figures

FIG. 0.1: ROYAL MILITARY ACADEMY SEMI-ANECHOIC ROOM.....	20
FIG. 0.2: REVERBERATION CHAMBER WITH ROTATING MECHANICAL TUNER/STIRRER	22
FIG. 1. 1: SOLUTIONS FOR N=1 AND $\omega t = 0$; N=1 AND $\omega t = \frac{\pi}{3}$	32
FIG. 1. 2: SOLUTIONS FOR N=1 AND $\omega t = \frac{2\pi}{3}$; N=1 AND $\omega t = \pi$	33
FIG. 1. 3: SOLUTIONS FOR N=2 AND $\omega t = 0$; N=2 AND $\omega t = \frac{\pi}{3}$	33
FIG. 1. 4: SOLUTIONS FOR N=2 AND $\omega t = \frac{2\pi}{3}$; N=2 AND $\omega t = \pi$	34
FIG. 1. 5: SOLUTIONS FOR N=3 AND $\omega t = 0$; N=3 AND $\omega t = \frac{\pi}{3}$	34
FIG. 1. 6: SOLUTIONS FOR N=2 AND $\omega t = \frac{2\pi}{3}$; N=2 AND $\omega t = \pi$	35
FIG. 1. 7: EUT IN A ONE-DIMENSION CAVITY, WITH NO PERTURBATION.....	36
FIG. 1. 8: EUT IN A 1-D CAVITY, WITH PERTURBATION: LENGTH OF THE CAVITY IS CHANGING FROM L=8 TO L=14 (L=12±2) PERIODICALLY, FOR EXAMPLE IN 60 SECONDS.....	37
FIG. 1. 9: IDEAL RESONATING CIRCUIT (LEFT) AND REAL RESONATING CIRCUIT (RIGHT) ...	40
FIG. 1. 10: DECREASING OF ENERGY IN A RESONATING CIRCUIT WITH TIME.....	40
FIG. 1. 11: ELECTRIC AND MAGNETIC ENERGIES IN A RESONATING CAVITY.	41
FIG. 1. 12: WAVEGUIDE AND RECTANGULAR CAVITIES	44
FIG. 1. 13: PARALLELEPIPED RESONATING CAVITY.....	46
FIG. 1. 14 : WORKING FREQUENCY AND FREQUENCY BANDWIDTH OF MODES.....	50
FIG. 1.15: STATISTICAL DISTRIBUTION OF THE POWER RECEIVED BY AN ANTENNA	61
FIG. 2. 1: SET-UP IN THE REVERBERATION CHAMBER WITH THE RAIL CONTROLLING SYSTEM AND THE MEASUREMENT INSTRUMENTS	69
FIG. 2.2: HORIZONTAL RAIL + VERTICAL RAIL + LPDA ANTENNAS + E-FIELD METER	70
FIG. 2.3: STANDARD DEVIATION FOR EACH POLARIZATION.....	74
FIG. 2.4: STANDARD DEVIATION FOR ALL THREE POLARIZATIONS	75
FIG. 2.5: E-FIELD MEASURED AT POINT P1 AND FOR X POLARIZATION.	76

FIG. 2.6: FIELD STRENGTH SPATIALLY AVERAGED OVER THE EIGHT POINTS DELIMITING THE WORKING VOLUME	77
FIG. 2.7: PDF FOR EX; RAIL; N=150 TUNER STEPS.	78
FIG. 2.8: CDF FOR EX; RAIL; N=150 TUNER STEPS.....	79
FIG. 2.9: PDF FOR EY; RAIL; N=150 TUNER STEPS.	79
FIG. 2.10: CDF FOR EY; RAIL; N=150 TUNER STEPS.	80
FIG. 2.11: PDF FOR EZ; RAIL; N=150 TUNER STEPS.	80
FIG. 2.12: CDF FOR EZ; RAIL; N=150 TUNER STEPS.	81
FIG. 2.13: PDF FOR EX; RAIL; N=24 TUNER STEPS.	83
FIG. 2.14: CDF FOR EX; RAIL; N=24 TUNER STEPS.....	83
FIG. 2.15: PDF FOR EY; RAIL; N=24 TUNER STEPS.	84
FIG. 2.16: CDF FOR EY; RAIL; N=24 TUNERS STEPS.	84
FIG. 2.17: PDF FOR EZ; RAIL; N=24 TUNERS STEPS.....	85
FIG. 2.18: CDF FOR EZ; RAIL; N=24 TUNERS STEPS.....	85
FIG. 2.19: PDF FOR ETOT; RAIL; N=150 TUNERS STEPS.	87
FIG. 2.20: CDF FOR ETOT; RAIL; N=150 TUNERS STEPS.....	87
FIG. 2.21: PDF FOR ETOT; RAIL; N=24 TUNERS STEPS.....	88
FIG. 2.22: CDF FOR ETOT; RAIL; N=24 TUNERS STEPS.....	89
FIG. 2.23: PDF FOR POWER ON ANTENNA 1; RAIL; N=51 TUNER STEPS.	90
FIG. 2.24: CDF FOR POWER ON ANTENNA 1; RAIL; N=51 TUNER STEPS.	91
FIG. 2.25: PDF FOR POWER ON ANTENNA 2; RAIL; N=51 TUNER STEPS.....	91
FIG. 2.26: CDF FOR POWER ON ANTENNA 2; RAIL; N=51 TUNER STEPS.	92
FIG. 3.1: SET-UP IN THE REVERBERATION CHAMBER WITH THE STATIC NETWORK OF 2X8 TRANSMITTING ANTENNAS.....	95
FIG. 3.2: POSITIONING OF THE ANTENNA NETWORK IN THE REVERBERATION CHAMBER.....	96
FIG. 3.3: GENERAL CABLING OF THE STATIC SOURCE-MODE TUNING SYSTEM.	97
FIG. 3.4: STANDARD DEVIATION OF THE E-FIELD (POL. X, Y AND Z), 64 TUNER STEPS (6 ANTENNAS PAIRS USED).	104
FIG. 3.5: TOTAL STANDARD DEVIATION OF THE E-FIELD, 64 TUNER STEPS (6 ANTENNA-PAIRS USED).	104
FIG. 3.6: STANDARD DEVIATION OF THE E-FIELD (POL. X, Y, Z AND TOTAL), 37 TUNER STEPS (8 ANTENNA-PAIRS USED).	106
FIG. 3.7: SPATIAL AVERAGE OF THE E-FIELD, 64 TUNER STEPS (6 ANTENNA-PAIRS USED)	107
FIG. 3.8: SPATIAL AVERAGE OF THE E-FIELD, 37 TUNER STEPS (8 ANTENNA-PAIRS USED).	108
FIG. 3.9: PDF FOR EX; STATIC; N=37 TUNER STEPS.	108
FIG. 3.10: CDF FOR EX; STATIC; N=37 TUNER STEPS.	109
FIG. 3.11: PDF FOR EY; STATIC; N=37 TUNER STEPS.	109

FIG. 3.12: CDF FOR E _Y ; STATIC; N=37 TUNER STEPS.	110
FIG. 3.13: PDF FOR E _Z ; STATIC; N=37 TUNER STEPS.	110
FIG. 3.14: CDF FOR E _Z ; STATIC; N=37 TUNER STEPS.	111
FIG. 3.15: PDF FOR E _{TOT} ; STATIC; N=37 TUNERS STEPS.	112
FIG. 3.16: CDF FOR E _{TOT} ; STATIC; N=37 TUNERS STEPS.....	113
FIG. 3.17: PDF FOR POWER ON ANTENNA; STATIC; N=37 TUNER STEPS.	114
FIG. 3.18: CDF FOR POWER ON ANTENNA; STATIC; N=37 TUNER STEPS.	114
FIG. 4.1: ILLUSTRATION OF THE WHEELER METHOD.....	120
FIG. 4.2: SET-UP FOR MEASUREMENTS WITH VNA	123
FIG. 4.3: THE QUARTER-WAVE ANTENNA ON GROUND PLANE (H = 3.9 CM; R = 18.5 CM; K _A = 6.8 @ 1.8 GHz; $\epsilon = 5.8 \times 10^7$ S/M	130
FIG. 4.4: THE DOUBLE RIDGED HORN ANTENNA. A = 23.5 CM; B = 14 CM	130
FIG. 4.5: THE LOG PERIODIC ANTENNA. C = 32 CM; D = 50 CM. 70 DIPOLES.	130
FIG. 4.6: ANTENNA EFFICIENCY MEASUREMENT, MEASUREMENT SET-UP.	134
FIG. 4.7: (A) PLAIN FLECTRON PIFA (FLPL); (B) PLAIN SHIELDIt PIFA (SHPL); (C) SLOTTED FLECTRON PIFA (FLSL) AND (D) SLOTTED SHIELDIt PIFA (SHSL)	139
FIG. 4.8: TOP VIEW OF THE WORKING VOLUME AND ANTENNA PLACEMENTS.....	139
FIG. 4.9: SETUP 1 WITH X-POLARIZED ANTENNAS (LABELLED AS 'P1') AND ANTENNA STAND ARRANGEMENT 1 (LABELLED AS 'R1'), OR P1R1	140
FIG. 4.10: SETUP 2 WITH Y-POLARIZED ANTENNAS (LABELLED AS 'P2') AND ANTENNA STAND ARRANGEMENT 1 (LABELLED AS 'R1'), OR P2R1	141
FIG. 4.11: SETUP 3 WITH Z-POLARIZED ANTENNAS (LABELLED AS 'P3') AND ANTENNA STAND ARRANGEMENT 1 (LABELLED AS 'R1'), OR P3R1	141
FIG. 4.12: SETUP 4 WITH Z-POLARIZED ANTENNAS (LABELLED AS 'P3') AND ANTENNA STAND ARRANGEMENT 1 (LABELLED AS 'R2'), OR P3R2	142
FIG. 4.13: SETUP 5 WITH Y-POLARIZED ANTENNAS (LABELLED AS 'P2') AND ANTENNA STAND ARRANGEMENT 1 (LABELLED AS 'R2'), OR P2R2	142
FIG. 4.14: SETUP 6 WITH X-POLARIZED ANTENNAS (LABELLED AS 'P1') AND ANTENNA STAND ARRANGEMENT 1 (LABELLED AS 'R2'), OR P1R2	143
FIG. 4.15: FRONT OF THE PATCH ANTENNA.....	146
FIG. 4.16: SIDE VIEW OF THE PATCH ANTENNA WITH ITS FEEDING NETWORKS	147
FIG. 5.1: SCHEMATICS OF A CEUT SINGLE CHANNEL	152
FIG. 5.2: THE CEUT, OPEN (LEFT) AND CLOSED (RIGHT) WITH ONE LOOP ON EACH FACE OF THE METALLIC BOX.	154
FIG. 5. 3: AVERAGE POWER P _R RECEIVED BY THE LOOP.	156
FIG. 5.4: CEUT AND ACCESSORY EQUIPMENT, FOR INTERLABORATORY TESTING.	158
FIG. 5.5: CEUT ELECTRONIC DRAWING	159

FIG. 5.6: CEUT ELECTRICAL CONNECTIONS, PART 1	160
FIG. 5.7: CEUT ELECTRICAL CONNECTIONS, PART 2.	161
FIG. 5.8: RESPONSE OF CEUT TO FREQUENCY AND IMMUNITY LEVEL IN A SAR	165
FIG. 5.9: RESPONSE OF CEUT TO FREQUENCY AND IMMUNITY LEVEL IN RC	167
FIG. 5.10: RESPONSE OF CEUT TO DIFFERENT TYPES OF TUNERS.	167
FIG. 5.11: INTERLABORATORY TESTING RESULTS (A PART), CEUT EXPOSED TO E-FIELD .	169
FIG. 6.1: SET-UP FOR CALIBRATION (LEFT) AND TESTING (RIGHT).	173
FIG. 6.2: GENERAL INTERCONNECTION SCHEME FOR THE RC WITH STATIC TUNER.....	174
FIG. 6.3: THE STATIC TUNER WITH 8-PAIRS ANTENNA ARRAY.....	176
FIG. 6.4: THE RAIL TUNER WITH TWO ORTHOGONAL RAILS.	177
FIG. 6.5: E-FIELD CALCULATIONS DETAILS.	179
FIG. 6.6: COMPARISON SAR v RC; 37 STEPS AND 50 V/M.....	182
FIG. 6.7: COMPARISON SAR v RC; 37 STEPS AND 35 V/M.....	183
FIG. 6.8: COMPARISON RC RAIL METHOD; 37 v 12 STEPS.....	184
FIG. 6.9: COMPARISON RC STATIC METHOD; 37 v 12 STEPS.....	184
FIG. 6.10: TRANSMITTED POWER, RAIL37 v RAIL12.....	185
FIG. 6.11: ERMS-AVG, STATIC 37 v STATIC 12.	186
FIG. 6.12: TENTATIVE OF UNIFICATION OF EXPERIMENTAL RESULTS.	189
FIG. 6.13: POWER REQUIREMENTS IN SAR AND RC.	190
FIG. 6.14: EXTRA POWER NEEDED TO INCREASE $E_{MAX-AVG}$ BY 3 DB.....	191
FIG. 6.15: ERMS-AVG VARIATION FOR RAIL 37 AND RAIL12.....	194
FIG. 6.16: RATIO FOR DIFFERENT TUNER STEPS AND METHODS.	195
FIG. 7.1: GAS MOLECULE COLLISION.....	206
FIG. 7.2: ELECTRIC FIELD STOCHASTIC VARIATION IN TIME DUE TO THE MOVING TUNER. ..	206
FIG. 7.3: TWO ORTHOGONAL RAILS TUNING METHOD IN RC.	215
FIG. 7.4: MEASUREMENT SET-UP	216
FIG. 7.5: ERGODICITY MEASUREMENT RESULTS FOR ERMS. EACH PLOT REPRESENTS A DIFFERENT FREQUENCY. THE INDICATION "SAMPLES" REFEREEING TO THE ABCISSA CORRESPONDS TO THE ROW OF THE MATRIX (THERE ARE 150 "SAMPLE" POINTS, EACH REPRESENTING A TIME STEP). ALL VALUES ON A ROW OF THE MATRIX HAVE BEEN DEPICTED IN THE PLOTS, YIELDING A RED ZONE RATHER THAN A SINGLE RED LINE, SEE ALSO FIG. 7.7 TOP LEFT PLOT FOR DETAILS.	219
FIG. 7.6: ERGODICITY MEASUREMENT RESULTS FOR ERMS (CONTINUATION OF FIG. 7.5).	220
FIG. 7.7: ERGODICITY MEASUREMENT RESULTS FOR ERMS, DETAILS.....	221
FIG. 7.8: STANDARD DEVIATION OF SPACE-TO-TIME RATIOS AS A FUNCTION OF	222

List of Tables

TABLE 1.1: LIMIT VALUES FOR THE KS TEST AS A FUNCTION OF THE TUNER STEPS.....	66
TABLE 2.1: POSITIONS, IN METERS, OF E-FIELD PROBE (X;Y;Z).....	71
TABLE 2.2: LIST OF FREQUENCIES, IN MHZ, FOR RAIL TUNING.....	72
TABLE 2. 3: KS TEST SUMMARY; E-FIELD; RAIL; N=150 TUNER STEPS; 1546 MHZ; P3.	82
TABLE 2.4: KS TEST SUMMARY; E-FIELD; RAIL; N=24TUNER STEPS; 1546 MHZ; P3. ...	86
TABLE 2.5: SCALE FACTORS RELATIONSHIP; RAIL; N=150 TUNER STEPS.	88
TABLE 2. 6: SCALE FACTORS RELATIONSHIP; RAIL; N=24 TUNER STEPS.	89
TABLE 2.7: KS TEST SUMMARY; POWER; RAIL; N=51TUNER STEPS; 2400MHZ.....	92
TABLE 3.1: LIST OF FREQUENCIES FOR STATIC TUNING (MHZ).....	101
TABLE 3.2: KS TEST SUMMARY; E-FIELD; STATIC; N=37TUNER STEPS; 1546 MHZ; P3.	112
TABLE 3.3: SCALE FACTORS RELATIONSHIP; STATIC; N=37 TUNER STEPS.	113
TABLE 3.4: KS TEST SUMMARY; POWER; STATIC; N=37 TUNER STEPS.	115
TABLE 3.5: TESTING TIME COMPARISON IEC 61000-4-3 VS IEC61000-4-21 (MEASURED)	116
TABLE 3.6: TESTING TIME REDUCTION FOR MIL-STD-461F (ESTIMATION)	117
TABLE 4.1: EFFICIENCY VALUES FOR QUARTER-WAVE ANTENNA	135
TABLE 4.2: EFFICIENCY VALUES FOR DRH ANTENNA	136
TABLE 4.3: EFFICIENCY VALUES FOR LOG PERIODIC ANTENNA	137
TABLE 4.4: EFFICIENCY MEASUREMENT RESULTS ON PIFA'S (PART I)	144
TABLE 4.5: EFFICIENCY MEASUREMENT RESULTS ON PIFA'S (PART II)	145
TABLE 4.6: EFFICIENCY MEASUREMENT RESULTS ON PIFA'S, SUMMARY	145
TABLE 4.7: DIMENSIONS OF THE PATCH ELEMENTS AND CHARACTERISTICS OF THE SUBSTRATE	147
TABLE 4. 8: PATCH ANTENNA EFFICIENCY RESULTS	148
TABLE 4.9: REPEATABILITY OF ANTENNA EFFICIENCY MEASUREMENTS	149
TABLE 6.1: RELATION BETWEEN E _{MAX} -AVG / E _{RMS} -AVG AND SPATIAL FIELD UNIFORMITY.	195
TABLE 7.1: STATISTICAL PHYSICAL MODELS COMPARISON.....	211
TABLE 7.2: POSITIONS, IN METERS, OF E-FIELD PROBE (X,Y,Z)	214
TABLE 7.3: LIST OF LOGARITHMICALLY SPACED FREQUENCIES, IN MHZ	215

Introduction

The evolution of modern society over the last five decades has been characterized by a growing impact of technology on the performance, reliability and security of various systems and equipment made by man to increase productivity, make some work less painful or improve life comfort. Electrical and electronic devices in particular are nowadays present and extensively used in almost all types of applications.

Hence, the electromagnetic compatibility of these devices/equipment/systems has become a very important issue. So important that it is now an integral part of the design process. "Electrical and electronic devices are said to be *electromagnetically compatible* when the electrical noise generated by each does not interfere with the normal performance of any of the others. Electromagnetic compatibility (EMC) is that happy and secure situation in which systems work as intended, both within themselves and in their environment" [1].

The term *emitter* is used to denote a source of electromagnetic energy that can unintentionally or eventually intentionally cause some disturbance or upset of other devices/systems, while the term *susceptor* is used to denote a device that responds to electromagnetic energy and could be a potential victim of it. Examples of emitters are automobile ignition systems, radar transmitters, fluorescent lights, computers and power lines. Examples of susceptors are navigation instruments, ordnance, displays devices, heart pacers, and industrial controls.

Electrical transmission paths of the undesired energy from the emitter to the susceptor are generally classified in two categories:

conducted and *radiated*. Conducted means carried by metallic paths (grounding, signal cables, power lines, microwave transmission lines), while radiated means coming from a structure radiating an electromagnetic field, like an antenna.

The level of emissions generated by an emitter and their spectral content can be experimentally determined by using special test and measurement facilities like anechoic rooms and reverberation chambers. The same facilities can be used as well for determining the level of immunity and the frequency sensitivity of a susceptor.

The semi-anechoic room (SAR) is very often a large Faraday room the walls of which are lined with RF absorbing material aimed at cancelling or substantially reducing the wall reflections in such a way that the propagation of the electromagnetic waves inside are just like in the free space (see Fig. 0.1).



Fig. 0.1: Royal Military Academy Semi-Anechoic Room.

If the floor is conductive, we speak of a SAR. If it is partly or completely covered by absorbers, it is called a FAR (Fully Anechoic Room).

When performing an immunity test in an anechoic room, the Equipment Under Test (EUT) is set on a turntable at a defined distance from the source antenna (1 m for military standards, 3 or

10 m for civil standards) which is transmitting in a well-defined polarization (first horizontal and then vertical) in order to stress the EUT under various angles of incidences and polarization states, this being repeated at all frequencies of interest.

Because the test time must be kept reasonable, only a limited set of aspect angles are chosen for the EUT and only vertical and horizontal polarizations are recommended in the standards. The standards impose a certain degree of field uniformity in the plane where the EUT is placed. They require also that the performance of the RF absorbers is good enough to obtain in the SAR an environment very close to that of the free space. A difference of only a few decibels is tolerated for the signal levels, which requires a very low reflectivity of the absorbers. As a consequence, most of the energy emitted by the source antenna is dissipated in the RF absorbers and only a small fraction is efficiently coupled to the EUT, a balance that becomes quite costly when high field strengths at high frequency are required by the standard.

An alternative way to assess the immunity of a EUT is to put it in a reverberation chamber.

Reverberation chambers (RC) are electrically large, high Q cavities without any absorbers that differ from empty ones in that they include a rotating stirrer in order to obtain statistically uniform electromagnetic fields. Imagine the stirring like the blades propeller action of a ship perturbing the water (see Fig. 0.2)



Fig. 0.2: Reverberation chamber with rotating mechanical tuner/stirrer

These chambers were first mentioned in 1968 [55]. Since then, a lot of work has been done to develop a theory in order to better understand the functioning [6], [18], and [56]. The orientations of the research studies were to use them as alternatives to anechoic rooms, in immunity and emission testing. It was probably first used as an immunity testing tool in the early seventies when an engineer from Boeing wondering how to test their planes in a large metallic hangar, had the brilliant idea to move the transmitting antenna at different locations.

But, nearly forty years later, it has not yet made a breakthrough in its evolutionary process. We mean that the official qualification testing in civil electronical/electrical equipment does not allow the use of reverberation chambers. Indeed, we do not know any European product or family standard that mentions the use of the basic standard IEC 61000-4-21 [2] relative to the reverberation chambers as reference for the radiated immunity to E-fields.

Even if it is allowed in the MIL-STD-461F¹ [3] as an alternative to the anechoic room, we can ask ourselves why it has been put aside by civil standards.

¹ military standard for immunity and emission assessment of equipment to electromagnetic fields

We see two reasons: the first one is that it seems that testing in reverberation chambers would be more severe for the equipment, so the lobbying of the manufacturers does not want to spend more money for better shielding their equipment; the second one is that the method is quite constraining and the testing time is longer compared to that of the anechoic room.

At the Laboratory of Electro Magnetic Applications (LEMA) of the Royal Military Academy both types of test facilities are available; a large semi-anechoic room for 1 or 3 m testing according to military or civil standards and a reverberation chamber. This is for us a unique opportunity to study and compare the severity of immunity testing in both types of test facilities. Simplifying the test method is one thing but reducing the testing time is a real challenge. So, aside from the severity issue, a second objective of the present research is to experiment new tuning methods in the Royal Military Academy reverberation chamber. If the results are concluding, the present study could be a contribution to a proposal of improvement of the MIL-STD-461F [3].

There are several methods generally used for mode tuning a reverberation chamber (RC). The rotating tuner is historically the first and largely used [4] [5], but is quite slow. This type is recommended in the IEC 61000-4-21 [2] and MIL-STD-461F RS103 [3] testing procedures. Because the mechanical tuner has to be electrically large to be efficient, it can be quite cumbersome at low frequencies and limit the free working volume available for the EUT, especially in small reverberation chambers. In large chambers with low LUF (Lowest Usable Frequency), huge stirrers can sometimes cause stability and vibration problems without paying specific attention to such issues.

A rotating mechanical tuner continuously changes the spatial location of its surface, where the boundary conditions are imposed to the fields. Hence, it changes the resonant frequencies of the

cavity modes. Wu and Chang [6] showed that this has some equivalence to frequency modulation of the source. Considering an idealized two dimensional cavity model with a line source having a band-limited white Gaussian noise excitation, Hill [7], [57], [61] has shown that the standard deviation on electric field homogeneity does not exceed 3 dB at an operating frequency of 4 GHz, and for a source bandwidth (BW) of 1 MHz. Standard deviation goes even down to 0.88 dB for a BW of 10 MHz. Real-world measurements made by Loughry [8], have confirmed Hill's modelling. Other types of mechanical tuner/stirrer have also been investigated [64].

The VIRC (Vibrating Intrinsic Reverberation Chamber) is a RC where the walls are made of a flexible conducting material attached in different points to mechanical vibrators that make the walls vibrate. It allows tuning without the use of a mechanical tuner inside the test volume. Thanks to the vibration the modal structure inside the chamber is changed, so only stirring is possible. When tuning a stepper motor drives a continuously rotating paddle wheel mechanically coupled to one or more walls [9].

Another technique consists in leaving the cavity walls static and getting the source of radiation in movement (source-stirring). Such a source-stirring method using an array of antennas has been first mentioned by Hong [10]. Theoretical analysis has been provided showing that by controlling the locations, polarizations, and phases of the sources the uniformity of field distributions can be improved. Source-stirring by rotating the transmitting antenna by 45 degrees at three different heights has also been investigated [11]. It is shown that source-stirring is capable of producing good statistics and is comparable to the standard mechanical-stirring technique. In [12], source-stirring is realized by moving two antennas on two orthogonal rails (one rail for each antenna) over a total distance of 3.5 m. The step distance between two successive positions is 2.5 cm in a 2.5 m cubic shape RC. The measurements show that the 3

dB field uniformity requirement can be met in the 800-2500 MHz frequency range for a reduced set of 24 steps.

This thesis starts with a theoretical introduction on Electromagnetic waves in cavities (Chapter 1) and continues with the investigation of two types of tuning.

The first one is a dynamic mode tuning with two antennas, each mounted on a separate rail (Chapter 2). The difference with the conventional tuning system is that, in this case, the antennas are moving.

The second tuning system is completely static, consisting in a network of eight antennas powered in such a manner that they produce efficient tuning (Chapter 3).

These two types of tuner differ fundamentally from the conventional systems usually described in literature. That is why we have made a lot of verifications for the assessment of their performance and their compliance with the applicable standard (IEC 61000-4-21). After a complete description of the tuner, its field uniformity has been assessed in accordance to the above mentioned standard in order to verify its compliance with it. Moreover, a statistical examination has been carried out by calculating the Probability Density Function (PDF) and its Cumulative Distribution Function (CDF) of the three components of the Electric field, the total Electric field and the power received by an antenna. This statistical examination is often used in literature in order to assess the performance of a tuning system, but very few are followed by the field uniformity examination as required for the compliance with the requirements of the IEC 61000-4-21 standard. The experimental CDF statistical parameter is compared to the theoretical CDF via the Kolmogorov-Smirnov (KS) hypothesis test.

One of the applications of a Reverberation Chamber (RC) is the measurement of the antenna efficiency. We have developed a

procedure in order to carry out these measurements with our new tuning system (Chapter 4). In a way, it can be considered as an additional means of assessment of the performance of our innovative tuning systems: what a conventional can do, the new tuning systems have to do as well. For the measurement of the antenna efficiency, the described procedure in the IEC 61000-4-21 standard is a relative method, that is to say, an antenna with known efficiency must be available. We have applied this, but go some steps further. We propose an absolute method for the measurement of the antenna efficiency without needing a reference antenna. These two methods for antenna efficiency measurements have been thoroughly applied to several types of antennas, a home-made quarter-wave monopole, two antennas available on the market: PIFA's (Planar Inverted-F Antenna) and a dual-band, dual-polarized and dual fed patch antenna array.

In order to make the comparison of the RC with our SAR, we have designed, developed and manufactured a reference (Chapter 5), called Canonical Equipment Under Test (CEUT). This equipment was intended to be placed both in the RC and SAR environments and linked via optical fibre to a PC outside the room. It was developed for the Electric Radiated Field immunity testing, that is to say, exposed to Electric fields around 50 V/m; it was supposed to react or not to react over the frequency range of interest (800 to 2500 MHz). Its functioning was so satisfactory during our work, that we proposed ABLE² to use it as reference for an interlaboratory testing campaign devoted to the immunity to the radiated Electric field. This has never been done before by lack of such reference equipment. The CEUT has made the tour of Belgium and has been tested in EMC laboratories in Germany and Japan.

² Association of Belgian Accredited Laboratories

Thanks to the CEUT, the efficiencies of the two innovative tuners have been stated and compared (Chapter 6). Moreover, the conditions for equivalence between RF radiated immunity tests, performed both in RC and in AC, are presented. The fact is that these tests may not be equivalent if a lot of tuner steps are used in RC, or, more or less exposed faces are presented in AC. Regarding the use of RC for military testing we come to an unexpected conclusion that is opposite to the common knowledge when thinking of RC because of the testing distance required in the MIL-STD-461F. More interesting findings are given regarding the power management and a new property in RC is exposed.

Finally, the ergodicity of the stochastic process of generation in a RC has been experimentally assessed (Chapter 7). What is called as “fundamental” and not easy to be experimentally proven [13], [14], has, as far as we know, been done here for the first time. The ergodicity is important in a way that it makes a link between the time average of the random electric field in a given spatial point and the spatial average over different points of the same field measured at a given time. So, in case of ergodicity it is possible to know the spatial average of the Electric field in the complete volume of an RC at a fixed time (measurement process that can be very long), by measuring this random value in a fixed spatial point in the RC volume but for a given duration of time, some minutes for example.

1. Electromagnetic wave equation and introduction to reverberation chamber

Before giving the theoretical background and the most important properties of the random fields generated in an RC, it is worthwhile to recall some fundamental equations of electromagnetics and to illustrate which type of solutions are derived for the boundary value problem of the metallic cavity.

1.1 Maxwell's and Helmholtz equations

1.1.1 Maxwell's equations

Starting from Maxwell's equations for time harmonic fields let us derive the Helmholtz equation expressing the wave propagation in the medium of interest (the time convention is $e^{-i\omega t}$).

$$\nabla \cdot \vec{D} = \rho \quad (1.1)$$

$$\nabla \cdot \vec{B} = 0 \quad (1.2)$$

$$\nabla \times \vec{E} = i\omega \mu \vec{H} \quad (1.3)$$

$$\nabla \times \vec{H} = \vec{J} - i\omega \epsilon \vec{E} \quad (1.4)$$

Applying a curl to both sides of (1.3) and rewriting (1.4) gives:

$$\nabla \times \nabla \times \vec{E} = i\omega \mu \nabla \times \vec{H} \quad (1.5)$$

$$\nabla \times \vec{H} = \vec{J} - i\omega \epsilon \vec{E} \quad (1.6)$$

Knowing that:

$$\nabla \times \nabla \times \vec{E} = \nabla \nabla \cdot \vec{E} - \nabla^2 \vec{E} \quad (1.7)$$

And making the following simplifications:

a) $\nabla \cdot \vec{E} = 0$ (no electrical charge in the volume defined of interest).

b) $\vec{J} = 0$ (no current in the volume of interest).

Equations (1.5) and (1.6) become:

$$-\nabla^2 \vec{E} = i\omega \mu \nabla \times \vec{H} \quad (1.8)$$

$$\nabla \times \vec{H} = -i\omega \epsilon \vec{E} \quad (1.9)$$

And, replacing (1.9) in (1.8) yields:

$$-\nabla^2 \vec{E} = \omega^2 \mu \epsilon \vec{E} \quad (1.10)$$

Or

$$\nabla^2 \vec{E} + \omega^2 \mu \epsilon \vec{E} = 0 \quad (1.11)$$

This is the Helmholtz equation for the electrical field and the same equation can be derived for the magnetic field.

1.1.2 Helmholtz equation

The product $\mu \epsilon$ is related to the speed of propagation of the wave by the following equation:

$$\mu \varepsilon = \frac{1}{c^2} \quad (1.12)$$

where c is the speed of light (m/s) in the medium.

Equation (1.11) becomes:

$$\nabla^2 \vec{E} + \left(\frac{\omega}{c} \right)^2 \vec{E} = 0 \quad (1.13)$$

The term $\frac{\omega}{c}$ is called the eigenvalue [7] and often noted k .

And, we have the final expression:

$$(\nabla^2 + k^2) \vec{E} = 0 \quad (1.14)$$

where \vec{E} is a complex quantity that is function of the spatial position and time t , according to the time harmonic expression.

$$\mathbf{E}(\vec{r}, t) = \sqrt{2} \operatorname{Re} \left[\vec{E}(\vec{r}, \omega) \cdot e^{(-i\omega t)} \right] \quad (1.15)$$

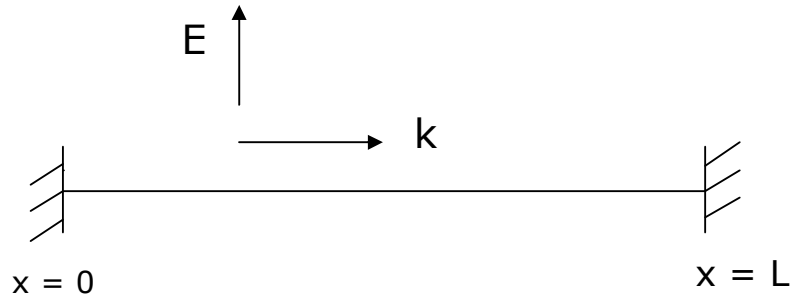
The theory of resonating cavities and the solutions of equation (1.14) in such cavities will be discussed extensively in section 1.4.

1.2 A one dimensional cavity

In order to allow the reader to have a first contact with the reverberation chambers and the way they work, let us consider the one dimensional case.

The one dimensional cavity can be seen as a rectilinear path of length L along which a wave can travel and bounce back at its terminations where the electric field must be compatible with some

boundary condition (like $E=0$ in case the boundaries are perfectly conducting).



Equation (1.14) becomes:

$$\frac{d^2 E}{dx^2} + k^2 E = 0 \quad (1.16)$$

And the solution is:

$$E = E_0 [\sin(\omega t + kx) - \sin(\omega t - kx)] \quad (1.17)$$

Two time harmonics waves propagating in opposite direction, the first toward the negative x and the second backward to the positive x .

Mathematically, we can write the solutions:

$$E = 2.E_0.\sin kx.\cos \omega t \quad (1.18)$$

To characterize this solution, let us set the conditions at the boundaries, i.e. $E=0$ at $x=0$ and $x=L$ (the total length of the one-dimension cavity).

To satisfy this, one should have $kL = n\pi$ (with $n=0, 1, 2, \dots$).

The solution (1.18) becomes:

$$E = 2.E_0.\sin\frac{n\pi}{L}x.\cos\omega t \quad (1.19)$$

This equation shows that there exists an infinite number of solutions depending on the value of n .

The solutions represent stationary waves that oscillate in time (the factor " $\cos \omega t$ "), but have a spatial dependence of the oscillation magnitude, i.e. standing waves.

To illustrate this, let us consider the graphical solutions for $n=1, 2$ and 3 .

$E = 0$, in $x=0$ and $x=L$, (we take $L=12$ length units, for example). And for four angle values (indirectly for time as time=angle/angular frequency, which is kept constant).

1.2.1 Graphical Solution for one dimension and $n=1$.

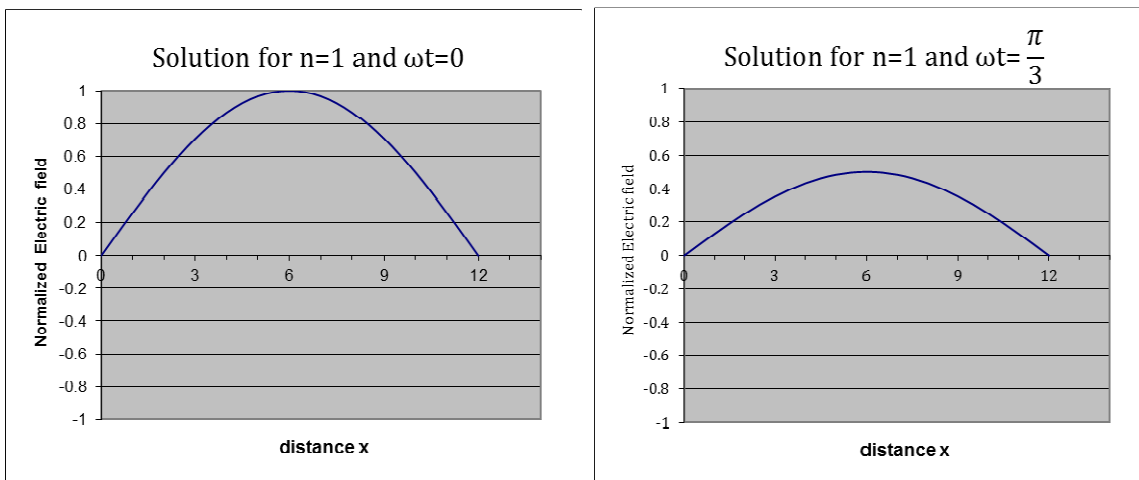


Fig. 1. 1: Solutions for $n=1$ and $\omega t = 0$; $n=1$ and $\omega t = \frac{\pi}{3}$

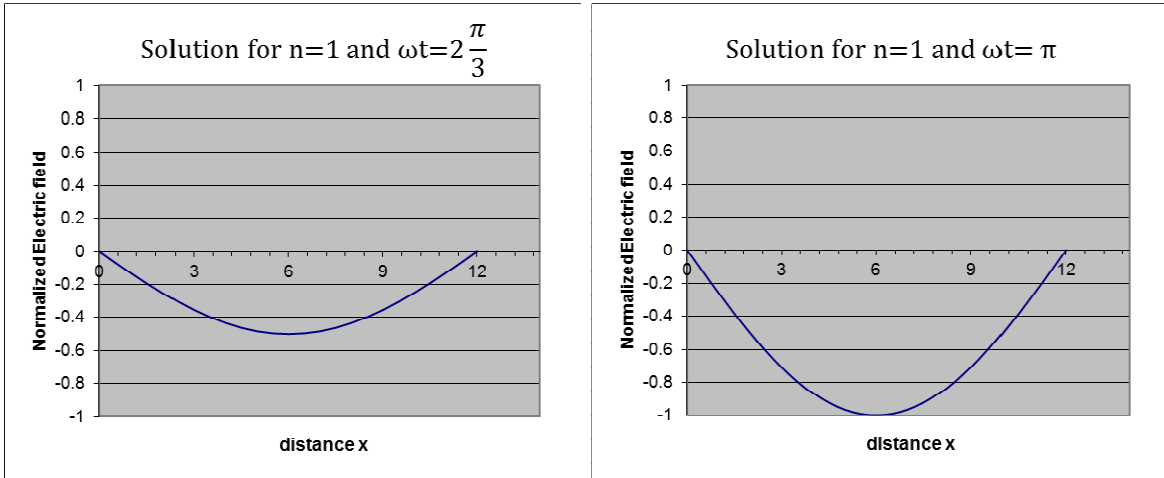


Fig. 1. 2: Solutions for $n=1$ and $\omega t = \frac{2\pi}{3}$; $n=1$ and $\omega t = \pi$

We observe that for $x=L/2$ there is a maximum variation of the normalized electric field.

1.2.2 Graphical Solution for one-dimension and $n=2$.

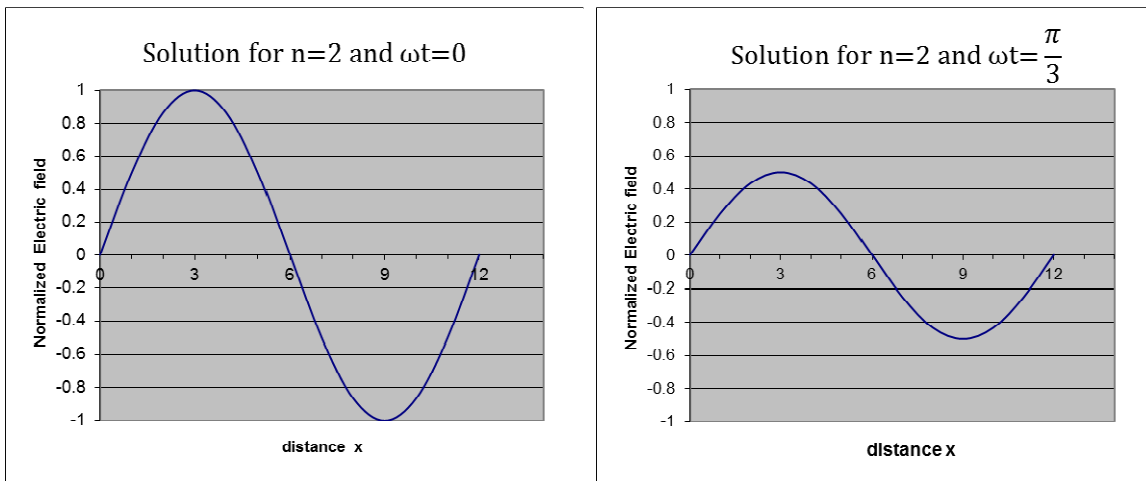


Fig. 1. 3: Solutions for $n=2$ and $\omega t = 0$; $n=2$ and $\omega t = \frac{\pi}{3}$

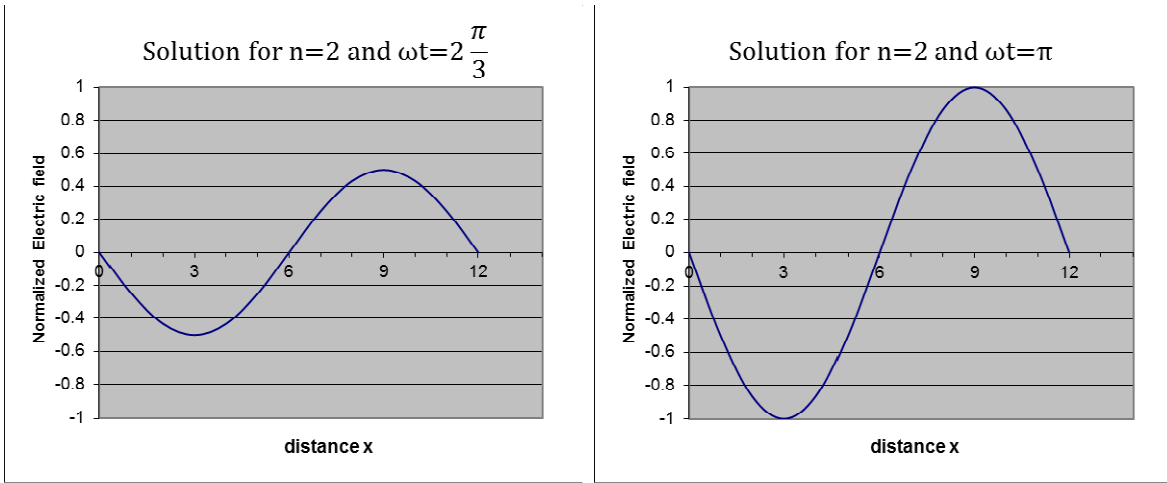


Fig. 1. 4: Solutions for $n=2$ and $\omega t = \frac{2\pi}{3}$; $n=2$ and $\omega t = \pi$

We observe that for $L/2$ the normalized electric field is zero at any time, so the variation is minimal.

And, for $L/4$ and $3L/4$ the variation is maximum.

1.2.3 Graphical Solution for one-dimension and $n=3$

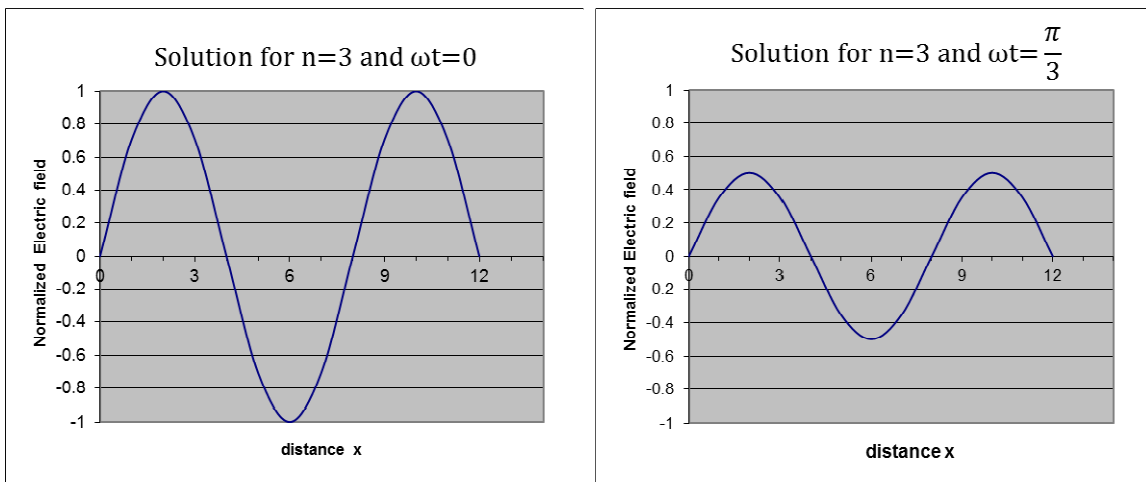


Fig. 1. 5: Solutions for $n=3$ and $\omega t = 0$; $n=3$ and $\omega t = \frac{\pi}{3}$

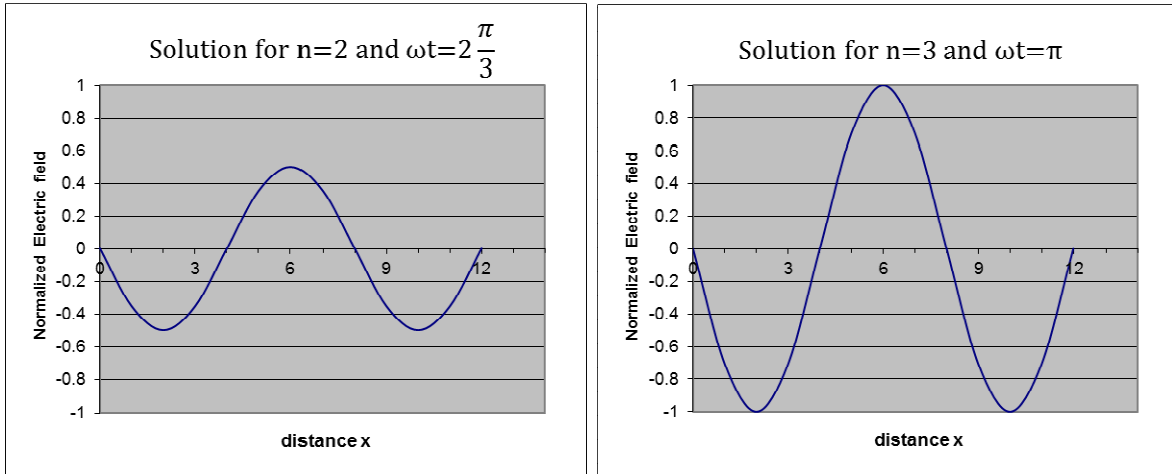


Fig. 1. 6: Solutions for n=2 and $\omega t = \frac{2\pi}{3}$; n=2 and $\omega t = \pi$

For n=3, we observe that for $L/3; 2L/3; 3L/3, \dots$ the normalized electric field is zero at any time, so the variation is minimum.

And, for $L/6; 3L/6; 5L/6; \dots$ the variation is maximum.

As a general rule, we observe nodes (amplitude is minimum) at $x=a.L/n$ (with $a = 1, 2, 3, \dots$) and anti-nodes (amplitude is maximum) at locations $x=a.L/2n$.

1.3 A «1D reverberation chamber»

Still considering the one dimensional cavity case, for simplicity, we note that an object (we will call it EUT=Equipment Under Test) of dimension that is a fraction (let us say $L/6$) of the total cavity length, placed in a random position in it, will be submitted to a spatially non-uniform electric field. In fact, a part of the EUT will never be submitted to an electric field, whereas another part will be exposed to a level that is maximum (see Fig. 1. 7) the EUT will not be submitted to an E-field at the point where the normalized electric field crosses the x-axis. At the opposite, the exposition of the EUT will be maximum at the abscissa where the

normalized electric field reaches its maximum. This is obviously not acceptable in a point of view of testing, as the requirement is that all the parts of the EUT be submitted to the same electric field within given limits (which are often $\pm 3\text{dB}$).

This part of EUT will not be submitted to an E-field

This part of EUT will be submitted to a maximum E-field

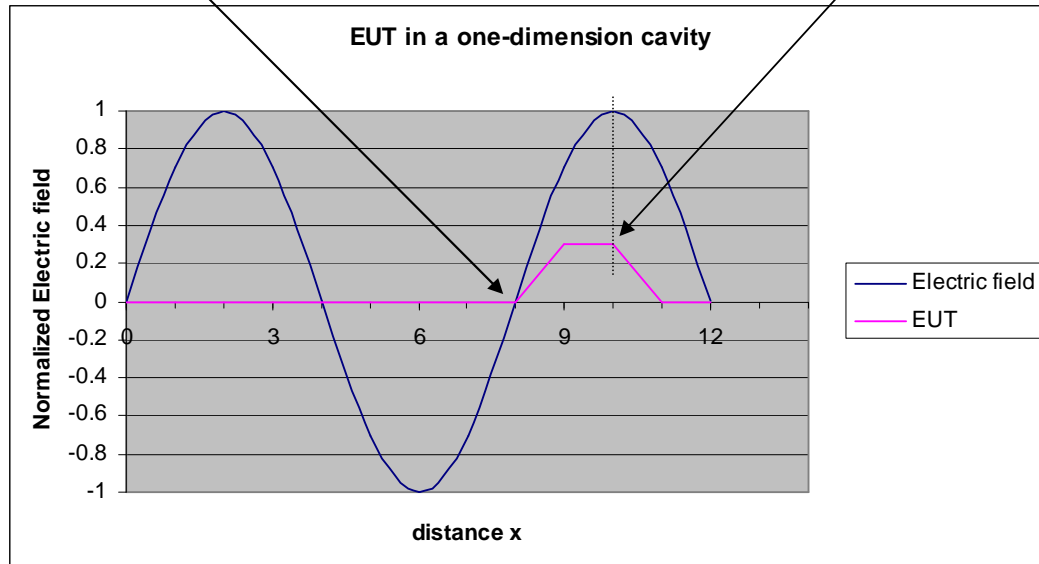


Fig. 1. 7: EUT in a one-dimension cavity, with no perturbation

In order to have a spatial (one dimension space) uniformity of the E-field, we introduce some perturbation in the cavity. Hence, a small deformation of the cavity introduces a change in the resonant frequency of the cavity mode. In this case a small deformation is made by changing the length L of the one dimension cavity. This is called *stirring* or *tuning* the modes of the cavity. And the system that allows changing these resonant frequencies is called the *stirrer* or *tuner*. The length changes as a function of time; suppose that we change it from $L-dl$ to $L+dl$ in 60 seconds. This value is rather reasonable as we will see later that the tuner cycle is of this order.

The graphical solutions will be as mentioned in the following Fig. 1. 8 :

This part of EUT will be submitted to a maximum E-field when L=10

This part of EUT will be submitted to a maximum E-field when L=14

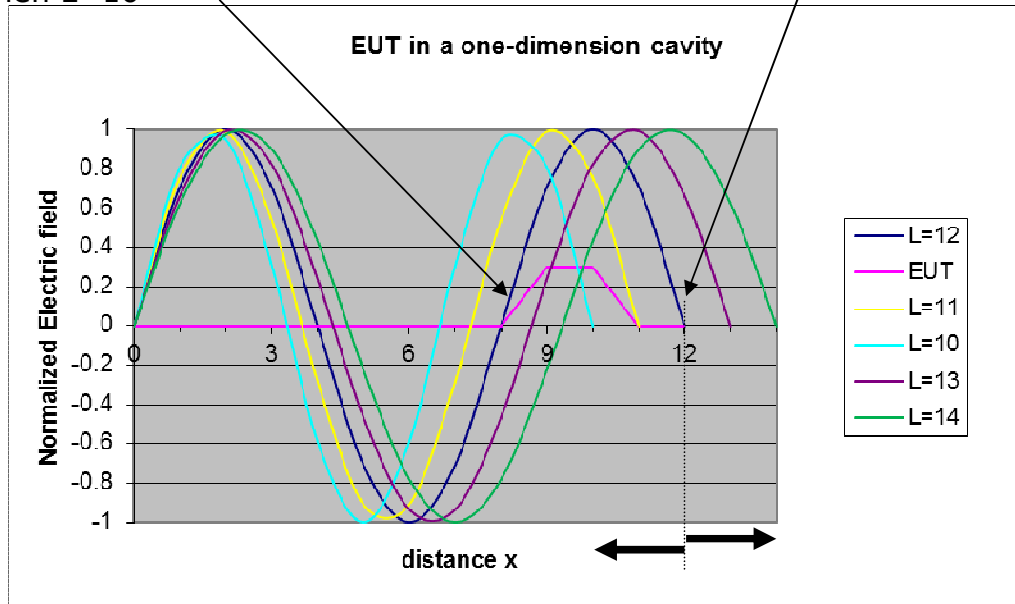


Fig. 1. 8: EUT in a 1-D cavity, with perturbation: Length of the cavity is changing from L=8 to L=14 ($L=12\pm 2$) periodically, for example in 60 seconds.

As we can see in the figure above, all parts of the EUT will be submitted to a maximum Electric field, not at the same time, but within a tuner cycle, which duration is about 60 seconds, for example. Now, we have fulfilled the requirement of spatial uniformity of the Electric field, as we can say that within a tuner cycle, all the parts of the EUT are submitted to the same maximum Electric field.

If, for example, $L(t) = L_0 + dl \cdot \cos \Omega t$ (with Ω the tuner cycle angular frequency, and dl the maximum variation of L_0), then (1.19) becomes:

$$E = 2.E_0 \cdot \sin \frac{n\pi}{L_0 + dl \cos \Omega t} x \cdot \cos \omega t \quad (1.20)$$

This expresses no longer the fields in a static cavity but in a reverberation room with a Ω tuner cycle angular frequency).

This is the principle of a Reverberation room, an electrically large cavity where the resonant frequencies are changed with a tuner in order to obtain a uniform maximum electric field in a defined space of the cavity, within a time cycle.

In our case, the tuning is made by changing the length of the one dimension cavity, but we will see later, that there are many types of tuners, having the same effect, changing the conditions at the boundaries of three dimensional cavities.

1.4 Theory of resonating cavities

1.4.1 Generalities

At low frequency, a resonating electrical circuit can be made from an inductor and a capacitor (Fig. 1. 9, left). The electric energy is contained in the capacitor, the magnetic energy is contained in the inductor and the total energy oscillates between these two types at the oscillation frequency of the circuit [15]. The electric energy accumulated in the capacitor at the voltage $V(t)$ is $W_e(t)=CV^2(t)/2$, whereas the current $I(t)$ passing through the inductor produces an energy $W_m(t)=LI^2(t)/2$. The total energy $W_t = W_e+ W_m$ is maximum when the circuit is excited at the resonating frequency given by the expression:

$$f_r = \frac{1}{2\pi\sqrt{LC}} \quad (1.21)$$

The resonating frequency is related to the capacitance and to the inductance. But, these elements are not ideal: the capacitor has always a leakage resistance, and the inductor has a series resistance, in such a way that the real resonating circuit has a

conductance G that expresses these imperfections (Fig. 1. 9, right). We recall that the quality factor Q of an oscillating circuit is defined as:

$$Q = 2\pi \frac{\textit{Total energy stored}}{\textit{dissipated energy over one cycle}} \quad (1.22)$$

The energy variation is represented in Fig. 1. 10. We can calculate the instantaneous total energy stored in the circuit by observing that when the magnetic energy comes to zero, the electric energy goes to a maximum [16]. The decreasing of energy in the circuit on a cycle is obtained by multiplying the mean power P_d dissipated in the resistance by the period T ($= 2\pi/\omega$). The relation (1.22) can then be rewritten:

$$Q = \frac{2\pi W_t}{T \left(\frac{dW_t}{dt} \right)} = \omega \frac{W_t}{P_d} \quad (1.23)$$

The resonating circuits at low frequency have typically a quality factor Q around 100.

At high frequencies, where the wavelength is of the same order than the size of the components (we mean normal size of resistors or capacitors that is around 3 cm, excluding surface mounted devices (smd) components), these do not behave any more as localized elements but as distributed elements, in such a way that the LC circuit does not function correctly. At these frequencies, the resonating function is realized thanks to cavities where the electromagnetic energy is confined by the conductive walls.



Fig. 1. 9: Ideal resonating circuit (left) and Real resonating circuit (right)

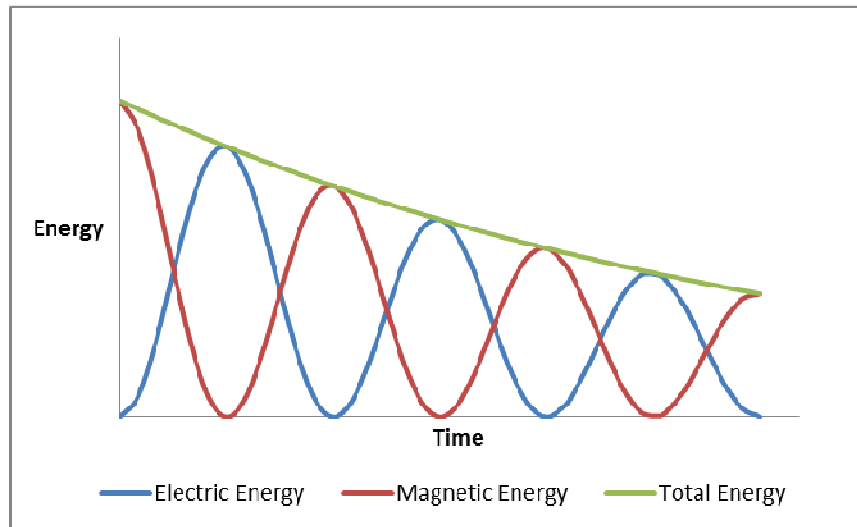


Fig. 1. 10: Decreasing of energy in a resonating circuit with time.

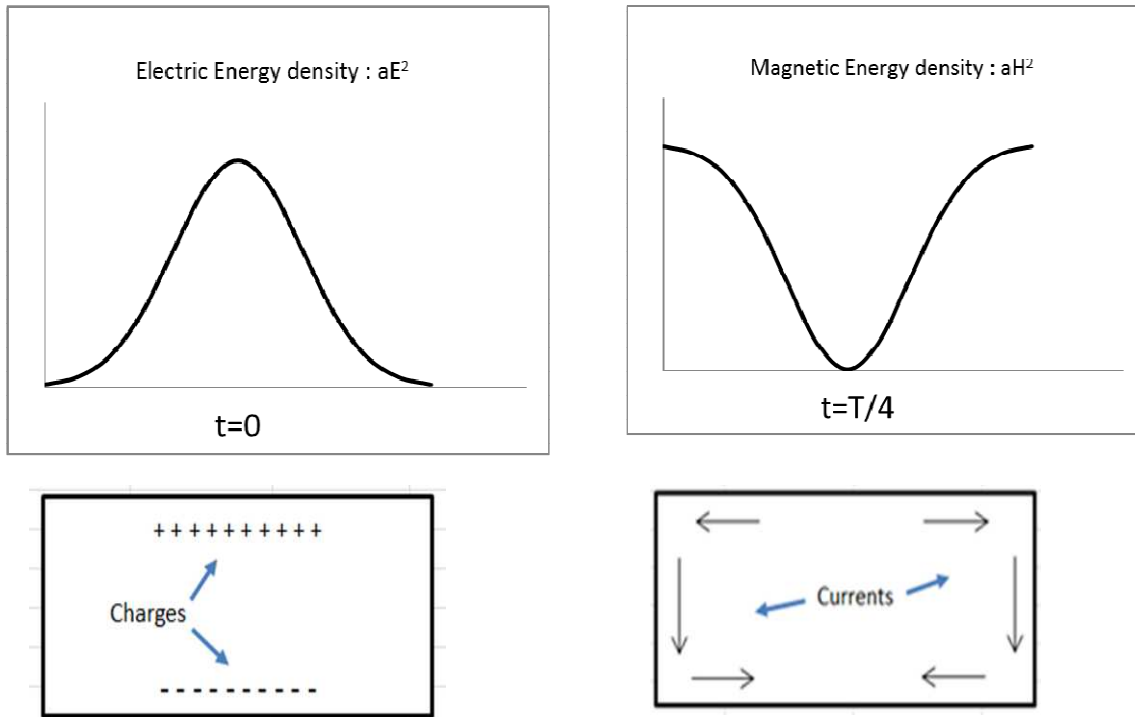


Fig. 1. 11: Electric and magnetic energies in a resonating cavity.

The electric energy is stored in the electric field and the magnetic energy is stored in the magnetic field. As we can see in Fig. 1. 11, at a given time $t=0$, the energy is entirely in its electrical type with electrical positive charges and negative charges accumulated on the superior and inferior sides, respectively. A quarter of a cycle later ($t=T/4$), the energy is entirely in its magnetic type with electric currents flowing along the side walls [16].

The total energy is maximum when the excitation frequency is one of the resonating frequencies of the cavity. As we will see, there exists an infinite number of resonating modes for a cavity. Each mode is characterized by a given charge distribution and currents on the walls. To each mode corresponds an equivalent scheme and a defined resonating frequency. The resonating frequencies are related to the shape of the cavity and to its dimensions. The mode

for which the resonating frequency is the lowest is called the *fundamental mode* of the cavity.

According to the way the cavity is excited, a TM (Transverse Magnetic) mode or TE (Transverse Electric) mode can exist.

A TM mode is associated with a characteristic current stationary wave at the surface of the walls. The current is oriented in such a way that it produces a magnetic field which has components only in the transverse plan. The current has a direction that is perpendicular to this plan. The intensity of the current surface density (A/m^2) in a point of the wall is equal to the intensity of the magnetic field tangent to the wall at this point.

A TE mode is characterized by a stationary wave of oscillating charges in such a way that it produces an electric field with components in one plan, called transverse plan.

The surface density of charges is distributed in such a way that the resulting electric field is perpendicular to the metallic walls. The intensity of the electric field E (V/m) at the surface, multiplied by the electric permittivity ϵ of the media (F/m) is equal to the charge surface density (C/m^2).

The conductivity of the walls is not infinite. Hence, just like in an oscillating circuit at low frequency, the equivalent scheme of a resonating cavity in a given mode has a shunt conductance. The quality factor of a cavity is, nevertheless, higher (10^2 to 10^4). An example of calculation of the Q factor for a cavity of given shape will be given later.

The operation of functioning of a cavity can be understood as well by reference to the concept of transmission line, which can be considered, under certain condition, as a 1D-cavity. According to the transmission line theory, the input impedance of a short-circuited lossless line of length d and characteristic impedance Z_c is:

$$Z_{IN} = j Z_C \operatorname{tg} \left(\frac{2\pi d}{\lambda_G} \right) \quad (1.24)$$

where λ_G is the wavelength on the line. We know that there will be resonance if we place at the input of this line an impedance whose value is the opposite of the above value. If we place a short-circuit, there will be resonance when we have: $Z_{IN}=0$, for this

$$d = n \frac{\lambda_G}{2} \quad (n=1, 2, \dots) \quad (1.25)$$

The extension of this reasoning to tri-dimensional structures is not difficult. Let us take, for example, a lossless rectangular waveguide of infinite length, where a TE_{mn} wave is propagating. The waveguide is short-circuited at a defined position A (Fig. 1. 12) with a perfect electrical conductor. The electric and magnetic field reflect with a reflection coefficient equal to -1 and 1 respectively (in such way that the boundary conditions are satisfied) and stationary waves appear in the waveguide.

At a fixed frequency, we can cut in the waveguide, a series of oscillating cavities, under the condition that the cut part has a length $a \cdot \lambda_G / 2$ ($a=1, 2, \dots$). For any other length of the part, the boundary conditions are not satisfied and it will not be possible to maintain oscillations at this fixed frequency.

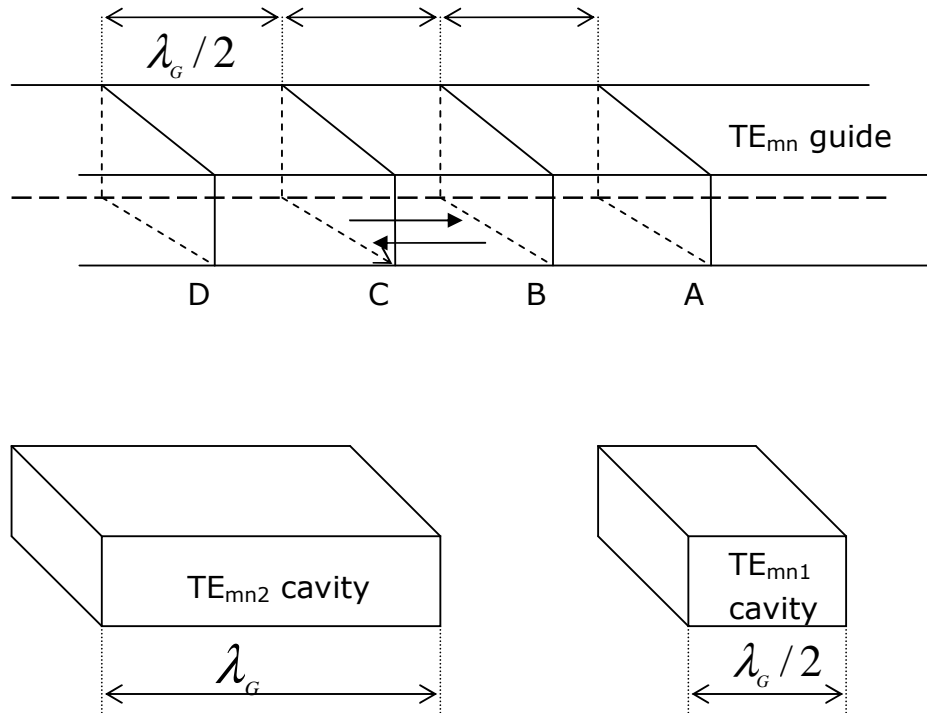


Fig. 1. 12: Waveguide and rectangular cavities

On the nodal planes A, B, C,... with a distance between them of $\lambda_g/2$, the transversal electric field is null. If a second metallic plate would be set in B or C, the new boundary conditions imposed to this surface would be compatible with the field existing in the guide. We obtain in this way closed cavities AB, AC,...for which we can say that it is possible for a wave to oscillate in this volume in the TE_{mn1} , TE_{mn2} , ... The indexes 1, 2, ... indicate the length of the cavity measured in multiples of $\lambda_g/2$.

1.4.2 The Helmholtz equation in 3-D parallelepiped cavity

Let us consider now the case of 3D-cavities (Fig. 1. 13). In order to find their solutions, we start from the vector Helmholtz equation (1.14), [7]:

$$(\nabla^2 + k^2)\vec{E} = 0 \quad (1.26)$$

$$(\nabla^2 + k^2)\vec{H} = 0 \quad (1.27)$$

where k is the wave number or the propagation vector.

The boundary conditions at the surface of the perfectly conducting walls require an electric field that is perpendicular and a magnetic field that is tangential to the surface, in other words:

$$\vec{n} \times \vec{E} = 0 \quad (1.28)$$

$$\vec{n} \cdot \vec{H} = 0 \quad (1.29)$$

where \vec{n} is the unit vector perpendicular to the wall surface.

For some simple shape as the parallelepiped one, it is possible to solve these equations analytically.

It is obtained by short-circuiting a z oriented rectangular waveguide in $z=0$ and $z=d$.

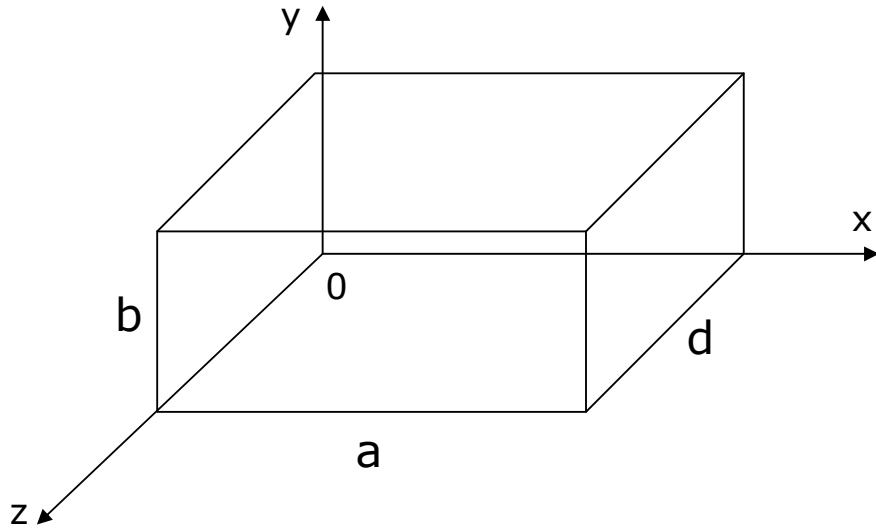


Fig. 1. 13: Parallelepiped resonating cavity

The equations (1.26) and (1.27) admit solutions only for some k values, called *eigenvalues*. To each eigenvalue corresponds an eigenfunction called *mode*. As explained above, these modes are those of the rectangular waveguide (TE_{mn} and TM_{mn}) to which a third index is added, indicating the number of half-wavelengths along the total length of the cavity. So, for each mode, the dimensions of the cavity in the three dimensions must be an entire multiple of the half-wavelength.

The values of $k = \omega/c$ (where c is the speed of light in the cavity) for which the equations (1.26) and (1.27) admit solutions are:

$$k_{mnp}^2 = \left(\frac{\omega_{mnp}}{c} \right)^2 = \left(\frac{m\pi}{a} \right)^2 + \left(\frac{n\pi}{b} \right)^2 + \left(\frac{p\pi}{d} \right)^2 \quad (1.30)$$

where:

$$\left. \begin{array}{l} m=0, 1, 2, \dots \\ n= 0, 1, 2, \dots \\ p= 1, 2, 3, \dots \end{array} \right\} \text{ for TE modes} \quad \left. \begin{array}{l} m=1, 2, 3, \dots \\ n= 1, 2, 3, \dots \\ p= 0, 1, 2, \dots \end{array} \right\} \text{ for TM modes}$$

The mode having the smallest order and the lowest resonant frequency is called the *fundamental mode* of the cavity. If $d > a > b$, this will be the TE_{101} mode.

For TE modes, the electric and magnetic fields in the cavity are derived from the solutions of the Helmholtz equation (1.27) and the boundary conditions:

$$H_z = H_0 \cos \frac{m\pi x}{a} \cos \frac{n\pi y}{b} \sin \frac{p\pi z}{d} \quad (1.31)$$

$$H_x = -\frac{H_0}{\left(\frac{m\pi}{a}\right)^2 + \left(\frac{n\pi}{b}\right)^2} \left(\frac{p\pi}{d}\right) \left(\frac{m\pi}{a}\right) \sin \frac{m\pi x}{a} \cos \frac{n\pi y}{b} \cos \frac{p\pi z}{d} \quad (1.32)$$

$$H_y = -\frac{H_0}{\left(\frac{m\pi}{a}\right)^2 + \left(\frac{n\pi}{b}\right)^2} \left(\frac{p\pi}{d}\right) \left(\frac{n\pi}{b}\right) \cos \frac{m\pi x}{a} \sin \frac{n\pi y}{b} \cos \frac{p\pi z}{d} \quad (1.33)$$

$$E_x = \frac{j\omega\mu H_0}{\left(\frac{m\pi}{a}\right)^2 + \left(\frac{n\pi}{b}\right)^2} \left(\frac{n\pi}{b}\right) \cos \frac{m\pi x}{a} \sin \frac{n\pi y}{b} \sin \frac{p\pi z}{d} \quad (1.34)$$

$$E_Y = -\frac{j\omega\mu H_0}{\left(\frac{m\pi}{a}\right)^2 + \left(\frac{n\pi}{b}\right)^2} \left(\frac{m\pi}{a}\right) \sin\frac{m\pi x}{a} \cos\frac{n\pi y}{b} \sin\frac{p\pi z}{d} \quad (1.35)$$

$$E_z = 0 \quad (1.36)$$

where H_0 is an arbitrary constant in A/m and $\vec{H} = \frac{1}{j\omega\mu} \nabla \times \vec{E}$.

For TE modes, there are two restrictions on the indexes: $m+n \neq 0$ and $p \neq 0$.

The first is due to the fact that if m and n are together equal to zero, $H_x = 0$ and $H_y = 0$. This means that there is no electric field and thus no electromagnetic wave.

The second restriction is needed because the boundary conditions impose that $H_z = 0$ on the two short-circuit faces, in $z=0$ and $z=d$.

For the TM modes, the electric and magnetic fields in the cavity are derived from the solutions of the Helmholtz equation (1.26) and the boundary conditions.

$$E_z = E_0 \sin\frac{m\pi x}{a} \sin\frac{n\pi y}{b} \cos\frac{p\pi z}{d} \quad (1.37)$$

$$E_x = -\frac{E_0}{\left(\frac{m\pi}{a}\right)^2 + \left(\frac{n\pi}{b}\right)^2} \left(\frac{p\pi}{d}\right) \left(\frac{m\pi}{a}\right) \cos\frac{m\pi x}{a} \sin\frac{n\pi y}{b} \sin\frac{p\pi z}{d} \quad (1.38)$$

$$E_Y = -\frac{E_0}{\left(\frac{m\pi}{a}\right)^2 + \left(\frac{n\pi}{b}\right)^2} \left(\frac{p\pi}{d}\right) \left(\frac{n\pi}{b}\right) \sin \frac{m\pi x}{a} \cos \frac{n\pi y}{b} \sin \frac{p\pi z}{d} \quad (1.39)$$

$$H_X = -\frac{j\omega\epsilon E_0}{\left(\frac{m\pi}{a}\right)^2 + \left(\frac{n\pi}{b}\right)^2} \left(\frac{n\pi}{b}\right) \sin \frac{m\pi x}{a} \cos \frac{n\pi y}{b} \cos \frac{p\pi z}{d} \quad (1.40)$$

$$H_Y = \frac{j\omega\epsilon E_0}{\left(\frac{m\pi}{a}\right)^2 + \left(\frac{n\pi}{b}\right)^2} \left(\frac{m\pi}{a}\right) \cos \frac{m\pi x}{a} \sin \frac{n\pi y}{b} \cos \frac{p\pi z}{d} \quad (1.41)$$

$$H_Z = 0 \quad (1.42)$$

where E_0 is an arbitrary constant in V/m and $\vec{E} = -\frac{1}{i\omega\epsilon} \nabla \times \vec{H}$.

Note that the longitudinal component E_z of the TM modes is proportional to the functions $\sin \frac{m\pi x}{a}$ and $\sin \frac{n\pi y}{b}$.

The E_z component would be equal to zero with m or n equal to zero. This explains why in (1.30), we must exclude the case $m=0$ and $n=0$. Indeed, a TM mode with $E_z = 0$ would be a TEM mode, that is only possible with a system with two conductors at least. In [17] some of the first modes of the parallelepiped cavity are presented.

1.4.3. RC = Resonating cavity + tuner

The energy of the input frequency spreads over the different modes. In other words, the input frequency initiates several modes in the cavity which resonating frequencies are close to the working frequency (Fig. 1. 14). The input frequency of the source can be CW or modulated, and do not produce new frequencies. The bandwidth in which the modes will be excited is given by [8]:

$$f_0 \left(1 - \frac{1}{2Q}\right) \leq f \leq f_0 \left(1 + \frac{1}{2Q}\right)$$

Where Q is the quality factor (see section 1.5.3 for more information).

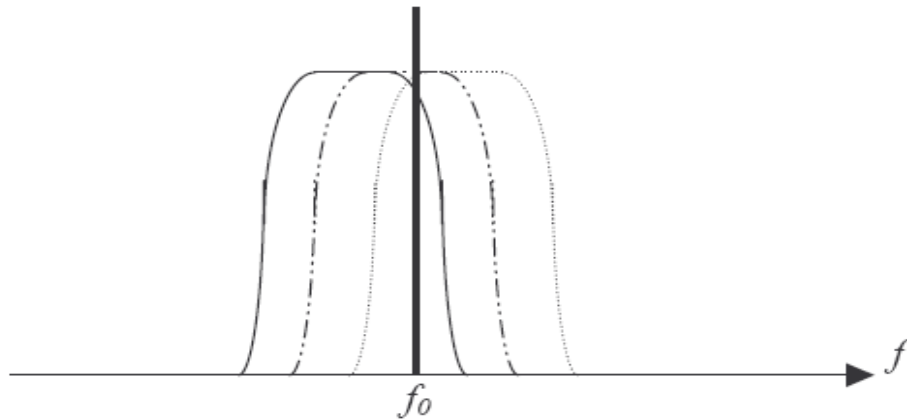


Fig. 1. 14 : Working frequency and frequency bandwidth of modes.

It is the random excitation, by the tuner, of the modes close to the working frequency which constitutes the fundamental mechanism leading to a random electromagnetic field in the reverberation chamber.

1.5 Statistical characterization of Electric field and Power in a RC

1.5.1 Introduction

In a testing chamber where the reverberation conditions are ideal, the field in a given point is the sum of a large number of independent electromagnetic waves coming from the reflections on the walls and the tuner. This independence results from the action of the tuner displacement which reflects and diffracts in time dependent spatial directions the waves incident to it. These directions depend, in fact, on the instantaneous position of the tuner at the moment when the waves impinge it, and, of the arrival directions.

1.5.2 Definitions

First of all, we define the Cumulative Distribution Function (CDF or cdf) $F(y)$ as the probability that the random variable Y takes a value less than or equal to y :

$$F(y) = \Pr [Y \leq y] \quad (1.43)$$

The CDF is nondecreasing with the following properties:

$$F(-\infty) = 0$$

$$F(\infty) = 1$$

We define the Probability Density Function (PDF or pdf) $f(x)$ as a function whose general integral over the range x_L to x_U is equal to the probability that the random variable X takes a value in that range:

$$\int_{x_L}^{x_U} f(x)dx = \Pr [x_L < X \leq x_U] \quad (1.44)$$

The CDF, $F(y)$, is related to the PDF, $f(x)$, as follows:

$$F(y) = \int_{-\infty}^y f(x)dx \quad (1.45)$$

So, for m independent normal random variables, a_1, a_2, \dots, a_m with zero mean and a standard deviation σ , the χ and χ^2 statistics are defined as:

$$\chi = \sqrt{a_1^2 + a_2^2 + \dots + a_m^2} \quad (1.46)$$

and,

$$\chi^2 = a_1^2 + a_2^2 + \dots + a_m^2 \quad (1.47)$$

The number m is the Degree of Freedom (DOF or dof) of these statistics.

Their respective Probability Density Functions (PDF or pdf) are:

$$f(\chi) = \frac{2}{2^{\frac{m}{2}} \sigma^m \Gamma\left(\frac{m}{2}\right)} \chi^{m-1} e^{-\frac{\chi^2}{2\sigma^2}} \quad (1.48)$$

$$f(\chi^2) = \frac{2}{2^{\frac{m}{2}} \sigma^m \Gamma\left(\frac{m}{2}\right)} (\chi^2)^{\frac{(m-2)}{2}} e^{-\frac{\chi^2}{2\sigma^2}} \quad (1.49)$$

Where: $\Gamma\left(\frac{m}{2}\right)$ is the Gamma function, with

- $\Gamma(1) = 1$;
- $\Gamma(m) = (m-1)!$;
- $\Gamma\left(\frac{1}{2}\right) = \sqrt{\pi}$;
- $\Gamma\left(m + \frac{1}{2}\right) = \frac{(2m)!}{4^m m!} \cdot \sqrt{\pi}$;
- With, "m" a non-negative integer.

1.5.3 PDF and CDF for the Electric field components

About the real and imaginary part of the three rectangular components of the electric field, we write:

- $E_x = E_{xr} + E_{xi}$;
- $E_y = E_{yr} + E_{yi}$;
- $E_z = E_{zr} + E_{zi}$.

Their instantaneous value is the sum of a large number of independent contributions (electromagnetic waves coming from the reflections on the walls and the tuner). According the Lyapunov central limit theorem, we know that the mean of a sufficiently large number of independent random variables, will be approximately normally distributed. In other words, the real and imaginary part follows a Gaussian pdf [7], [60] with zero mean and a given variance. This independence results from the action of the tuner

displacement which reflects and diffracts in time dependent spatial directions the waves incident to it.

The Gaussian pdf for the real part of E_x component is:

$$f(E_{xr}) = \frac{1}{\sqrt{2\pi}\sigma} \cdot e^{-\frac{E_{xr}^2}{2\sigma^2}} \quad (1.50)$$

The same Gaussian pdf applies for the real and imaginary part of the E_y and E_z components.

Since, $E_a = \sqrt{E_{ar}^2 + E_{ai}^2}$, with $E_a = E_x, E_y$ or E_z and according to (1.48), E_a behaves as a χ pdf with two degree of freedom, or as a Rayleigh pdf:

$$pdf \equiv f(E_a) = \frac{E_a}{\sigma^2} e^{-\frac{E_a^2}{2\sigma^2}} \quad (1.51)$$

With : σ^2 being a scale factor.

This scale factor depends on the numerical value of the electric field. An estimator is given hereafter (1.54).

The characteristics of the pdf are the following:

$$mean \equiv \mu = \sigma \sqrt{\frac{\pi}{2}} \quad (1.52)$$

$$variance \equiv \sigma_a^2 = \sigma^2 \left(2 - \frac{\pi}{2} \right) \quad (1.53)$$

It is interesting to note that the ratio of the variance to the square of the mean of a Rayleigh random variable is a constant equal to $4/\pi - 1 \approx 0,273$.

$$\text{scale factor estimator} \equiv \hat{\sigma}^2 = \frac{1}{2n} \sum_{i=1}^n E_{a_i}^2 \quad (1.54)$$

Where n is the number of samples or tuner steps (see also point 2.2).

The Maximum-Likelihood Estimator (MLE) of σ^2 is calculated by taking the derivative of the pdf (1.51) with respect to σ^2 and setting it equal to zero, yielding (1.54).

In [18], it is defined in function of the characteristics of the RC:

$$\sigma^2 = \frac{4\pi Q}{3\epsilon_0 \omega V} \cdot P_{in} \quad (1.55)$$

Where:

- Q is the quality factor of the RC [59];
- $\epsilon_0 = 8.854 \times 10^{-12}$ (F/m), the vacuum permittivity;
- ω is the angular frequency in (rad/s);
- V is the volume of the RC;
- P_{in} is the power delivered to the RC by an external source of energy (W).

The MLE will be very useful when comparing the theoretical and experimental data. In fact, the $\hat{\sigma}^2$ will be calculated from the

measured Electric field and will be used instead of σ^2 in the theoretical cdf (cumulative density function):

$$cdf \equiv F(E_a) = 1 - e^{-\frac{E_a^2}{2\sigma^2}} \quad (1.56)$$

When comparing the theoretical and experimental cdf's in the Kolmogorov-Smirnov (KS) hypothesis test, we will take for σ^2 , in the theoretical cdf, its estimator $\hat{\sigma}^2$ calculated from the experimental data according to (1.54).

So, all six rectangular components of the electromagnetic field (E_x , E_y , E_z , H_x , H_y and H_z) follow a χ pdf with two degrees of freedom (or as a Rayleigh pdf) [7], [18], [65].

This is valid for an ideal world, but in reality, the efficiency of the tuner is not perfect and one can show [19] [20] that the magnitude of the rectangular field component E_a is rather characterized by a *Rice-Nakagami* pdf [58], which depends, first, on a "tuned part", E_a of the field (which is purely random) described by its standard deviation, and, second, on a residual "untuned part" noted \tilde{E}_a , corresponding to some deterministic residue in the field.

The pdf of the resulting rectangular component of the electric field can be written as:

$$f(E_a) = \frac{E_a}{\sigma^2} I_0\left(\frac{E_a \tilde{E}_a}{\sigma^2}\right) e^{-\frac{E_a^2 + \tilde{E}_a^2}{2\sigma^2}} U(E_a) \quad (1.57)$$

Where $I_0(\cdot)$ is the first type modified Bessel function of zero order and $U(\cdot)$ is the Heaviside step function.

a) If the “untuned part” of the field is larger than the “tuned part” in such a way that:

$$E_a \cdot \tilde{E}_a \gg \sigma^2 \quad (1.58)$$

We can replace $I_0(\cdot)$ by its asymptotic development:

$$I_0(x) \approx \frac{e^x}{\sqrt{2\pi x}} \left(1 + \frac{1}{8x} + \frac{9}{128x^2} + \dots \right) \quad (1.59)$$

And limiting to the first order term, the relation (1.57) becomes:

$$f(E_a) \approx \frac{1}{\sqrt{2\pi\sigma^2}} \sqrt{\frac{E_a}{\tilde{E}_a}} e^{-\frac{(E_a - \tilde{E}_a)^2}{2\sigma^2}} U(E_a) \quad (1.60)$$

This is close to a Gaussian pdf.

b) If, on the other side, $\tilde{E}_a = 0$ (perfect tuning, no deterministic field), then the Rice-Nakagami pdf reduces to:

$$f(E_a) = \frac{E_a}{\sigma^2} e^{-\frac{E_a^2}{2\sigma^2}} U(E_a) \quad (1.61)$$

Known as χ pdf with two dof, or Rayleigh pdf. This distribution is only characterized by the variance σ^2 of the two Gaussian elementary distributions of the real and imaginary parts of E_a .

In order to quantify the difference between the actual statistical distribution and the reference distribution, we introduce the *Rice factor* defined by:

$$RF = \frac{\tilde{E}_a}{2\sigma^2} \quad (1.62)$$

It expresses the ratio of the “untuned part” to the “tuned part” of the field component. When the reverberation chamber is close to the ideal world, the tuned part is high, then $RF \approx 0$. In the opposite case, if the “untuned part” is predominant, then $RF > 1$.

By analogy with a propagation environment, the first case ($RF \approx 0$) corresponds to propagation dominated by multiple paths variable with time yielding a purely random field, whereas the second case ($RF > 1$) is corresponding to a situation where line-of-sight path is predominant, introducing a deterministic component in the random field.

1.5.4 PDF and CDF for the total Electric field

We recall that the magnitude of the total electric field is defined as:

$$|E_t| = \sqrt{|E_x|^2 + |E_y|^2 + |E_z|^2} \quad (1.63)$$

The total electric field behaves as a χ pdf with six degrees of freedom (the three rectangular components times the real and imaginary part, of each rectangular component). So, the pdf is obtained from (1.48) with $m=6$:

$$pdf \equiv f(E_t) = \frac{E_t^5}{8\sigma^6} e^{-\frac{E_t^2}{2\sigma^2}} \quad (1.64)$$

With σ^2 being a scale factor.

The characteristics of the pdf are the following:

$$\text{mean} \equiv \mu = \frac{15\sigma\sqrt{2\pi}}{16} \quad (1.65)$$

$$\text{variance} \equiv \sigma_a^2 = \sigma^2 \left(6 - \frac{225\pi}{128} \right) \quad (1.66)$$

$$\text{scale factor estimator} \equiv \hat{\sigma}^2 = \frac{1}{6n} \sum_{i=1}^n E_{t i}^2 \quad (1.67)$$

Where n is the number of samples.

The Maximum-Likelihood Estimator (MLE) of σ^2 is calculated by taking the derivative of the PDF (1.64) with respect to σ^2 and setting it equal to zero, this yields (1.67).

The MLE will be very useful when comparing the theoretical and experimental data. In fact, the $\hat{\sigma}^2$ will be calculated from the measured total electric field and will replace the σ^2 in the theoretical pdf.

From (1.45) and (1.64), one obtains:

$$\text{cdf} \equiv F(E_t) = 1 - e^{-\frac{E_t^2}{2\sigma^2}} \left(\frac{E_t^4}{8\sigma^4} + \frac{E_t^2}{2\sigma^2} + 1 \right) \quad (1.68)$$

To our knowledge, it is the first time this formula is presented; there is no direct reference in literature. It will be useful when comparing the theoretical and experimental cdf's in the Kolmogorov-Smirnov (KS) hypothesis test.

The same kind of pdf (χ with six degrees of freedom) applies to the total magnetic field.

1.5.5 PDF and CDF for the Power received on an antenna in a RC

Up to now, we have spoken about the electromagnetic field, but what about the statistical distribution of the power received by an antenna in a reverberation chamber?

The power received at the termination of a matched antenna in a statistically homogeneous, isotropic and non-polarized electromagnetic field is a χ^2 random variable with two degrees of freedom (see Fig. 1. 15). So, the pdf is obtained from (1.49) with $m=2$:

$$pdf \equiv f(P) = \frac{1}{2\sigma^2} e^{-\frac{P}{2\sigma^2}} \quad (1.69)$$

With P the power received by the antenna, and σ^2 being a scale factor.

The characteristics of the pdf are the following:

$$mean \equiv \mu = 2\sigma^2 \quad (1.70)$$

$$variance \equiv \sigma_a^2 = (2\sigma^2)^2 \quad (1.71)$$

$$scale \ factor \ estimator \equiv \hat{\sigma}^2 = \frac{1}{2n} \sum_{i=1}^n P_i \quad (1.72)$$

Where n is the number of samples.

The Maximum-Likelihood Estimator (MLE) of σ^2 is calculated by taking the derivative of the pdf (1.69) with respect to σ^2 and setting it equal to zero, yielding (1.72).

The MLE will be very useful when comparing the theoretical and experimental data. In fact, the $\hat{\sigma}^2$ will be calculated from the measured received power and will replace the σ^2 in the theoretical PDF.

$$cdf \equiv F(P) = 1 - e^{-\frac{P}{2\sigma^2}} \quad (1.73)$$

This will be useful too when comparing the theoretical and experimental CDF's in the Kolmogorov-Smirnov (KS) hypothesis test.

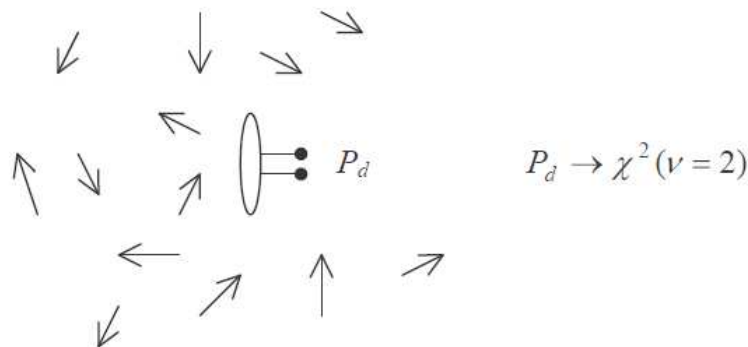


Fig. 1.15: Statistical distribution of the power received by an antenna

1.6 Statistical properties of the Electric field in RC

As we have seen in section 1.5 that the real and imaginary parts of the electric field components follow a Gauss statistic with zero mean and a given variance, we can write the following properties (this applies to an ideal RC):

$$\langle E_{xr} \rangle = \langle E_{xi} \rangle = \langle E_{yr} \rangle = \langle E_{yi} \rangle = \langle E_{zr} \rangle = \langle E_{zi} \rangle = 0 \quad (1.74)$$

$$\langle E_{xr}^2 \rangle = \langle E_{xi}^2 \rangle = \langle E_{yr}^2 \rangle = \langle E_{yi}^2 \rangle = \langle E_{zr}^2 \rangle = \langle E_{zi}^2 \rangle = \sigma^2 \quad (1.75)$$

σ^2 is the variance of the underlying Gauss statistic and the scale factor of the pdf's and cdf's expressed in section 1.5.

The objective is to find the relation between σ^2 and the components of the electric field and between σ^2 and the total electric field.

From (1.74):

$$\sigma^2 = \frac{1}{n} \sum_{i=1}^n E_{xr}^2 \quad (1.76)$$

Note that (1.75) is still valid if we replace E_{xr}^2 by E_{xi}^2 , E_{yr}^2 , E_{yi}^2 , E_{zr}^2 or E_{zi}^2 .

Moreover, $E_x^2 = E_{xr}^2 + E_{xi}^2$, and as $\langle E_{xr}^2 \rangle = \langle E_{xi}^2 \rangle$ from (1.75), equation (1.76) becomes:

$$\sigma^2 = \frac{1}{2n} \sum_{i=1}^n E_x^2 \quad (1.77)$$

Note that (1.76) is still valid if we replace E_x^2 by E_y^2 or E_z^2 . This very important relation has to be compared with (1.54) that gives the scale factor estimator of the pdf of E_x , E_y and E_z from their measured values. We understand that the scale factor is the variance of the underlying Gauss statistic. And thanks to (1.54) or

(1.77), we can calculate the pdf and cdf of the electric field component.

Note that (1.77) can also be written and completed as:

$$\sigma^2 = \frac{\langle E_x^2 \rangle}{2} = \frac{\langle E_y^2 \rangle}{2} = \frac{\langle E_z^2 \rangle}{2} \quad (1.78)$$

Looking for the total electric field, now, we write:

$$E_t^2 = E_{xr}^2 + E_{xi}^2 + E_{yr}^2 + E_{yi}^2 + E_{zr}^2 + E_{zi}^2 \quad (1.79)$$

From (1.74), $\langle E_t^2 \rangle = 6 \cdot \langle E_{xr}^2 \rangle$, and using (1.76), we obtain:

$$\sigma^2 = \frac{1}{6n} \sum_{i=1}^n E_t^2 \quad (1.80)$$

Again, this very important relation has to be compared with (1.78) that gives the scale factor estimator of the pdf of E_t from its measured values. We understand that the scale factor is the variance of the underlying Gauss statistic. And thanks to (1.67) or (1.80), we can calculate the theoretical pdf and cdf of the total electric field.

Coming back to (1.75), we can write (1.80) also as:

$$\sigma^2 = \frac{\langle E_t^2 \rangle}{6} \quad (1.81)$$

And, from (1.78) and (1.81), we can write that:

$$\langle E_x^2 \rangle = \langle E_y^2 \rangle = \langle E_z^2 \rangle = \frac{\langle E_t^2 \rangle}{3} \quad (1.82)$$

These two important properties are given by Hill in [7], without proof.

1.7 The Kolmogorov-Smirnov (KS) hypothesis test

The Kolmogorov-Smirnov (KS) test will be used to compare the theoretical and experimental CDFs of the components of the electric field, the total electric field and the power, and to find if they are in agreement or not.

A short presentation of the KS test is the following: We have an experimental random process $F_e(x)$ and a theoretical one $F_t(x)$. Then we define as the test statistic the random variable

$$q = \max |F_e(x) - F_t(x)| \quad (1.83)$$

for a specific experiment, let us say, the measurement of the electric field component E_x at a given frequency and spatial point in the RC, and this at n tuner steps. If the function $F_t(x)$ is the probabilistic CDF modelling the underlying stochastic process (hypothesis H_0), then the empirical statistics $F_e(x)$ obtained from n samples should be considered as a good estimator of it as $F_e(x) \rightarrow F_t(x)$ for $n \rightarrow \infty$. From this it follows that

$$E[F_e(x)] = F_t(x) \quad (1.84)$$

Where $E[F_e(x)]$ is "the expected value" or mean of $F_e(x)$.

It shows that for large n , q is close to 0 if H_0 is true and is close to $\max |F_e(x) - F_t(x)|$ if H_1 is true. In other words, we will reject H_0 if

q is larger than constant c which is determined in terms of the significance level α :

$$\alpha = P\{q > c \mid H_0\} \approx 2e^{-2nc^2} \quad (1.85)$$

With $H_0 : F_e(x) \equiv F_t(x)$ and $H_1 : F_e(x) \neq F_t(x)$.

Applied to our measurements, the hypothesis test will proceed as follows. We obtain, from the measurements, the experimental CDF of the electric field component, the total electric field or the power received, then, we obtain the theoretical respective CDF, and we will determine q with (1.83).

We will accept the hypothesis H_0 (i.e. that the experimental CDF tends to the theoretical one) in the confidence interval of 95 % if (from 1.85):

$$q < \sqrt{-\frac{1}{2n} \ln \frac{\alpha}{2}} \quad (1.86)$$

With $\alpha = 0.05$ and n being the number of tuner steps.

We have calculated with (1.86), the following values of q as a function of the number of tuner steps, n , we have used during our experimentations, in the table below:

Table 1.1: Limit values for the KS test as a function of the tuner steps

n Number of tuner steps	q Limit value of KS test
150	0.1109
52	0.1883
51	0.1902
37	0.2233
24	0.2772
12	0.3921

These values of n are linked to the measurements. The values of 150, 24 and 12 are linked to the tuner steps used in the dynamic source-mode tuning (chapter 2). The value of 37 is used in the static source-mode tuning (chapter 3) and the values of 52 and 51 are used in the antenna efficiency measurements (chapter 4).

2. Dynamic source-mode tuning with two orthogonal LPDA antennas scanning system

2.1 Introduction

The method usually applied for mode tuning in a reverberation chamber (RC) consists in placing a rotating stirrer that breaks the waves coming from a fixed source antenna, reflecting and scattering them in various time-dependent directions. It has been applied with success in many facilities over the world and has also been used at LEMA. Not conceived originally for reverberation purpose but rather as a Faraday cage, the cubic shape of the small LEMA chamber (15m^3) was a priori expected to be a penalty for obtaining a good separation of the resonance frequencies. In fact the parallelepiped shape is the preferred one (because there are no degenerate modes as it is the case in a cubic shape). From the studies done the last years on this chamber [21][22][23][24], it turns out that the drawback of the cubic shape can be overcome if the mechanical stirrer is properly designed and if the "factor 6" rule of thumb (the minimum ratio of the operating frequency to the fundamental resonance frequency of the cavity to have enough modes in the chamber [6]) is relaxed to a "factor 9" rule of thumb. Because the mechanical stirrer has to be electrically large to be efficient, it can be quite cumbersome and limits the working volume available for the EUT, especially in small reverberation chambers. In large chambers with low LUF (Lowest Usable Frequency), huge stirrers can cause stability and vibration problems [12].

The innovative method of dynamic source-mode tuning presented here could be an interesting alternative to mechanical tuning. The RAIL tuner is based on the use of two orthogonal rails

placed close to the chamber walls on which LPDA transmitting antennas are moved in order to obtain a source-tuned reverberation chamber.

The work has been carried out in the perspective of making immunity testing according to the IEC 61000-4-21 standard at HIRF (High Intensity Radiated Fields) in the frequency band of mobile phone and GPS systems (800-2500MHz). The three components of the E-field, the forward and reverse output powers and the displacement of the two LPDA (Log Periodic Dipole Array) antennas have been measured for each of the 150 tuner positions, at eight locations of the working volume and at twenty two frequencies within the frequency range of interest. The results are oriented and analysed in terms of the requirements of the standard, i.e., the field uniformity. The results show that this source tuning method using two orthogonal scanning systems that are less cumbersome than the conventional mechanical mode stirrer, is quite efficient.

2.2 Set-up and measurement method

With 2.48 m on a side the LEMA cubic chamber has its fundamental resonance at 85.15 MHz according to (1.30). Considering the abovementioned "factor 9" rule of thumb, it exhibits a LUF at about 800 MHz. It is equipped with a 35 W amplifier in order to achieve high levels of electric field (>35 V/m) in the frequency range of 800 to 2500 MHz. For assessing the efficiency of the dynamic source-tuner, a calibration has been performed as a function of the method described in the IEC 61000-4-21 [2], but without measuring the received power.

The RAIL tuner consists of two rails (Fig. 2. 1 and Fig. 2.2). The horizontal one (rail A) is 2.48 m long and set at 1.25 m from the floor. The vertical one (rail B) is 2.08 m long and placed at 1.39 m from the back wall and at 1.09 m from the front wall. The number of steps for rail A (used length: 2.05 m) and for rail B (used length: 1.65 m) is 83 and 67 respectively. This gives a total of 150 steps or

tuner positions. The length of a single step is 2.5 cm. Considering the lowest frequency of interest (800 MHz), rails A and B are 5.5λ and 4.5λ long respectively, while the step length is $\lambda / 15$ at 800 MHz and $\lambda / 4.8$ at 2500 MHz. So, both rails are electrically long structures, but are much less cumbersome than the rotating stirrer. They are placed near the walls in order to maximize the working volume, but the distance between the antennas, mounted on it and the walls is kept higher than $\lambda / 4$. The rails are placed perpendicular (one horizontal and one vertical) in order to improve the independency of the electromagnetic waves.

The working volume (dotted in red in Fig. 2. 1) is delimited by spatial points P1, P2,... to P8. It is 1.20 m long, 0.90 m large and 0.60 m high.

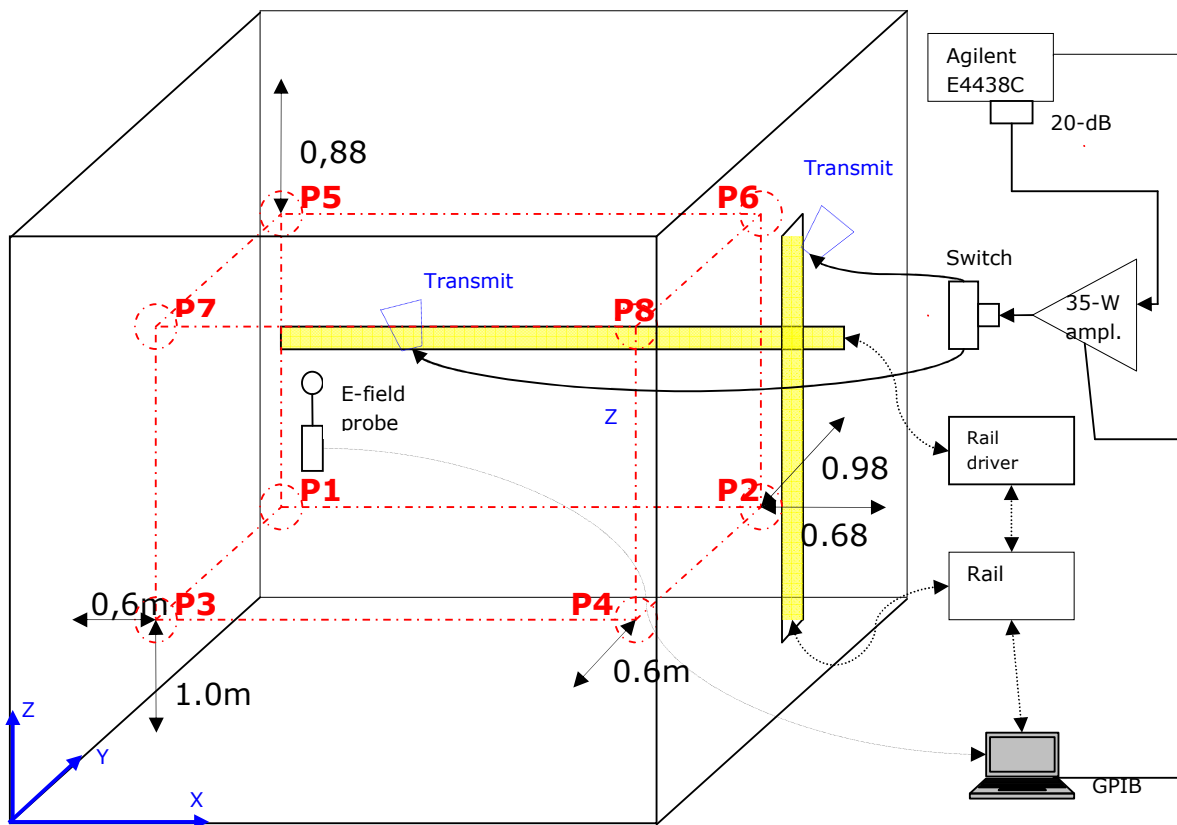


Fig. 2. 1: Set-up in the reverberation chamber with the rail controlling system and the measurement instruments

The working volume is the same as for the second tuning method in order to compare both methods.

The transmitting LPDA (Log Periodic Dipole Array) antenna on each rail has a (900-2500 MHz) bandwidth and a 10 W maximum input power. They are directed towards the walls of the chamber for preventing a direct coupling from the source antenna to the EUT. Now, due to the fact that the LPDA radiation pattern becomes broader below 1 GHz, one can expect some direct illumination of the working volume. In practice, some degree of direct coupling from the source to the EUT would alter the expected Rayleigh probability density function of the field yielding a Rice-Nakagami distribution due to the presence of some deterministic part in the stochastic field.

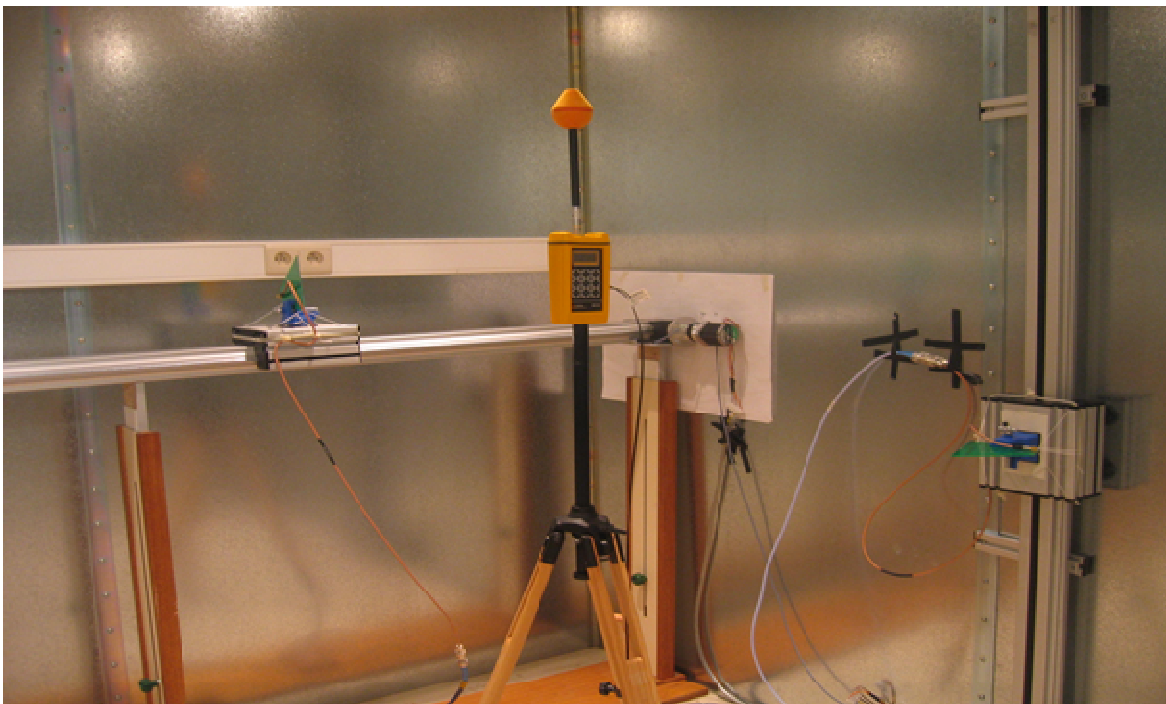


Fig. 2.2: Horizontal rail + Vertical rail + LPDA antennas + E-field meter

The Narda EMR-300 meter with a (3 MHz -18 GHz) E-field probe type 9.2 has been used. It gives the three components of the E-field in one read operation.

During all the measurements, the output of the Agilent generator (E4438C) is set to 0 dBm. As this passes through a 20 dB attenuator, the input of the 35 W amplifier is powered with -20 dBm. The amplifier needs -5 dBm to give full power. The output forward and reverse powers of the amplifier are given directly by the amplifier (no external directional coupler and power meter have been used). The output forward power of the amplifier is about 1.5 W. The power is given to the antenna of rail A during the first 83 steps; then the power is manually switched to the antenna of rail B during the last 67 steps. A software has been developed with LabVIEW for instruments controlling and data acquisition. The E-Field probe is placed on eight spatial points (P1 to P8), delimiting the working volume. The separation distances between the surfaces bounding the working volume and any chamber surface are kept higher than $\lambda/4$, i.e. 9 cm at 800 MHz, in accordance with the $\lambda/4$ rule of thumb. Closer to the walls, the field meter would stand in the wall boundary layer, where the electric field orientation is rather dictated by the local boundary condition and thus more deterministic than stochastic in terms of polarization.

Table 2.1: Positions, in meters, of E-Field probe (X;Y;Z)

P1	(0.60;1.50;1.00)
P2	(1.80;1.50;1.00)
P3	(0.60;0.60;1.00)
P4	(1.80;0.60;1.00)
P5	(0.60;1.50;1.60)
P6	(1.80;1.50;1.60)
P7	(0.60;0.60;1.60)
P8	(1.8;0.6;1.6)

The efficiency of this new tuning method has been assessed at a total of twenty two frequencies logarithmically spaced (in accordance with the requirements of IEC 61000-4-21), at each of the eight spatial points (Table 2.1). The list of frequencies is given in Table 2.2.

Table 2.2: List of frequencies, in MHz, for RAIL tuning

800.00	1463.88
845.17	1546.54
892.90	1633.87
943.32	1726.13
996.58	1823.60
1052.86	1926.58
1112.31	2035.37
1175.12	2150.30
1241.48	2271.72
1311.58	2400.00
1385.64	2513.50

2.3 Tests Results

2.3.1 Field uniformity

For each of the three components of the E-field the uniformity is given by the normalized standard deviation:

$$\sigma_{ij}(dB) = 20 \text{Log}_{10} \left(\frac{\sigma_{ij} + \langle \vec{E}_{ij} \rangle_8}{\langle \vec{E}_{ij} \rangle_8} \right) \quad (2.1)$$

where i stands for the field component of interest (X, Y, Z), j stands for the test frequency with

$$\sigma_{ij} = \sqrt{\frac{\sum_{k=P1}^{P8} (\overrightarrow{E}_{kij} - \langle \overrightarrow{E}_{ij} \rangle_8)^2}{7}} \quad (2.2)$$

$$\langle \overrightarrow{E}_{ij} \rangle_8 = \frac{\sum_{k=P1}^{P8} \overrightarrow{E}_{kij}}{8} \quad (2.3)$$

$$\overrightarrow{E}_{kij} = \frac{E_{\max \ kij}}{\sqrt{P_{ave \ input \ kij}}} \quad (2.4)$$

where $E_{\max \ kij}$ is the maximum value over the 150 steps of the tuner, in a given point k , for a given field component i and at a given frequency j , while $P_{ave \ input \ kij}$ is the average output forward power of the amplifier. The graphical results are given in Fig. 2.3. As one can see, the standard deviation of each component is less than the 3 dB limit over the whole frequency range of interest.

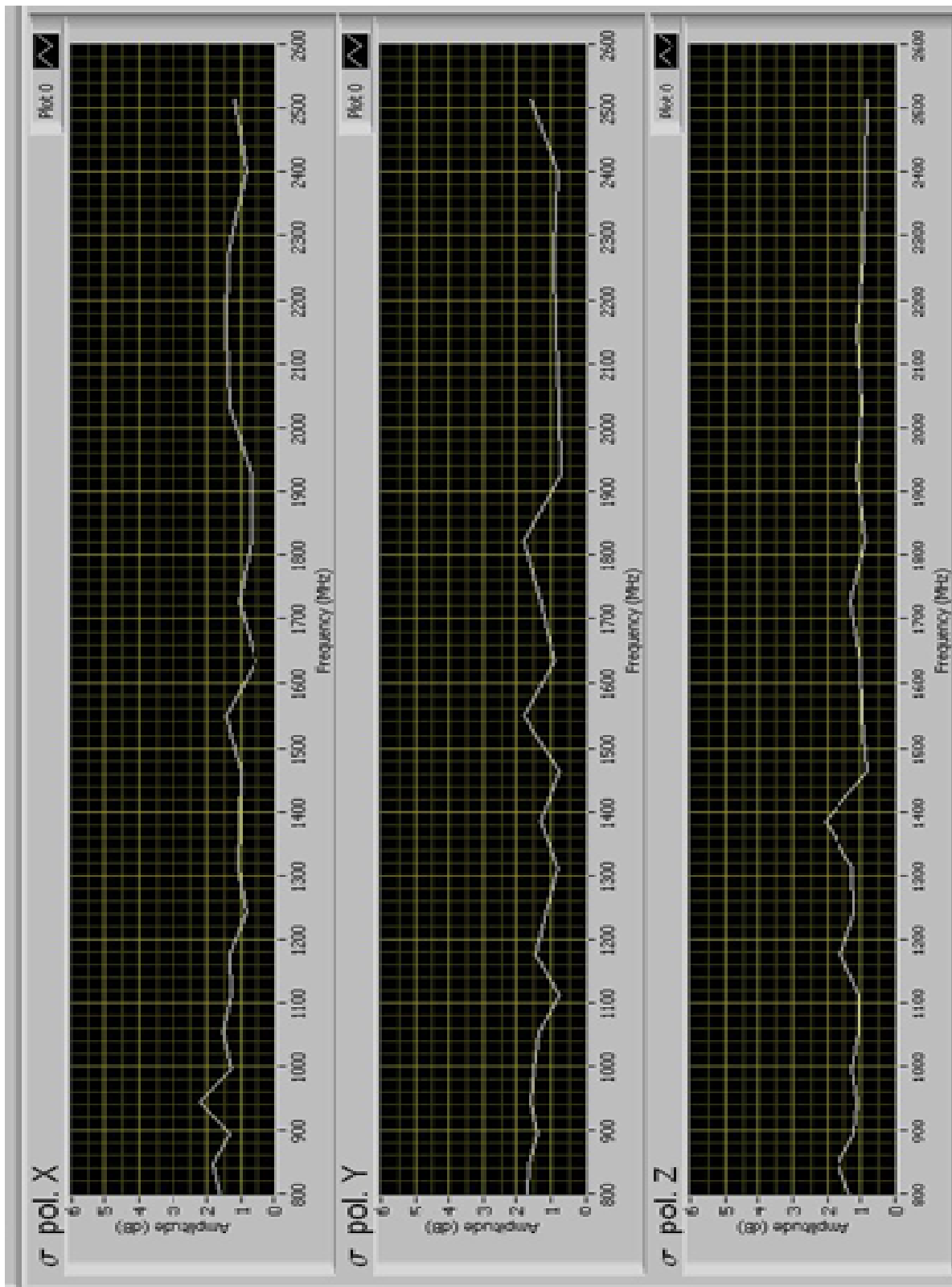


Fig. 2.3: Standard deviation for each polarization

The IEC standard defines the overall field uniformity too, taking into account the three polarizations of the E-field; the standard deviation is then expressed by:

$$\sigma_j(dB) = 20 \text{Log}_{10} \left(\frac{\sigma_j + \langle \vec{E}_j \rangle_{24}}{\langle \vec{E}_j \rangle_{24}} \right) \quad (2.5)$$

Where j stands for the 22 frequencies as given in Table 2.2.

$$\sigma_j = \sqrt{\frac{\sum_{k=P1}^{P8} \sum_{i=X}^Z (\vec{E}_{kij} - \langle \vec{E}_j \rangle_{24})^2}{23}} \quad (2.6)$$

$$\langle \vec{E}_j \rangle_{24} = \frac{8 \langle \vec{E}_{xj} \rangle_8 + 8 \langle \vec{E}_{yj} \rangle_8 + 8 \langle \vec{E}_{zj} \rangle_8}{24} \quad (2.7)$$

The graphical results are given in Fig. 2.4. The overall standard deviation turns out to be less than the 3 dB limit.

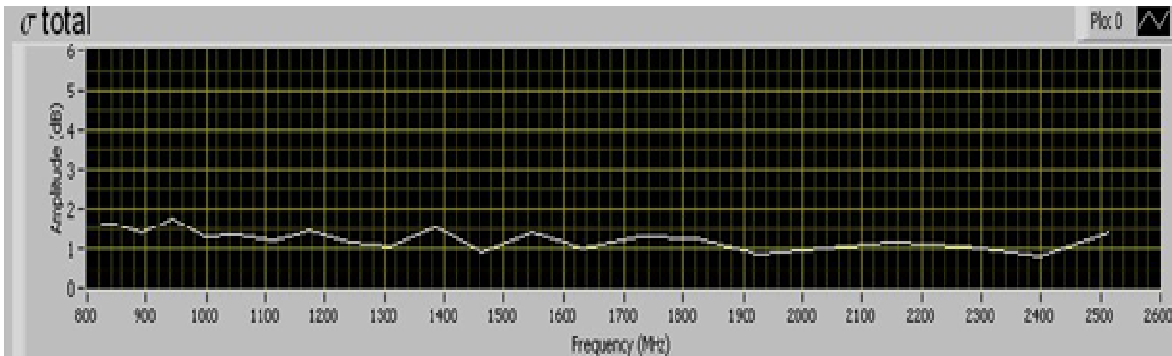


Fig. 2.4: Standard deviation for all three polarizations

2.3.2 Field strength obtained

Fig. 2.5 shows, as an example, the E-field measured, in V/m, as a function of the tuner steps and the frequency at spatial point P1 and for X polarization.

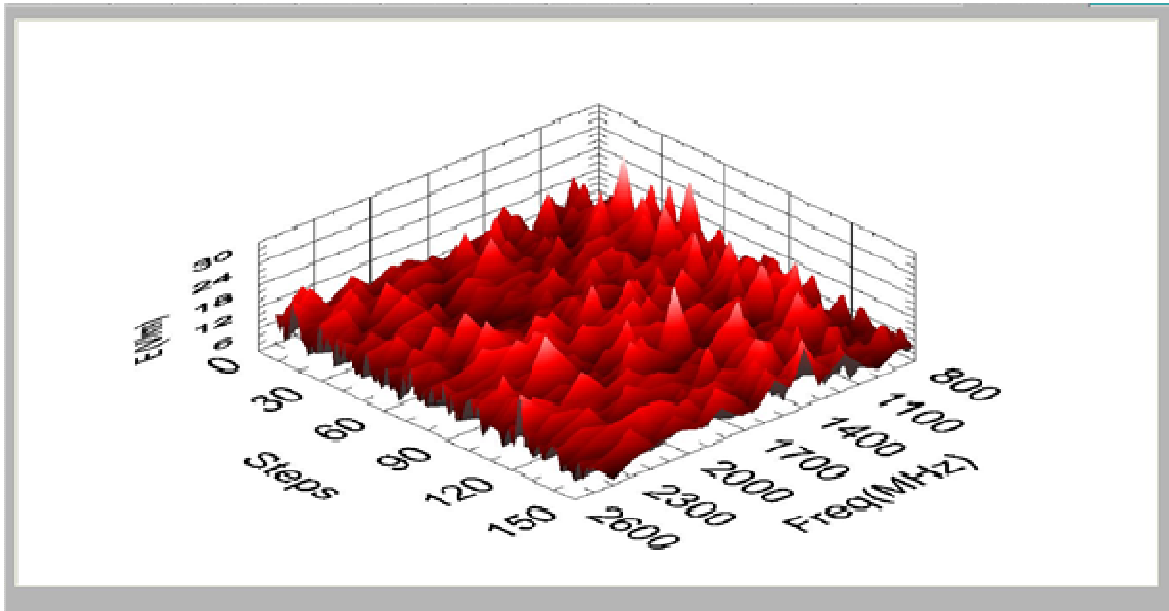


Fig. 2.5: E-field measured at point P1 and for X polarization.

The vertical scale of the figure is E (V/m). The maximum (over the 150 tuner steps) field strength averaged over the eight spatial points is given in Fig. 2.6, for each of the three components. It ranges from 10.9 V/m at 800 MHz to 21.5 V/m at 1053 MHz, with a mean value of 16.9 V/m and a 3σ deviation of 6 V/m (or +2.6 dB to -3.8 dB). These values are obtained for a constant level of -20 dBm at the amplifier input, and an output forward power of about 1.5 W. The normalized values show that less power is needed in frequencies above 1500 MHz to obtain the same level of electric field.

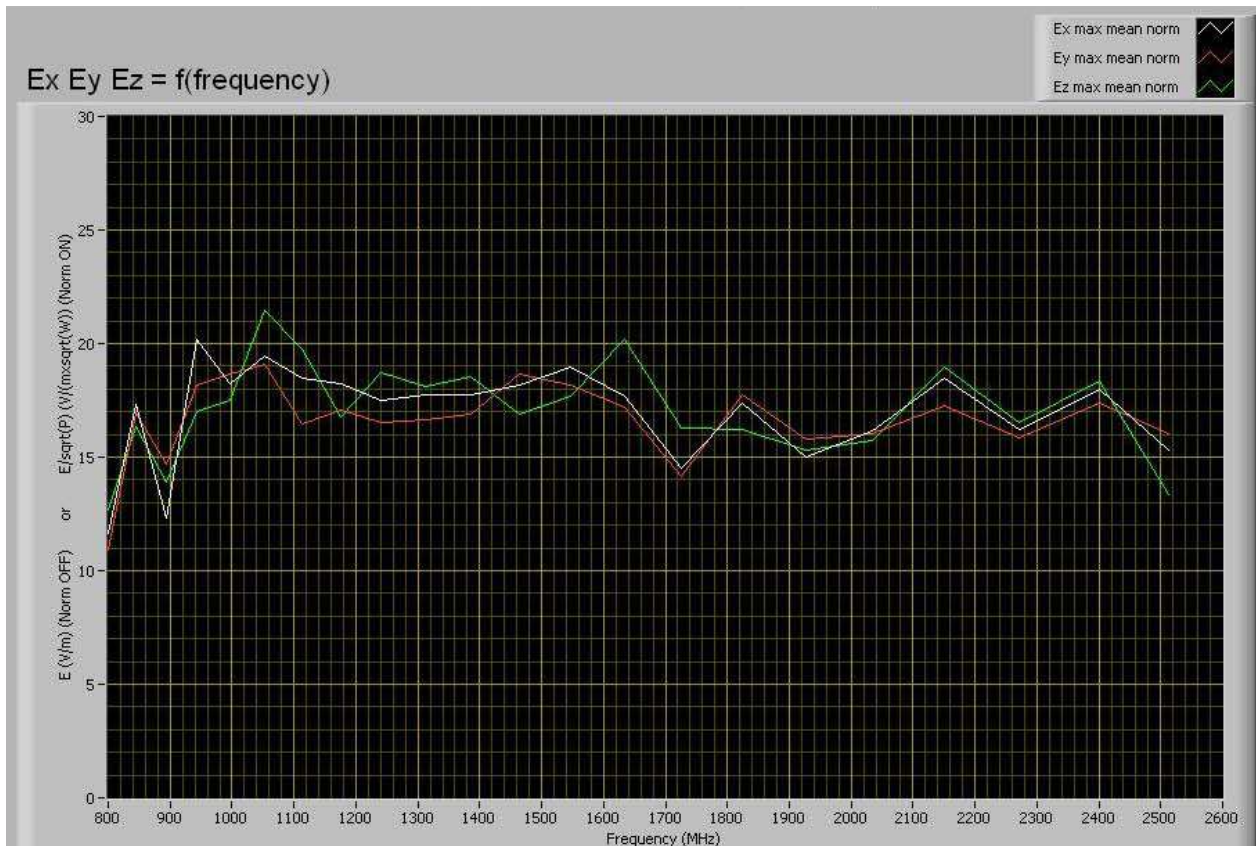


Fig. 2.6: Field strength spatially averaged over the eight points delimiting the working volume

Hence one can estimate that, with the antennas used, field strengths of about 30 V/m with 80% AM modulation and 54 V/m without modulation are expected (the electric field with AM modulation, $E_{AM_{mod.}}=30$ V/m, have to be reduced by a factor $1+m$ compared to $E_{CW}=54$ V/m, in function to the available power), when the amplifier input power is higher than the -20 dBm but remains at values limiting the amplifier output at levels lower than the maximum input power of the LPDAs. And, for 20 W maximum power input antennas, field strengths of about 36 V/m with 80 % AM modulation and 65 V/m without modulation could be generated, with maximum available amplifier input power (30 W).

2.3.3 PDF, CDF and KS test for the Electric field components

Although the IEC standard requirements for RC are focused on spatial uniformity and obtainable field strengths, to be in line with the uniformity requirements in SAR. The author's opinion is that the ultimate test for assessing the stochastic environment in a RC consists in verifying that the experimental PDF and CDF obtained in the chamber are, in the statistical sense, in good agreement with the theoretical ones expected in ideal reverberation conditions. To check this we will apply the Kolmogorov-Smirnov hypothesis test on a large set of tuner steps, for each of the three field components and for the total field.

2.3.3.1 For n=150 tuner steps

A lot of measurements have been done. Only a sample is given below. It is corresponding to a frequency of 1546 MHz and at point P3 (see Fig. 2. 1 and Table 2.1). With b, the scale factor, equals to σ of point 1.5.3. It is calculated with formula (1.54).

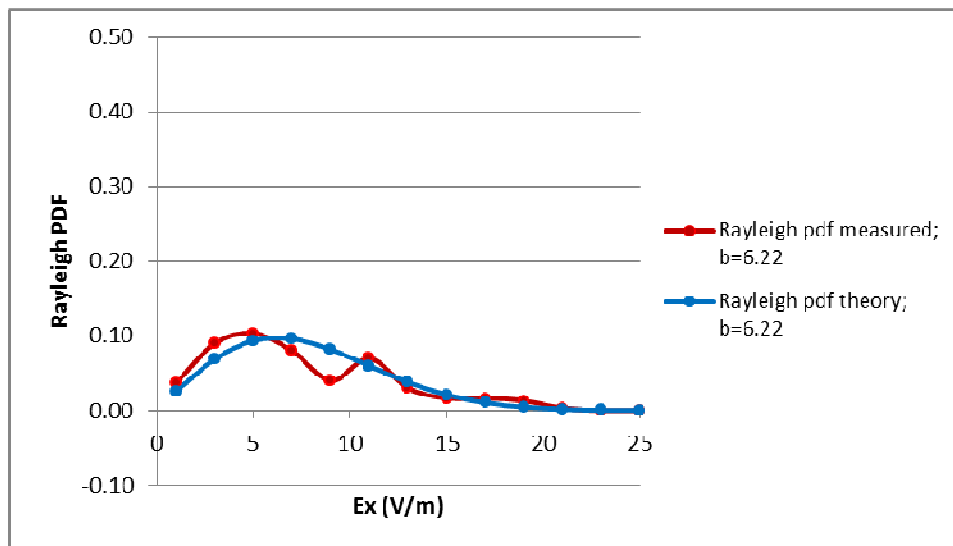


Fig. 2.7: PDF for Ex; RAIL; n=150 tuner steps.

The use of the PDF graph above is as follows: suppose we want to know the probability to have an Ex electric field strength between 5 and 10 V/m, then according to the definition of PDF (see section 1.5.2):

$$\int_5^{10} \frac{E_x}{6,22^2} e^{-\frac{E_x^2}{2 \cdot 6,22^2}} dx = \Pr [5 < E_x \leq 10] = 0,449 \text{ or } 44,9\%.$$

Comparing to Fig. 2.7, it is coherent, as the total surface below the blue curve is equal to 1.

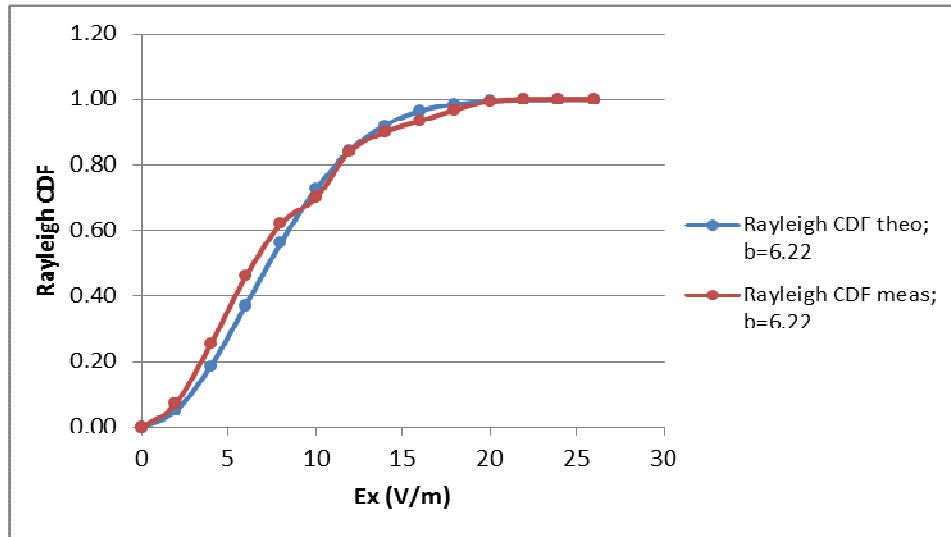


Fig. 2.8: CDF for E_x ; RAIL; $n=150$ tuner steps.

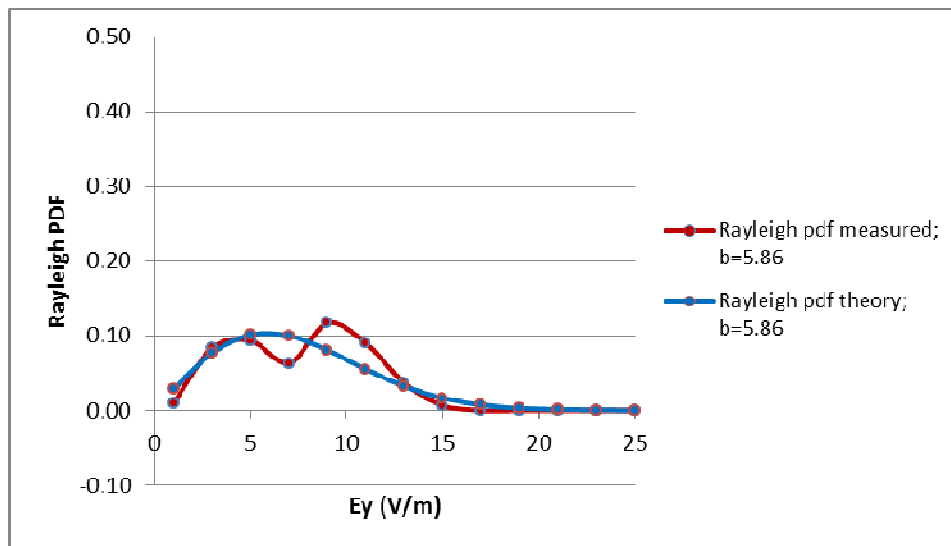


Fig. 2.9: PDF for E_y ; RAIL; $n=150$ tuner steps.

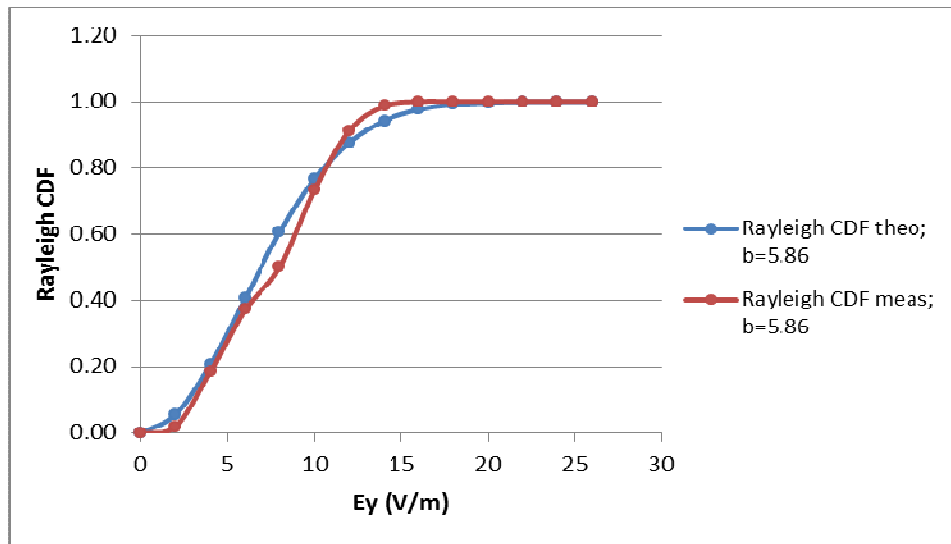


Fig. 2.10: CDF for E_y ; RAIL; $n=150$ tuner steps.

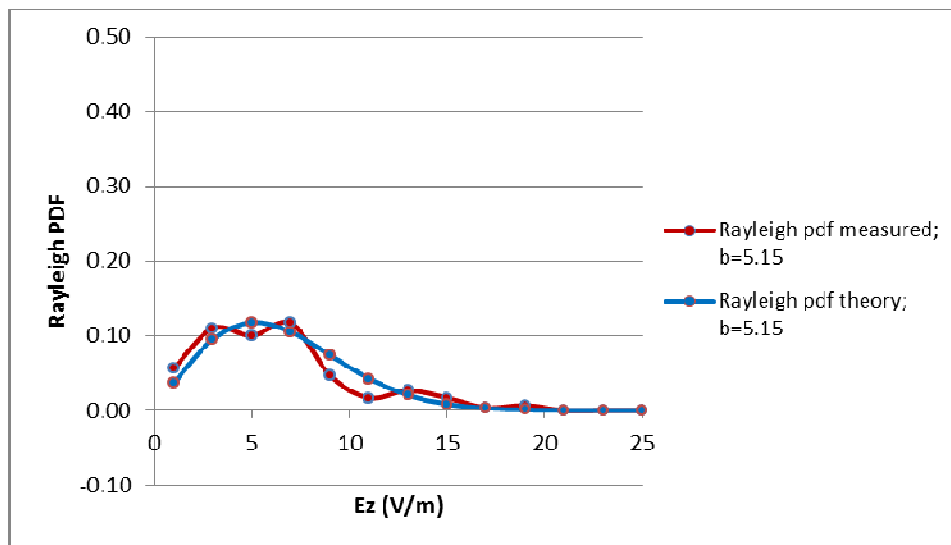


Fig. 2.11: PDF for E_z ; RAIL; $n=150$ tuner steps.

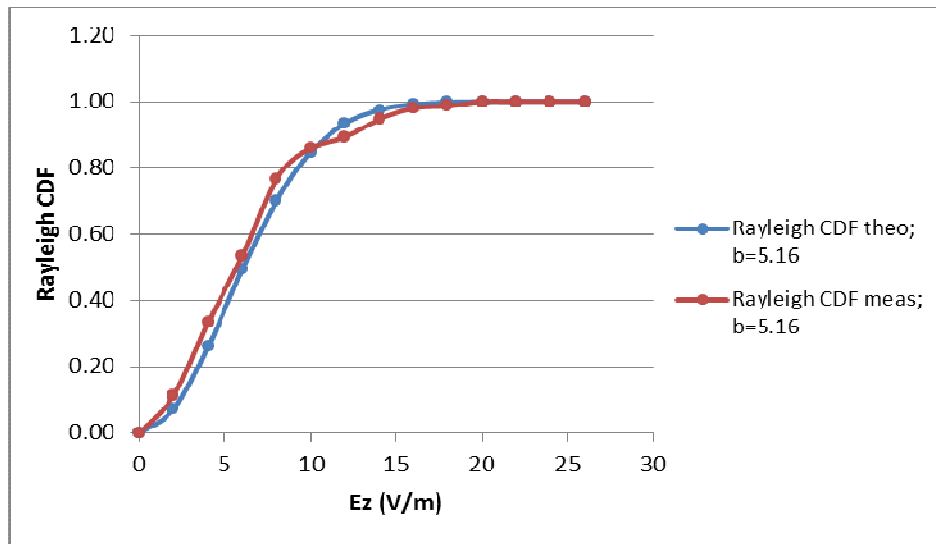


Fig. 2.12: CDF for E_z ; RAIL; $n=150$ tuner steps.

The differences, in the Rayleigh PDF above graphs, between the theoretical curves and the experimental ones can be explained by the imperfection of the tuner and the number of the tuner steps (the higher the tuner steps the lower the difference between the theoretical and measured values). In reality, the magnitude of the field is characterized by a Rice probability density function, which depends, on a tuned part of the field, which is purely random, and, on a residual untuned part corresponding to a deterministic residue of the field. The Rayleigh pdf being a particular case of the Rice pdf when there is no deterministic part.

The table below gives the results of the KS test when comparing the theoretical and experimental CDF's given in Fig. 2.8, Fig. 2.10 and Fig. 2.12. We have added the comparison of the CDF's for the total Electric field given later.

Table 2. 3: KS test summary; E-field; RAIL; n=150 tuner steps; 1546 MHz; P3.

Electric field	KS test result	KS test limit	KS test Conclusion
Ex	0,0880	0,1109	Pass
Ey	0,1062	0,1109	Pass
Ez	0,0729	0,1109	Pass
Etot	0,0404	0,1109	Pass

Note (see also section 1.7):

- KS test result is $\max|F_e(x) - F_t(x)|$.

- KS test limit is $\sqrt{-\frac{1}{2n} \ln \frac{\alpha}{2}}$ (with n=150 and $\alpha=0.05$).

We will accept the hypothesis H_0 (experimental CDF tends to theoretical CDF) in a confidence interval of 95 %, $\alpha = 0.05$ and $n = 150$. The KS test limit is extracted from Table 1.1. (see section 1.7).

The test with 150 tuner steps takes a long time, using 24 tuner steps allows for a substantial gain of time, but is H_0 still verified?

2.3.3.2 For n=24 tuner steps

Here too, a lot of measurements have been done, but only a sample is given below. For comparing the results we will obtain with those discussed in the preceding section (n=150), we present

here also the results obtained at the same location and frequency, i.e. 1546 MHz and point P3 (see Fig. 2. 1 and Table 2.1).

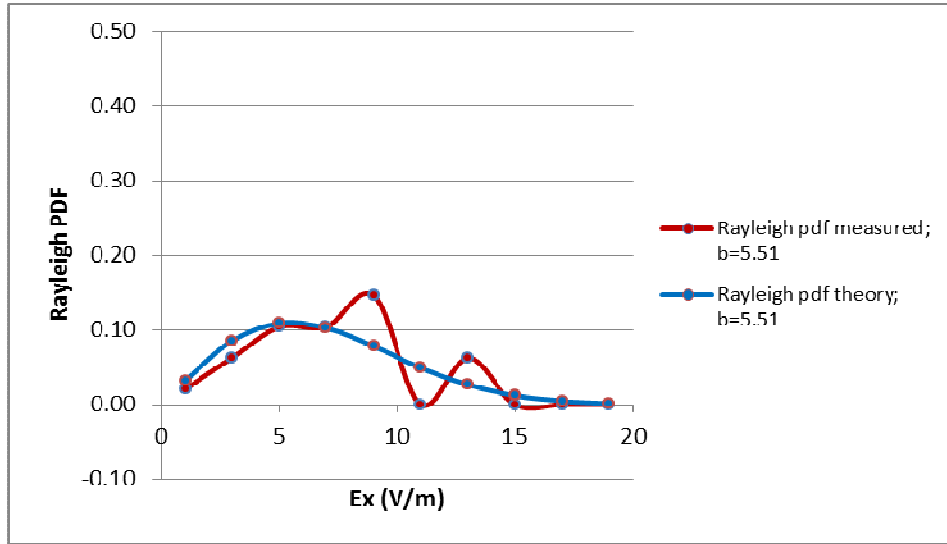


Fig. 2.13: PDF for E_x ; RAIL; $n=24$ tuner steps.

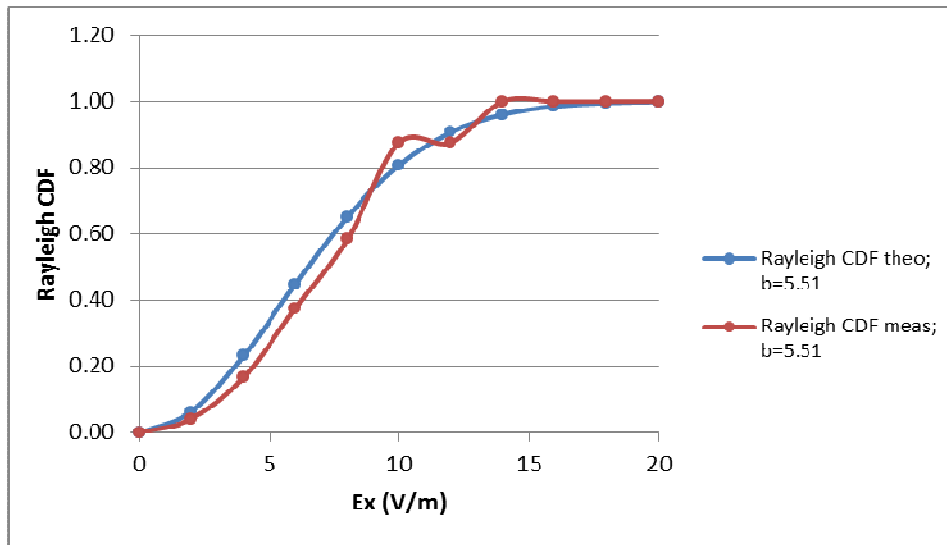


Fig. 2.14: CDF for E_x ; RAIL; $n=24$ tuner steps.

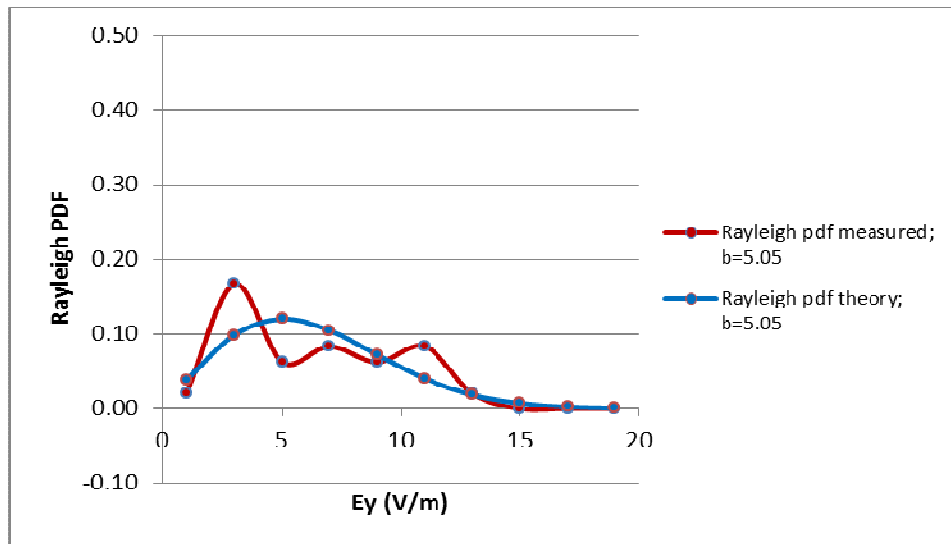


Fig. 2.15: PDF for Ey; RAIL; n=24 tuner steps.

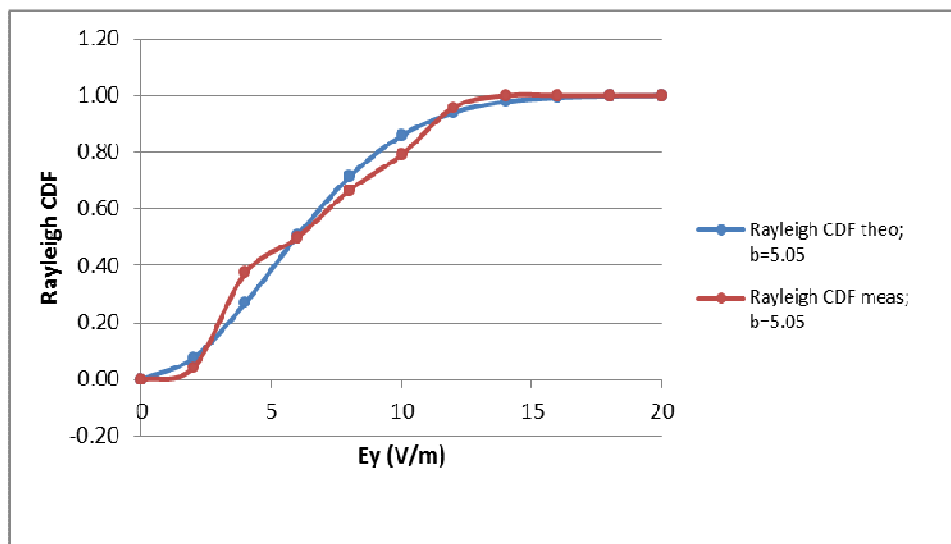


Fig. 2.16: CDF for Ey; RAIL; n=24 tuners steps.

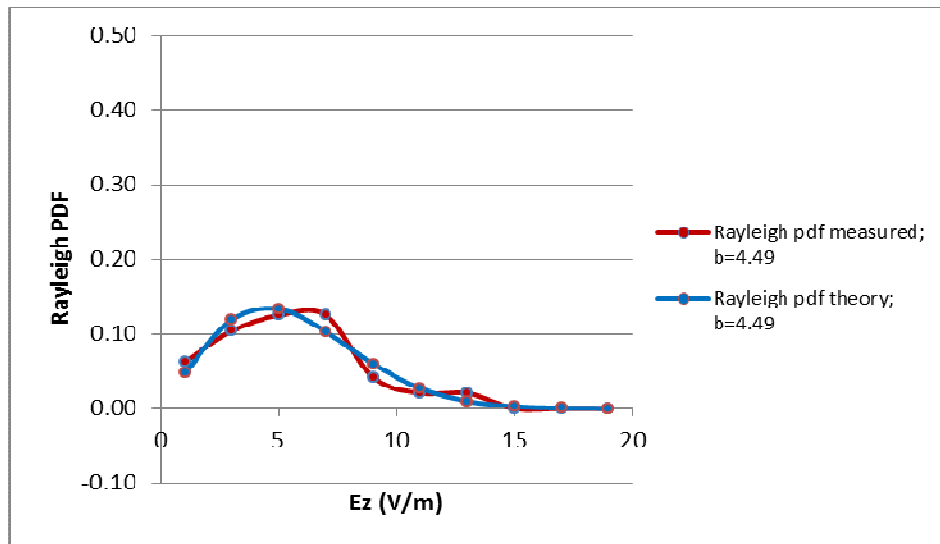


Fig. 2.17: PDF for E_z ; RAIL; $n=24$ tuners steps.

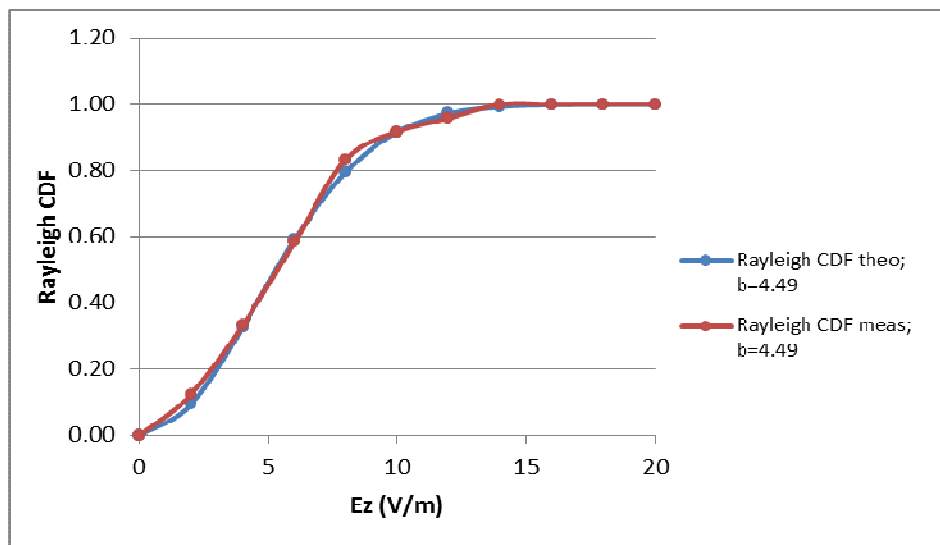


Fig. 2. 18: CDF for E_z ; RAIL; $n=24$ tuners steps.

The table below gives the results of the KS test when comparing the theoretical and experimental CDF's given in Fig. 2.14, Fig. 2.16 and Fig. 2. 18. We have added the comparison of the CDF's for the total Electric field given later.

Table 2.4: KS test summary; E-field; RAIL; n=24tuner steps; 1546 MHz; P3.

Electric field	KS test result	KS test Limit	KS test Conclusion
Ex	0,0723	0,2772	Pass
Ey	0,1060	0,2772	Pass
Ez	0,0377	0,2772	Pass
Etot	0,0479	0,2772	Pass

We accept the hypothesis H_0 (experimental CDF tends to theoretical CDF) in a confidence interval of 95 %, $\alpha = 0.05$ and $n = 24$. The KS test limit is extracted from Table 1.1. (see section 1.7).

2.3.4 PDF, CDF and KS test for the total Electric field

2.3.4.1 For n= 150 tuner steps

We recall that:
$$E_{tot} = \sqrt{E_x^2 + E_y^2 + E_z^2} .$$

Its PDF and CDF are given below:

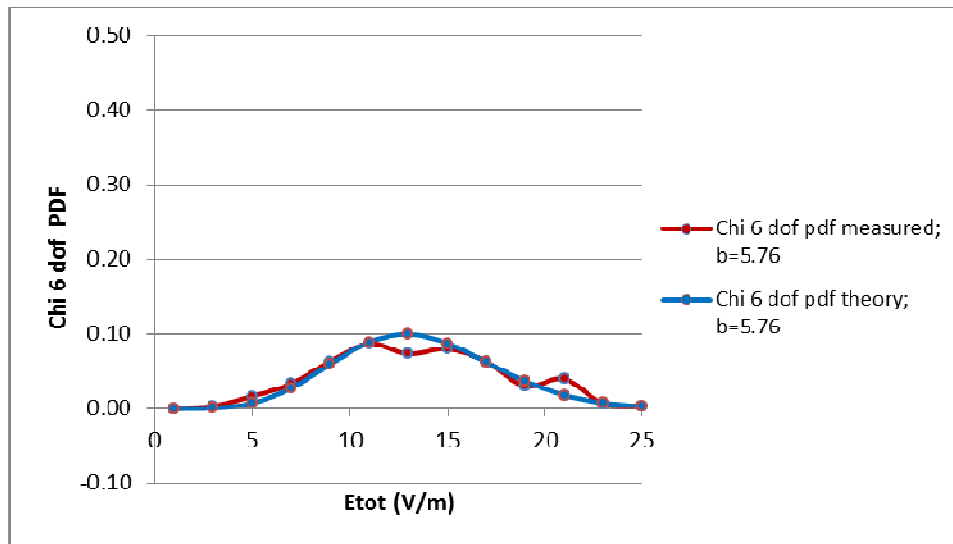


Fig. 2.19: PDF for Etot; RAIL; n=150 tuners steps.

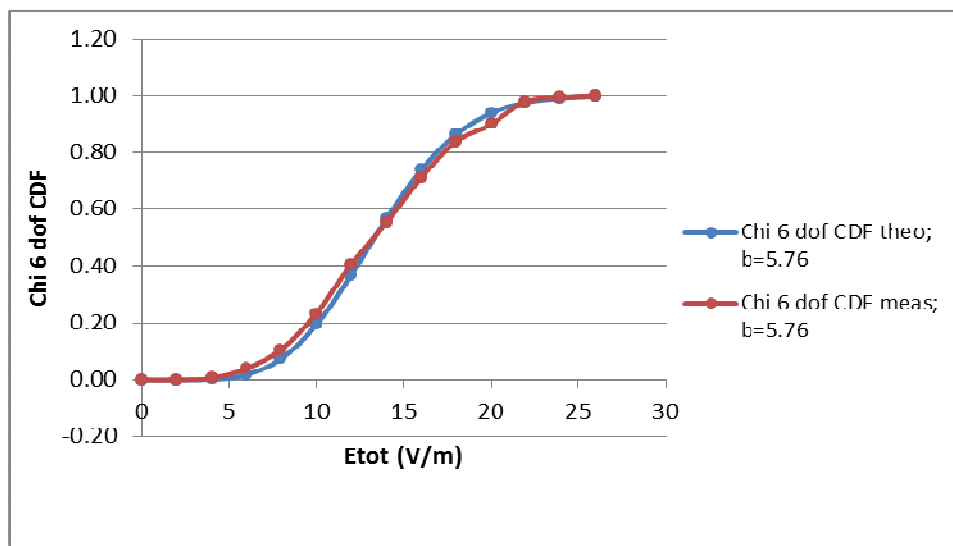


Fig. 2.20: CDF for Etot; RAIL; n=150 tuners steps.

It turns out that the experimental and theoretical CDF's passes the KS test (see Table 2.3)

In the table below, it is shown that the scale factor b of the total Electric field is very close to the arithmetic mean of the scale factors of the components of the Electric field. We recall that the scale factor is the standard deviation of the underlying Gauss pdf.

Table 2.5: Scale factors relationship; RAIL; n=150 tuner steps.

Scale Factors				
b_{Ex}	b_{Ey}	b_{Ez}	b_{Etot}	b_{Etot}
Measured	Measured	Measured	Measured	Arithmetic mean
6,22	5,86	5,15	5,76	5,74

The scale factor measured values are calculated from formula (1.54) of section 1.5.3.

2.3.4.2 For n=24 tuner steps

The PDF and CDF of the total Electric field are given below:

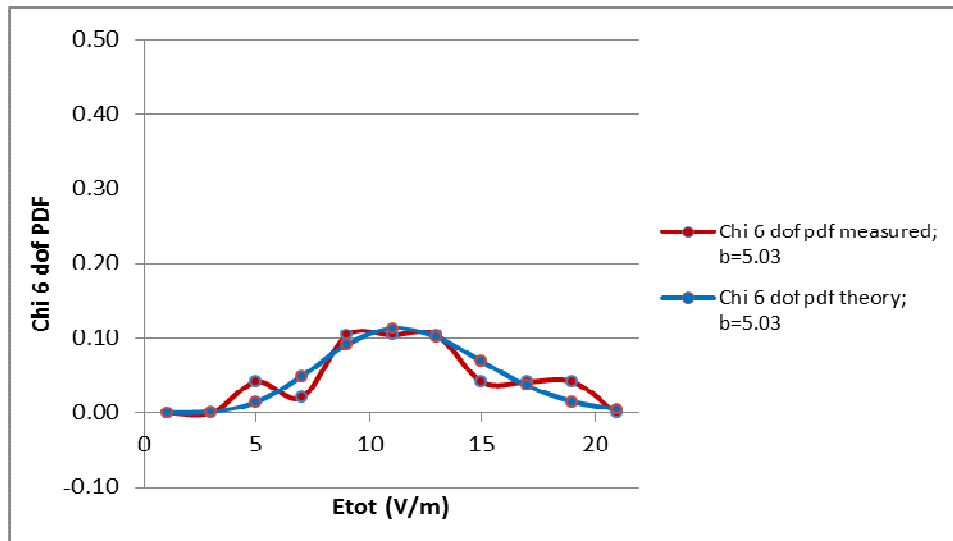


Fig. 2.21: PDF for Etot; RAIL; n=24 tuners steps.

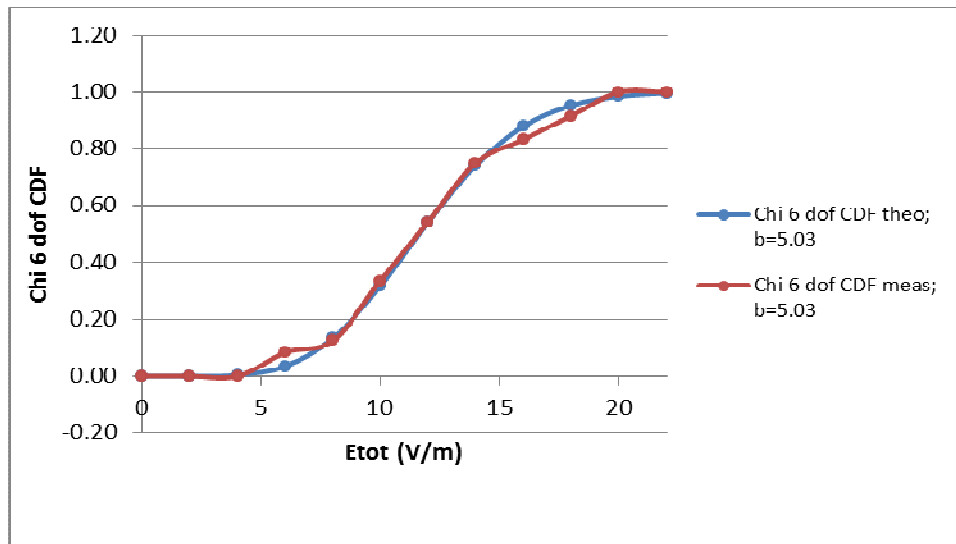


Fig. 2. 22: CDF for Etot; RAIL; n=24 tuners steps.

It turns out that the experimental and theoretical CDF's passes the KS test (see Table 2.4.)

The scale factors relationship is still valid for n=24 tuner steps as indicated in the table below:

Table 2. 6: Scale factors relationship; RAIL; n=24 tuner steps.

Scale Factors				
b_{Ex}	b_{Ey}	b_{Ez}	b_{Etot}	b_{Etot}
Measured	Measured	measured	Measured	Arithmetic mean
5,51	5,05	4,49	5,03	5,02

Before concluding this validation of the field statistics obtained with the LPDA scanning system, let us consider the experimental PDF and CDF for the power received at the termination of an antenna placed into the RC. This power shall indeed be essential when the RC will be used for determining experimentally the radiation efficiency of some antenna.

2.3.5 PDF, CDF and KS test for the Power received on an antenna

When assessing antenna efficiency (see chapter 4), the power received on each of the two antennas was measured, with the RAIL method, using n=51 tuner steps at 2400 MHz (the measurements are described in section 4.3.). Below is their treatment.

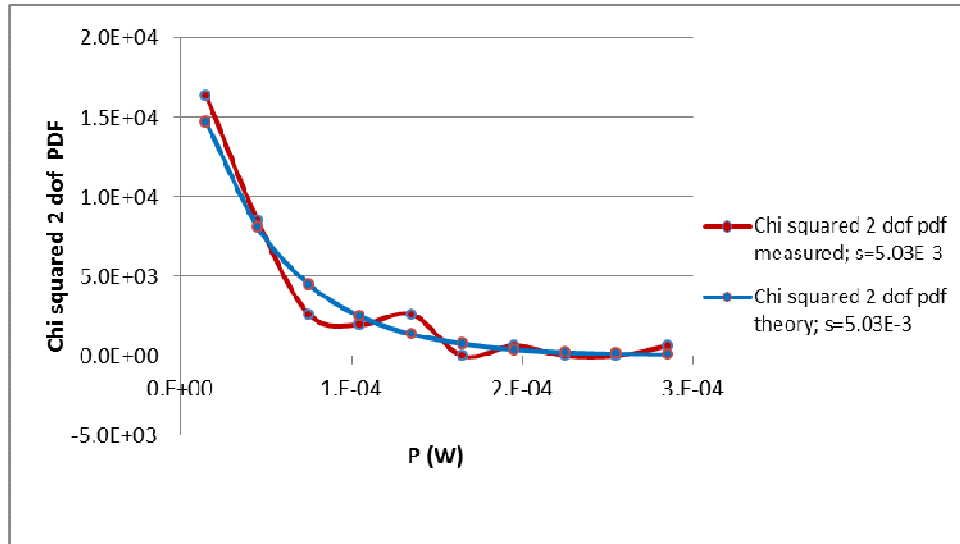


Fig. 2. 23: PDF for Power on antenna 1; RAIL; n=51 tuner steps.

At the first glance, it could be surprising to note values of PDF above 1 on the ordinate axis (see Fig. 2. 23), but it is not abnormal because the probability is the surface below the curves. For example, if we want to know the probability to have a power between 0,1 mW and 0,2 mW, then according to the definition of PDF (see point 1.5.2):

$$\int_{0,1mW}^{0,2mW} \frac{1}{2.(5,03)^2} e^{-\frac{P}{2.5,03^2}} dx = \Pr [0,1mW < P \leq 0,2mW] = 0,12 \text{ or } 12\%.$$

Fig. 2. 23 is coherent, as the total surface below the blue curve is equal to 1, as shown in Fig. 2.24 and Fig. 2.26 for antenna 1 and 2 respectively.

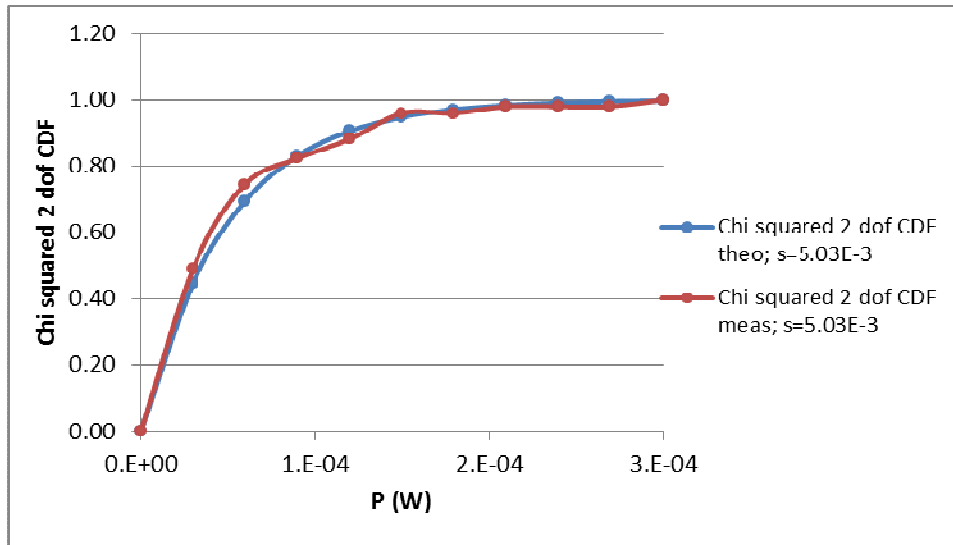


Fig. 2.24: CDF for Power on antenna 1; RAIL; n=51 tuner steps.

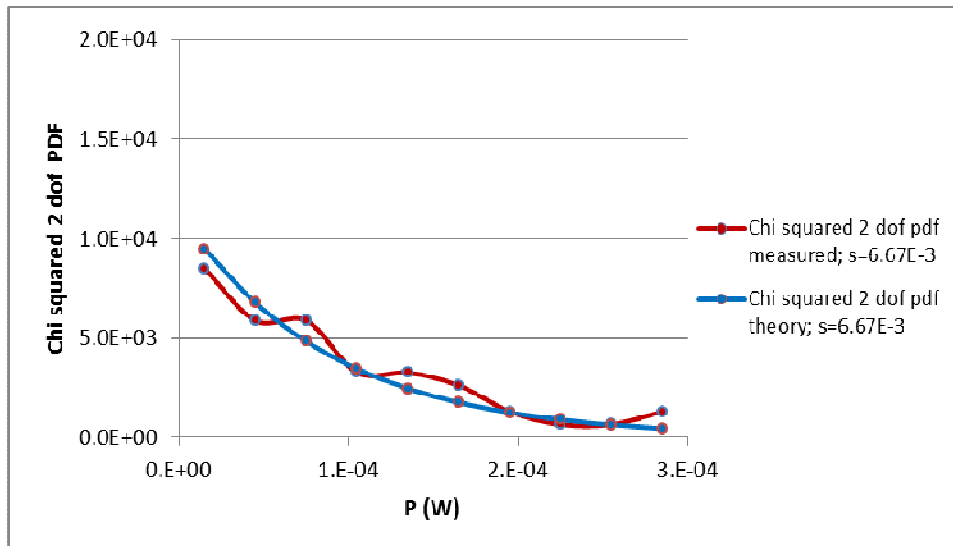


Fig. 2.25: PDF for Power on antenna 2; RAIL; n=51 tuner steps.

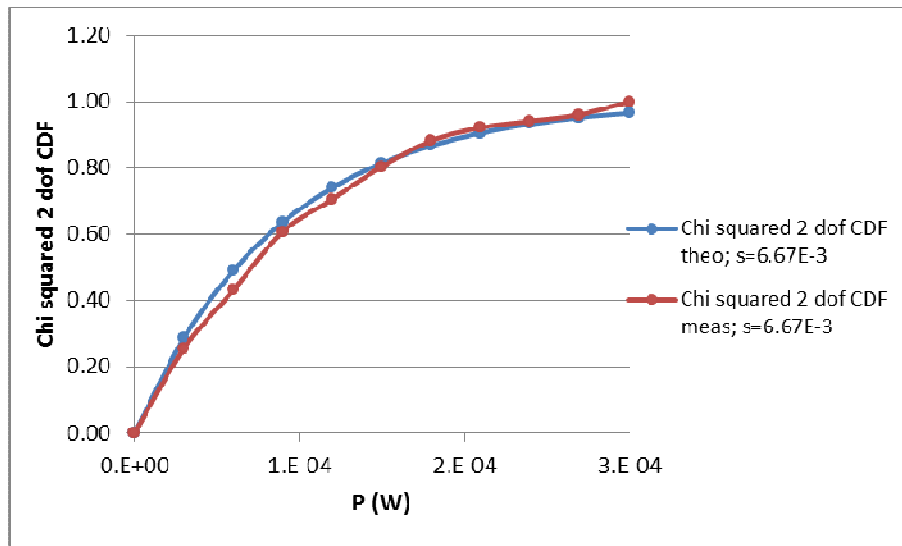


Fig. 2.26: CDF for Power on antenna 2; RAIL; n=51 tuner steps.

The table below gives the results of the KS test when comparing the theoretical and experimental CDF's given in Fig. 2.24 and Fig. 2.26.

Table 2.7: KS test summary; Power; RAIL; n=51tuner steps; 2400MHz.

Power	KS test result	KS test Limit	KS test Conclusion
Antenna 1	0,0509	0,1902	Pass
Antenna 2	0,0588	0,1902	Pass

2.4 Conclusion

A new method for source-tuning the modes in a reverberation chamber has been proposed and investigated. The method is based on the dynamic use of two orthogonal rails supporting moving LPDA transmitting antennas. From the efficiency analysis carried out in the frame of the IEC 61000-4-21 standard, it turns out that the 3 dB field uniformity requirement is met, in the working volume, in the 800 to 2500 MHz frequency range, where

the upper frequency limit is set by the maximum frequency of the presently used amplifier. Depending on the frequency, maximum field strengths achieved over 150 tuner steps and averaged over the working volume of the LEMA chamber are of the order of 11 to 22 V/m, and this for a forward power injected in the RC of only 1.5 W. Hence, this method could be a good alternative to the cumbersome mechanical stirrer, especially in small chambers where the working volume has to be optimized, but also in large chambers aiming at low LUF (<500 MHz) where one could get rid of the stability and vibration problems inherent to large stirrers. Moreover, the statistical treatment of the random Electric fields and power show that their experimental PDF and CDF are close to the theory. This is confirmed by the KS hypothesis test, even for a very limited number of tuner steps (n=24).

3. Static source-mode tuning with an electronically switched antenna network

3.1 Introduction

The second innovative source-mode tuning of electromagnetic fields we have conceived and experienced in the LEMA reverberation chamber is presented. The STATIC tuner is based on a LPDA antenna network placed in the RC. The fixed antennas are commuted sequentially in order to change with time the position of the point which the electromagnetic waves are emitted from, rather than using a moving mechanical stirrer like a rotary paddle wheel. The objective is to get rid of any moving part and to decrease the testing time, thanks to the short response time of electronic switching. The efficiency of this new tuner is assessed as a function of the field uniformity requirements of the IEC 61000-4-21 [2] which states the 3 dB limit above 400 MHz. As already mentioned, in our case we will work within the frequency band of mobile phone and GPS systems (800-2500 MHz). The three components of the E-field, the forward and reverse output powers and the binary code associated with the emitting antennas have been acquired for each of the tuner positions, at the same eight locations delimiting the testing volume, and at the number of frequencies as required in the standard. The first results show a promising method for tuning in an RC as the field uniformity complies with the standard deviation requirement of the IEC 61000-4-21.

3.2 Set-up and measurement method

The LEMA reverberation chamber is of a cubic shape (2.48 m side). It has its fundamental resonance at 85.15 MHz. According to MIL-STD-461F, test RS103 (susceptibility to electric field, 2 MHz to 40 GHz) the LUF (Lowest Usable Frequency) is given by:

$$f = c_0 \sqrt[3]{\frac{N.3}{8.\pi.a.b.c}} \quad (3.1)$$

where N is the number of modes ($= 100$ for the LUF), c_0 is the speed of light, while a , b and c are the dimensions of the RC. We obtain a rounded LUF of 280 MHz. We work from 800 MHz on because our testing amplifier operated in the 800 to 2500 MHz range. So, in practice, the lower operating frequency is about 10 times larger than the cavity fundamental resonance frequency and about 3 times the LUF recommended by the MIL-STD-461F.

In the chamber we have placed a network consisting of 2 sets of eight antennas (see Fig. 3.1 and Fig. 3.2).

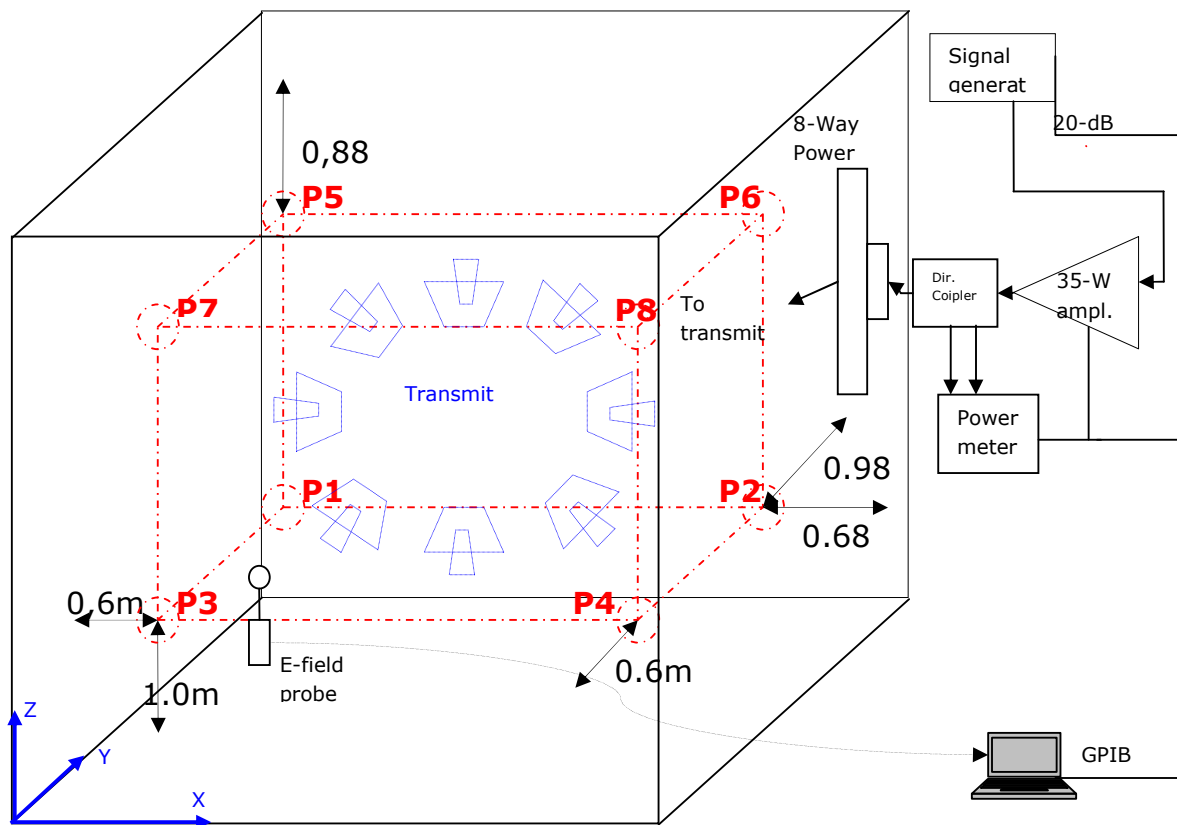


Fig. 3.1: Set-up in the reverberation chamber with the static network of 2x8 transmitting antennas.

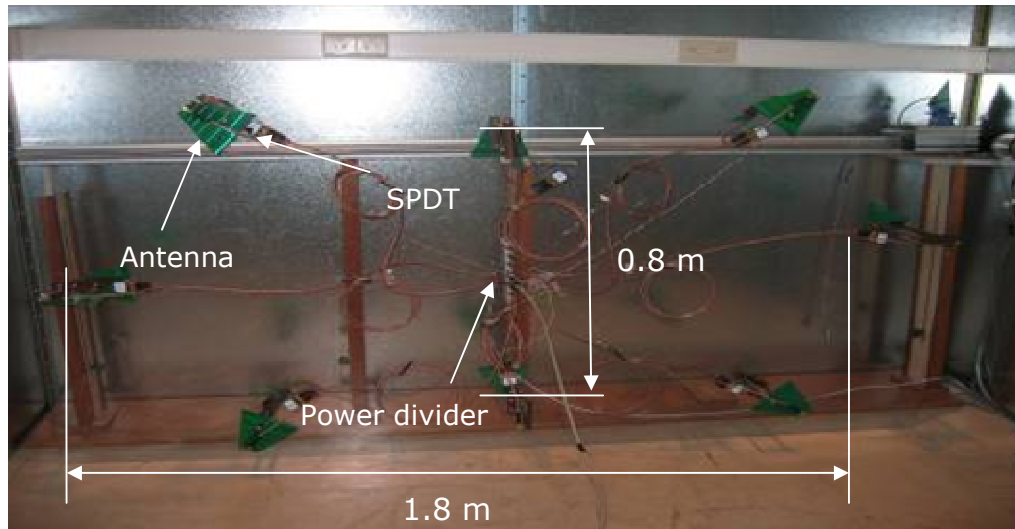


Fig. 3.2: Positioning of the antenna network in the reverberation chamber.

The antennas are fixed on a rectangular plexiglas plate of 2.5 m long, 1.25 m wide, and 6 mm thick. It is placed at 46 cm in front of one of the walls of the chamber. The largest distance between any two antennas is 1.8 m and the smallest is 0.8 m, so the total surface covered is about 1.44 m^2 . Each of the 8 pairs of antennas (see Fig. 3.3) is connected to an SPDT (Single Pole Double Throw) RF switch that has a bandwidth from DC to 6 GHz and an RF power handling of 100 W @ 2.5 GHz.

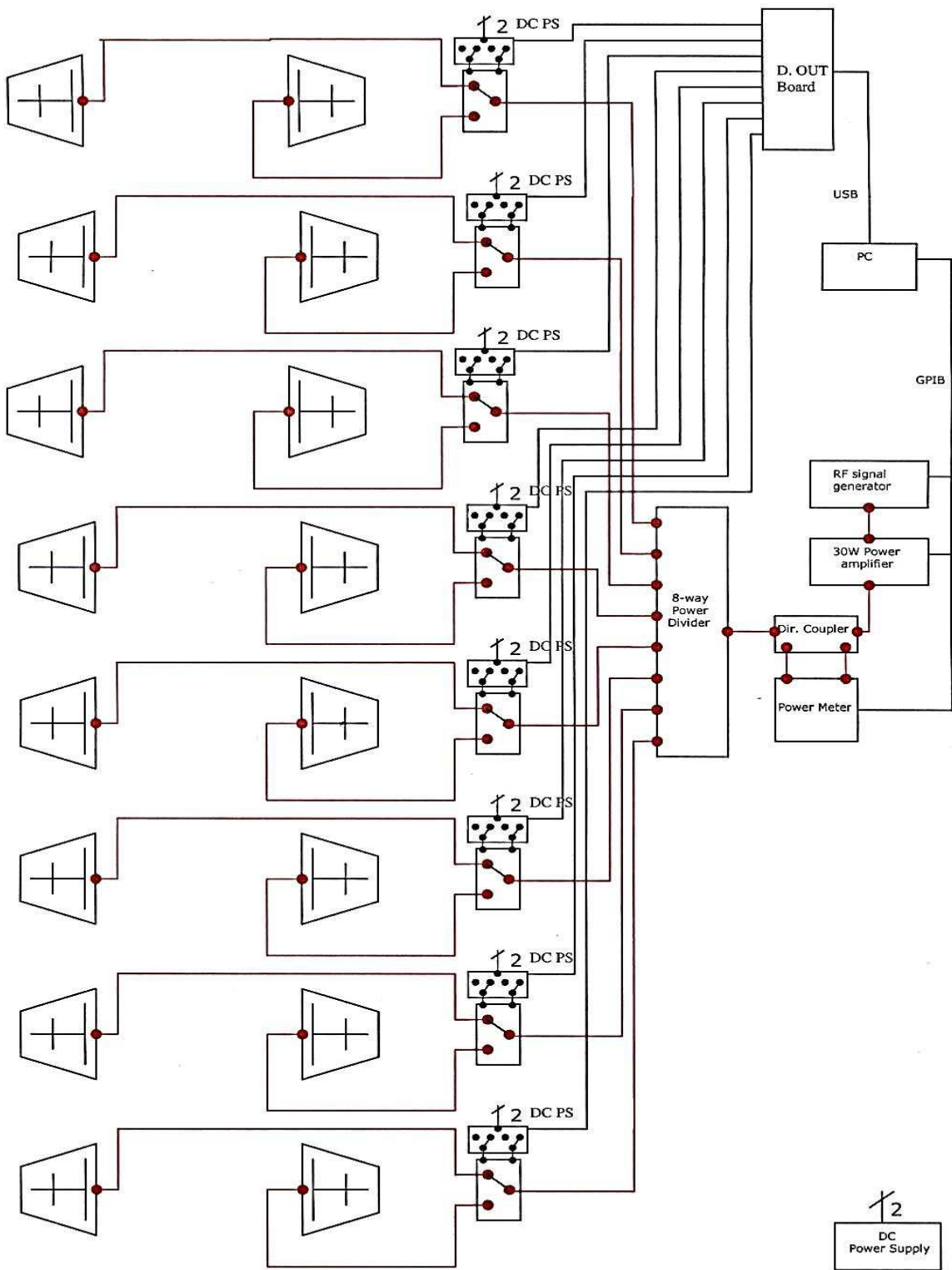


Fig. 3.3: General cabling of the static source-mode tuning system.

The input of the RF switch is connected to the 8-way power divider and the two complementary outputs are connected to the pair of antennas, via RF cables (0.3 dB@2.5GHz attenuation). The switch is controlled in such a way that at any time the RF power is radiated into the RC by 8 antennas. Each SPDT switch is used in conjunction with a pair of antennas and is connected to one of the output ports of the 8-way of the power divider. So, the power applied to the input of this last one is divided in 8 equal parts and transmitted through the SPDT switches to 8 antennas, the position of each switch determining which one of the antennas making a pair will radiate. The input of the power divider is connected to the 35 W power amplifier. This receives on its input a -20 dBm power level from the signal generator. Each of the eight RF switches is powered by a DC switch that gives +12 V DC or -12 V DC. As a function of the polarity, they switch to the first or the second state. The control is given by an 8-digital output board placed outside the chamber. This board is connected to a PC via a USB bus and allows for the sequencing. The signal generator, the power amplifier and the power meter are connected to the PC via a GPIB bus. Software has been self-developed with LabVIEW for the instruments controlling data acquisition and analysis. This allows complete automatic sequences of testing, i.e. put RF power into the chamber, wait for the dwell time, acquire the test metrics, and sweep to another frequency automatically.

Let us consider now the total path attenuation of the RF power. Starting from the amplifier we have the cable to the power divider with an attenuation of 3.6 dB @ 2.5GHz. The insertion loss (IL) of the power divider is $10.5 \text{ dB} \pm 0.2 \text{ dB}$, which is 1.5 dB higher than the theoretical IL of an 8-way power divider (we recall that the theoretical insertion loss of a power divider/combiner is $IL = 10 \cdot \log N$, with N is the number of inputs or outputs, for $N=8$, we find $IL=9 \text{ dB}$), the real loss at the output is 1.5 dB, as adding the power of each 8 outputs we come back to the input power. Each of the eight

cables from the output of the power divider to the RF switch has an attenuation of 1.6 dB that give a total of 12.8 dB (1.6x8). The IL of the RF switch is 0.2 dB and the cable from the RF output to the antenna has 0.26 dB attenuation. As we have eight RF switches and cables, this gives a total of 3.68 dB. So, the total attenuation is $3.6+1.5+12.8+3.68=21.58$ dB and this is high compared to the RAIL method. That is also the reason why the electric field is lower. Clearly it appears that the eight cables from the power divider to the RF switches should be of very low attenuation in order to have the best attenuation budget. If these cables have 0.3 dB instead of 1.6 dB, then the total attenuation will be 11.18 dB.

The working volume (dotted in red) is delimited by the spatial points P1, P2,..., to P8. It is 1.20 m long, 0.90 m wide and 0.60 m high (see Fig. 3.1).

Each transmitting LPDA antenna has a 900-2500 MHz bandwidth and a 10 W maximum input power. The antennas are directed towards the walls of the chamber and do not directly illuminate neither the working volume nor the E-field meter in order to prevent direct coupling. In practice, some degree of direct coupling to the EUT can be expected and that would alter the Rayleigh probability density function of the field, yielding a Rice-Nakagami distribution due to the presence of some deterministic part in the stochastic field [25].

The Narda EMR-300 meter with a 3 MHz-18 GHz E-field probe has been used. It gives the three components of the E-field in a single read operation. The E-Field probe is placed at eight spatial points (P1 to P8), delimiting the working volume. The separation distances between the surfaces bounding the working volume and any chamber surface are kept higher than $\lambda/4$, i.e. 9 cm at 800 MHz.

During all the measurements, the output of the signal generator is set to -20 dBm. The amplifier needs -5 dBm to give full power, so the set-up is free of any harmonics. The output forward and reverse

powers of the amplifier are measured by means of a directional coupler AR DC7420 that has a 20 dB coupling ratio, connected to a R&S NRP power meter connected via GPIB to a PC. The output forward power is about 1.5 W. The input power has been measured at the termination of a Horn antenna.

The sequencing of the RF switch control has been chosen in such a way to minimize the amount of switching over a whole tuning cycle. Three sequencing schemes are considered: Natural binary, Binary reflected Gray, Binary Balanced Gray. We chose to work with a 6-bit code. The type of code has been selected in order to obtain a minimum number of transitions (Hamming distance of 1). This contributes to reduce the Mean Time Between Failure of the RF and DC switches. Moreover, the transitions should be spread over all the RF and DC switches to avoid any accelerated wear of more often used switches. The transitions for the three types of sequencing are the following: 63, 31, 15, 7, 3, 1 (total: 120); 32, 16, 8, 4, 2, 1 (total: 63); 10, 11, 11, 10, 10, 11 (total 63), respectively. The first number of the series corresponds to the number of transitions of the first bit or switch, the second number corresponds to the second bit or switch, etc... The Binary Balanced Gray strategy is used for generating the codes we used [26]. The coordinate sequence forms our input data and we have written a code to generate the 64 binary words of 6 bits.

As for the RAIL tuner, the efficiency of the STATIC tuner has been assessed at a total of twenty two frequencies logarithmically spaced (in accordance with the IEC 61000-4-21), (Table 3. 1), at each of the eight spatial points):

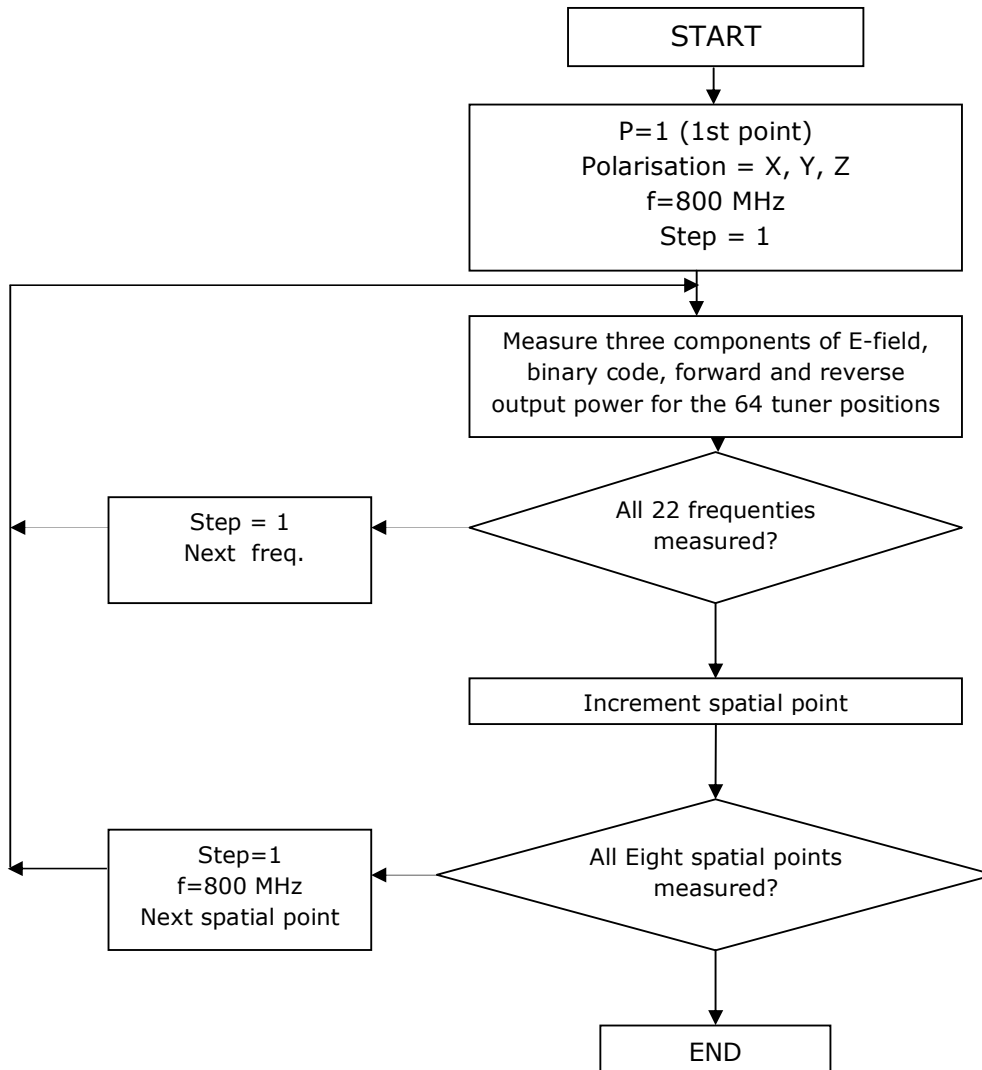
Table 3.1: List of frequencies for STATIC tuning (MHz)

800.00	1463.88
845.17	1546.54
892.90	1633.87
943.32	1726.13
996.58	1823.60
1052.86	1926.58
1112.31	2035.37
1175.12	2150.30
1241.48	2271.72
1311.58	2400.00
1385.64	2513.50

3.3 Tests Results

3.3.1 Field Uniformity

For each spatial point delimiting the working volume and at each frequency, we measured the three polarizations of the electric field (E_x , E_y , and E_z).



The 64 binary codes (representing the samples) were also saved, together with the forward and reverse power at the output of the power amplifier. These results are saved in a single file and the consecutive frequency is applied. When all the frequencies are done, the next spatial point is set. The total number of data collected in this way was 67584 (8 spatial points x 22 frequencies x 64 binary codes x 6 chamber measured data).

From these data the field uniformity is calculated based on the formula given in the IEC standard:

$$\sigma_{ij} (dB) = 20 \text{Log}_{10} \left(\frac{\sigma_{ij} + \langle \overleftrightarrow{E}_{ij} \rangle_8}{\langle \overleftrightarrow{E}_{ij} \rangle_8} \right) \quad (3.2)$$

where i indicates the field component of interest (X, Y, Z), j indicating the test frequency.

$$\sigma_{ij} = \sqrt{\frac{\sum_{k=P1}^{P8} (\overleftrightarrow{E}_{kij} - \langle \overleftrightarrow{E}_{ij} \rangle_8)^2}{7}} \quad (3.3)$$

$$\langle \overleftrightarrow{E}_{ij} \rangle_8 = \frac{\sum_{k=P1}^{P8} \overleftrightarrow{E}_{kij}}{8} \quad (3.4)$$

$$\overleftrightarrow{E}_{kij} = \frac{E_{\max \text{ } kij}}{\sqrt{P_{\text{aveinput } kij}}} \quad (3.5)$$

$E_{\max \text{ } kij}$ is the maximum value over the 64 steps of the tuner, in a given point k , for a given component i and at a given frequency j . $P_{\text{aveinput } kij}$ is the average output forward power of the amplifier. The graphical results, for 64 tuner steps and 6 antenna pairs used, are given in Fig. 3.4. and Fig. 3.5. In this case we use 64 tuner steps as it is a power of 2 and because it is a binary system.

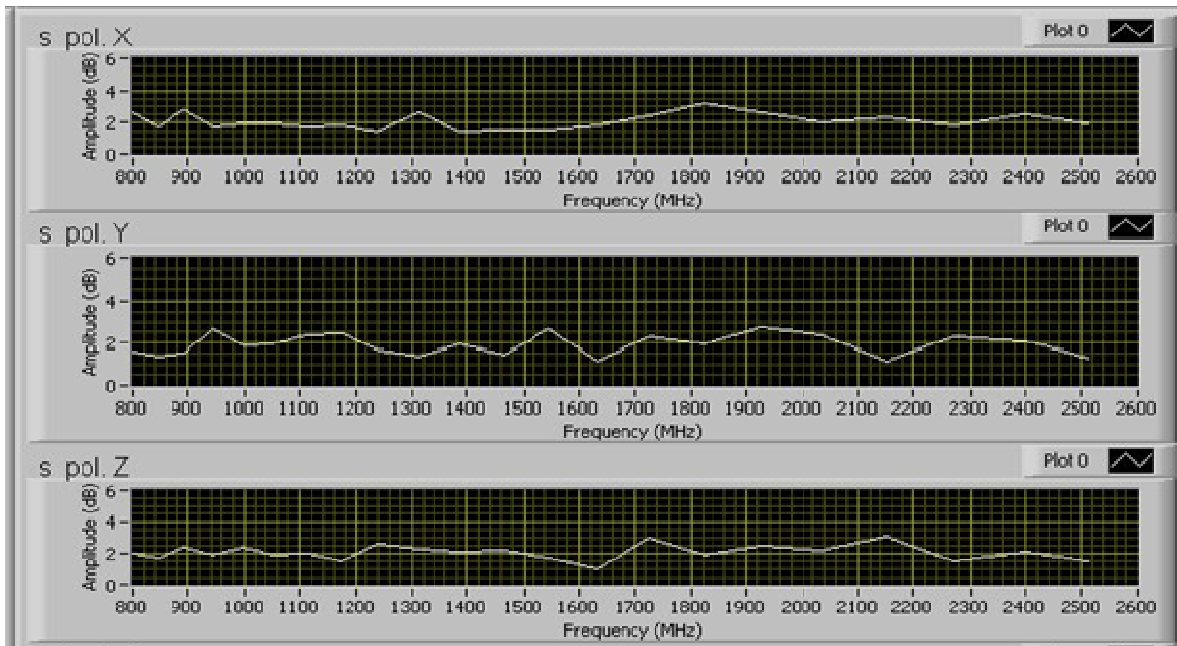


Fig. 3.4: Standard deviation of the E-field (pol. X, Y and Z), 64 tuner steps (6 antennas pairs used).

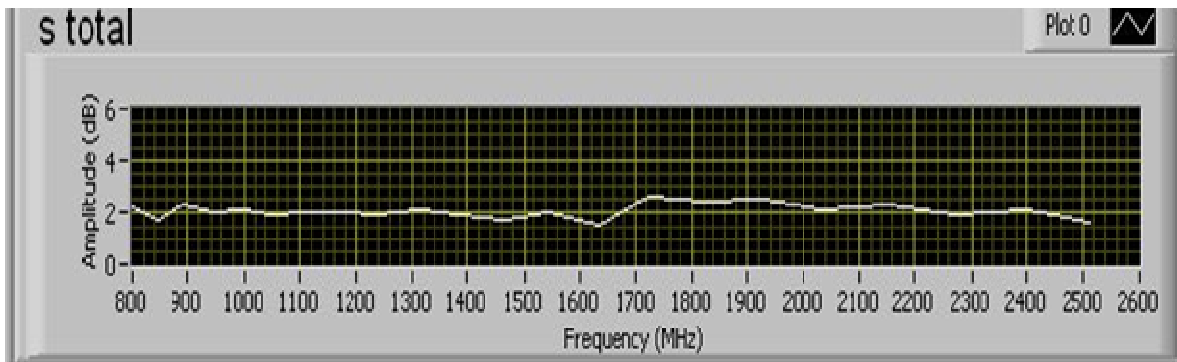


Fig. 3.5: Total standard deviation of the E-field, 64 tuner steps (6 antenna-pairs used).

As one can see, the standard deviation for the components are less than or equal to (for the X polarization at one frequency) the 3 dB limit over the whole frequency range of interest; so, it complies but there is no margin.

Before realizing the described spatial configuration, we had decided to start with another configuration with antennas closer to each other, with a maximum distance between two antennas of 0.8 m

and a minimum distance of 0.6 m (Instead of 1.8 m and 0.8 m, respectively as described in Fig. 3.2. a 5-bit sequencing code (32 samples) was used. In this case, the standard deviation exceeded the requirement of 3 dB. We obtained about 3.7 dB for a given polarization and frequency. That is why we moved to the described configuration. However, as can be seen it is not completely satisfactory because we do not have any margin (standard deviation is 3 dB for X polarization at 1823 MHz and Z polarization at 2150 MHz). In fact, we can easily improve the results by selecting a sequencing binary code that involves all eight antennas. In the discussed case, six pairs of antennas were switching, two pairs were not.

Finally, in order to gain some margin to deal with the drift of the characteristics of the tuner components over time (indeed, the gain of the antenna can become lower or the path loss of the cables and switches can increase, in this case the field uniformity will become higher than 3 dB and does not comply any more), the same work has been done but with all 8 antenna pairs and 37 tuner steps.

We face a dilemma, the higher the tuner steps the better the field uniformity, but the longer the testing time. Previously we worked with 64 tuner steps, now we choose a lower value i.e. 37 steps, and in order to compensate for a loss of field uniformity, the vertical and horizontal distances of the antennas, see Fig. 3.2 (in other words the surface covered by the tuner) is increased. With these changes, we obtain a better field uniformity with lower testing time. The results are given in Fig. 3.6. It can be seen that a margin of 0.3 dB or greater has been obtained. That is to say that the maximum measured standard deviation "s" or σ is 2.7 dB and the maximum normalized standard deviation value is 3 dB.

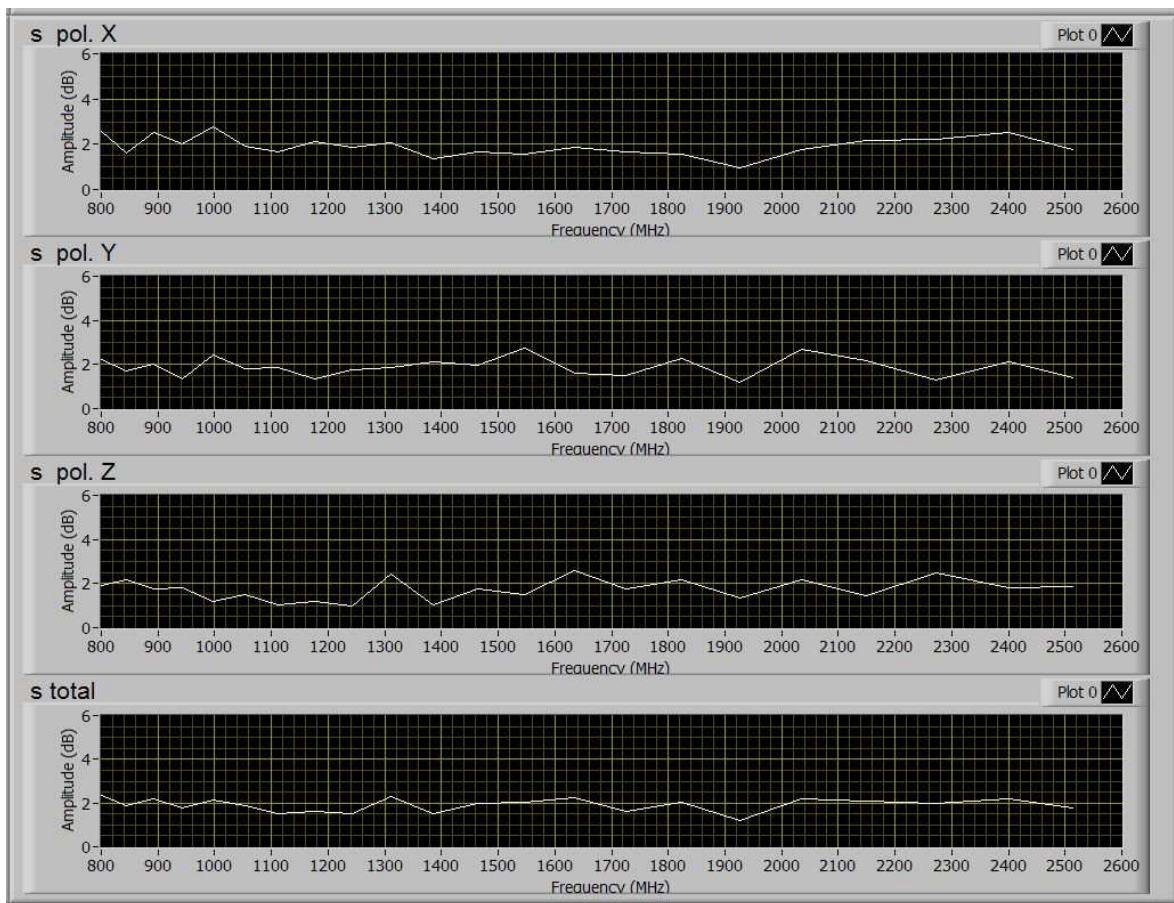


Fig. 3.6: Standard deviation of the E-field (pol. X, Y, Z and total), 37 tuner steps (8 antenna-pairs used).

3.3.2 Field strength obtained

For the 6 antenna-pairs used, the measured E-field has a mean value of 9.95 V/m (over the whole frequency range, and the 8 spatial points, of E_{max} , the electric field expressed in equation (2.7)), with a standard deviation of 1.65 V/m (see Fig. 3.7).

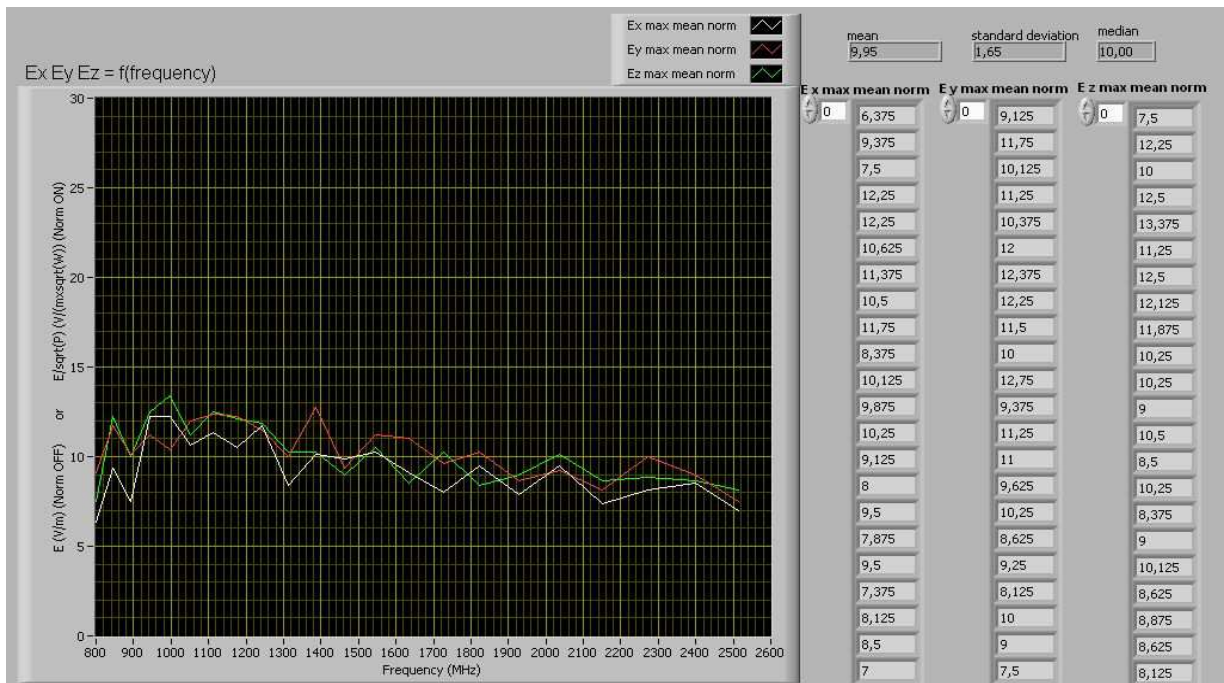


Fig. 3.7: Spatial average of the E-field, 64 tuner steps (6 antenna-pairs used)

This value is obtained for a forward power of 1.5 W. This value is lower than the one measured with the orthogonal rails dynamic tuner [12]. In this case the E-field was about 15 V/m. This is due to the loss in the eight cables connecting the power divider to the RF switches. Hence, by selecting low loss cables we could achieve higher values of the electric field, close to 15 V/m.

With 8 antenna-pairs used, the measured E-field has a mean value of 9.69 V/m with a standard deviation of 1.51 V/m (see Fig. 3.8).

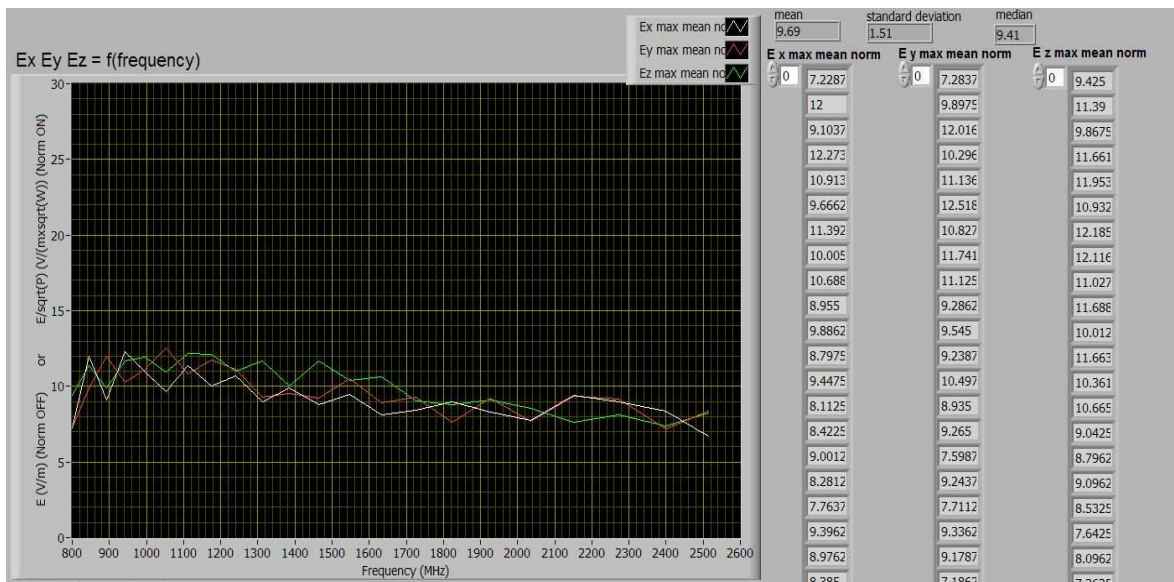


Fig. 3.8: Spatial average of the E-field, 37 tuner steps (8 antenna-pairs used).

So, we conclude that using 8 antenna-pairs is the best choice.

3.3.3 PDF, CDF and KS test for the Electric field components

As for the dynamic tuning method, a lot of measurements have been done for the static one. Only a sample is given below. It is corresponding to a frequency of 1546 MHz and at point P3 (see Fig. 3.1 and Table 3.1), the same starting parameters as for the RAIL tuning method.

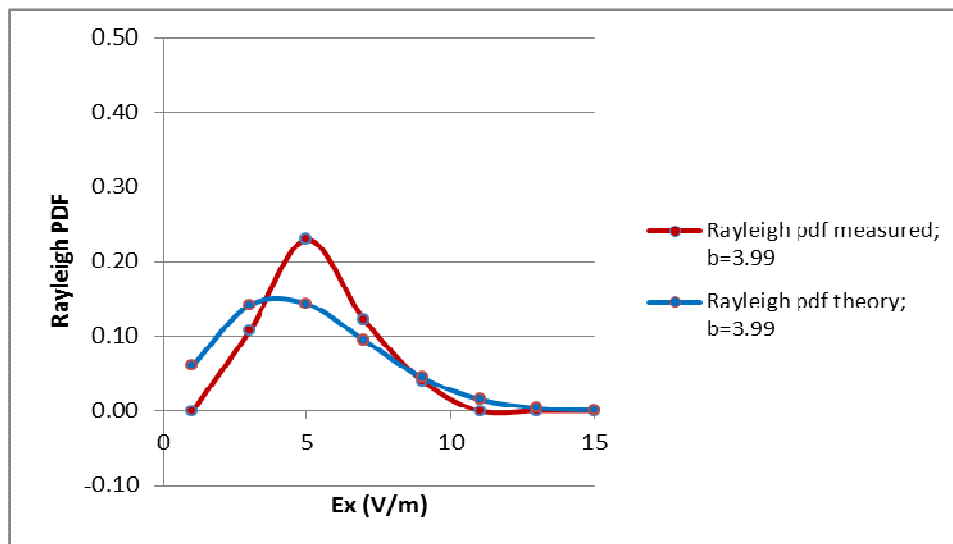


Fig. 3.9: PDF for Ex; STATIC; n=37 tuner steps.

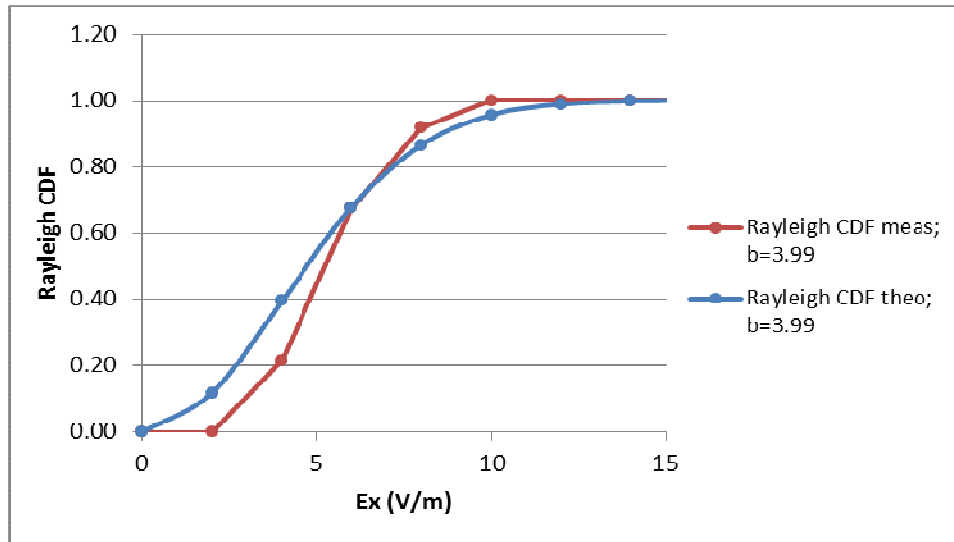


Fig. 3.10: CDF for E_x ; STATIC; $n=37$ tuner steps.

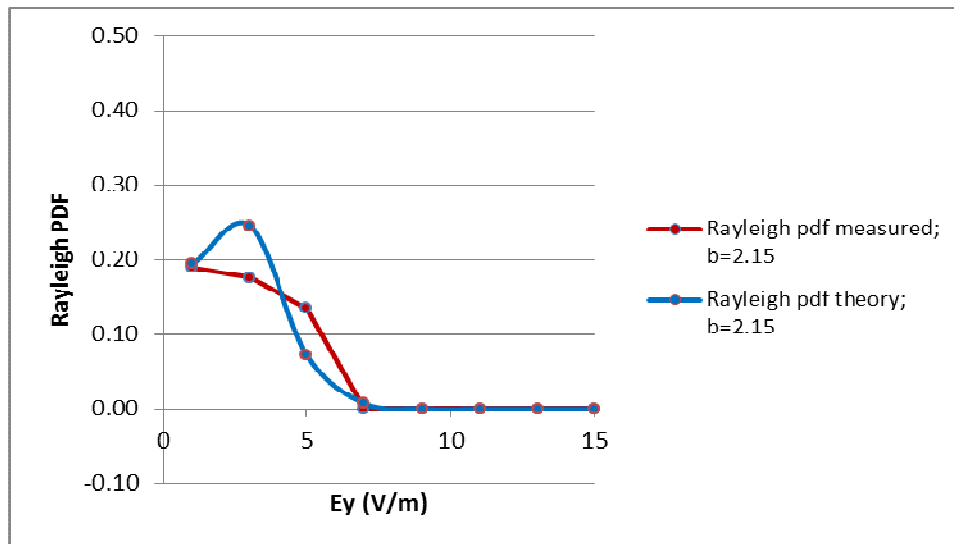


Fig. 3.11: PDF for E_y ; STATIC; $n=37$ tuner steps.

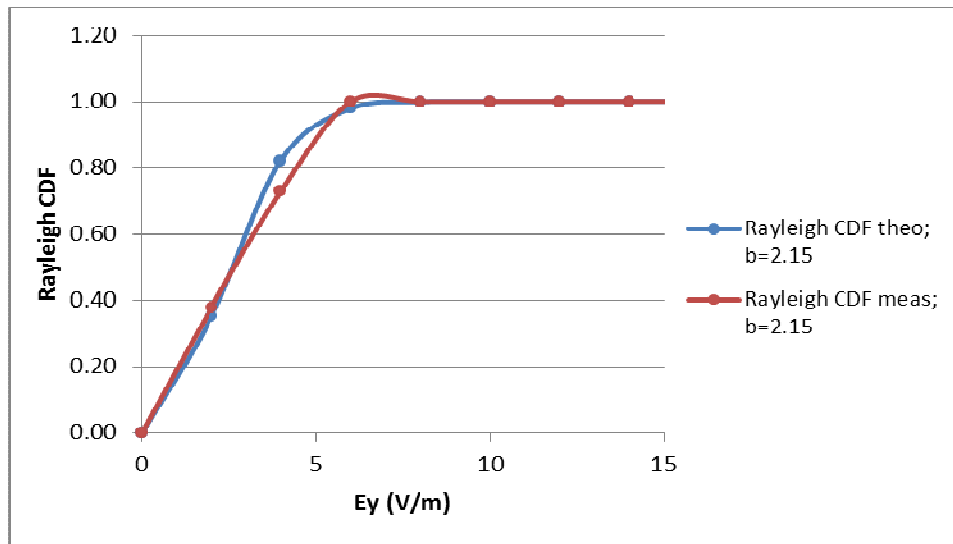


Fig. 3.12: CDF for E_y ; STATIC; $n=37$ tuner steps.

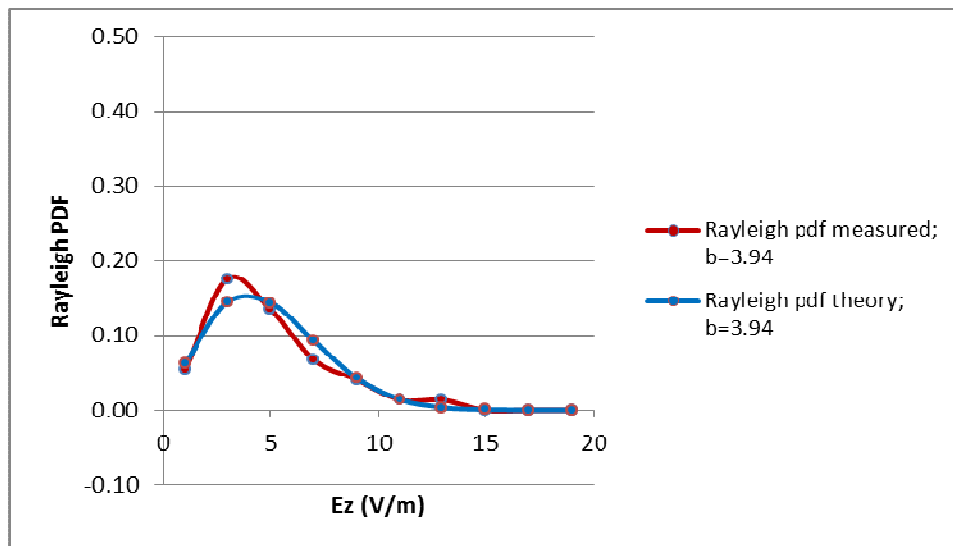


Fig. 3.13: PDF for E_z ; STATIC; $n=37$ tuner steps.

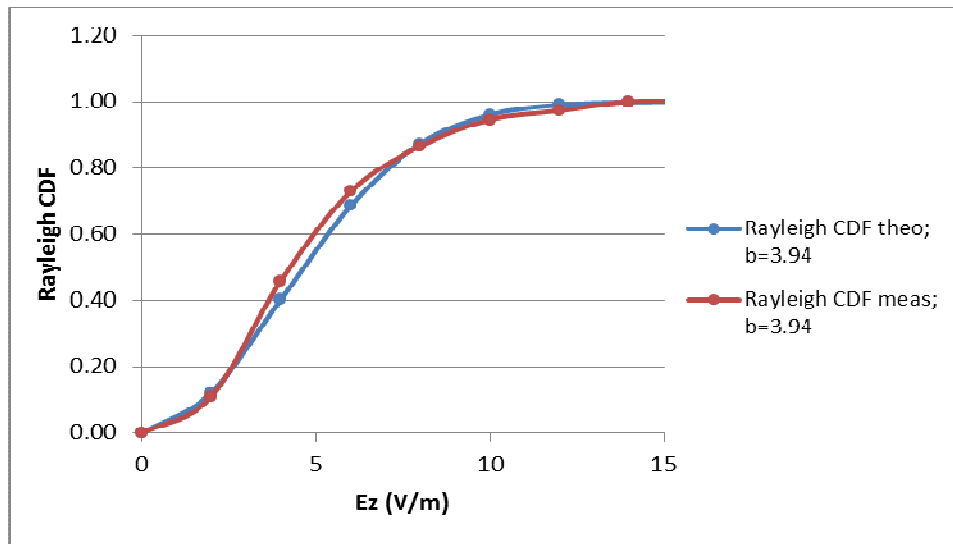


Fig. 3.14: CDF for E_z ; STATIC; $n=37$ tuner steps.

The differences, in the Rayleigh PDF above graphs, between the theoretical curves and the experimental ones can be explained by the imperfection of the tuner and the number of the tuner steps (the higher the tuner steps the lower the difference between the theoretical and measured values). In reality, the magnitude of the field is characterized by a Rice probability density function, which depends first, on a tuned part of the field, which is purely random, and, on a residual untuned part corresponding to a deterministic residue of the field. The Rayleigh pdf being a particular case of the Rice pdf when there is no deterministic part.

The discrepancies in the graphs between the theory and measurements are due to minimal direct coupling of the emitting antennas to the measuring instruments. In theory the field is purely random and follows the Rayleigh pdf, but with direct coupling, a residual untuned part corresponding to a deterministic residue of the field is present, this is called the Rice-Nakagami pdf.

The table below gives the results of the KS test when comparing the theoretical and experimental CDF's given in Fig. 3.10, Fig. 3.12 and Fig. 3.14. We have added the comparison of the CDF's for the total Electric field given later.

Table 3.2: KS test summary; E-field; STATIC; n=37tuner steps; 1546 MHz; P3.

Electric field	KS test result	KS test limit	KS test conclusion
Ex	0,1788	0,2233	Pass
Ey	0,0931	0,2233	Pass
Ez	0,0568	0,2233	Pass
Etot	0,0987	0,2233	Pass

3.3.4 PDF, CDF and KS test for the total Electric field

The results are for a frequency of 1546 MHz and at point P3 (see Fig. 3.1 and Table 3.1).

We recall that: $E_{tot} = \sqrt{E_x^2 + E_y^2 + E_z^2}$.

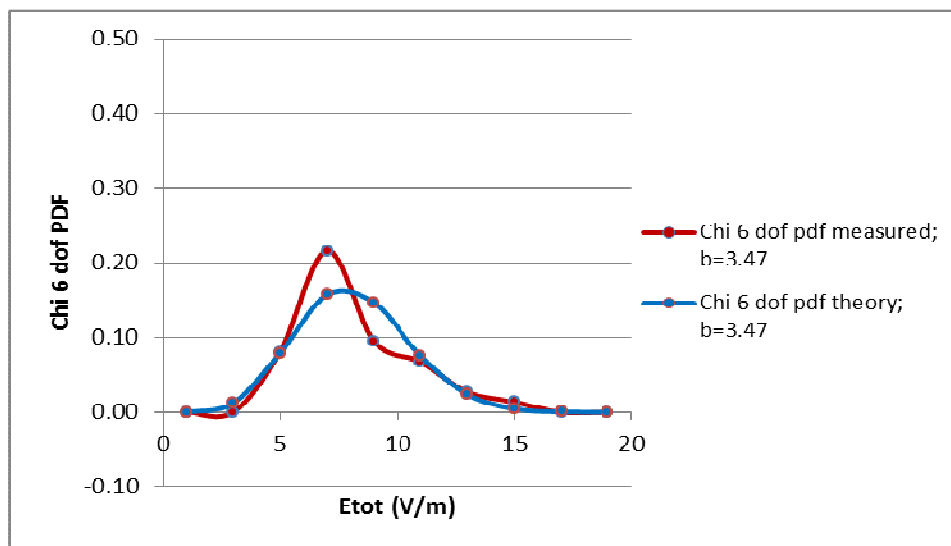


Fig. 3.15: PDF for Etot; STATIC; n=37 tuners steps.

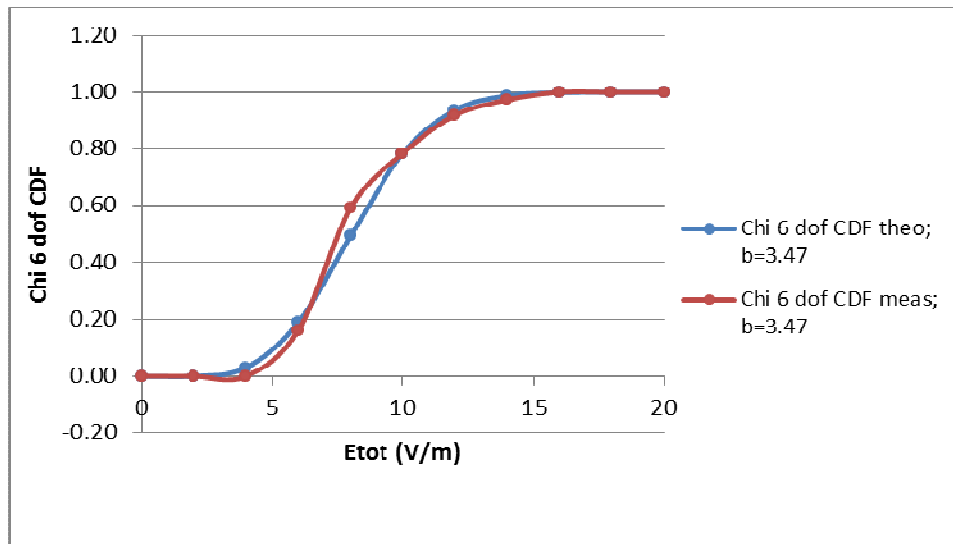


Fig. 3.16: CDF for Etot; STATIC; n=37 tuners steps.

The experimental and theoretical CDF's pass the KS test (see Table 3.2).

The scale factors relationship found for the RAIL tuning method is still valid for the STATIC tuning, with, in this case, n=37 tuner steps as indicated in the table below:

Table 3.3: Scale factors relationship; STATIC; n=37 tuner steps.

Scale Factors				
b_{Ex}	b_{Ey}	b_{Ez}	b_{Etot}	b_{Etot}
Measured	Measured	Measured	Measured	Arithmetic mean
3,99	2,15	3,94	3,47	3,36

3.3.5 PDF, CDF and KS test for the Power received on an antenna

The power has been measured at the termination of a Horn antenna during the general measurements aiming at the determination of the Electric field uniformity (see section 3.3.1).

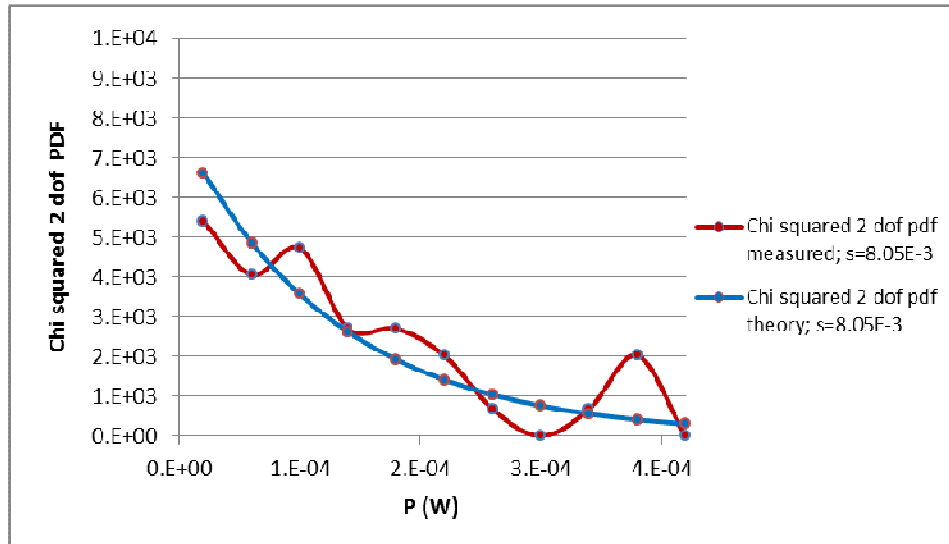


Fig. 3.17: PDF for Power on antenna; STATIC; n=37 tuner steps.

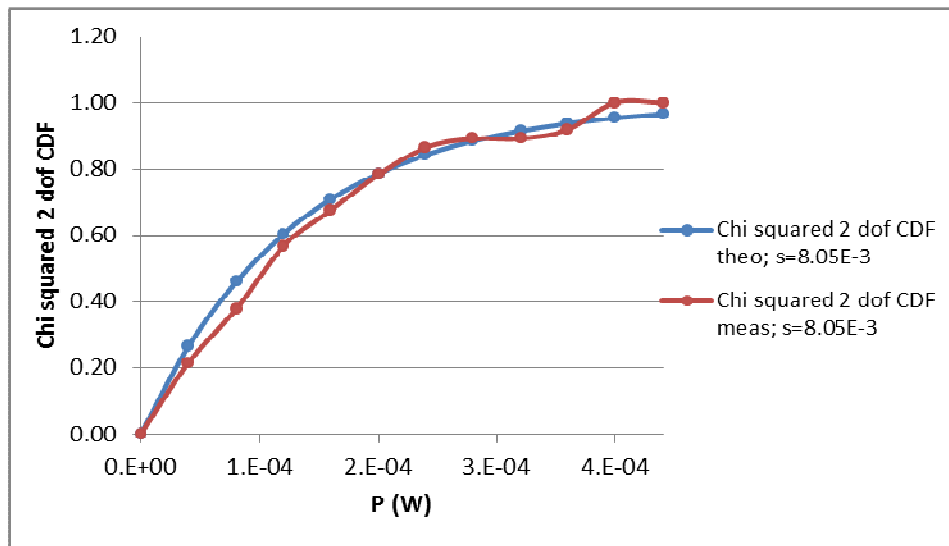


Fig. 3.18: CDF for Power on antenna; STATIC; n=37 tuner steps.

The table below gives the results of the KS test when comparing the theoretical and experimental CDF's given in Fig. 3.18.

Table 3.4: KS test summary; Power; STATIC; n=37 tuner steps.

Power	KS test result	KS test limit	KS test conclusion
Antenna	0,0822	0,2233	Pass

Now that the method of static source-mode tuning based on the electronic switching of an LPDA antenna network has been fully validated in terms of field uniformity and probability density function, let us consider the time needed for performing a calibration with our method in comparison with the conventional one.

3.3.6 Testing Time and Costs

A comparison of testing times between the IEC 61000-4-3 [27] and the IEC 61000-4-21 has been given in [12] for 150 and 24 samples or tuner steps. In our case, analysis of the result files shows that the calibrating time for our 24 steps procedure with the two orthogonal rails is approximately equal to the time needed to calibrate with a 6-bit binary sequence of 64 tuner steps. We need 1h06 min, while 47 minutes are needed to calibrate with a 5 bit binary sequence of 32 tuner steps, a reduction of 29 %. However, this 5-bit sequencing has to be rejected because the field uniformity does not comply with the standard. So, for the comparison, we keep only the configurations (shown in Table 3.5) that complies with the standard IEC 61000-4-21. It can be seen that the testing time in a semi-anechoic room will always be lower than in a reverberation chamber when working in tuning mode (i.e. stopping during a defined dwell time, for example 3 seconds, at each frequency, in order to observe the behaviour of the equipment under test).

Table 3.5: Testing time comparison IEC 61000-4-3 vs IEC61000-4-21
(measured)

	Testing time for 800 to 2500 MHz (Log steps 5%) n=22 frequencies
IEC 61000-4-3 2 pol./ 3 pol.	25 min / 35 min
IEC 61000-4-21 24 steps (moving antennas)	1.1 h
IEC 61000-4-21 64 steps (static antennas 6 pairs)	2 h
IEC 61000-4-21 37 steps (static antennas 8 pairs)	1.1 h

Now, we compare the testing time reduction between a conventional mechanical tuner and our new static tuner. The testing time reduction for MIL-STD-461F is described in Table 3.6. We estimate that the static tuner is 1 second quicker, at least, than a mechanical one. Because the iteration from one tuner step to the next for the static tuner is made by toggling the RF switches, this takes less than one hundred milliseconds, but the movement of the mechanical tuner from one position to the next takes, at least, one second.

Table 3.6: Testing time reduction for MIL-STD-461F (estimation)

Testing frequencies	Number of steps	Testing time reduction for 12 mechanical tuner steps	Testing time reduction for 37 mechanical tuner steps
30 MHz – 1 GHz	703	2.3 h	7.2 h
800 MHz – 2.5 GHz	412	1.4 h	4.2 h
1 GHz – 18 GHz	1158	3.9 h	11.9 h

According to MIL-STD-461F, from 30 MHz to 1 GHz, the ratio between two successive frequencies is 0.005, and from 1 GHz to 18 GHz this ratio is 0.0025, so the number of steps for the considered testing frequencies can be calculated and figure in the second column. Now, if this number of steps is multiplied by one second and the applicable tuner step (12 or 37), we find the time reduction expressed in hours in columns 4 and 5 respectively. The approximate costs related to this static tuner are 2300 Euros (this includes the 8-way power divider (which has the higher cost), the RF SPDT switches and the cables).

3.4 Conclusion

A new method for source-tuning the modes in a reverberation chamber has been proposed and investigated. The method is based on the use of eight pairs of LPDA antennas covering a surface parallel to a wall of the chamber. This method shows that the 3 dB field uniformity requirement can be met in the 800 to 2500 MHz frequency range for a 6-bit sequencing (64 tuner steps), and for an 8-bit sequencing (37 tuner steps). A 5-bit sequencing (32 tuner steps) technique has been tested on a surface

that is smaller than the one for the 6-bit (the surface is the one covered by the static tuner and delimited by the eight pair of antennas to form an ellipse, the horizontal length is 1.8 m and vertical length is 0.8 m, see Fig. 3.2), however, this 5-bit sequencing is rejected because the associated standard deviation is 0.7 dB higher than the minimum requirement of the standard (i.e. 3 dB).

Finally, the testing time with this method is lower than with conventional mechanical ones for the same number of tuner steps. Hence, a laboratory equipped with such a tuning system would spare hours of testing for the same performance quality.

The statistical treatment and analysis of the random Electric fields and power show that their experimental PDF and CDF are close enough to the theoretical Rayleigh distribution to pass the KS hypothesis test. This important result demonstrates at the same time that the stochastic fields obtained by the present method do not contain any significant deterministic part, which guarantees the absence of a direct coupling between the source of radiation and the EUT placed in the testing volume.

4. Application of RC new tuning method to antenna efficiency determination

4.1 Introduction

One way to evaluate the efficiency of the new tuning method using the two orthogonal rails described in Chapter 2 is to use it in one of the several applications of a reverberation chamber, i.e. the determination of the radiation efficiency of an antenna, called for short "antenna efficiency".

We start with the relative method for antenna efficiency measurement in a reverberation chamber (RC) already described in the IEC 61000-4-21 standard. It is then applied to the measurement of antenna efficiency without the use of a reference antenna, but with the data acquisition of the electrical field strength (E-field). This new E-field method is to the RC what the gain/directivity radiation pattern method is to anechoic chambers. The antenna efficiency values are obtained from measurements done with equipment used for EMC immunity testing, such as E-field meter, spectrum analyser and power meter. The knowledge of antenna efficiency measured in RC is useful, for mobile antenna designers who have to characterize their antenna in multipath and stochastic environments.

The radiation efficiency value of antennas mounted on RFID (radio frequency identification used to automatically identifying and tracking of goods) equipment, cellular mobile phones or wireless communication equipment like Bluetooth or Wifi (Wireless fidelity) is an important component of the link budget. The higher the efficiency, the larger the communication range, the longer the battery lifetime and the lower the communication errors. Antennas like PIFA (Planar Inverted-F antenna), short whip or RFID tags exhibit an approximate efficiency of 65 % and operate within the

800-2400 MHz frequency range. Antenna arrays for MIMO system can also be measured [62].

Several methods are used to measure the efficiency, like the one proposed by Wheeler in 1959 [28] (see Fig. 4.1). The radiansphere is a hypothetical sphere having a radius of one radian length ($\lambda/2\pi$) from the centre of an antenna that is much smaller than the sphere. Physically, it marks the transition between the near and the far field regions, for electrically small antennas. It is interesting to point out that, in his original paper, Wheeler considered a small spherical antenna, uniformly pitched with windings in the axial direction. This small loop antenna was part of an oscillating circuit so the radiation shield caused an increase in the amplitude of oscillation. This increase in amplitude was a measure of the radiation efficiency.

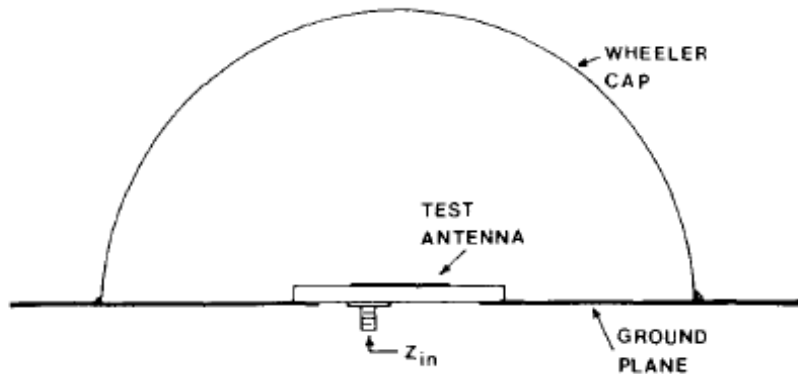


Fig. 4.1: Illustration of the Wheeler method.

This method is best suited for antennas whose size is lower than $\lambda/2\pi$. Considering the above mentioned frequency range we can say that the maximum antenna size for applying the Wheeler Cap method to PIFA and RFID antennas should be 6 cm. For any larger size, a more suited method should be searched for.

Integrating the measured antenna gain over all 4π steradians of a spherical surface, and dividing by 4π is another way to find the

antenna efficiency. This can be done in an anechoic room with a mechanical tri-dimensional positioning system as described in [29], [30], [31], [32]. This method is called gain/directivity or radiation pattern method (see (4.1)) and gives good results if we accept an accuracy of $\pm 20\%$ in comparison to $\pm 2\%$ with the Wheeler one, and the costly measurement platform.

$$\eta = \frac{P_{rad}}{P_{IN}} = \frac{G}{D} \quad (4.1)$$

where,

- P_{rad} is the power radiated by the antenna;
- P_{IN} is the power delivered to the antenna terminals;
- G is the Gain and D the directivity.

One of its advantages is that it can be extended to antennas whose size is larger than $\lambda/2\pi$, like log periodic or DRH (Double Ridge Horn) antennas.

Remembering that communication equipment is mostly used in urban areas or indoor environments where a lot of waves are coming in from almost all directions on the antenna, the use of a reverberation chamber becomes evident. Indeed, thanks to the mode stirring, the fields in it are stochastic and cause a large number of plane waves to come from all directions. Over one stirrer scan, we can assume that the electric and magnetic fields, in a reverberation chamber of good quality, are statistically homogeneous, isotropic and unpolarised. The method consists in connecting port 1 (Tx) of a Vector Network Analyser (VNA) to a

transmitting antenna and port 2 (Rx) successively at a Reference antenna and at the unknown antenna (see Fig. 4.2)

Let us define the two ports consisting of the transmitting antenna (including its feeder), the propagation channel between antennas and the antenna under test (reference or unknown) with its cable. The scattering parameters of it, S_{21} and S_{22} are measured over one stirrer scan, for a fixed frequency, and the unknown radiation efficiency η_u is computed from the following formula [33], [34], [35]:

$$\eta_u = \frac{\langle |S_{21u}|^2 \rangle}{\langle |S_{21r}|^2 \rangle} \times \frac{1 - \langle |S_{22r}| \rangle^2}{1 - \langle |S_{22u}| \rangle^2} \times \eta_r \quad (4.2)$$

where:

- $\langle |S_{21u}|^2 \rangle$ is the ensemble average over one stirrer scan of the ratio of the forward power P_2 received at the unknown antenna terminals to the forward power P_1 applied to the transmitting antenna terminals.
- $\langle |S_{21r}|^2 \rangle$ is the ensemble average over one stirrer scan of the ratio of the forward power P_2 received at the Reference antenna terminals to the forward power P_1 applied to the transmitting antenna terminals.
- $\langle |S_{22r}| \rangle^2$ is the square of the ensemble average over one stirrer scan of the reflection coefficient at the termination 2 of the 2-Port equipped with the Reference antenna.

- $\langle |S_{22u}| \rangle^2$ is the square of the ensemble average over one stirrer scan of the reflection coefficient at the termination 2 of the 2-Port equipped with the Unknown antenna.
- η_r is the known radiation efficiency of the Reference antenna.

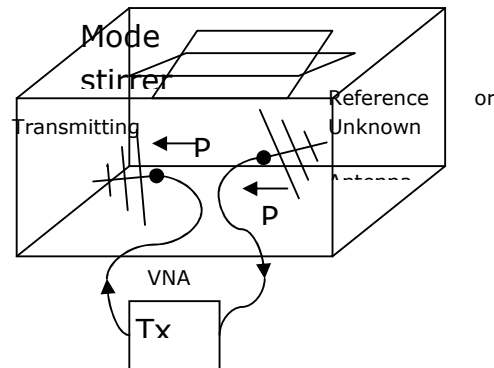


Fig. 4.2: Set-up for measurements with VNA

Now, if we assume that both unknown and Reference antennas are impedance-matched antennas, with $S_{22} \leq -10$ dB, assuming an accuracy in between 10 and 20 %, and that the reflection coefficient of the 2-Port at its termination 2 is close to that of the antenna connected at the point, the formula (4.2) reduces to:

$$\eta_u = \frac{\langle |S_{21u}|^2 \rangle}{\langle |S_{21r}|^2 \rangle} \times \eta_r \quad (4.3)$$

that expresses the radiation efficiency as a ratio of averaged normalized powers multiplied by a known value of radiation efficiency.

In section 4.2, we present the theoretical background, section 4.3 being an exhaustive presentation of our radiation efficiency measurement methods yielding the results given in sections 4.4. and 4.6.

4.2 Theory

4.2.1 Definition

Antenna efficiency is defined as the total radiated power divided by the total input power, when the antenna is assumed to be impedance matched [36]:

$$\eta = \frac{P_r}{P_r + P_l} \quad (4.4)$$

Where:

- P_r is the total radiated power;
- P_l is the power lost in conductors and dielectrics;
- $P_r + P_l$ is the total power at the antenna terminals.

It is important to make the distinction with the *total antenna efficiency* which takes into account the impedance mismatch:

$$\eta_T = \eta \times \left(1 - |S_{11}|^2\right) \quad (4.5)$$

where S_{11} is the reflection coefficient of the antenna (and the well-known scattering parameter). The expression $(1 - S_{11}^2)$ is called the *impedance mismatch efficiency* and is ≥ 90 % for satisfactory antenna impedance matching ($S_{11} \leq -10$ dB).

From (4.4), we have easily developed the formula given in [37] for the quarter-wave circular cylindrical antenna, which yields:

$$\eta = \left(1 + \left(\frac{l^2 f \mu_0}{4\pi a^2 R_r^2} \right)^{\frac{1}{2}} \sigma^{-\frac{1}{2}} \right)^{-1} \quad (4.6)$$

where:

- l is the length of the wire;
- f is the operating frequency;
- μ_0 is the magnetic permeability of free space ($= 4\pi \cdot 10^{-7}$ V.s/A.m);
- a is the radius of the wire;
- R_r is the radiation resistance ($= 36.5 \Omega$ for the electrically thin quarter-wave antenna);
- σ is the conductivity of the conductor (assumed the same for wire and ground plane).

As Reference antenna, we have made a thin quarter-wave antenna on a finite ground plane, as depicted in Fig. 4.3. According to [38] the radiation resistance of a thin quarter-wave element at a centre of a circular ground plane of radius $0 \leq ka \leq 8.5$ can be calculated by the oblate spheroidal wave-function method and by the method of moments. In the present case of $ka = 6.8$ the radiation resistance turns out to be 30.1 according to the first method and 43.5 according to the second one. Hence, the best estimator taken in [38] for the radiation resistance is 36.5 Ohm. Using this last value in (4.6) we obtain a computed efficiency of 99 %. Moreover, King [39] gives a value very close to 99 %. So, we keep this value as best estimator.

4.2.2 Relative method (with Reference antenna)

The average power received by an impedance-matched reference antenna given by Hill [7], can be generalized to an antenna for which $S_{11r} \neq 0$ as follows:

$$\langle P_{Rr} \rangle = \frac{\langle E_0^2 \rangle}{Z_0} \times \frac{\lambda^2}{8\pi} \times \eta_r \times (1 - |S_{11r}|^2) \quad (4.7)$$

where:

- $\langle P_{Rr} \rangle$ is the ensemble average of the power received at the Reference antenna terminals;
- $\langle E_0^2 \rangle$ is the ensemble average, over one stirrer scan, of the square electric field in the RC;
- Z_0 is the free space plane wave impedance (=377 Ohm);
- λ is the operating wavelength;
- $|S_{11r}|^2$ is the square modulus of the reflection coefficient of the Reference antenna.

For the unknown antenna (with $S_{11u} \neq 0$), we have:

$$\langle P_{Ru} \rangle = \frac{\langle E_0^2 \rangle}{Z_0} \times \frac{\lambda^2}{8\pi} \times \eta_u \times (1 - |S_{11u}|^2) \quad (4.8)$$

where:

- $\langle P_{Ru} \rangle$ is the ensemble average of the power received at the unknown antenna terminals;
- $|S_{11u}|^2$ is the square modulus of the reflection coefficient of the unknown antenna.

By dividing (4.8) by (4.7), we obtain:

$$\eta_u = \frac{\langle P_{Ru} \rangle}{\langle P_{Rr} \rangle} \times \frac{(1 - |S_{11r}|^2)}{(1 - |S_{11u}|^2)} \times \eta_r \quad (4.9)$$

This shows equivalence with formula (4.2). For further computation of our radiation efficiency, equation (4.9) will be used.

4.2.3 E-field method (without Reference antenna)

Let us compare the radiation efficiency derived from (4.8) with those given in IEC 61000-4-21 [3].

Solving (4.8) for η_u gives:

$$\eta_u = \frac{\langle P_{Ru} \rangle}{\frac{\langle E_0^2 \rangle}{Z_0}} \times \frac{1}{\frac{\lambda^2}{8\pi}} \times \frac{1}{(1 - |S_{11u}|^2)} \quad (4.10)$$

The discussion about (4.10) is the following. The radiation efficiency is presented as the ratio of the average power received at the antenna terminals divided by the average scalar power density

$\langle E_0^2 \rangle / Z_0$ in the space occupied by the antenna. This gives a result in square meters. If we divide this result by the effective area (in square meters) of the antenna $\lambda^2 / 8\pi$ taking into account a polarization mismatch factor of 0.5, as justified in [40] (there is some controversy over whether to use 1 or 0.5 as polarization factor in a RC, we choose 0.5 as it has been confirmed experimentally in [40]) and with $G=1$ (antennas with dimensions lower than λ have low directivity and are considered isotropic), we obtain a dimensionless value, just as the radiation efficiency is. This means that measuring and averaging the E-field makes it possible to obtain the radiation efficiency without the need of any Reference antenna.

According to the IEC 61000-4-21 standard,

$$\langle E_0 \rangle = \frac{8\pi}{\lambda} \sqrt{5 \frac{P_{RMax}}{\eta_u}} \quad (4.11)$$

where:

- $\langle E_0 \rangle$ is the ensemble average of the electric field;
- P_{RMax} is the measured maximum value of the received power on the AUT over one stirrer scan;
- η_u is the unknown antenna efficiency.

Solving (4.11) for η_u , gives:

$$\eta_u = \frac{1}{3} \times \frac{P_{RMax}}{\langle E_0^2 \rangle / Z_0} \times \frac{1}{\lambda^2 / 8\pi} \quad (4.12)$$

It is interesting to compare (4.12) and (4.10) and to point out that, according to the IEC standard, the maximum to average value is equal to 3. In (4.12) an impedance-matched antenna is considered. This maximum to average value is coherent with the following. It is known from [41] that the power received by an antenna in a RC has a χ^2 probability density function with two degrees of freedom and [40] gives a table of maximum to average ratios as a function of the number of samples. A ratio of 3 is associated with 12 samples, which is the minimum number of samples allowed by the IEC standard. As a conclusion, we will derive the radiation efficiency by applying (4.10).

4.3 Measurement on home-made and two commercial antennas

4.3.1 Set-up description

Three antennas are measured: a coaxially fed quarter-wave monopole on a circular ground plane at an operating frequency around 1.8 GHz (Fig. 4.4), a Double Ridged Horn (DRH) with a range from 700 MHz to 18 GHz (Fig. 4.5) and a Log periodic antenna with a range from 300 MHz to 18 GHz (Fig. 4.5). We will measure the efficiencies of the DRH and the log periodic according to the relative method (the quarter-wave is the Reference antenna). The efficiencies of all three antennas will be measured according to our E-field, absolute method, all this at frequencies around 1.8 GHz.

The efficiency computed for the quarter-wave is 99 %. The efficiency of a DRH is around 90 % according to [2].

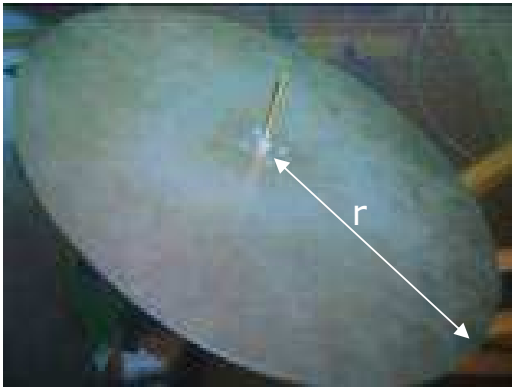


Fig. 4.3: the quarter-wave antenna on ground plane ($h = 3.9$ cm; $r = 18.5$ cm; $ka = 6.8$ @ 1.8 GHz; $\sigma = 5.8 \times 10^7$ S/m)

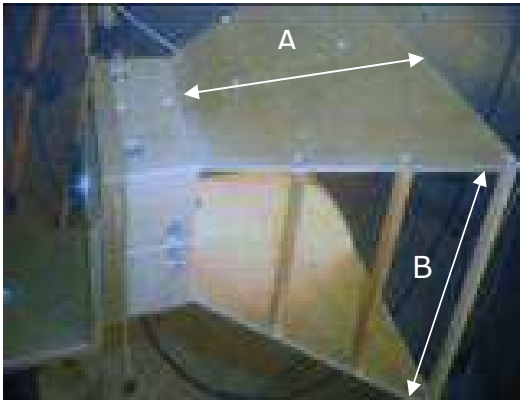


Fig. 4.4: the Double Ridged Horn antenna. $A = 23.5$ cm; $B = 14$ cm

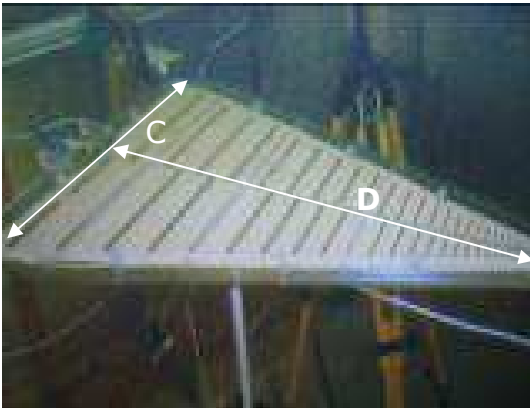


Fig. 4.5: the log periodic antenna. $C = 32$ cm; $D = 50$ cm. 70 dipoles.

We use the 15 m^3 Reverberation Chamber (RC) of LEMA, with a LUF (Lowest Usable Frequency) of 800 MHz. The electronic tuner consists of two rails (Fig. 4.6) (in yellow). The horizontal one is 2.48 m long and set at 1.25 m from the floor. The vertical one is 2.08 m long and placed at 1.39 m of the back wall and at 1.09 m from the front wall. On each rail a transmitting LPDA (Log Periodic

Dipole Antenna) directed towards the walls of the chamber is moving. The RC is equipped with common EMC equipment like a Narda EMR-300 E-field meter (3 MHz -18 GHz), a power meter NRP from Rohde & Schwarz with a bidirectional coupler from Amplifier Research, spectrum analysers and signal generators. Section 2 and [12] gives an extensive description of it. The spatial uniformity is 2 dB or less for 150 samples and, maximum 2.5 dB for 24 samples.

4.3.2 General considerations

It is worthwhile to mention the major precautions/sources of errors that influence the accuracy of efficiency measurements:

- a) The Reference antenna should be placed far from the chamber walls ($> \lambda / 4$) in order to avoid the deterministic bias of field statistics existing in the boundary layer;
- b) Residual polarization unbalance can be removed by polarization stirring, i.e. by using three orthogonally polarized fixed antennas instead of one [42];
- c) Moving the unknown antenna to several positions inside the RC is a technique called "platform stirring" and is supposed to improve accuracy [43];
- d) Change of the equipment between the measurements gives a systematic error. This can be avoided by using as much as possible the same equipment and place them in symmetric spatial positions [44].

We have taken care of the above recommendations as follow:

- a) The reference and the unknown antennas have been placed inside the working volume as determined in [12]; this volume delimited by points P1-P8 (Fig. 4.6.) is at a distance of least 0.6 m from the vertical walls, 1 m from the floor and 0.88 m from the ceiling, so the separation distance is kept higher than $\lambda / 4$,

i.e. 9 cm at 800 MHz. Moreover, the two transmitting antennas are directed towards the chamber vertical walls.

b) Polarization imbalance is reduced because the two transmitting antennas are orthogonally polarized. Moreover, Reference and unknown antennas are placed sequentially in three identical orthogonally polarized positions.

c) Platform steering is done in some way, because, once the measurement is done for a given orthogonal polarization, we do a spatial swap, that is to say, we place the AUT in the former spatial position of the Reference antenna, and we place the Reference antenna in the former spatial position of the unknown antenna.

d) Change of loading is reduced to a minimum, because we pay attention not to introduce/retrieve equipment during the measurement process and during the spatial swap as described in "c)" above.

4.3.3 Procedure for Relative method

The coaxially fed quarter-wave monopole is used as Reference antenna. The unknown antennas are the DRH and the Log periodic. We use the equipment and connections as described in Fig.4.6. The unknown and the Reference antennas are connected to a spectrum analyser. They are placed in a first identical orthogonal polarization inside the working volume delimited by points P1-P8 (Fig.4.6.). The tuner (horizontal and vertical rails) produces 51 samples. We then measure 2×51 values of received power. After that, another orthogonal polarization is set and again received power measurements are done. Then, a third orthogonal polarization is set and power measurements are performed. Finally, a spatial swap is done and the three orthogonal polarizations are set sequentially. A total of $2 \times 3 \times 2 \times 51$ power measurements are

carried out. The mean values of $\langle P_{Ru} \rangle_{1X}$, $\langle P_{Ru} \rangle_{1Y}$, $\langle P_{Ru} \rangle_{1Z}$, $\langle P_{Ru} \rangle_{2X}$, $\langle P_{Ru} \rangle_{2Y}$, $\langle P_{Ru} \rangle_{2Z}$, are computed and the mean values of $\langle P_{Rr} \rangle_{1X}$, $\langle P_{Rr} \rangle_{1Y}$, $\langle P_{Rr} \rangle_{1Z}$, $\langle P_{Rr} \rangle_{2X}$, $\langle P_{Rr} \rangle_{2Y}$, $\langle P_{Rr} \rangle_{2Z}$ are computed too. Then, we use the formula (4.9) to obtain the efficiency. The values between brackets are the ensemble averages of the received power over 51 samples in three polarizations and two spatial positions in the RC.

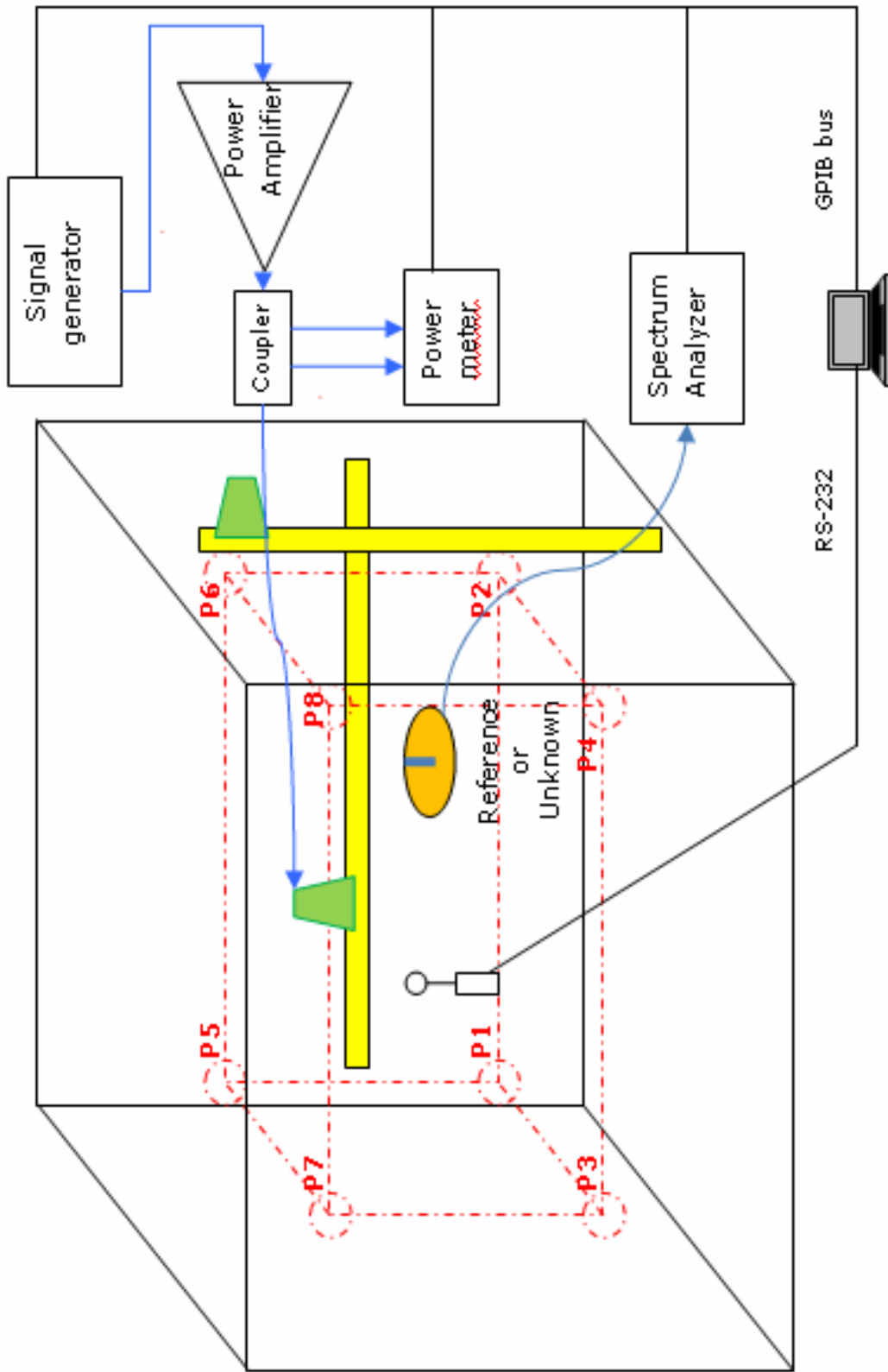


Fig. 4.6: Antenna efficiency measurement, measurement set-up.

4.3.4 Procedure for E-field method

We measure the efficiency of the three antennas. The E-field meter and the unknown antenna are placed in the working volume (Fig. 4.6.). The unknown antenna is connected to a spectrum analyser. The E-field, the received power of the unknown antenna, the forward and reverse power to the transmitting antenna and the information about the stirrer steps are acquired automatically by home-made LabVIEW software. There are 148 tuner steps (82 on the horizontal stirrer and 66 on the vertical one). The number of tuner steps is different in this case because the software was set at this value. The unknown antenna is placed sequentially in three orthogonal polarizations within the working volume. The signal is amplified by a power amplifier, E-fields around 10 V/m are measured. The formula (4.10) is used to compute the efficiency.

4.3.5 Results for the home-made Quarter-wave antenna

Table 4.1: Efficiency values for Quarter-wave antenna

Frequency (GHz)	Efficiency (%)	
	Calculated	E-field method
1.7	99	74.9
1.75		86.8
1.8 ($\lambda/4$)		99.4
1.85		98.1
1.9		78.5

As we can see, at the quarter-wavelength resonance (1.8 GHz) the experimental efficiency given by the E-field method is in very good agreement with the calculated one (99%). The discrepancy (24 %) observed at other frequencies is partly due to measurement errors (for example, a spatial uniformity around 1 dB introduces an error of about 12 %), and partly to frequency sensitive impedance matching of the antenna. Errors could be reduced by doing a spatial swap.

4.3.6 Results for the Double Ridged Horn antenna

Table 4.2: Efficiency values for DRH antenna

Frequency (GHz)	Efficiency (%)		
	Announced	Relative method	E-field method
1.7	90	93.4	100.8
1.75		99.1	78.8
1.8		99.5	81.2
1.85		96.5	77.2
1.9		91.3	69.6

Note: the value «100.8 %» is obviously an impossible one and should be limited to 100 %.

The relative method gives results within 10 % of the announced value. The E-field method gives results within 20%; in comparison with the 20 % accuracy of the equivalent gain/directivity method [32] in an anechoic environment, the present results are quite satisfactory.

4.3.7 Results for the Log periodic antenna

Table 4.3: Efficiency values for Log periodic antenna

Frequency (GHz)	Efficiency (%)		
	Informative	Relative method	E-field method
1.7	75	49.5	32.2
1.75		44.7	32.2

The results obtained by the two methods are much closer to each other than to the informative value which is given as a “typical” figure, so the actual efficiency value of the unknown antenna is probably around 35-40 %. To the best knowledge of the authors no other experimental value has been reported in the literature for Log periodic antennas. Fundamentally, a Log periodic antenna consists of an alignment of a large number of linear dipoles of various lengths in order to make the antenna broadband but with a same directivity. At a given frequency, not all the dipoles are radiating, but only the ones whose length is close to $\lambda/2$ the other ones being passive. So, taking into account the fact that only a fraction of the antenna structure contributes to the radiation at a given frequency and that the antenna is not considered to be efficient in directions other than its axis, a value as high as 75% for the claimed efficiency is at least surprising for us. The measured values we have obtained seem to be more realistic and in better correspondence with what we expect from a directive and linearly polarized antenna placed in a multipath and depolarized environment. But this should be confirmed by other authors to enhance the confidence one could have to the results.

4.4 Measurement on PIFA antennas

This work has been done in the reverberation chamber of Royal Military Academy with a PhD student of KUL.

4.4.1 Set-up description

We choose to measure the efficiency of some PIFA antennas made from ShieldIt (SH) and Flectron (FL) conductive textiles. Both are sourced from LessEMF USA, and have surface resistivities, R_s , of less than $0.05 \Omega/\text{sq}$. Both textiles are polyester-based fabric coated using copper (Flectron) and both copper and nickel (for ShieldIt fabric). The thickness, t , of Flectron is estimated at 0.08 mm , and ShieldIt is about twice of the former, 0.17 mm . The PIFAs' design, optimization and simulated efficiencies are gathered from CST Microwave Studio.

Two topologies of the antennas were tested in this work. One is PIFA with a plain radiator (labelled as SHPL for ShieldIt fabric and FLPL for Flectron), while another incorporates a notched radiator (labelled as SHSL for ShieldIt and FLSL for Flectron). The operating frequencies of these antennas are at 2.4 GHz , which is also the frequency of efficiency measurements. The summary of the topologies are given in Fig. 4.7.

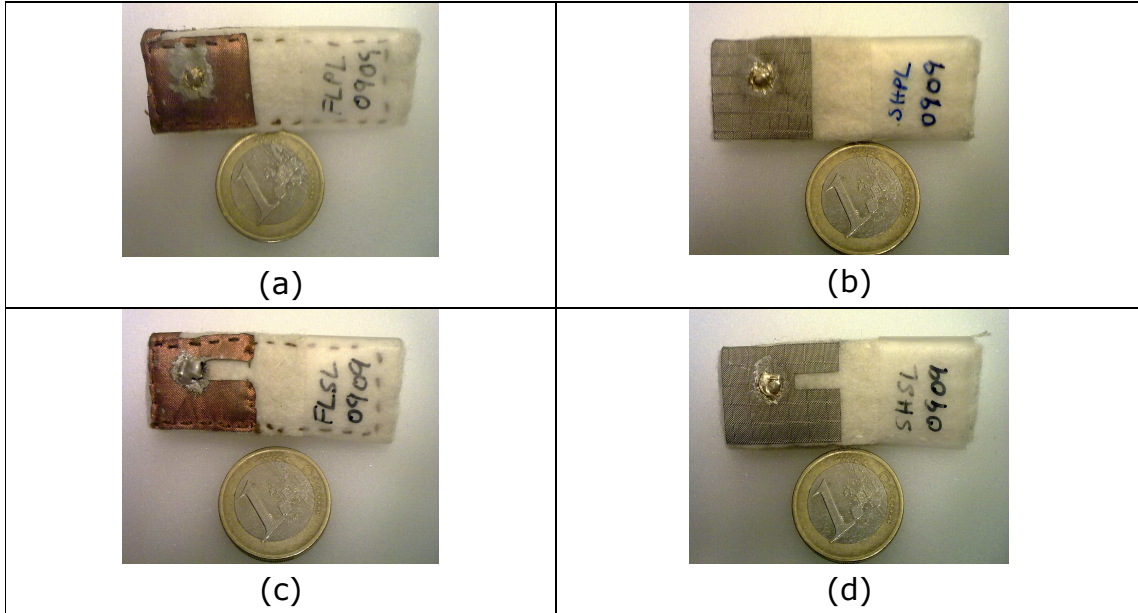


Fig. 4.7: (a) Plain Electron PIFA (FLPL); (b) Plain ShieldIt PIFA (SHPL); (c) Slotted Electron PIFA (FLSL) and (d) Slotted ShieldIt PIFA (SHSL)

4.4.2 General considerations

- a) Three antenna stands/holders are placed in the working volume (1.2 m long, 0.9 m wide and 0.6 m high) of the reverberation chamber side by side. The working volume is denoted as the volume between points P1 to P8 in Fig. 4.6. The rectangular working volume is divided equally into a 3 x 2 cell (3 columns and 2 rows). The two antennas are placed in the centre of the left- and right-most columns, respectively, while the E-field meter is centred at the top-centre cell, as shown in Fig. 4.8.

	E-field meter	
Hor		AUT

Fig. 4.8: Top view of the working volume and antenna placements

- b) Polarization unbalance is reduced as the two transmitting antennas are orthogonally polarized. Moreover, Reference and unknown antennas are placed sequentially in three identical orthogonally polarized positions.
- c) In order to compensate for spatial lack of uniformity (3 dB uniformity is higher when an accuracy of around 10 % is targeted), we do a swap, that is to say, we place the unknown antenna in the former spatial position of the Reference antenna, and we place the Reference antenna in the former spatial position of the unknown antenna.
- d) The reading difference between the two spectrum analysers is compensated, by relative calibration of the two spectrums and taking into account the difference.

Note: Physical setup of different antenna polarizations and antenna holder locations illustrating points "b)" and "c)" above are shown in Fig. 4.9 to Fig. 4.14.



Fig. 4.9: Setup 1 with X-polarized antennas (labelled as 'P1') and antenna stand arrangement 1 (labelled as 'R1'), or *P1R1*



Fig. 4.10: Setup 2 with Y-polarized antennas (labelled as 'P2') and antenna stand arrangement 1 (labelled as 'R1'), or $P2R1$



Fig. 4.11: Setup 3 with Z-polarized antennas (labelled as 'P3') and antenna stand arrangement 1 (labelled as 'R1'), or $P3R1$

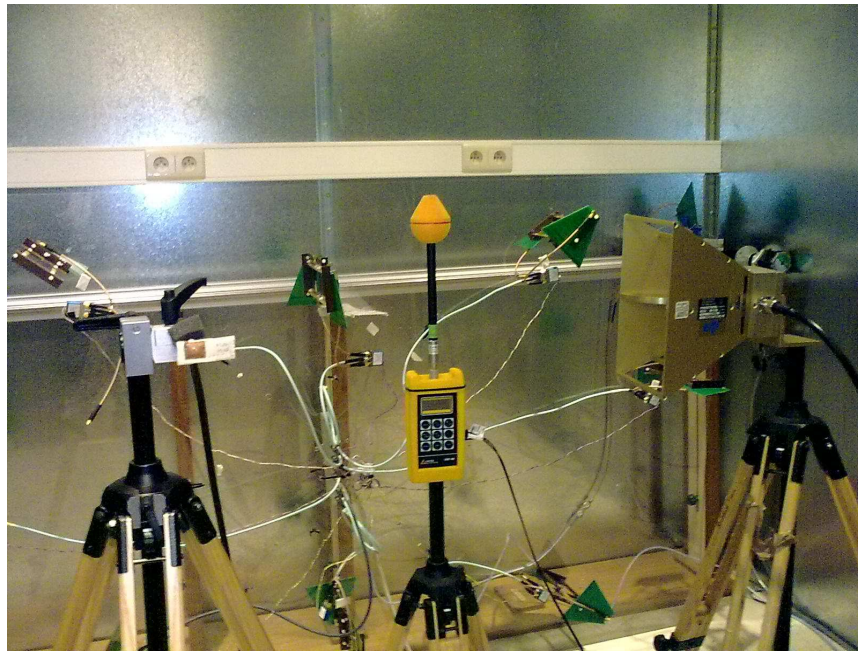


Fig. 4.12: Setup 4 with Z-polarized antennas (labelled as 'P3') and antenna stand arrangement 1 (labelled as 'R2'), or $P3R2$



Fig. 4.13: Setup 5 with Y-polarized antennas (labelled as 'P2') and antenna stand arrangement 1 (labelled as 'R2'), or $P2R2$



Fig. 4.14: Setup 6 with X-polarized antennas (labelled as 'P1') and antenna stand arrangement 1 (labelled as 'R2'), or $P1R2$

4.4.3 Procedure for Relative method

We use a wideband Double Ridged horn antenna as the Reference antenna. Its efficiency is assumed to be 90%. The unknown antennas are the PIFAs presented and illustrated above. The unknown and the Reference antennas are each connected to their spectrum analyser. They are placed in a first identical orthogonal polarization inside the working volume. The stirrer (horizontal and vertical rails) produces 51 samples (29 for the horizontal and 22 for the vertical). Then, we measure 2×51 values of received power. After that another orthogonal polarization is set and received power measurements are done again. Then, a third orthogonal polarization is set and power measurements are performed. Finally, a spatial swap is done and the three orthogonal polarizations are set sequentially as illustrated by Fig. 4.9 to Fig. 4.14. A total of $2 \times 3 \times 2 \times 51$ power measurements are done. The mean value of the received power is computed. Finally, we use the formula (4.9) to obtain the efficiency.

4.4.4 Procedure for E-field method

The E-field meter and the unknown antenna are placed in the working volume. The unknown antenna is connected to a spectrum analyser. The E-field, the received power of the unknown antenna, and information about the stirrer steps are acquired automatically by internally-developed LabVIEW software. Again, there are 51 stirrer steps. The unknown antenna is placed sequentially in three orthogonal polarizations within the working volume. The signal is amplified by a power amplifier, E-fields around 10 V/m are measured. The formula (4.10) is used to compute the efficiency.

4.4.5 Results for PIFA antennas

A total of 15 antenna topologies/materials were measured in RMA.

Table 4.4: Efficiency measurement results on PIFA's (part I)

	Sim	Gain/dir.	RMA (Abs)	RMA (Rel)
FLPL0510	82.20	60.14	78.66	62.66
FLSL0510	81.61	46.93	76.36	53.09
SHPL0510	78.27	81.88	89.09	75.67
SHSL0510	81.68	76.26	68.74	60.35
CTPL0909	83.02	81.38	81.78	76.45
CTSL0909	83.03	81.70	78.87	68.46
FLPL0909	82.20	67.14	72.63	65.99
FLSL0909	76.50	60.60	60.90	60.26
SHPL0909	78.27	78.99	82.49	71.40
SHSL0909	81.05	76.43	86.18	68.61

Table 4.5: Efficiency measurement results on PIFA's (part II)

	Sim	Gain/dir.	RMA (Rel)	RMA (Abs)
FSHP9	84.39	78.09	104.80	91.27
FFLP5	91.51	65.48	59.03	50.87
CPPL	98.88	NA	105.17	92.73
SHPL0909(L)	NA	NA	70.79	68.48
SHPL0909(W)	NA	NA	19.95	17.97

The "Sim" column gives the results obtained by the KUL PhD student with the 3D electromagnetic simulation software CST.

A summary is given below:

Table 4.6: Efficiency measurement results on PIFA's, summary

Method	Sim	Gain/Dir	E-field	Relative
FLPL	82.2	67.1	72.6	66.0
FLSL	76.5	60.6	60.9	60.3
SHPL	78.3	79.0	82.5	71.4
SHSL	81.1	76.4	86.2	68.6

Analysing the results, difference between simulated and measured FLPL PIFA is about 0.4 dB or 6 %. The simulation calculation seems to be slightly over-optimistic, considering ideal materials and simulation environments. For SHPL PIFA, the difference between the E-field method and the gain/directivity are -0.2 dB and 0.4 dB, respectively, compared to the relative method. On the other hand, the difference between SHSL efficiency measured using the E-field method and measurements results obtained in another laboratory

according the gain-directivity method is -0.5 dB. This difference is 0.5 dB for the relative method.

4.5 Measurements on Dual-Band, Dual-Polarized and Dual fed perforated Array Patch antenna pair

In the frame of its end study work a student of the Polytechnic faculty of the RMA has designed, realized and characterized the performances of a dual band and dual polarized array patch antenna. This was an opportunity to measure the radiation efficiency of another antenna type than the previous ones and to compare it to its value obtained by electromagnetic simulation of the modelled antenna using FEKO. A complete description of the antenna is given in [45].

4.5.1 Set-up description and procedure

The same set-up and procedure have been used as for the PIFA antennas, see points 4.4.1 to 4.4.4.

Picture of the antenna is given in Fig. 4.15 and Fig. 4.16.

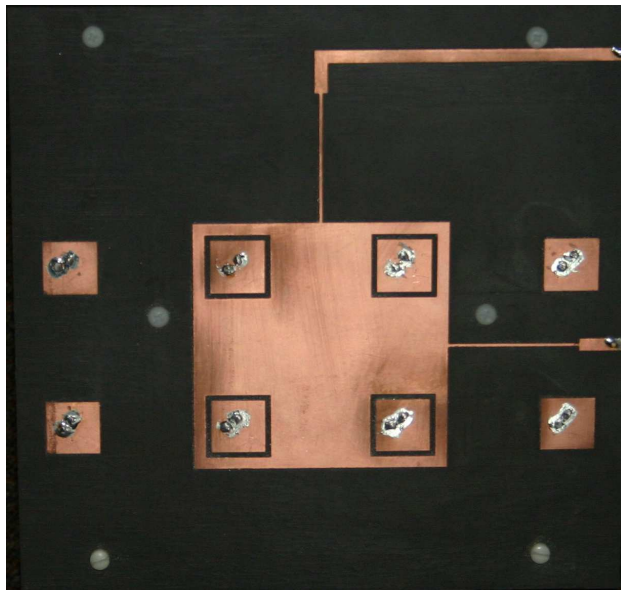


Fig. 4.15: Front of the patch antenna.

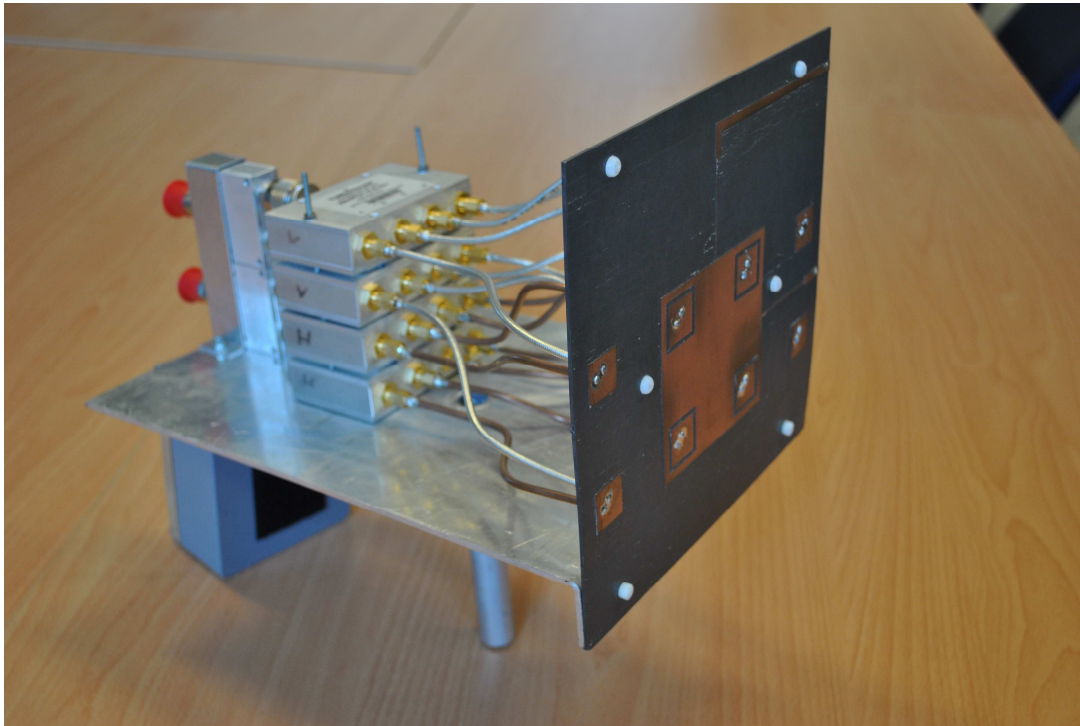


Fig. 4.16: Side view of the patch antenna with its feeding networks

The two resonant frequencies of the patch are:

- a) L-band: 1.15 GHz;
- b) C-Band: 5.3 GHz.

Table 4.7: Dimensions of the patch elements and characteristics of the substrate

Band	f_0	L	L_{eff}	h	ϵ_r	$\tan \gamma$
	(GHz)	(mm)	(mm)	(mm)	-	-
L	1.15	85	86.6	1.57	2.33	0.0014
C	5.3	18	19.6	1.57	2.33	0.0014

The two feeding networks at the back side of the C-band patch array, one for each polarization, consist of RG 402 flexible cables of

equal length directly soldered to the antenna backplane followed by a cascade of divider-combiners. These networks ensure equi-amplitude and equi-phase feeding of all eight C-band patches. The L-band patch element is fed by two 50 Ω microstrip lines.

4.5.2 Results for the Dual-Band, Dual-Polarized patch antenna

Table 4. 8: Patch antenna efficiency results

Band	Efficiency (%)	
	FEKO sim.	Measured
L	55	78.5
C	87.3	81.5

As one can see, the results obtained by simulation and by measurements are in good agreement for the C-band. But for the L-band, one notes a discrepancy of about 33%. Further investigation is needed to clarify the reason of such a difference.

4.6 Repeatability Tests

Four PIFA antennas were tested to investigate the repeatability of the measurement facility.

Antenna measurements carried out for repeatability tests:

- a) Plain Flectron (FLPL 0909) – 2x
- b) Plain ShieldIt (SHPL 0510) – 2x
- c) Plain ShieldIt (SHPL0909) – 2x
- d) Plain ShieldIt with Large Fleece (SHPL0909L) – 2x

Table 4.9: Repeatability of antenna efficiency measurements

	Date (2011)	Sim	Satimo	RMA1 (Abs)	RMA1 (Rel)	RMA2 (Abs)	RMA2 (Rel)	Diff (Abs)	Diff (Rel)
FLPL0909	16/2	82.20	67.14	70.17	70.22	72.63	65.99	2.46	4.23
SHPL0510	14/2 and 16/2	78.27	81.88	89.09	75.67	82.54	80.28	6.55	4.61
SHPL0909	16/2	78.27	78.99	82.49	71.40	75.08	65.62	7.41	5.78
SHSL0909L	16/2	NA	NA	70.79	68.48	76.45	66.29	5.66	2.19

Max difference of 7.5 % was found between the same antennas measured twice. Satimo is an industry leader in electromagnetic field measurements in the microwave frequency range.

4.5 Conclusions

For the quarter-wave reference antenna, the efficiency measured is in good agreement with the calculated one at the operating frequency. For the Double Ridged Horn antenna, the estimated accuracy of the E-field method is $\pm 20\%$, which is the same as the accuracy of the equivalent gain-directivity method performed in an anechoic environment. The accuracy of the relative method is even better, i.e. $\pm 10\%$. For the Log periodic antenna, the uncertainty related to the measuring equipment or the method itself cannot explain the discrepancy between the informative and the measured values. Taking into account the results of the two methods, we estimate that the efficiency of the measured Log periodic antenna should be closer to 40 % than to 75 %. Feedback on radiation efficiency of log periodic antennas is welcome. The advantage of the methods presented here is that there is no need for Wheeler caps adapted to the antenna to be measured. Moreover, the E-field method does not need any reference antenna.

On top of that, this method has been applied to the measurement of PIFA antennas. It provided a maximum difference of 0.5 dB or 10 % compared to the conventional gain-directivity or relative method. The measured reproducibility is 7.5 %. The benefit is that there is no need for a reference antenna. The accuracy can be improved by doing a larger number of stirrer steps, but the 45 minutes measurement time is then increased.

It has to be pointed out that the tuning method is the new one using two orthogonal rails as described in point 2. As the antenna efficiency results are satisfactory, this implicitly consolidates this new method. Finally, in the future, an antenna factor method can be developed in the RC [63].

5. The Canonical Equipment Under Test (CEUT)

5.1 Introduction

The CEUT has been designed and manufactured, initially, in order to make the comparison between the two types of tuning in the reverberation chamber, and for comparison with the semi-anechoic room. To the knowledge of the author, it is an original realization and has no equivalent in the EMC-community.

It has yielded unexpected developments, as it has been used for interlaboratory testing for the radiating immunity tests by the EMC Laboratories in Belgium, including the LEMA laboratory of Royal Military Academy. The testing report of the results can be found in annex 4.

5.2 Working mechanism

The CEUT (Canonical Equipment Under Test) has been designed and constructed to be representative of most of modern digital electronics and which susceptibility is not linked to some polarization state. Hence, it consists of a coupling part, a sensitive electronic part and some electronic modules for the remote control and visualization of the status of the CEUT. It is battery-powered.

The coupling part of the CEUT is composed of three orthogonal loop antennas. For sensitivity purpose the loop circumference has been chosen equal to the mean wavelength in the frequency range of interest. It is well known that electrically small loops have the advantage to have a response directly proportional to the magnetic flux of the incident wave without any resonance problem, but exhibit a low sensitivity. Electrically large loops on the contrary offer a better sensitivity, but suffer from resonances due to a mixed response to both magnetic and electric fields. Hence, the circumference of the loop antenna of the CEUT has been chosen to be a fraction of the wavelength, but not too

small so that it offers enough sensitivity, without any resonance problem.

The sensitive part is composed of three identical channels, one per polarization. Each channel contains a square wave pulse generator, an envelope generator, a counter and a comparator. In order to reduce any interference, all the electronics are placed in a metallic box, Fig. 5.1. The square wave generator is connected to the counter through the two-turn circular loop (diameter = 6 cm).

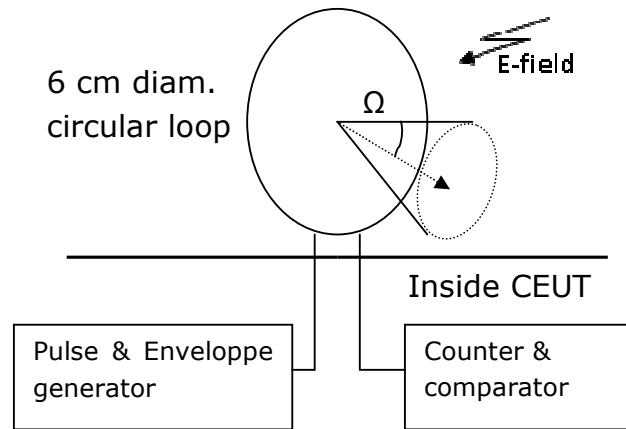


Fig. 5.1: Schematics of a CEUT single channel

The theory of operation is as follows: when the electromagnetic incident field is established into the room (SAR or RC), the pulse generator is remotely triggered to produce a burst of 100 square pulses with 50% duty cycle, during 2 seconds. These pulses are applied through the loop antenna conductor to the counter and the comparator. The number of pulses has to be equal to the one set by an 8-bit dip-switch (in our case equal to 100). If not, an output greater or lower is issued. After a 2-s delay, results (= ; > or <) are available, and recorded. Finally, a reset pulse is sent to the three counters. The data are handled as follows: if the counter

state is smaller than 100, the output is set to 0; if it equals 100, it is set to 1, and if it is larger than 100, it is set to 2.

In order to decide whether the CEUT has been disturbed, a pass-fail criterion has to be established. This is defined as follows. A pass is obtained if all outputs are at 1 for any tuner step at each frequency. Otherwise, there is a fail, and this for the three channels. During the tuner scan, if at least one of n steps is 0 or 2, then reaction is accounted for 0 or 2. If several 0's and 2's are observed, then the higher is the winner. If at least one 0 or 2 is detected during tuner scan then reaction is accounted for FAIL. If all counts are 1 (OK), then reaction is accounted as PASS, all this at three polarizations. Let's take an example: for 12 tuner steps, we acquire 3x12 CEUT reaction data, the result for the given frequency is considered as PASS if all the 36 values are 1, if at least one is 0 or 2, then the result is considered as FAIL.

5.3 Electrical and Mechanical description

The characteristics of the CEUT (see Fig. 5.2) are the following:

- 1) Six digital data inputs (three for triggering and three for clearing the counters);
- 2) Nine digital data output (three data output for each polarization);
- 3) Count 100 Pulses (adjustable) during 2 seconds (adjustable);
- 4) Pulse duration: 20 ms;
- 5) Duty cycle: 50%.
- 6) Driver developed with LabVIEW software for remote controlling;
- 7) Five-meter optic fibre link;
- 8) Battery powered, 4-h autonomy;

- 9) Shielded metallic box (24.5 cm x 20 cm x 25 cm), with 3-mm wall thickness.



Fig. 5.2: The CEUT, open (left) and closed (right) with one loop on each face of the metallic box.

5.4 Power received by CEUT in RC

Due to the presence of the shielding, the circular loop is the only coupling element through which energy from the incident field can be transferred to the electronics [1.5, p. 113]. The spatial average power received by this circular loop is:

$$\langle P_r \rangle = \frac{E_0^2}{2} \cdot \frac{R_r}{4\pi} \cdot \iint_{4\pi} [|S_{r\alpha}(\Omega)|^2 + |S_{r\beta}(\Omega)|^2] d\Omega \quad (5.1)$$

with the components of the receiving function:

$$S_{r\alpha} = 0 \quad \text{and} \quad S_{r\beta} = \frac{-i \omega \mu A \sin \alpha}{2 \eta R_r} \quad (5.2)$$

and where:

- E_0^2 the squared electric field strength incident on the loop (V^2/m^2);
- R_r the loop radiation resistance (Ohm);
- Ω the solid angle (sr), see Fig. 5.1;

- A the area of the loop (m^2);
- η the wave impedance (Ohm);
- ω the angular frequency (rad/s);
- μ the free space magnetic permeability (H/m);
- α the angle between propagation vector of the incident wave and the axis perpendicular to the plane of the loop ($^\circ$).

Substituting (5.2) in (5.1) and calculating the angular integration gives:

$$\langle P_r \rangle = \frac{E_0^2 \omega^2 \mu^2 A^2}{12 \eta^2 R_r} \quad (5.3)$$

Because the loop diameter stands from $\lambda/6$ to $\lambda/2$ over the frequency range of interest, we examine two models: the small loop and the Alford loop (dimensions not negligible comparing to the wavelength). The following relation gives the radiation resistance of a small loop [46]:

$$R_r = 31200 \cdot \left(N \cdot \frac{A}{\lambda^2} \right)^2 \quad (5.4)$$

where, N is the number of turns (2 turns in our case).

Then, replacing (5.4) in (5.3) yields:

$$\langle P_r \rangle = \frac{E_0^2 \lambda^2}{8 \pi \eta N^2} \quad (5.5)$$

Considering that loop dimensions are not negligible comparing to the wavelength for the upper part of the frequency band of interest,

we use the semi empirical equation of the radiation resistance given by Alford [47]:

$$R_r = 320N^2 \cdot \left[\sin\left(\pi \frac{l}{\lambda}\right) \right]^4 \tag{5.6}$$

Where: l is the diameter of the loop (6 cm).

Fig. 5. 3 shows both powers calculated from (5.5) on one hand and by substituting (5.6) in (5.3), with $E_0=50$ V/m:

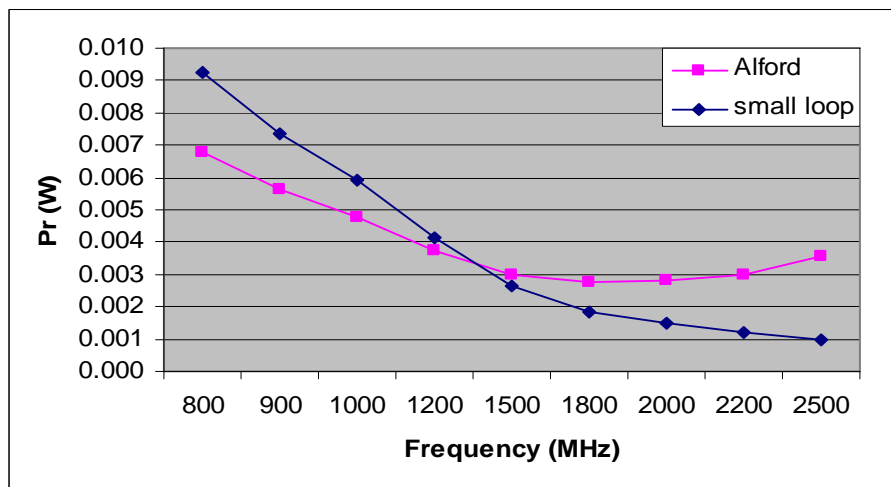


Fig. 5. 3: Average power P_r received by the loop.

This graph expresses the power transferred to the CEUT. It shows that whatever be the modelling of the loop, the maximum power picked up by the loop is at the low frequencies. So, one would expect that the CEUT electronics is more exposed at these frequencies. We will see later that this is in good agreement with the immunity tests, as the FAIL status will occur mainly from 800 MHz to around 1600 MHz. Beyond, the CEUT will mainly produce a PASS status, which can be explained by the low level of power received by the antenna.

Fig. 5.4 shows the CEUT, prepared for the interlaboratory testing, as it is presented in the user’s manual. It is linked by optical fibre (up to 20 meter has been tested) to a portable PC, on which

LabVIEW home-made software is running for control and acquisition of the status of the three loops.

The small grey box with four blue buttons is a testing emitter for checking before use.

Fig. 5.5 gives the internal electronic connections. The generation of the pulses is done by an assembler software running in a PIC16F630 microcontroller from MICROCHIP. Initially, the pulses were generated with NE555, but they were replaced due to temperature drift. Finally, Fig. 5.6 and Fig. 5.7 show the electrical connections. As this CEUT has to travel from one laboratory to another, the removal of fuses F1 and F2 assure the complete disconnection of the two batteries for security reasons. This is indicated in the user's manual.



Fig. 5.4: CEUT and accessory equipment, for interlaboratory testing.

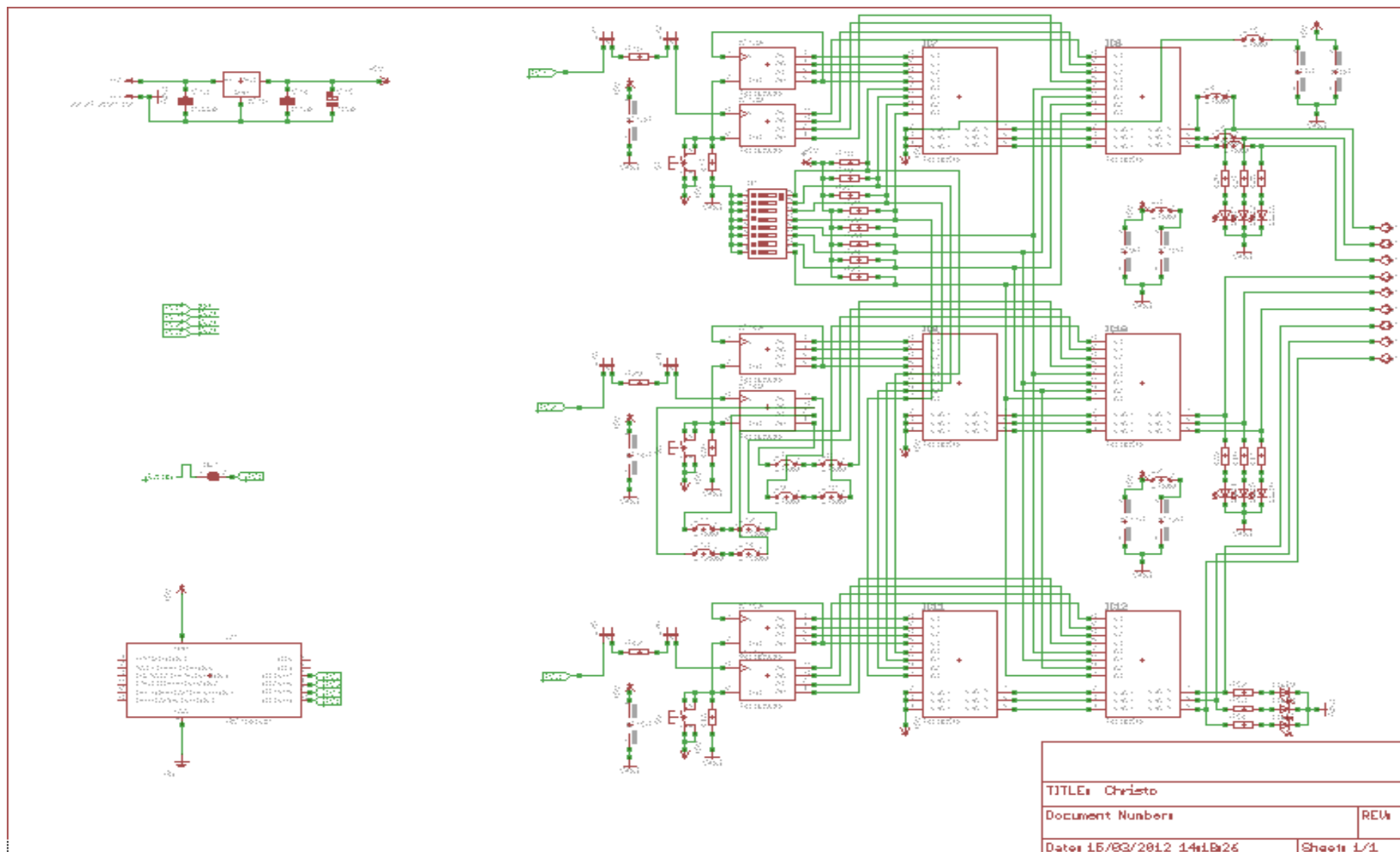


Fig. 5.5: CEUT Electronic drawing

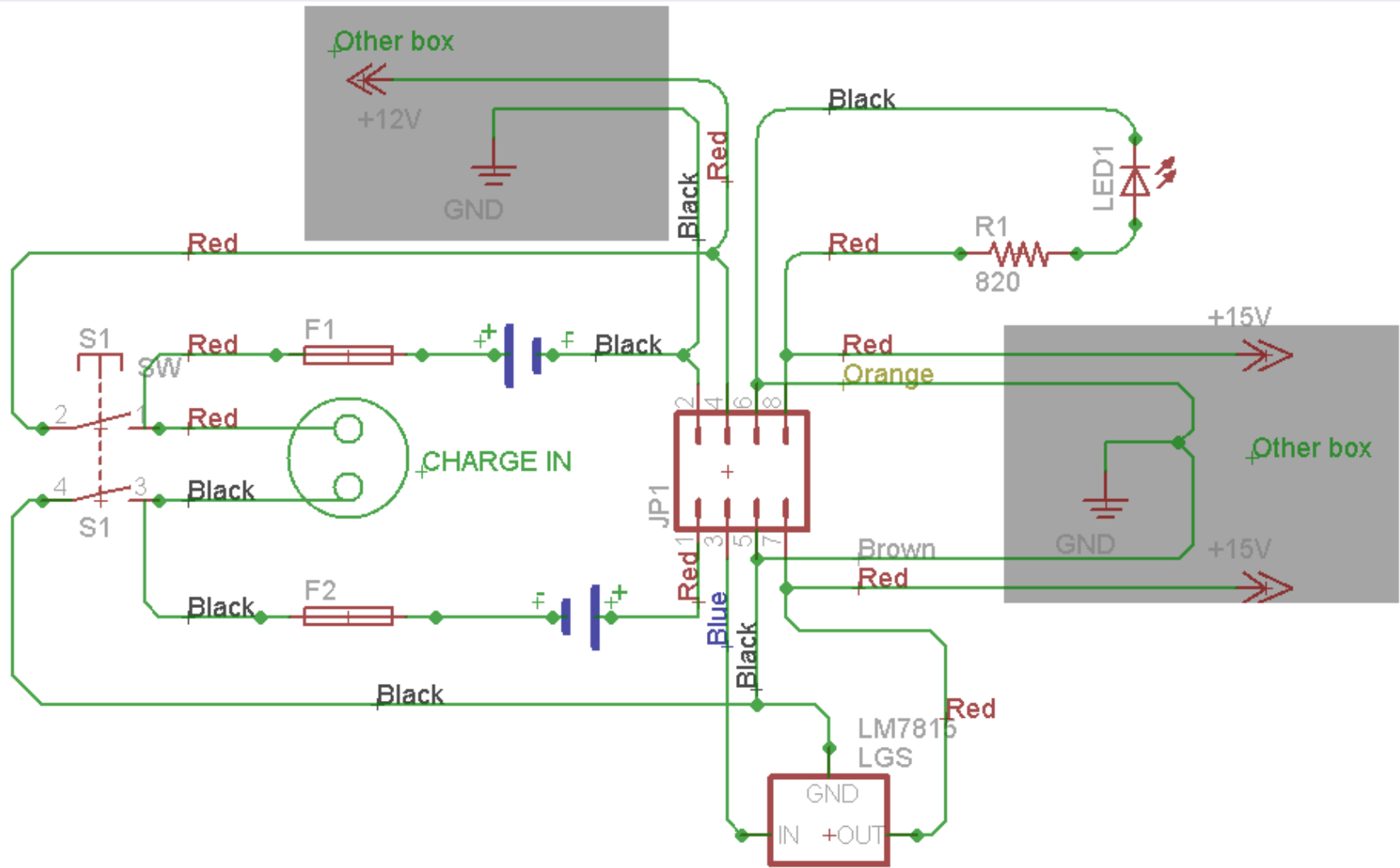


Fig. 5.6: CEUT Electrical connections, part 1

CIRCUIT DE PUISSANCE

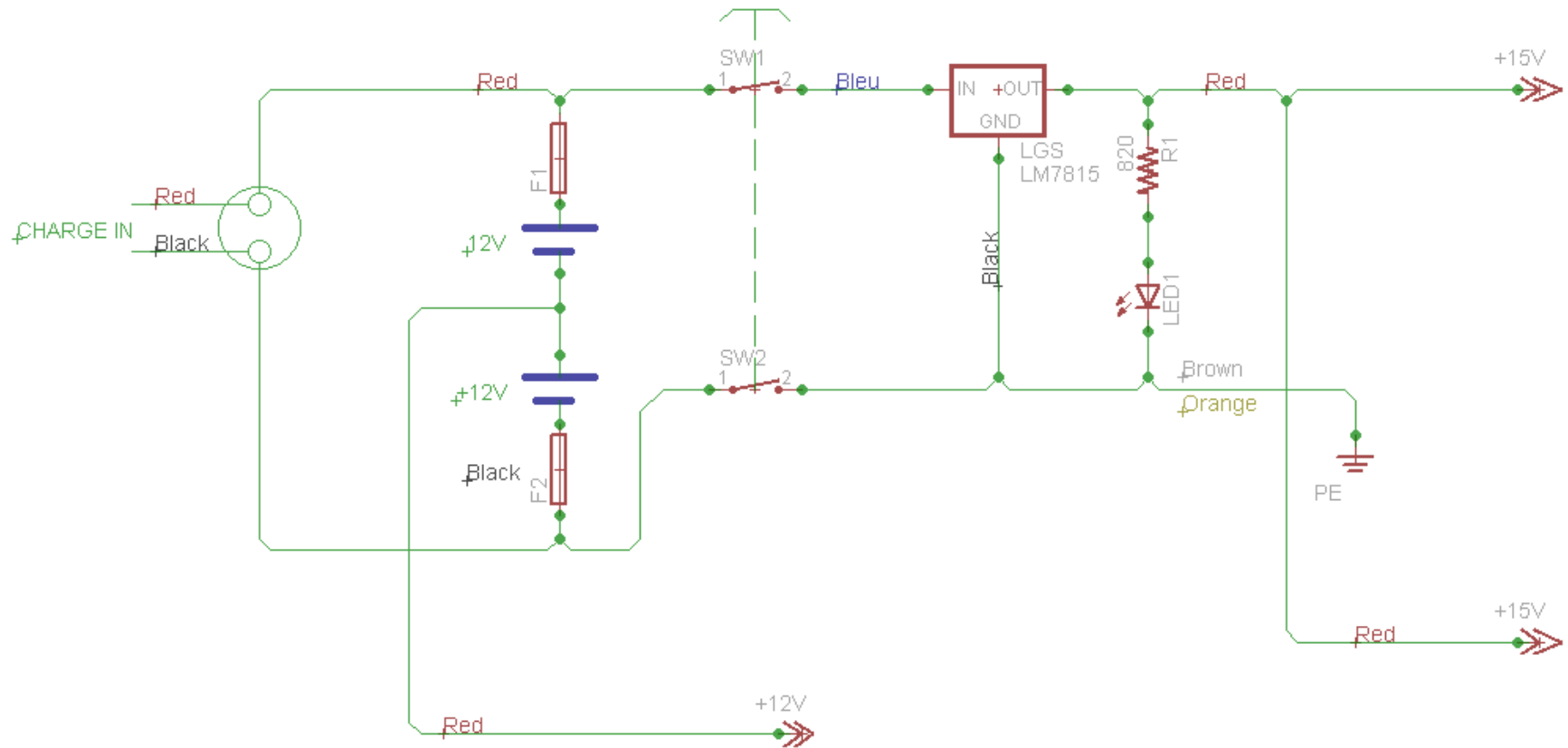


Fig. 5.7: CEUT Electrical connections, part 2.

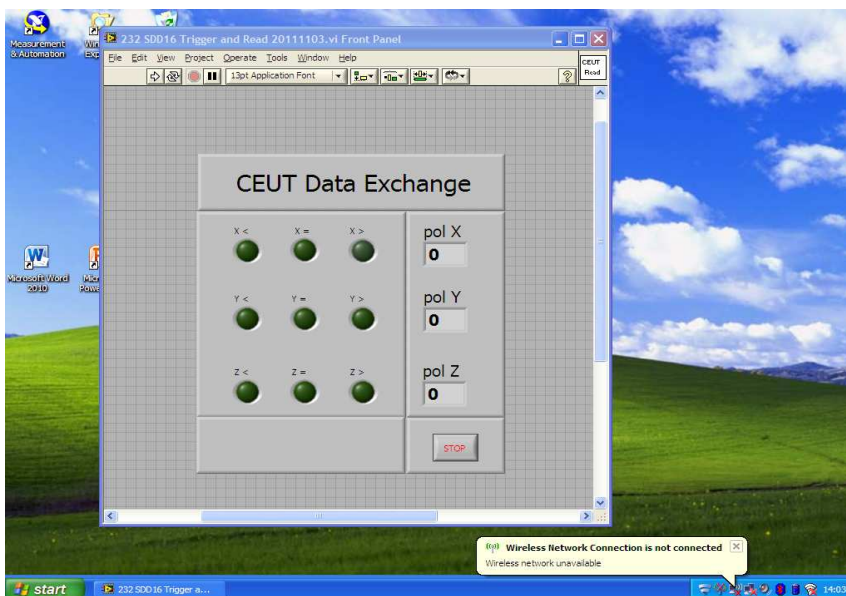
5.5 User's quick reference guide

- Turn on the notebook and open test program

Wait until the desktop screen appears.

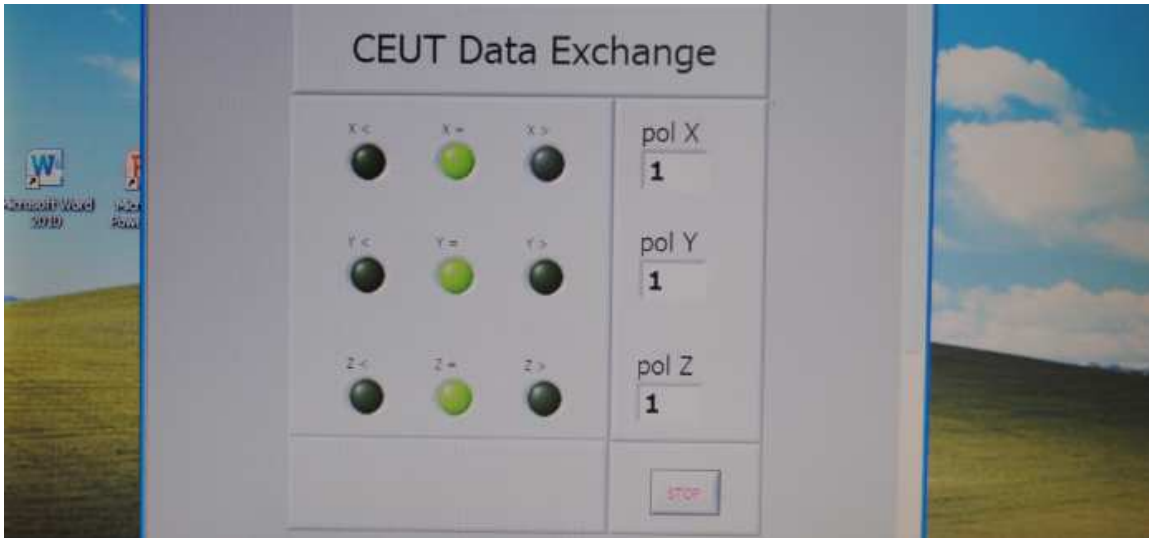


When you open test program, the communication interface appears next



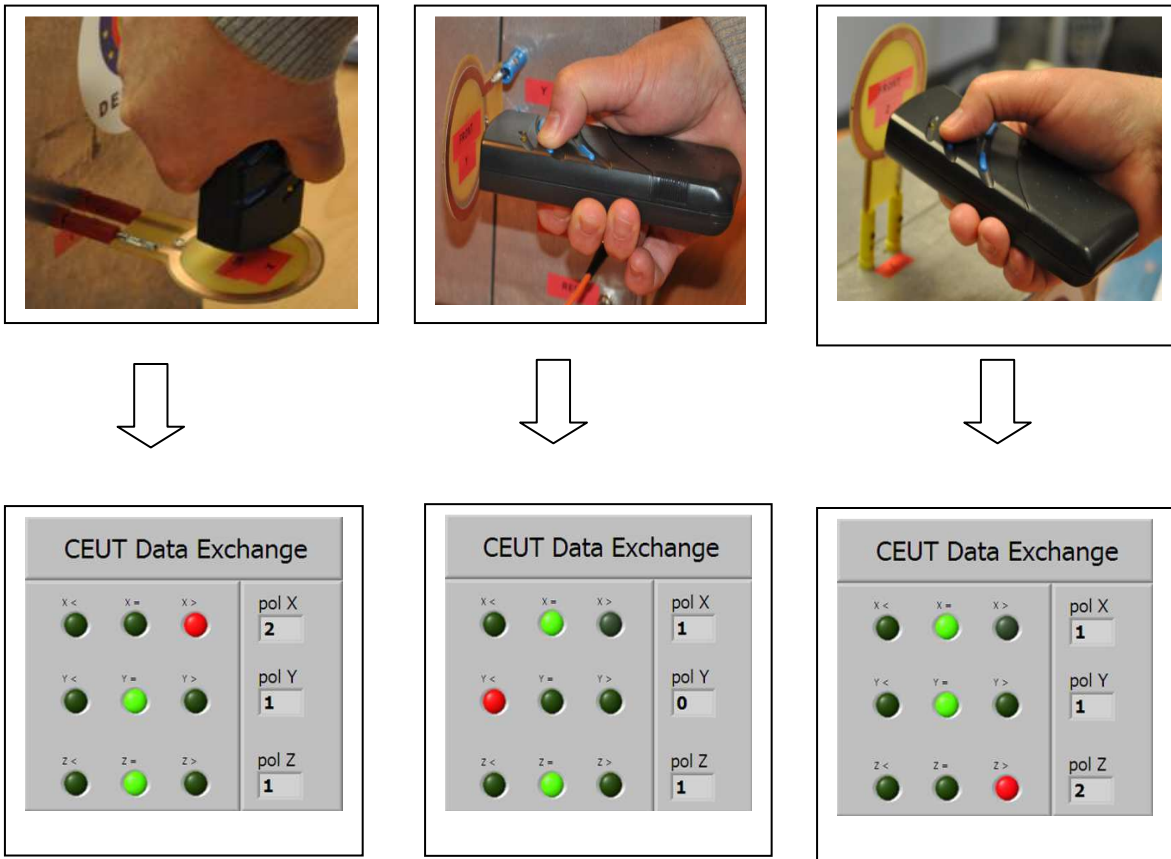
- **Run the program**

In the menu bar, click on **“Operate”** and then **“Run”** or simply make a click in the arrow below the menu bar. When it is running, the green LEDs light up.



- **Verification test with the transmitter**

Approach the transmitter a few centimetres from each antenna, press on one of the buttons and see change on the communication interface



Now the CEUT is ready for use.

5.6 CEUT measurements in SAR then in RC

Before starting, some verifications of the CEUT have been performed. First, the CEUT has been measured in a SAR. It is

placed at 1 meter distance from the emitting antenna and submitted to immunity levels of 50 and 35 V/m with a pulse modulation of 1 kHz and 50 % duty cycle (Fig. 6.1). Then, the response as a function of frequency and immunity level has been recorded (

Fig. 5.8). In the RC, the CEUT is placed in the working volume and submitted to immunity levels of 50 and 35 V/m with the same modulation as in SAR. The response as a function of frequency, immunity level and type of tuner is recorded (Fig. 5.9 and Fig. 5.10).

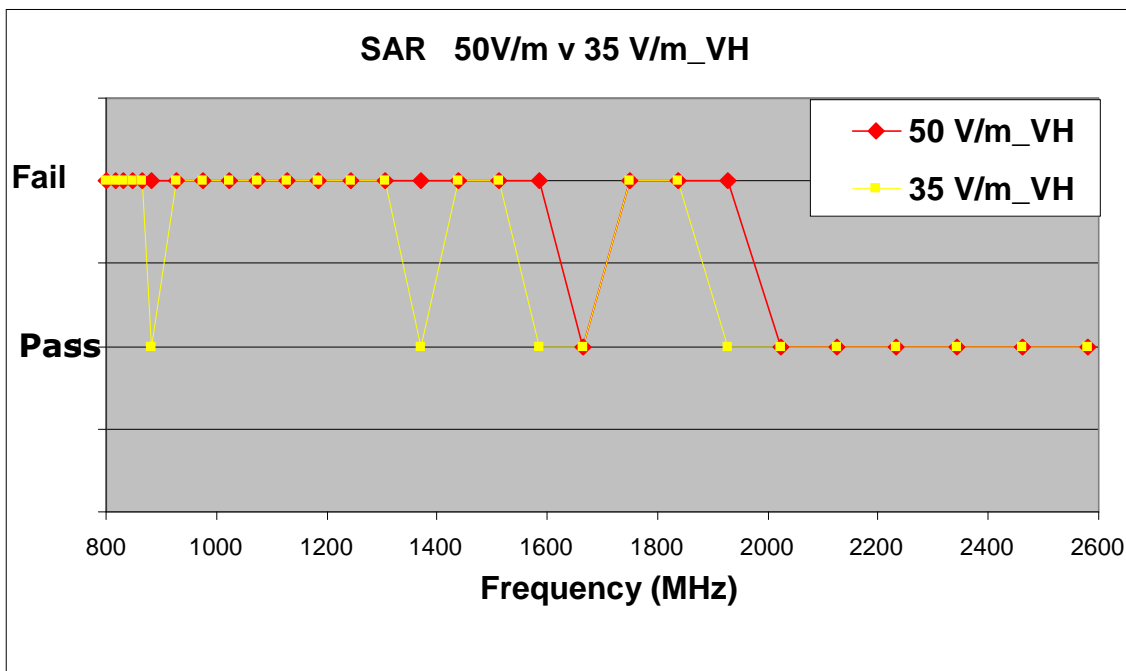


Fig. 5.8: Response of CEUT to Frequency and Immunity level in a SAR

Fig. 5.8, Fig. 5.9 and Fig. 5.10 give the reaction of the CEUT to the electric field as a function of frequency. This reaction is characterized by the status "Pass" or "Fail" given on the y-axis. "Pass" means that the CEUT does not react to the electric field and "Fail" means that the CEUT has reacted (one or more of the three

channels give counting results lower or higher than the expected value, which is 100).

From Fig. 5.8, two observations can be made. Firstly, the frequency response is as designed and predicted in Fig. 5. 3. At frequencies below about 1600 MHz, the average power picked up by the loop is higher and sufficient to disturb the counting process and to give a FAIL. Above 1600 MHz, as the average power is lower, the opposite happens. This means also that by adapting the dimensions of the loop, the CEUT can fit any desired frequency BW. Secondly, the CEUT becomes less reactive when the immunity level is reduced (from 50 to 35 V/m).

The behaviour in the RC (with 37 tuner steps) is given in Fig. 5.9 and Fig. 5.10. As in the SAR, the susceptibility becomes lower when the frequency increases, and the system is less reactive when the immunity level is reduced (with one exception). Note that at the maximum frequency, for 50 V/m, we have a FAIL. Maybe this can be explained by the trend in the behaviour of the Alford loop when the frequency increases.

The last acceptance test for the CEUT is to verify that the frequency response does not change when modifying the tuner (STATIC or RAIL) (see Fig. 5.10). The response is the same with the two types of tuners (STATIC or RAIL, with 37 tuner steps), with one exception out of the 28 frequencies analysed. It can be concluded that there is a good reproducibility.

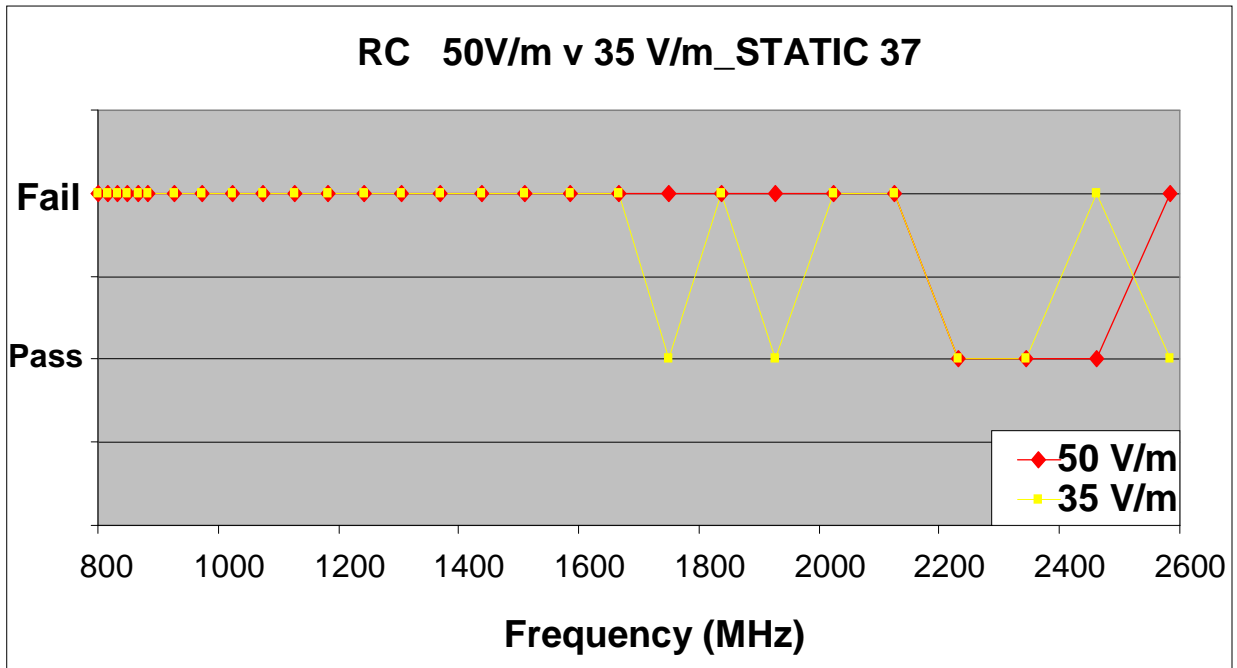


Fig. 5.9: Response of CEUT to Frequency and Immunity level in RC

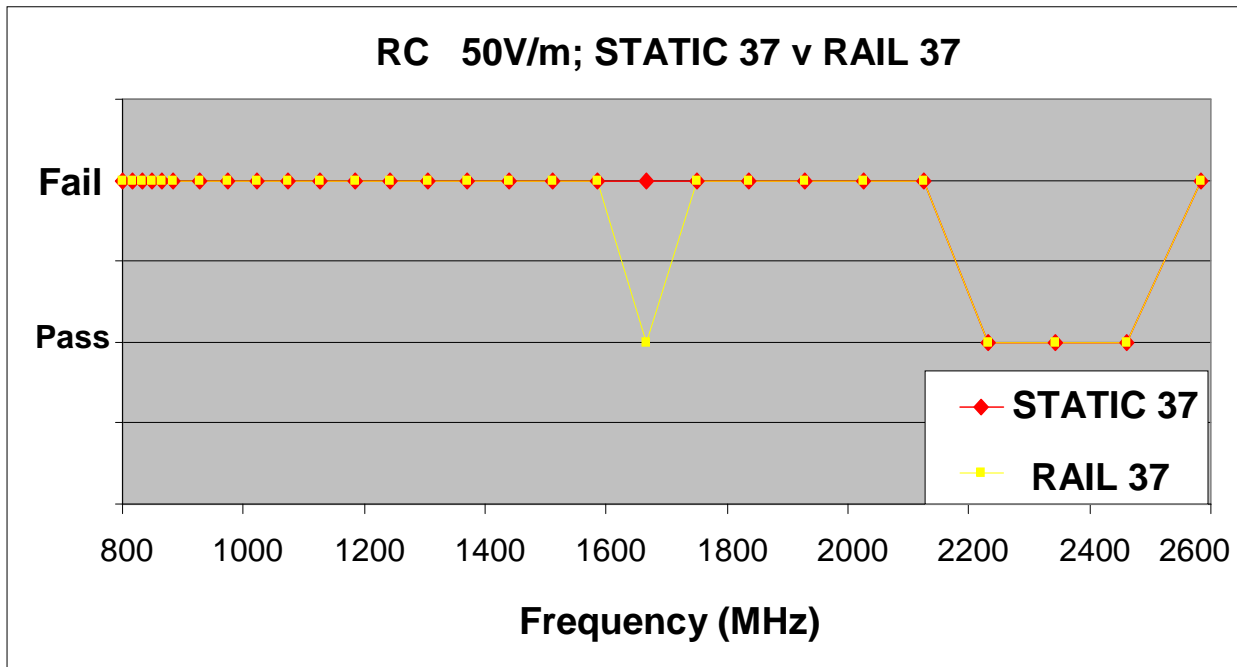


Fig. 5.10: Response of CEUT to different types of tuners.

5.7 Interlaboratory testing in Belgium and Japan

The CEUT has been presented during a meeting of ABLE (Accredited Bodies and Laboratories in Electrotechnics, www.ce-able.eu) during the year 2011. As one of the objectives of ABLE is Interlaboratory or Round Robin testing and, also, because a Round Robin in radiated immunity has never been done, the members decided to use the CEUT as reference material for a Round robin testing in radiated immunity to electric field according IEC 61000-4-3.

The Royal Military Academy coordinated this interlaboratory testing for the technical aspects and ANPI asbl for the administrative aspects. The following EMC testing laboratories have participated to the Interlaboratory testing between May and Augustus 2012:

- 1) Laborelec;
- 2) Lemcko;
- 3) More@Mere (BGEMC);
- 4) Université de Liège (Laboratoire CEM);
- 5) BARCO;
- 6) PHILIPS (EMC Test lab) (Netherlands);
- 7) Royal Military Academy;
- 8) ANPI asbl;
- 9) Laboratoria De Nayer;
- 10) Pioneer (Japan);

11) Fuji Xerox (Japan);

The tests have been carried out according IEC 61000-4-3, on a discrete series of frequencies and at different Electric field values. One part of the results is given in Fig. 5.11.

Orientation 1

Frequency	85	95	150	250	350	450	550	650	750	850	950	1.3	1.6	1.9	2.2	2.5	2.9	
Pol V	1	1	1b		1	1	1	1	1	1	1							
	1b	1b			1b	2												
	2	2			2	2	2	2	2	2	2							
	3	3			3	3	3	3	3	3	3							
	4	4			4	4	4	4	4	4	4							
	5	5	5		5	5	5	5	5	5	5							
	6	6			6	6	6	6	6	6	6							
	7			7	7	7	7	7	7	7	7							
	8	8	8			8	8	8	8	8	8	8	8	8	8	8	8	8
	9	9	9	9		9	9	9	9	9	9	9	9	9	9	9	9	9
10	10	10	10	10	10	10	10	10	10	10	10	10	10	10	10	10	10	
Fail			1	1														
			2	1b														
			3	2														
	4		4	3														
			6	4														
		7	7	5														
			8	6														
				7														
				8	8													

Fig. 5.11: Interlaboratory testing results (a part), CEUT exposed to E-field

We see that at 150 and 250 MHz the CEUT fails and most of the EMC laboratories detect it. The complete report is given in Annex 4.

The third-party comes to the conclusion that the CEUT remains stable during the interlaboratory testing except at some frequencies, see the conclusion, point G of the report, in Annex 4.

We see also the large coherence in the results obtained by the participating Laboratories. From 450 MHz to 2900 MHz, the result was the same (PASS) for all the labs. At 85 MHz and 350 MHz, only one lab obtained a FAIL while for all the others, it was a PASS.

This enhances the confidence we can have in the CEUT as a common reference equipment under test.

And this is also the case in horizontal polarization, as can be seen in annex 4.

6. Comparison of radiated immunity testing performed both in a reverberation chamber and in a semi-anechoic room

6.1 Introduction

In MIL-STD-461F [3], test RS103 (radiated immunity testing to electric field) allows the use of a RC as an alternative to the SAR. As military equipment can be related to life safety, it is of great importance that the testing results are independent of the types of room used. It can have dramatic consequences to allow the use of a RC while the testing results are less severe than in a SAR. We will give recommendations on the use of RC's for immunity testing. We will see that **the testing severity depends on the number of tuner steps**. As the method is quite similar, the recommendations will be extended to the civil IEC 61000-4-3 standard [27].

With this purpose, we have used the SAR and the RC at RMA equipped with the two innovative tuning systems previously described; the first one is the RAIL, extensively described in chapter 2, and the second one is the static tuning (STATIC), described in chapter 3.

We limited our work to the 800 – 2600 MHz frequency bandwidth. This range covers most of the cellular mobile phone networks. The lower limit is equal to ten times the eigen resonance frequency of the RC and is dictated by field uniformity requirements, while the upper limit is determined by the power amplifier high frequency cut-off. The experimental plan is as follows: tests are made in both environments. For RC both types of tuners (RAIL & STATIC) are

evaluated, with two values of tuner steps (12 and 37). All this at 50 V/m and 35 V/m. The figure of 12 is a requirement of the standard. With the assumption that a figure of 12 could be insufficient to obtain the same severity level as in the SAR, we have extended this figure to 37. This last figure assures good field uniformity within an acceptable testing time. All this has been performed at 50 V/m as required by the standard. In order to investigate the possible dependence between stirrer type and field-power relation in our RC, it has also been carried out at 35 V/m.

The CEUT (presented in chapter 5) has been designed and constructed to be representative of most of modern digital electronics and which susceptibility is not linked to some polarization state. Hence, it consists of a coupling part, a sensitive electronic part and some electronic modules for the remote control and visualization of the status of the CEUT. It is battery-powered.

During the study, we found some unexpected links between the ratio of the maximum to the average value of the rms electric field in one spatial point, and the "quality" of the field uniformity, as defined in IEC 61000-4-21 [2]. This link will be further explained in section 6.6.

6.2 Measurement Set-up

6.2.1 Semi-Anechoic Room (SAR)

The dimensions of the SAR are 8.55 m x 5.4 m x 5.2 m (L x l x H). The floor is covered with metal and the walls and ceiling with RF absorbers. The CEUT is placed at 1 meter from the antenna aperture (see Fig. 6.1). Calibration and testing are made according to MIL-STD-461F. The calibration is performed at both vertical and horizontal polarizations for 50 and 35 V/m and from 800 to 2600 MHz. First, the electric field is calibrated without modulation (see

Fig. 6.1, left); then, the test is done (see Fig. 6.1, right) with modulation; the field strength sensor is only for monitoring and not for levelling.



Fig. 6.1: Set-up for calibration (left) and testing (right).

6.2.2 RC with the STATIC tuner

The cubic RC with sides of 2.48 m has its fundamental resonance at 85.15 MHz. It is worth to note that the LEMA RC was originally a cubic Faraday cage that has been converted to an experimental RC by setting a mode stirrer in it. The cubic shape is quite inconvenient because of the mode degeneration but this has been partially compensated by high-quality mode tuner design. Considering a “factor 9” rule of thumb with regard to the minimum number of cavity modes to assure statistical field homogeneity, it exhibits an LUF of about 800 MHz, which is low enough for the present experimental purpose. A general scheme showing the interconnections is given in Fig. 6.2.

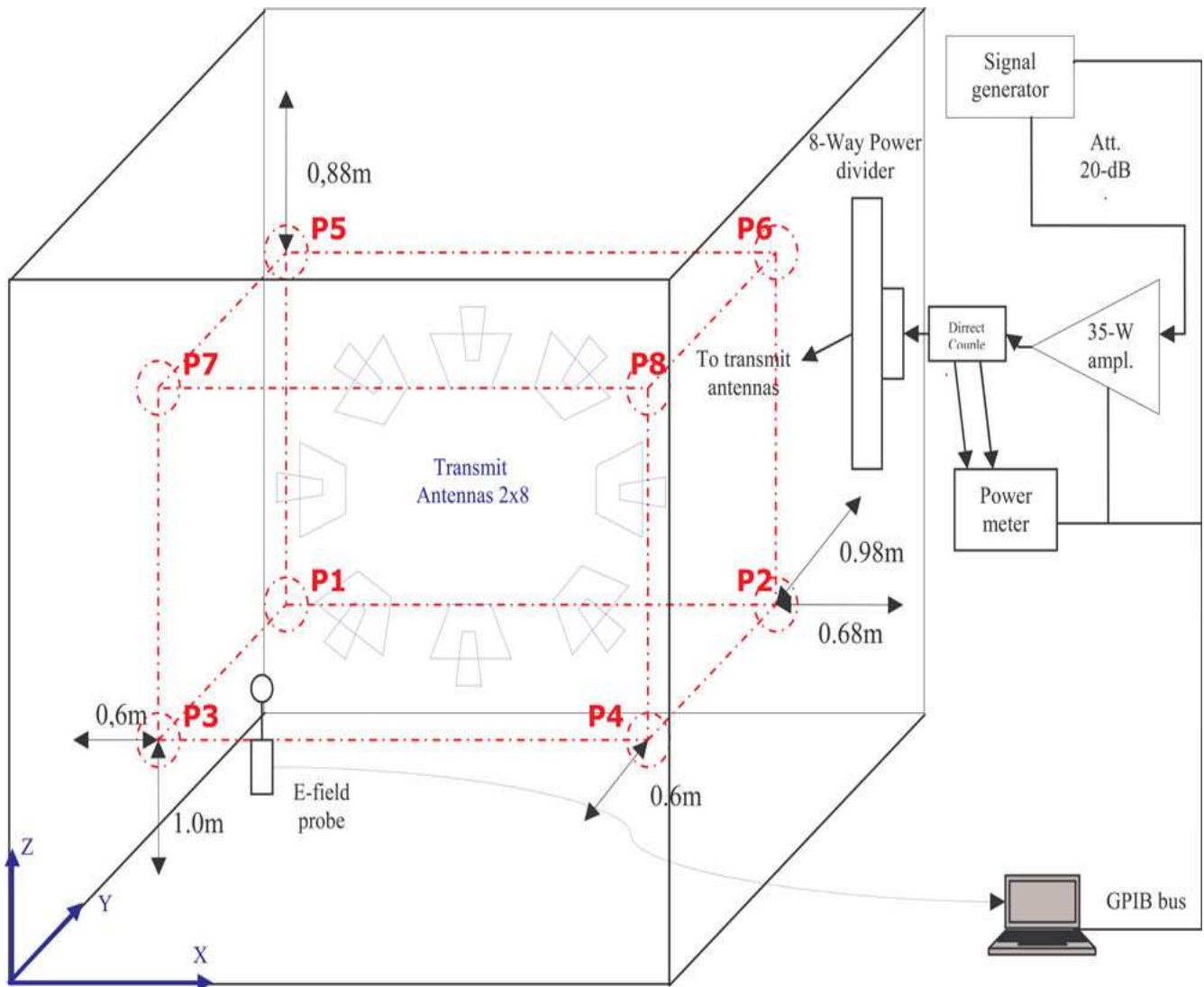


Fig. 6.2: General interconnection scheme for the RC with STATIC tuner.

The first innovative tuner is composed of an array of 2×8 antennas (see Fig. 6.3). They are fixed on a rectangular plexiglas plate of 2.5 m long, 1.25 m wide, and 6 mm thick. It is placed at 46 cm in front of one of the walls of the chamber. The largest distance between any two antennas is 1.8 m and the smallest is 0.8 m, so the total surface delimited by the eight antennas is about 1.44 m^2 . The antennas are directed towards the walls of the chamber and do

not directly illuminate neither the working volume nor the E-field meter for preventing direct coupling from the sources. In practice, direct coupling to the EUT would alter the expected Rayleigh probability density function of the field, yielding a Rice–Nakagami distribution due to the presence of some deterministic part in the stochastic field [20], [48].

Each of the eight pairs of antennas is connected to a single pole double throw RF switch. The input of each RF switch is connected to the eight-way power divider. The two complementary outputs of a switch are connected to a pair of antennas in such a way that, at any time, the RF power is radiated into the RC by eight antennas. An eight-digital output board placed outside the chamber controls the RF switches. This board is connected to a PC via an USB bus and allows for the sequencing. A complete description of this tuning method can be found in [49] and in Chapter 3. The input of the power divider is connected to the 35-W power amplifier.

The advantages of such a system in comparison with the conventional paddle are that it requires no rotating part, is less cumbersome and saves space in medium and small sizes chambers, and that the electronic tuning reduces the time between steps. The disadvantage of the STATIC tuner is that it requires more antennas, a more complicated feeding network with cables and switches, losses in power splitter and cables and, as a consequence, a more powerful amplifier.

The sequencing of the RF switch control has been chosen in such a way that it minimizes the amount of switching over a whole tuning cycle. It also realizes the same number of transitions for the eight switches. For 37 tuner positions, there are about ten transitions by switch, meaning that the antenna-pair associated emits ten times over a scan.

An electric field uniformity validation has been conducted according to the requirements of IEC 61000-4-21. The working volume considered is 1.2 m × 0.9 m × 0.6 m centred at 0.8 m height, in the middle of the RC (it is delimited by points P1–P8 of Fig. 6.2). The standard deviation of each component is less than the 3-dB limit of the standard, over the whole frequency range of interest, with a margin of 0.5 dB.

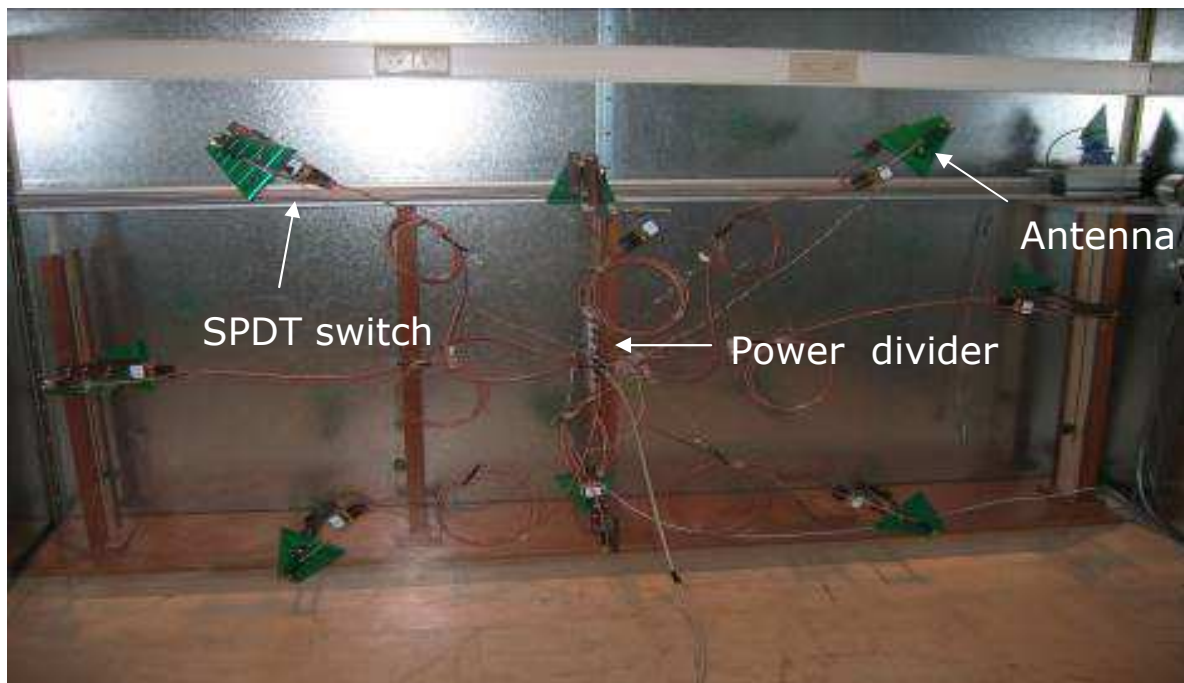


Fig. 6.3: The STATIC tuner with 8-pairs antenna array.

6.2.3 RC with the RAIL tuner

The RAIL tuner is installed in the same RC as the STATIC one. It is composed of two orthogonal rails with an antenna mounted on each of the moving cart (Fig. 6.4). The horizontal one (rail A) is 2.48 m long and set at 1.25 m from the floor. The vertical one (rail B) is 2.08 m long and placed at 1.39 m from the back wall and at 1.09 m from the front wall. The number of steps for rail A (used length: 2.05 m) and for rail B (used length: 1.65 m) is 20 and 17 respectively for 37 total tuner steps or positions. The length

of a single step is 2.5 cm; 10 cm and 15 cm for 150; 37 and 12 total tuner (rail A + rail B) positions, respectively. The advantages of this system are the same as for the STATIC one, except that it requires moving antennas on the rails. The disadvantage of the RAIL tuner is the need for a rail controller and the movement of the antenna cables.

An electric field uniformity validation has been conducted in the same manner as for the STATIC tuner. The standard deviations are below the 3-dB limit for each polarization and for the total field, for the two numbers of steps (150 and 24). The results for the case of 150 steps are the best (a margin of 1 dB). The margin is reduced to 0.5 dB for 24 steps. This margin is worse than the previous one, because this value is closer to the maximum limit of 3 dB given by the standard. This is equivalent to the STATIC tuner with 37 steps. A complete description of this tuning method can be found in [12] and Chapter 2.



Fig. 6.4: The RAIL tuner with two orthogonal rails.

6.2.4 Data acquisition of E-field and others

The PC is the centre of the test system. The following elements are connected to it:

- 1) NARDA EMR-300 + E-field probe AC-0004 (3 MHz-18 GHz) (RS232 connection);
- 2) Electronic circuit board for the control of the Static tuner (USB connection);
- 3) An SMR-40 signal generator from R&S (GPIB connection);
- 4) A 35 W amplifier from MILMEGA (GPIB connection);
- 5) An NRP power meter from R&S (GPIB connection);
- 6) The two rails controller (USB connection);
- 7) The CEUT (USB connection).

Moreover, LabVIEW software has been developed. It allows for the calibration and testing according MIL-STD-461F, RS103 in a reverberation chamber.

At each frequency, measurement is done of the three components (E_{rmsx} , E_{rmsy} and E_{rmsz}) of the E-field for the N steps of the tuners (STATIC and RAIL):

$$\begin{array}{l}
 \cdot E_{rmsx1} \quad E_{rmsy1} \quad E_{rmsz1} \quad \longrightarrow \quad E_{rms1} \\
 \cdot E_{rmsx2} \quad E_{rmsy2} \quad E_{rmsz2} \quad \longrightarrow \quad E_{rms2} \\
 \cdot E_{rmsxN} \quad E_{rmsyN} \quad E_{rmszN} \quad \longrightarrow \quad E_{rmsN}
 \end{array}
 \left. \vphantom{\begin{array}{l} \cdot E_{rmsx1} \quad E_{rmsy1} \quad E_{rmsz1} \quad \longrightarrow \quad E_{rms1} \\ \cdot E_{rmsx2} \quad E_{rmsy2} \quad E_{rmsz2} \quad \longrightarrow \quad E_{rms2} \\ \cdot E_{rmsxN} \quad E_{rmsyN} \quad E_{rmszN} \quad \longrightarrow \quad E_{rmsN} \end{array}} \right\} E_{rms-avg} = \frac{1}{N} \sum_{i=1}^N E_{rmsi}$$

$$\begin{array}{ccc}
 \downarrow & \downarrow & \downarrow \\
 \underbrace{E_{x-max} \quad E_{y-max} \quad E_{z-max}} & &
 \end{array}$$

$$E_{max-avg} = \frac{E_{x-max} + E_{y-max} + E_{z-max}}{3}$$

Fig. 6.5: E-field calculations details.

The E_{rms1} , for example, is calculated as the square root of the squares of E_{rmsx1} , E_{rmsy1} and E_{rmsz1} . At the end of the tuning cycle, $E_{rms-avg}$ and $E_{max-avg}$ are calculated as indicated in Fig. 6.5.

Note that E_{x-max} does not necessary occur at the same step as E_{y-max} or E_{z-max} .

6.2.5 Calibration of RC

The RC has to be calibrated for 50 and 35 V/m, i.e., the power needed at the input of the amplifier for generating such field strength in the chamber has to be determined. We place the E-field probe at one spatial point inside the working volume (as defined in 6.2.2) and we calibrate according MIL-STD-461F. In this case the calibrated field E_{cal} is:

$$E_{cal} = \frac{E_{x-max} + E_{y-max} + E_{z-max}}{3} \quad (6.1)$$

The calibration process uses the following relation in order to find the new output value of the signal generator

$$LVL_{Test} = LVL_{cal} \times \frac{E_{Test}^2}{E_{Cal}^2} \quad (6.2)$$

where E_{Test} is the requested calibration level (50 V/m for example for MIL-STD-461F). If this level is not obtained, a new value for LVL (LVL_{Test} : Level output at the SMR-40 signal generator) is calculated, taking into account the measured E_{Cal} and the actual LVL_{cal} . This iterative process is quite efficient, because in approximately 2 searches the appropriate LVL_{Test} value is found for the requested calibration level, within an accuracy of $\pm 7.5\%$.

At the end, a calibration file is created, containing, an index, the frequency, the level (LVL) that will be used to program the signal generator, the electric field requested, the electric field measured and the forward power of the amplifier P_{Fwdcal} . In order to take into account different output power levels of the amplifier when testing, in comparison with the levels present when calibrating, an adjustment is made during testing by the measurement of the amplifier output power $P_{Fwdtest}$ and using the relation below:

$$LVL_{New} = LVL_{Old} + P_{Fwdcal} - P_{Fwdtest} \quad (6.3)$$

where,

- 1) LVL_{Old} is the generator output level from calibration;
- 2) LVL_{New} is the generator output level during the test.

The order of magnitude of the adjustments is from 0 to 0.3 dBm.

It is important to note that, in the SAR, 50 V/m represents the rms value of E-field as directly measured by a common E-field meter, while in the RC, we have to measure the rms values of the three polarizations for each tuner step, then take the maximum over the tuner cycle and finally do the mean, the results is $E_{\max-avg}$ (as calculated in Fig. 6. 5), this corresponds to "case 2" described in [50].

6.3 Immunity testing results: SAR versus RC

We recall the CEUT has been exposed in the SAR to 50 V/m in one aspect angle and two polarizations. In the RC, it was exposed to the same immunity level, both for the RAIL and STATIC tuning method, using each 37 steps.

The intercomparison of the results obtained in the SAR and in the RC gives a very important result.

One can see that **testing in an SAR (with one aspect angle and two polarizations) is less severe than testing in a reverberation environment with 37 tuner steps.**

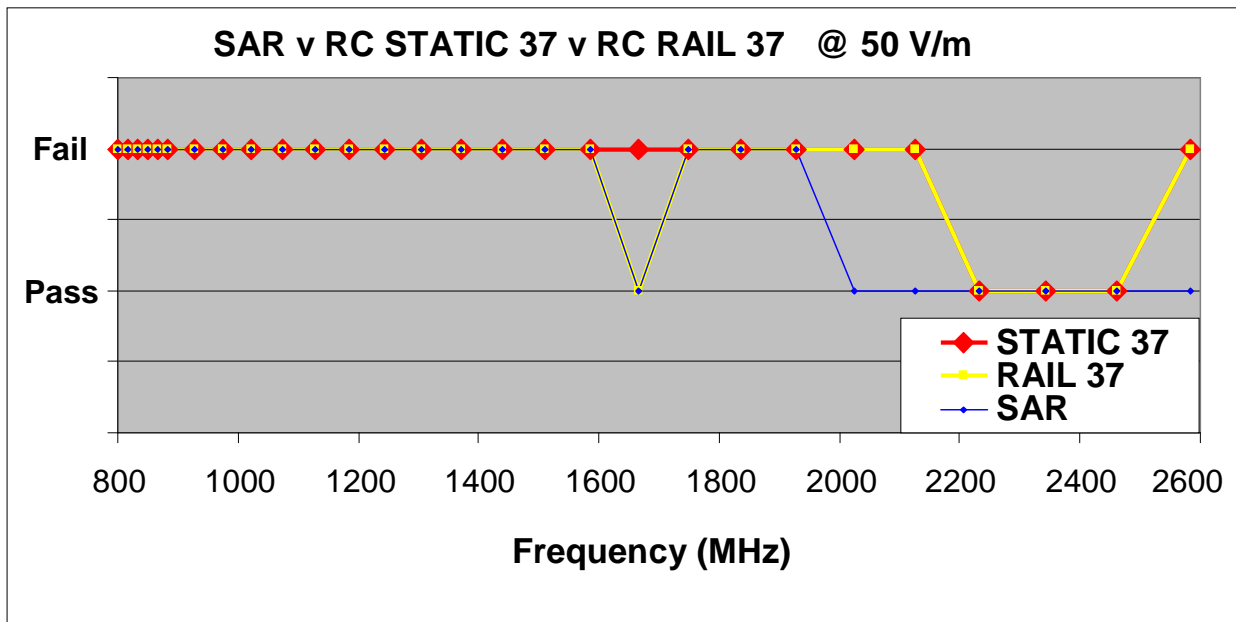


Fig. 6.6: Comparison SAR v RC; 37 steps and 50 V/m.

The semi-anechoic environment yields a Pass for four (three) frequencies out of 28, whereas in a reverberation room, using the STATIC (RAIL) method, there is a Fail. Note that at about 1650 MHz, where there is a difference for the RC tuning methods, the semi-anechoic and RC RAIL methods agree. They indicate both a Pass.

The same conclusion holds for the 35-V/m immunity level, see Fig. 6.7. Testing in an SAR (one aspect angle and two polarizations) is less severe than testing in a reverberation environment with 37 tuner steps. The semi-anechoic environment yields a Pass for seven frequencies out of 28, whereas in a reverberation room, using the static method, there is a Fail. This is also a good point for the reproducibility.

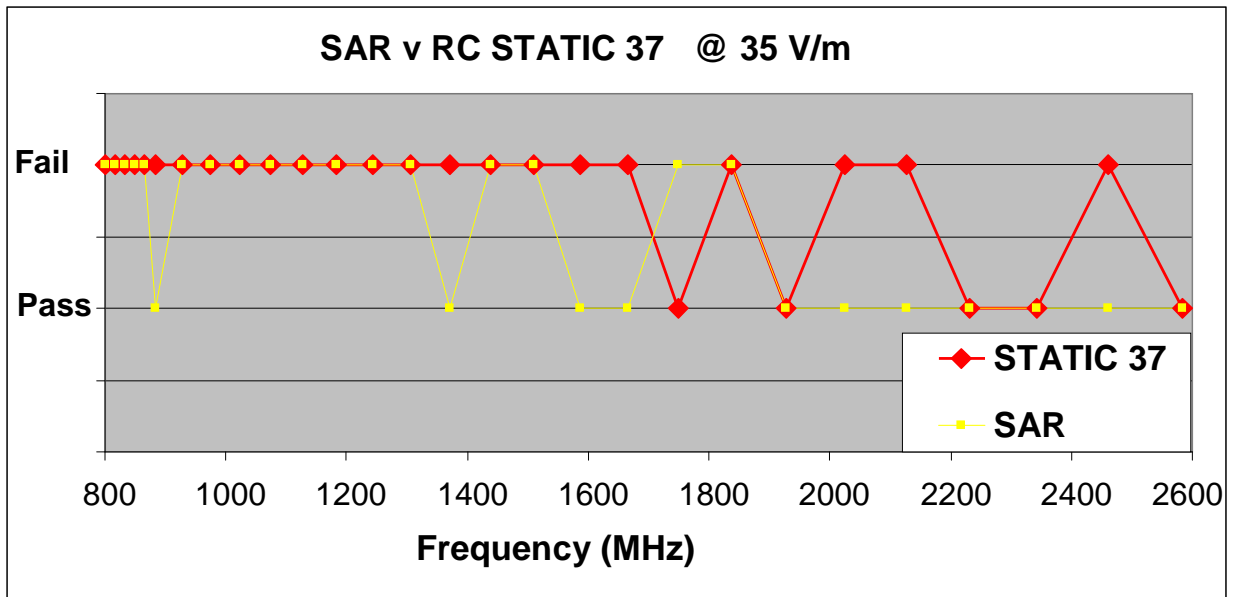


Fig. 6.7: Comparison SAR v RC; 37 steps and 35 V/m.

What about the influence of the tuner steps.

Fig. 6.8 and Fig. 6.9 show clearly the influence of the number of tuner steps. The higher the number of tuner steps, the higher the test severity, and this for both methods.

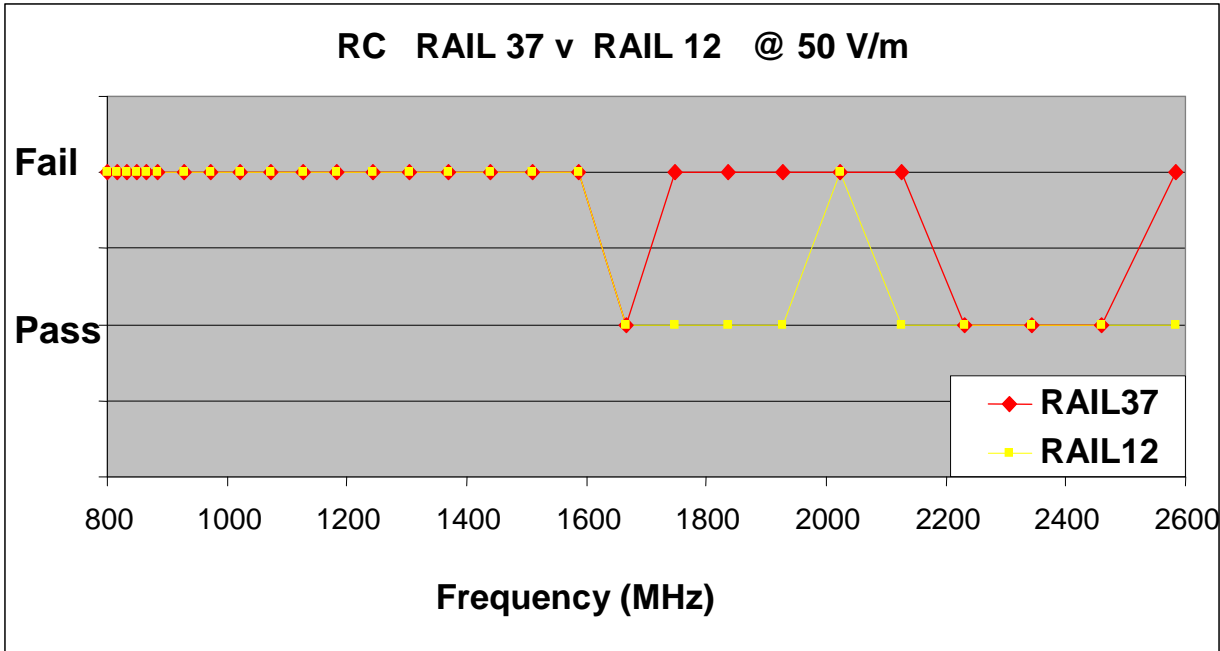


Fig. 6.8: Comparison RC RAIL method; 37 v 12 steps.

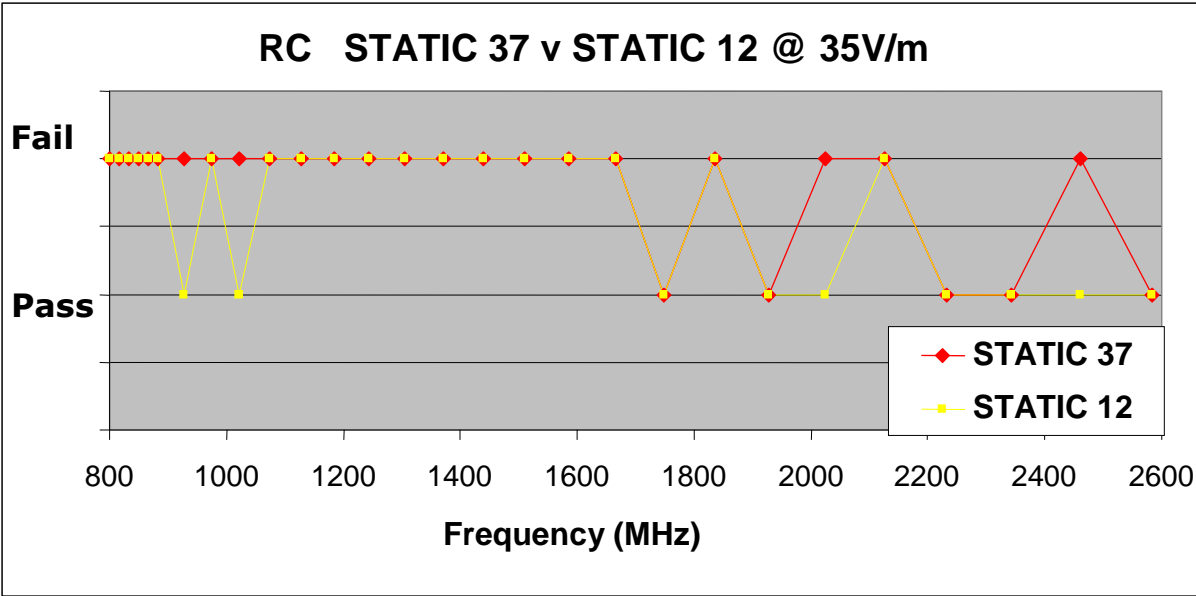


Fig. 6.9: Comparison RC STATIC method; 37 v 12 steps.

Let us resume: we found that RC testing is more severe than anechoic for high values (37) of tuner steps (Fig. 6.6 and Fig. 6.7). But also that reducing the tuner step will lower the severity (Fig. 6.8 and Fig. 6.9). So, intuitively, we can easily conclude that within

about 20 to 30 tuner steps the equivalence in testing results in a RC comparing with a semi-anechoic environment is achieved with one aspect angle and two polarizations in the SAR. But, why is the test with less tuner steps less severe? Is it because of the fact that the power with less tuner steps is lower or because of a lower Erms-avg field or because of the angles of incidence?

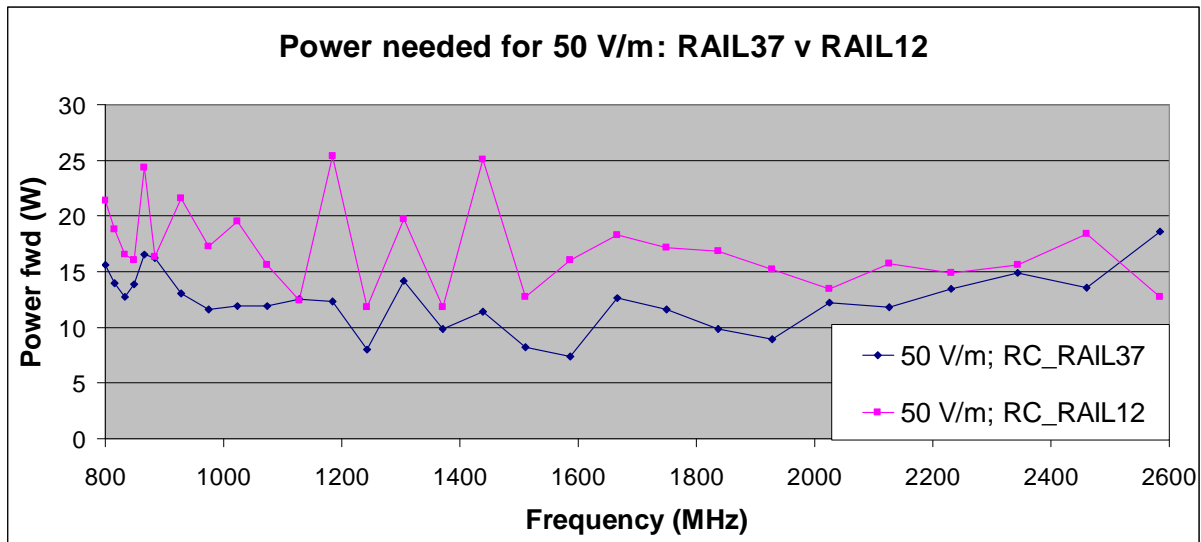


Fig. 6.10: Transmitted power, RAIL37 v RAIL12.

The severity is not linked to the transmitted power (written P_{fwd}) as more power is needed for 12 steps in order to achieve the $E_{max-avg}$ (see Fig. 6. 10) level of 50 V/m. Even with this supplementary power the CEUT remains less disturbed with 12 steps than with 37.

The fact that less power is needed when increasing the tuner steps, this is in accordance with theory [51]:

$$\frac{\langle P_{fwd2} \rangle}{\langle P_{fwd1} \rangle} = \frac{\gamma + \ln(N_1 + 1) - \frac{1}{2 \cdot (N_1 + 1)}}{\gamma + \ln(N_2 + 1) - \frac{1}{2 \cdot (N_2 + 1)}} \quad (6.4)$$

Where:

$\langle P_{fwd2} \rangle$ and $\langle P_{fwd1} \rangle$ are the mean forward powers transmitted to antennas over one tuning cycle, corresponding to N_2 and N_1 number of tuner steps, respectively, (W);

- $\gamma = 0.57722$.

Applying (6.4) to our measurements (Fig. 6.10) gives a ratio

$\frac{\langle P_{fwd2} \rangle}{\langle P_{fwd1} \rangle} = 0.726$ averaged from 800 to 2600 MHz, and taking for

$N_1=12$

and $N_2=37$, we obtain a value of 0.739, i.e. -1.7 % relative deviation from theory.

What about the Erms-avg (see Fig. 6. 5)? We recall that this is not controlled, contrary to Emax-avg which is the calibration level.

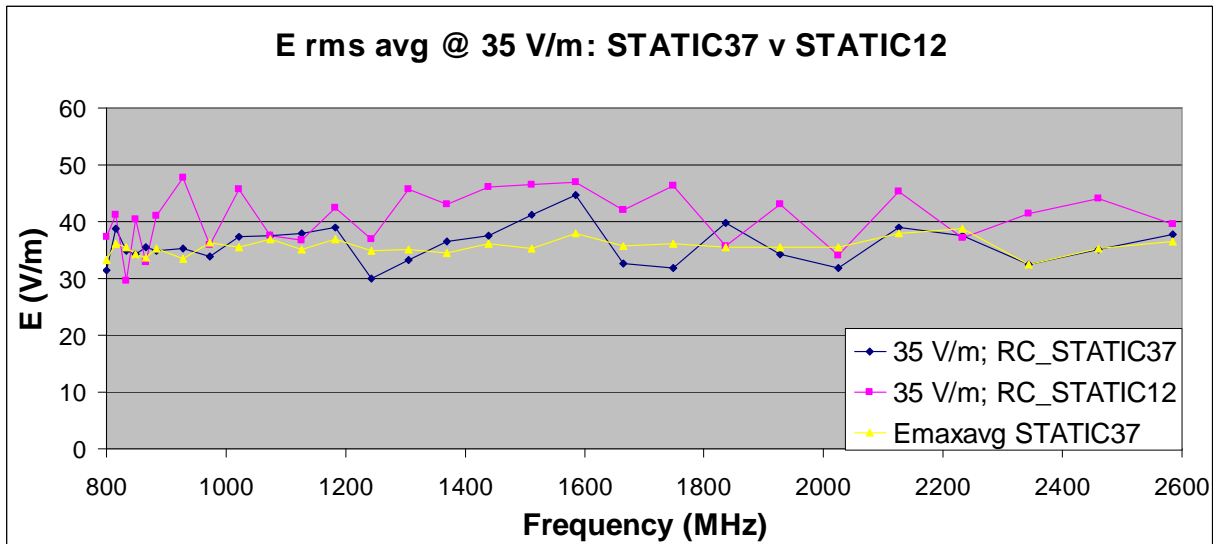


Fig. 6.11: Erms-avg, STATIC 37 v STATIC 12.

The severity is not linked to the Erms-avg as this value is higher for 12 steps (STATIC 12) than for 37 steps (STATIC 37). The testing is more severe with 37 steps because there are more angles of incidences.

6.4 Conditions for radiated immunity testing equivalence SAR v RC

These results allow giving general recommendations about the use of RC's in immunity testing, and, at the same time, trying to unify the testing and measurement results found in literature.

Up to now, we found that RC testing is more severe than SAR testing for a high number (37) of tuner steps (see Fig. 6.6 and Fig. 6.7). We also found that reducing the number of tuner steps lowers the severity (see Fig. 6.8 and Fig. 6.9). Intuitively, we may expect that with about 20–30 tuner steps, the equivalence in testing results between a RC and a SAR is achieved with one aspect angle and two polarizations in the SAR.

The results are summarized in Fig. 6. 12. There, the relation is established between the number of aspect angles in an SAR and the number of tuner steps in an RC. This figure yields very practical results. It can be seen that for MIL-STD-461F, RS103 radiated immunity testing (one aspect angle), it is recommended to use 20–30 tuner steps in order to have equivalence in the testing results. For IEC 61000-4-3 radiated immunity testing in an SAR (four aspect angles), it is recommended to use 40–60 tuner steps in order to obtain equivalence for the testing results.

In literature, several comparisons between SAR and RC have been made. We point out three of them. Firstly, in [52], where

a device with an external wire was tested, it is shown that the SAR with ten aspect angles is more severe than an RC with 50 tuner positions, which is in agreement with Fig. 6. 12. Secondly, in [53], a gas analyser was tested for one aspect angle in the RC and 20 tuner positions. A “good agreement” between the SAR and the RC was announced. Again, this is confirmed by Fig. 6. 12. Finally, we compare with the important work of Freyer and Bäckström. In [54], an error bias difference (the error bias is defined as the ratio of a measured response to the true maximum response) of 3 dB between a four and six aspect angle measurement in an SAR and a 12 tuner steps testing in an RC has been observed. This means that the SAR test is 3 dB more severe than the RC one, for the specified conditions. This is in agreement with Fig. 6. 12. Moreover, in further work [50], a four aspect angle testing in an SAR is found to have less error bias than a 12 tuner steps testing in an RC (comparison of Fig. 2 and 3 in [50]; only the maximum values are considered in Fig. 2. This means that the testing in an SAR is more severe. This is again in agreement with Fig. 6. 12.

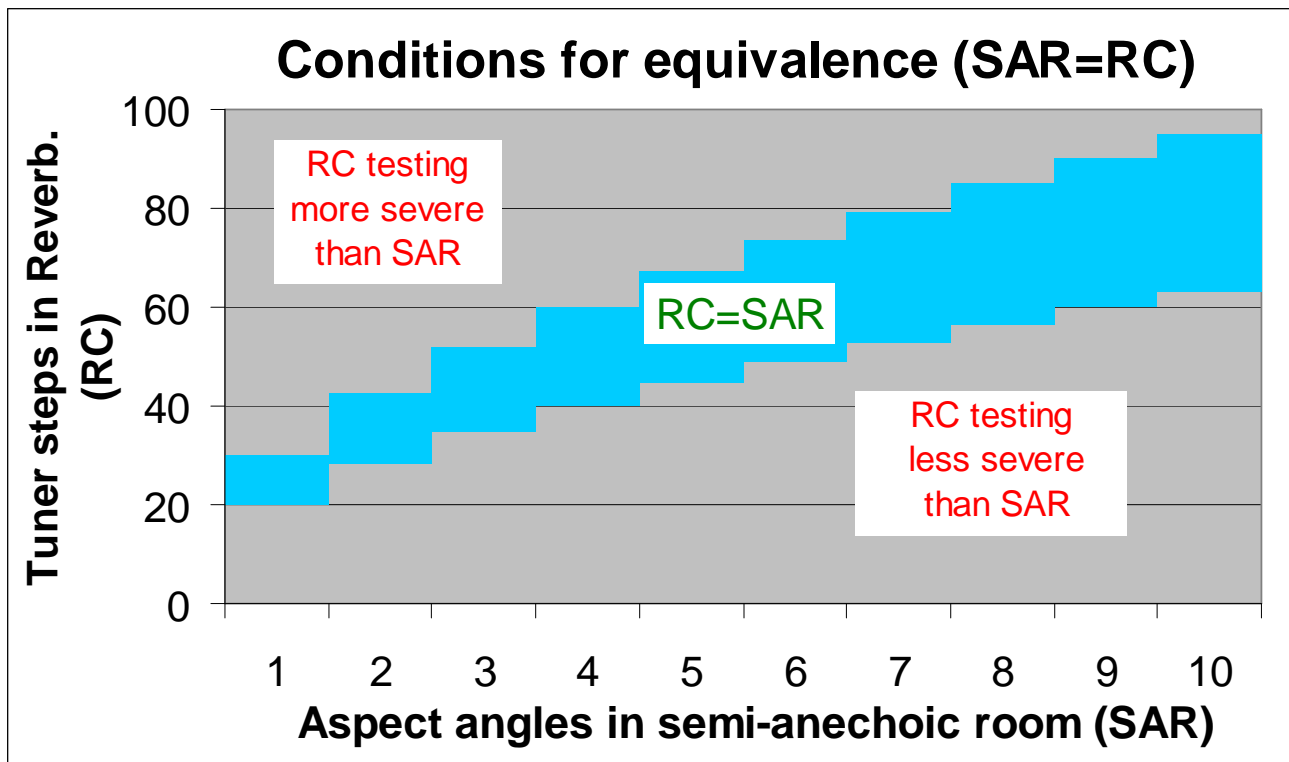


Fig. 6. 12: Tentative of unification of experimental results.

6.5 Power management

Two important practical questions to be answered are:

- 1) What is the power needed in SAR in order to obtain the required 50 V/m immunity level? Same question for the RC, for the two tuning methods.
- 2) Is it interesting to perform testing in RC rather in SAR taking into account only the power requirements aspect?

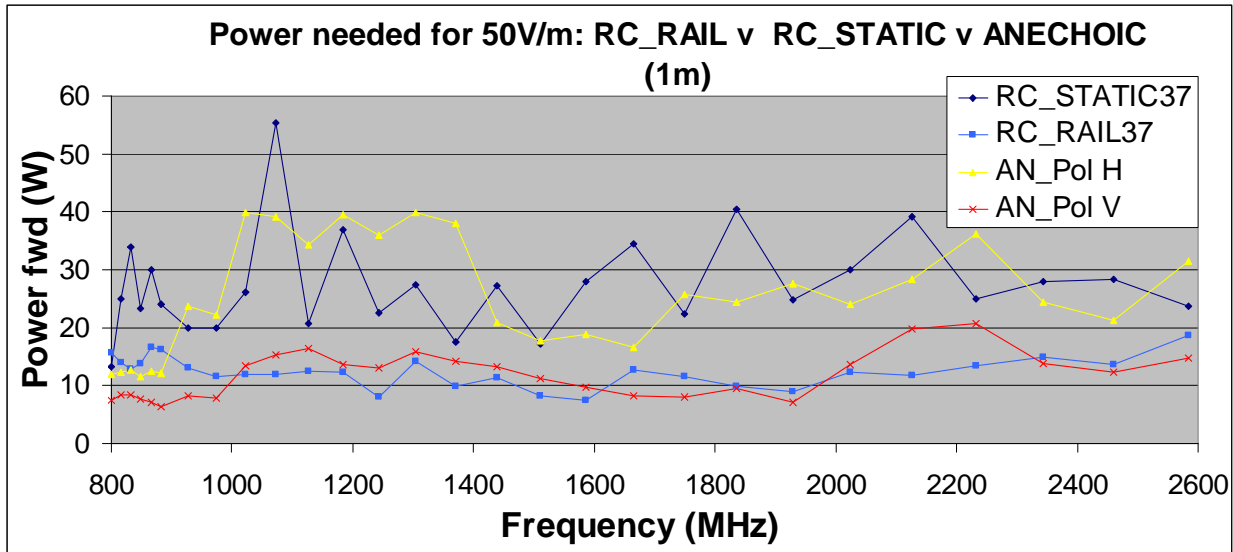


Fig. 6.13: Power requirements in SAR and RC.

From Fig. 6.13, we learn two things: firstly, rather the same power is needed by the RAIL method compared to the vertical polarization in a semi-anechoic environment, and the power needed for the horizontal polarization is rather the same as the one needed for the STATIC method. Secondly, the power needed for the RAIL method is 3 times (or 4.8 dB) lower than the power necessary to the STATIC method.

Note that in the MIL-STD-461F, RS103, the testing distance is 1 meter, compared to a testing distance of 3 meter required in the civil immunity standard IEC 61000-4-3. This implies that the power requirements in order to obtain the same electric field are 9 times (or 9.5 dB) higher when testing according the civil standard compared to the MIL-STD-461F. The attractiveness of RC's are reduced because the level of input power needed for a test in a RC is rather equivalent to the level of power needed in a semi-anechoic chamber for a 1 meter distance.

In a SAR:

$$E_{rms} = \frac{\sqrt{30.P_t.G}}{R} \quad (6.5)$$

Where P_t is the power, G the antenna gain and R the distance between the antenna and the spatial point where E_{rms} exists.

From this, we can deduce that:

$$\frac{\partial P_t}{P_t} = 2 \cdot \frac{\partial E_{rms}}{E_{rms}} \quad (6.6)$$

In other words, if 2 times more electric field is required, 4 times more power is needed. But what about this in a RC? Does the same kind of relation apply? What is the extra power we need if it is necessary to go from $E_{max-avg} = 35$ V/m to 50 V/m (or to increase by 3 dB)?

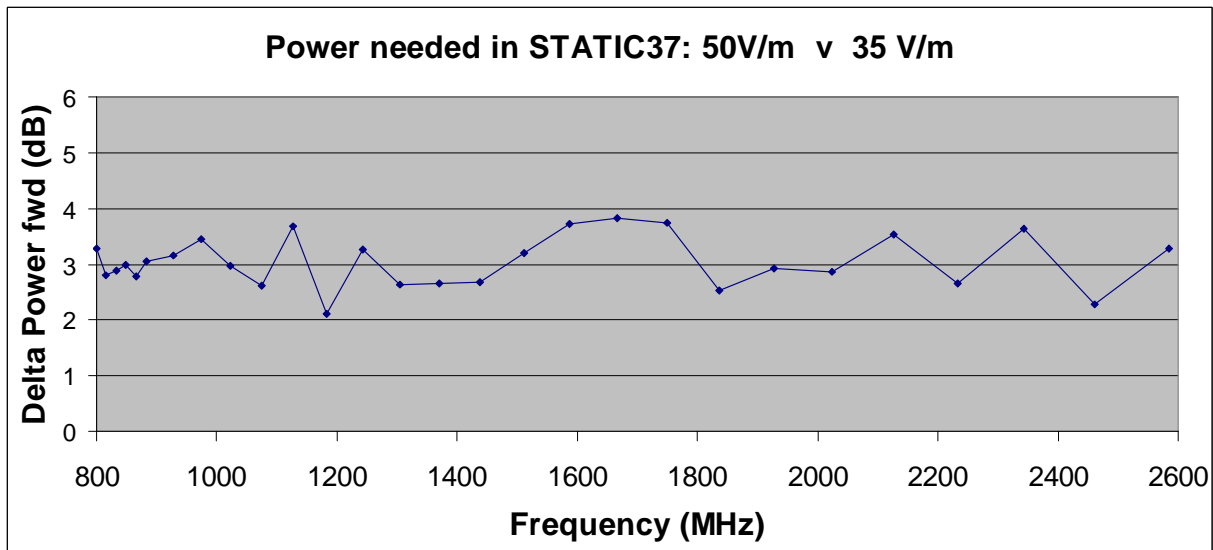


Fig. 6.14: Extra power needed to increase $E_{max-avg}$ by 3 dB.

By measurement (Fig. 6.14), this extra power turns out to be 3 dB, so a ratio of $\sqrt{2}$ for $E_{\max\text{-avg}}$ becomes a ratio of 2 in power. The theoretical demonstration is as follows: from [7], we have (assuming matched and lossless antennas):

$$P_t = \frac{16 \cdot \pi^2 \cdot V}{\lambda^3 \cdot Q} \cdot \langle P_r \rangle \quad (6.7)$$

Where:

- P_t is the transmitted power (W);
- V is the volume of the RC (m^3);
- λ is the wavelength (m);
- $\langle P_r \rangle$ is the average received power over N tuner steps (W).

Moreover, we know that:

$$\langle P_r \rangle = \frac{E_{rms}^2}{\eta} \cdot \frac{\lambda^2}{8\pi} \quad (6.8)$$

Where:

- E_{rms}^2 is the squared magnitude of the total electric field (V^2/m^2),
- η is the wave impedance of the medium (377 Ohm in free space).

From [7]:

$$\frac{E_{rms}^2}{3} = \langle |E_x|^2 \rangle = \langle |E_y|^2 \rangle = \langle |E_z|^2 \rangle \quad (6.9)$$

and from [5]:

$$\langle |E_i|^2 \rangle = \frac{E_{\max-i}^2}{A(N)} \quad (6.10)$$

Where: $A(N)$ is the max-to-average ratio of the squared magnitude of a rectangular component of the electric field. This ratio is a function of the number of tuner steps (N).

Replacing $\langle |E_i|^2 \rangle$ from (6.10) in (6.9) and, replacing E_{rms}^2 from (6.9) into (6.8). And finally, replacing $\langle P_r \rangle$ from (6.8) into (6.7), gives:

$$P_t = \frac{E_{\max-avg}^2}{\eta} \cdot \frac{6.\pi.V}{\lambda.Q.A(N)} \quad (6.11)$$

Differentiating (6.11) gives:

$$\frac{\partial P_t}{P_t} = 2 \cdot \frac{\partial E_{\max-avg}}{E_{\max-avg}} \quad (6.12)$$

It is the same kind of relation as in a semi-anechoic chamber and in agreement with the measurements of Fig. 6.14.

6.6 New property in a RC

During the course of our research, unexpectedly, we found that Erms-avg in a single spatial point goes lower, as the spatial field uniformity is getting better for a fixed value of Emax-avg (see Fig. 6.5).

Fig. 6.11 already shows that the Erms-avg goes lower from STATIC 12 to STATIC 37, and we know that the spatial uniformity is better for STATIC 37 than for STATIC 12. Emax-avg being the same for STATIC 12 and STATIC 37 as it has been calibrated according to it. As this assumption regards the STATIC method, does it hold for the RAIL one?

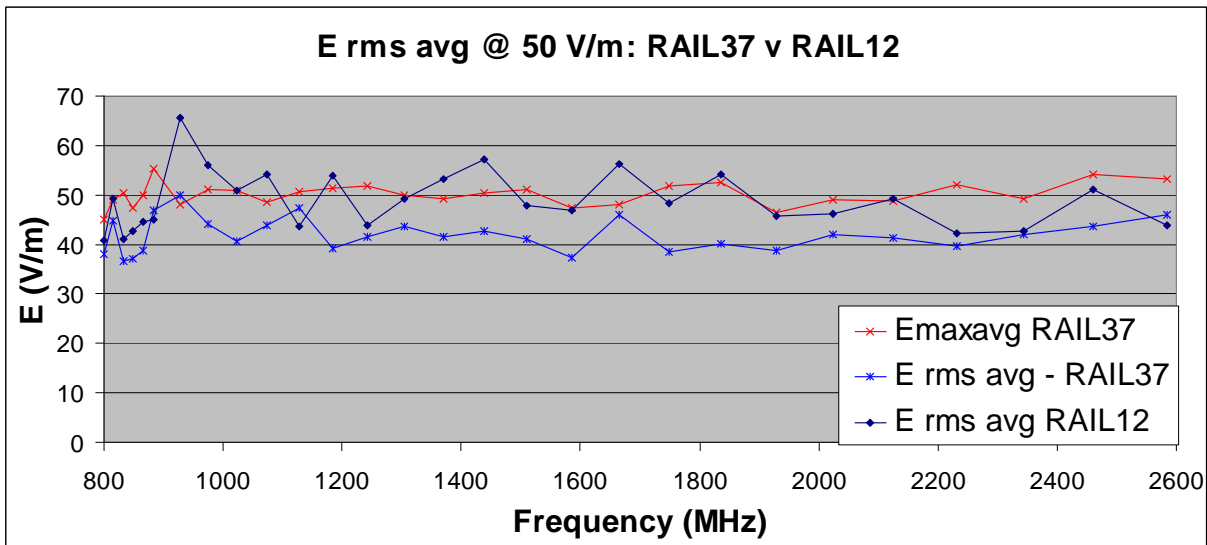


Fig. 6.15: Erms-avg variation for RAIL 37 and RAIL12

Fortunately, yes, we see that Erms-avg is getting lower from RAIL 12 to RAIL 37, and we know that RAIL 37 has a better spatial uniformity than RAIL 12, which has a better spatial uniformity than STATIC 12.

Extensive testing shows:

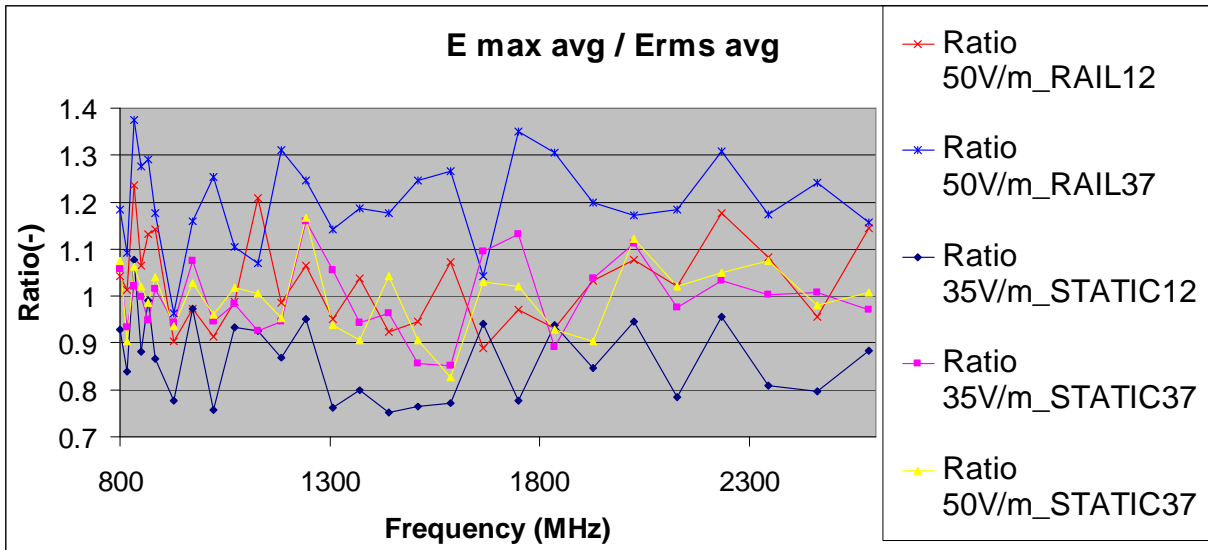


Fig. 6.16: Ratio for different tuner steps and methods.

Table 6.1: Relation between Emax-avg / Erms-avg and spatial field uniformity

Spatial Uniformity	STATIC (Step Nb)	RAIL (Step Nb)	$\frac{E_{\max-avg}}{E_{rms-avg}}$
> 3 dB	N=1	N=1	0.58
	N=12		0.85
= 3 dB	N=37	N=12	1
< 3 dB		N=37 N=150	1.19

Generalizing, the ratio Emax-avg / Erms-avg is considered and we learn from Fig. 6.16 that it goes up, firstly, when the tuner method gives a better spatial field uniformity (RAIL is better than STATIC) and, secondly, when the number of tuner steps increases (the higher the tuner steps the better the uniformity), and, Table 6.1 summarizes our findings.

The fact that the Emax-avg/Erms-avg ratio is a function of the number N of tuner steps can be demonstrated as follows:

We know that the magnitude of a component of the electric field (X, Y or Z) has a χ pdf (Probability Density Function) distribution with 2 dof (degree of freedom), also called a Rayleigh pdf, [7]:

$$f(|E_i|) = \frac{|E_i|}{\sigma^2} e^{-\frac{|E_i|^2}{2\sigma^2}} \quad (6.13)$$

where, $|E_i|$ can be the $|E_x|$, $|E_y|$ or $|E_z|$, the magnitude of a rectangular component of the Electric field.

(these values have been measured as Ermsx1, Ermsy1 and Ermsz1, etc..., see Fig. 6.5.).

The mean value of this pdf is:

$$\langle |E_i| \rangle = \sigma \sqrt{\pi/2} \quad (6.14)$$

From [40], we extract the maximum value of a rectangular component of the electric field from its mean value:

$$E_{i-\max} = B(N) \cdot \langle |E_i| \rangle \quad (6.15)$$

Where: $B(N)$ is the max-to-average ratio of the magnitude of a rectangular component of the electric field. This ratio is a function of the number of tuner steps (N).

Moreover, we know that the magnitude of the total electric field

($|E| = \sqrt{|E_x|^2 + |E_y|^2 + |E_z|^2}$) has a χ pdf distribution with 6 dof, [7]:

(these values have been measured as Erms1, Erms2, etc., see Fig. 6. 5)

$$f(|E|) = \frac{|E|^5}{8\sigma^6} e^{-\frac{|E|^2}{2\sigma^2}} \quad (6.16)$$

The mean value of this pdf is:

$$E_{rms-avg} = 15\sigma \frac{\sqrt{2\pi}}{16} \quad (6.17)$$

From Fig.6.5.:

$$E_{max-avg} = \frac{E_{x-max} + E_{y-max} + E_{z-max}}{3}$$

Replacing E_{i-max} by its value in (6.15), and $\langle |E_i| \rangle$ by its value in (6.14) gives:

$$E_{max-avg} = B(N) \cdot \sigma \cdot \sqrt{\frac{\pi}{2}} \quad (6.18)$$

Coming back to the ratio $\frac{E_{\max-avg}}{E_{\text{rms-avg}}}$ and replacing $E_{\max-avg}$ by its value in (6.18) and $E_{\text{rms-avg}}$ by its value in (6.17) gives:

$$\frac{E_{\max-avg}}{E_{\text{rms-avg}}} = \frac{8}{15} \cdot B(N) \quad (6.19)$$

According to [40], for N=37 tuner steps, B(N)=2.26, so,

$\frac{E_{\max-avg}}{E_{\text{rms-avg}}} = 1.20$, this should be compared to the measured value of 1.19, see Table 6.1.

Finally, the new property can be enounced:

If the ratio $\frac{E_{\max-avg}}{E_{\text{rms-avg}}} > 1$ in a single spatial point, then spatial uniformity of the electric field, in close vicinity, is < 3 dB.

With, "in close vicinity" one means a cube of about 50 cm side around the single spatial point considered.

6.7 Conclusions

a) A relation (illustrated in Fig. 6. 12) has been found between the number of aspect angles in an SAR and the number of tuner steps in an RC in order to obtain equivalence in radiated immunity testing results.

Fig. 6. 12 applies only to the tested device (CEUT, described in chapter 5), but it has been shown that comparison testing (SAR versus RC) of other type of devices also complies with this figure. In the future, it will be interesting to verify the compliance with many other testing results in such a way that the validity of Fig. 6. 12 can be extended to any type of device. In a SAR, the Erms has been considered, and in a RC, the Emax-avg of the rectangular components of the electric field has been taken into account.

This relation can directly be used in practice. For example, for MIL-STD-461F, RS103 radiated immunity testing, with one aspect angle in a SAR, it is recommended to use between 20 to 30 tuner steps in a RC, in order to achieve equivalence of testing results. For IEC 61000-4-3 testing, with four aspect angles in a SAR, between 40 to 60 tuner steps in a RC are recommended in order to achieve equivalence in testing results.

b) The advantage of performing a radiated immunity testing according MIL-STD-461F in a reverberation room is not so clear, because it will need equal or 2.5 less power, for the STATIC and RAIL tuners respectively, and the testing time is longer (about 3x, taking into account a dwell time of 5 seconds between each of the 37 tuner steps). The power advantage of reverberation room falls because the testing distance is 1 meter for MIL-STD-461F. Otherwise, for IEC 61000-4-3, where the testing distance is 3 meters, testing in a RC requires 9 times less power and becomes advantageous.

7. Ergodicity

7.1 Introduction

The notion of ergodicity was first introduced by Boltzmann in 1868 [67], [68], [69] for his Kinetic Theory of Gases (KTG). Boltzmann studied a special case of a gas molecule M in a plane, describing the ergodic kind of motion as follows: "If M were a shining point and the motion extremely swift, the whole surface traversed by M would appear uniformly illuminated.". The term was invented by physicists (Boltzmann, Maxwell, Gibbs and Einstein) in trying to determine whether dynamical systems evolve as expected from nonequilibrium to equilibrium. These systems were studied using statistical mechanics, with no insight in the dynamical behaviour (momentum and position evolution over time). The Ergodic hypothesis appeared when they wanted to pass from the statistical to the dynamical analysis of a physical system. The hypothesis was used to prove equipartitioning of energy (or velocity), meaning that the ensemble (or spatial) averages of the system equals time averages. Generally speaking, a physical system is ergodic if left to itself for long enough time, it will pass close to nearly all the dynamical states compatible with conservation of energy.

From the sixties until now, mathematicians (Sinai, Cornfeld, Fomin, Bunimovich, Petersen, Simanyi, etc...), [70], [71], [72] have developed the Ergodic theory. In 1963, Sinai [73], [74] gave a mathematical version of Boltzmann's hypothesis (what is called today the Boltzmann-Sinai ergodic hypothesis): the system of an arbitrary fixed number N of identical elastic hard balls moving in the m -torus T^m ($m \geq 2$) is ergodic. In the early seventies, [75], [76],

Sinai and Bunimovich proved this hypothesis for 2-D disks on the two-dimensional unit torus T^2 . The proof for 3-D balls was given in 1987 by Chernov and Sinai [77]. The proof uses so-called “billiard” containing particles whose trajectory is a straight line in between reflections at the boundaries (in accordance with the rule: “the angle of incidence is equal to the angle of reflection”, this means that the tangential components of the velocity are preserved and the normal component changes sign). A particular case is the Sinai billiard which is a square with a disk removed from its center, where 2-D particles move in straight lines and reflect either at the boundaries of the square or on the disk. Billiards can be considered as dynamical Hamiltonian systems that naturally appear in many important problems in physics. From a mathematical point of view, the ergodic hypothesis has proved to be one of the most difficult problems in the last hundred years. Only in two cases, both billiards, flows (or trajectories) have been proven to be ergodic.

There are examples in other fields. In acoustics, in [78] Sabine’s reverberation time expression is derived in an ergodic auditorium. Note that existence of ergodicity is determined by both the shape of the enclosure and the reflection law at the boundaries. In mechanics, there is the example of the simple harmonic

oscillator, whose Hamiltonian is $H(q, p) = \frac{1}{2}\omega.(p^2 + q^2)$, where p is the position, q the momentum (product of mass and velocity) and ω is the angular frequency, [79]. In 2012, an experimental test was given in [80], by measuring the diffusivities of molecules inside a nanostructured porous glass, using two conceptually different approaches. The data obtained through the direct observation of dye molecule diffusion by single-molecule tracking experiments,

that is the time average, was in perfect agreement with the ensemble value obtained in pulse-field gradient NMR experiments.

Let us take simple examples clearly illustrating the meaning of ergodicity. In an ideal factory of electronic components, the manufacturing of capacitors would be an ergodic process. The mean value over N days of the capacitance measured each day on a different capacitor is equal to the mean value of the capacitance of N capacitors measured on a single day. On the contrary, after a long period of time (ten years for example), according to Arrhenius' law, the capacitance value will drift due to ageing, and, the time average will no longer be equal to the ensemble average. In this case, the process is no more ergodic. Another example of non-ergodicity is the average height of men in a country. The mean value of the height of N men measured in a given year is not the same as the mean value over time measured on a single arbitrary man over N years. Macroeconomic studies show that the height of a population varies over longer periods of time.

In ElectroMagnetic field Theory in a Reverberation Chamber (RC), further called EMTRC, ergodicity is found to be a fundamental property of RCs, allowing estimating statistics by means of appropriate time averaging [13]. In [81] ergodicity is used to determine the Q factor with a spectral approach. In [82] it is used to proof that the Q factor behaves as a Fisher-Snedecor probability density function. In [83], ergodicity is used in the evaluation of the National Physical Laboratory (NPL) reverberation chamber. Finally, in [84] the simulations performed and the discussion on the properties of the ratio of maximum to mean amplitude rely on the ergodism principle. In this paper, an experimental test of the ergodic hypothesis for fields in reverberation chambers is given based on an extensive measurement campaign.

7.2 Ergodic Theory

Ergodic theory is the mathematical study of the long-term average behaviour of systems [85]. An Ergodic system or process is a system or process for which the time average of every measurable function coincides almost everywhere with its space average [85]. This is also known as the Birkhoff's Ergodic Theorem (1931) [85]. This means that the time average μ_t tends to the spatial average μ_s as $n \rightarrow \infty$ [66] with

$$\mu_t = \frac{1}{n} \sum_{t=0}^n x(t, s_i) \quad (7.1)$$

Where s_i represents a fixed spatial point in the chamber and n is the number of time steps considered for time averaging, and

$$\mu_s = \frac{1}{n} \sum_{s=0}^n x(t_k, s) \quad (7.2)$$

Where t_k represents a fixed time and n is here the number of spatial points considered for spatial averaging.

We will now show that the electric field in a RC can be considered as a mean-ergodic random process. This will be done by calculating the ratio of the space average to the time average and verifying that it is equal to 1. In other words, knowing the time average of the electric field in a given spatial point allows us to predict or

estimate the spatial average of this electric field at a given time in the entire volume of the RC. This fundamental property allows avoiding extensive electric field measurements in the volume of the RC at a fixed time, which is very tedious and time consuming. When it is needed to analyze the ergodic hypothesis from a physical point of view, a dynamical approach applied to a physical system with many degrees of freedom, such as a gas or an electromagnetic field is impossible, and a statistical one is preferred.

7.3 Ergodicity in reverberation chamber

In this section the kinetic theory of gases in an enclosure is compared to the theory of electromagnetic fields in a reverberation chamber. We will show that there are a lot of similarities.

First the most essential concepts of statistical theory are briefly recalled. For m independent Gaussian random variables a_1, a_2, \dots, a_m with zero mean and a standard deviation σ (m is thus the number of degrees of freedom (dof)) the χ statistics are defined as [18]:

$$\chi = \sqrt{a_1^2 + a_2^2 + \dots + a_m^2} \quad (7.3)$$

The probability density function (pdf) is:

$$f(\chi) = \frac{2}{2^{\frac{m}{2}} \sigma^m \Gamma\left(\frac{m}{2}\right)} \chi^{m-1} e^{-\frac{\chi^2}{2\sigma^2}} \quad (7.4)$$

where Γ is the Gamma function.

7.3.1 Velocities and Fields

According to Bernoulli's theory, a gas is made up of a great number of molecules moving chaotically through space in all directions. Assume that an enclosure having the form of a rectangle parallelepiped contains N molecules each of mass m , at thermal equilibrium. Consider the speed as a physical property of the gas, then we can write that [87]:

$$\langle v_x \rangle = \langle v_y \rangle = \langle v_z \rangle = 0 \quad (7.5)$$

In other words, the mean velocity components (in the x , y and z -direction) of all molecules passing over time through a given spatial point are equal to zero. This is called the isotropic property.

The fundamental reason for this property is the fact that each molecule undergoes statistical collisions with other molecules and with the enclosure. This changes its velocity in celerity and direction in a way that delivers the zero averages, see Fig. 7.1. For the total mean square velocities we can write [86], [87]:

$$\langle v_x^2 \rangle = \langle v_y^2 \rangle = \langle v_z^2 \rangle = \frac{\langle v_{rms}^2 \rangle}{3} \quad (7.6)$$

$$v_{rms} = \sqrt{\langle v_x^2 \rangle + \langle v_y^2 \rangle + \langle v_z^2 \rangle} \quad (7.7)$$

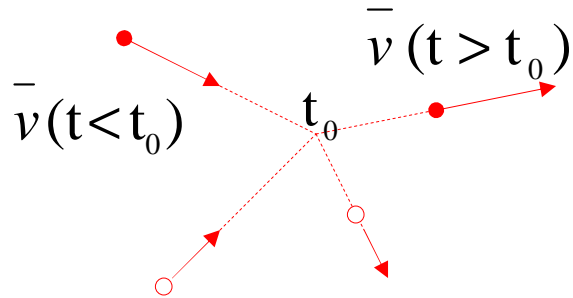


Fig. 7.1: Gas molecule collision.

In an RC, putting the tuner in a new position changes the boundary conditions and thus the relative phase shift between waves arriving at a specific point after reflection against walls and tuner. As a consequence, observed over periods of time which are large with respect to the time frames in which the tuner is moving, the electric field in any point (both field strength and polarization) is varying stochastically with time, see Fig. 7.2.

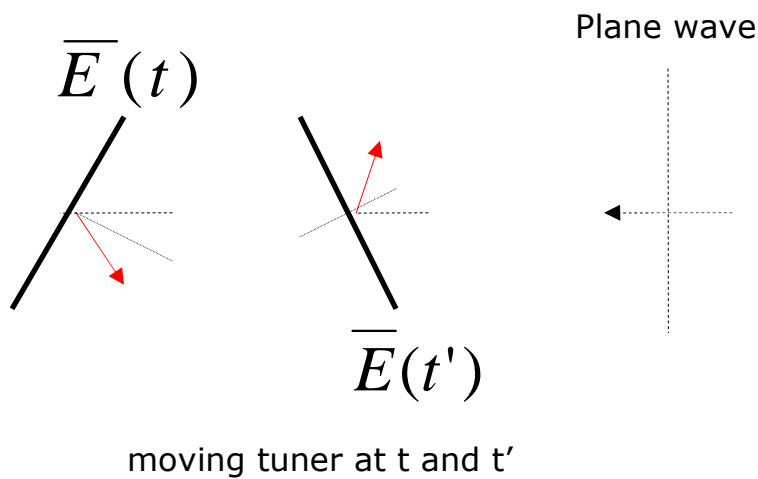


Fig. 7.2: Electric field stochastic variation in time due to the moving tuner.

When the tuner is set to a fixed position, each component of the electric field in any point is a time harmonic variable. However,

its value at any specific time is not the same from point to point because of the field inhomogeneity in the chamber resulting from the different phase combinations of the waves reflected against the chamber walls and the tuner. As a consequence, observed over sufficiently large volumes compared to the wavelength, the electric field at any time (both field strength and polarization) is varying stochastically over space.

This is exactly what the theory of electromagnetic fields in RC's states when considering the electric field:

$$\langle \mathbf{E}_x \rangle = \langle \mathbf{E}_y \rangle = \langle \mathbf{E}_z \rangle = 0 \quad (7.8)$$

which can be decomposed in real and imaginary parts as

$$\langle \mathbf{E}_{xr} \rangle = \langle \mathbf{E}_{xi} \rangle = \langle \mathbf{E}_{yr} \rangle = \langle \mathbf{E}_{yi} \rangle = \langle \mathbf{E}_{zr} \rangle = \langle \mathbf{E}_{zi} \rangle = 0$$

According to EMTRC also [7]:

$$\langle \mathbf{E}_x^2 \rangle = \langle \mathbf{E}_y^2 \rangle = \langle \mathbf{E}_z^2 \rangle = \frac{\langle \mathbf{E}_{rms}^2 \rangle}{3} \quad \text{and}$$

$$\mathbf{E}_{rms} = \sqrt{\langle \mathbf{E}_x^2 \rangle + \langle \mathbf{E}_y^2 \rangle + \langle \mathbf{E}_z^2 \rangle} \quad (7.9)$$

7.3.2 Probability Density Functions

In the KTG, only three degrees of freedom are considered corresponding to the x, y and z components of the speed. There are no real and imaginary parts. So, the pdf of the distribution of the gas velocities, v_{rms} as defined in (7.7), is a χ distribution with three degrees of freedom. Taking $m=3$ in (7.4) yields:

$$f(v_{rms}) = \frac{4}{\sqrt{\pi}} \cdot \frac{v_{rms}^2}{\sqrt{(2\sigma^2)^3}} \cdot e^{-\frac{v_{rms}^2}{2\sigma^2}} \quad (7.10)$$

Where an estimator of σ^2 is given by (note that this estimator is derived from the similarities with the EMTRC):

$$\hat{\sigma}^2 = \frac{1}{3n} \sum_{i=1}^n v_{rmsi}^2 \quad (7.11)$$

The right side of (7.11) is equal to $\frac{kT}{m_0}$ [88], where $k = 1.3807 \cdot 10^{-23}$

J.K⁻¹ is the Boltzmann constant, T is the gas temperature (K), and m_0 is the mass of a gas molecule (kg). Substituting it in (7.10) gives the well-known Maxwell-Boltzmann pdf of the velocity of a gas at thermal equilibrium [86], [88]:

$$f(v_{rms}) = \frac{4}{\sqrt{\pi}} \cdot \frac{1}{\sqrt{\left(2 \cdot \frac{kT}{m_0}\right)^3}} \cdot v_{rms}^2 \cdot e^{-\frac{v_{rms}^2}{2 \cdot \frac{kT}{m_0}}} \quad (7.12)$$

The pdf of a single orthogonal component of the velocity (x, y, or z) follows a χ distribution with one degree of freedom [88]

$$f(v_x) = \frac{1}{\sqrt{\pi \frac{kT}{m_0}}} \cdot e^{-\frac{v_x^2}{2 \frac{kT}{m_0}}} \quad (7.13)$$

Note that if we consider only the real part of each Electric field component, the pdf will be a χ distribution with one dof, exactly as in (7.13).

Studying electric fields in RC's, there are differences with gases concerning the pdf's. The magnitude of the electric field components (E_x, E_y, E_z) behaves as a χ pdf random variable with two degrees of freedom, because both the real and imaginary parts have to be considered. So, the pdf for a given component E_a is obtained from (7.4) with $m=2$:

$$f(E_a) = \frac{E_a}{\sigma^2} e^{-\frac{E_a^2}{2\sigma^2}} \quad (7.14)$$

With $E_a = E_x, E_y$ or E_z , and σ^2 is a scale factor. The Maximum-Likelihood Estimator (MLE) of σ^2 is calculated by taking the derivative of the pdf (7.14) with respect to σ^2 and setting it equal to zero [41], yielding:

$$\hat{\sigma}^2 = \frac{1}{2n} \sum_{i=1}^n E_{a i}^2 \quad (7.15)$$

where n is the number of time samples. According to [18]:

$$\sigma^2 = \frac{4\pi Q}{3\epsilon_0 \omega V} \cdot P_{in}$$

where Q is the quality factor of the RC, $\epsilon_0 = 8.854 \times 10^{-12}$ (F/m) the vacuum permittivity, ω the angular frequency in (rad/s), V the volume of the RC, and P_{in} the power delivered to the RC by an

external source. The pdf of the total electric field is given by a χ distribution of 6 degrees of freedom because the x , y , and z components are considered and for each component the real and imaginary part [7].

Further on, when working with energies, we will also need to consider only the real part of the electric field components. We can write:

$$E_{rms,r} = \sqrt{E_{xr}^2 + E_{yr}^2 + E_{zr}^2}$$

So, remembering (7.3) and taking $m=3$ in (7.4) yields:

$$f(E_{rms,r}) = \frac{4}{\sqrt{\pi}} \frac{E_{rms,r}^2}{\sqrt{(2\sigma^2)^3}} e^{-\frac{E_{rms,r}^2}{2\sigma^2}} \quad (7.16)$$

with the following estimator of σ^2 :

$$\hat{\sigma}^2 = \frac{1}{3n} \sum_{i=1}^n E_{rms,r}^2 \quad (7.17)$$

We observe that v_{rms} and $E_{rms,r}$ behave as a χ pdf with 3 dof.

7.3.3 Energies

In EMTRC the partial energy density is [18]:

$$W_d = \frac{\epsilon_0}{2} \cdot (E_{xr}^2 + E_{yr}^2 + E_{zr}^2) \quad (7.18)$$

Where E_{ar}^2 is the square of the real part of the electric field component considered ($a = x, y, \text{ or } z$). W_d behaves as a χ^2 pdf with three dof:

$$f(W_d) = \frac{2\pi\sqrt{W_d}}{(2\pi)^{3/2} \cdot \beta^3} \cdot e^{-\frac{W_d}{2\beta^2}} \quad (7.19)$$

Where, in EMTRC, $\beta^2 = \frac{\epsilon_0 \cdot \sigma_s^2}{2}$, and $\sigma_s^2 = \sigma_x^2, \sigma_y^2 \text{ or } \sigma_z^2$ as defined in (7.15).

In KTG, inserting $\beta^2 = \frac{k.T}{2}$ in (7.19) we obtain the well-know Maxwell-Boltzmann distribution for energy density, which behaves as a χ^2 pdf with three dof [88], [89].

As a conclusion of this section, it can be safely stated that there are a considerable number of similarities between the kinetic theory of gases (KTG) and electromagnetic theory in reverberation chambers (EMTRC). Table 7.1 resumes this.

Table 7.1: Statistical physical models comparison

	Kinetic Theory of Gases (KTG)	Electromagnetic Theory in Reverberation Chambers (EMTRC)
Historical landmark	Around 1870	Around 1990
Wave - particle	Particle (gas molecule)	Electromagnetic wave

Physical quantity	Velocity	Electric field
Properties of Physical quantity	$\langle v_x \rangle = \langle v_y \rangle = \langle v_z \rangle = 0$	$\langle E_x \rangle = \langle E_y \rangle = \langle E_z \rangle = 0$
	$\langle v_x^2 \rangle = \langle v_y^2 \rangle = \langle v_z^2 \rangle = \frac{\langle v_{rms}^2 \rangle}{3}$	$\langle E_x^2 \rangle = \langle E_y^2 \rangle = \langle E_z^2 \rangle = \frac{\langle E_{rms}^2 \rangle}{3}$
	$v_{rms} = \sqrt{\langle v_x^2 \rangle + \langle v_y^2 \rangle + \langle v_z^2 \rangle}$	$E_{rms} = \sqrt{\langle E_x^2 \rangle + \langle E_y^2 \rangle + \langle E_z^2 \rangle}$
Statistics	pdf of v_x , v_y and v_z is a χ with one dof	pdf of E_{xr} , E_{yr} and E_{zr} is a χ with one dof and E_s is a χ with two dof
	pdf of v_{rms} is a χ with three dof (Maxwell-Boltzmann distribution of velocity)	pdf of $E_{rms,r} = \sqrt{E_{xr}^2 + E_{yr}^2 + E_{zr}^2}$ is a χ with three dof and E_{rms} is a χ with six dof
	Energy density behaves as a χ^2 with three dof (Maxwell-Boltzmann distribution)	Energy density behaves as a χ^2 with three dof considering $E_{rms,r}$
Energy	Delivered by heating the gas enclosure	Delivered by injecting power in the RC
Ergodicity	Assumed since 1870, still to be proved experimentally	Experimentally found in our work

7.3.4 Ergodicity of electric fields in reverberation chambers

The total electric field is defined as :

$$E_{rms} = \sqrt{E_x^2 + E_y^2 + E_z^2} \quad (7.20)$$

Let $E_{rms s_i}$ be the spatial average of the total electric field over a limited number of spatial points in a reverberation chamber, at a given time i . This time corresponds to the i_{th} tuner step position over a limited total number of time (tuner) steps. Let $E_{rms t_k}$ be the time average of the total electric field, over a limited number of time (tuner) steps, at a given spatial point k . This k_{th} spatial point is one of a limited total number of spatial points. Similar definitions for the x , y , and z components of the field can be given.

To assess the ergodic hypothesis, one has to determine whether:

$$E_{rms s_i} = E_{rms t_k} \quad \text{or} \quad \frac{E_{rms s_i}}{E_{rms t_k}} = 1$$

According to Birkhoff's Ergodic Theorem, this has to be evaluated in the limit for an infinite number of spatial points and an infinite number of time steps.

7.4 Experimental test of ergodicity of electric fields in reverberation chamber

7.4.1 Measurement set-up

The reverberation chamber (RC) used has a volume of 15 m³. Its lowest useable frequency is about 800 MHz. The RC is

equipped with a RAIL tuner, described in detail in [12]. This tuner has been shown to satisfy the uniformity requirements of the IEC 61000-4-21 [12]. It is composed of two orthogonal rails with an LPDA (Log Periodic Dipole Array) antenna mounted on each of the moving carts (Fig. 7.3). The horizontal one (rail A) is 2.48 m long and positioned at 1.25 m from the floor. The vertical one (rail B) is 2.08 m long and placed at 1.39 m from the back wall and at 1.09 m from the front wall. The length of a single step is 2.5 cm. The number of steps for rail A (used length: 2.05 m) and for rail B (used length: 1.65 m) is 83 and 67 respectively. This gives a total of 150 steps or tuner positions. There is no other tuner type present in the RC, for example the conventional rotating tuner. The three components of the E-field, the forward and reverse output powers and the displacement of the two LPDA antennas have been measured for each of the 150 tuner positions, at eight locations of the working volume (see Table 7.2) and at twenty two frequencies within the frequency range of interest (800 to 2500 MHz, see Table 7.3). A total of 79200 electric field measurements have been done. The RC is equipped with a 35 W amplifier in order to achieve high levels of electric field in the frequency range, see Fig. 7.4.

Table 7.2: Positions, in meters, of E-Field probe (x,y,z)

P1	(0.6;1.5;1.0)
P2	(1.8;1.5;1.0)
P3	(0.6;0.6;1.0)
P4	(1.8;0.6;1.0)
P5	(0.6;1.5;1.6)
P6	(1.8;1.5;1.6)
P7	(0.6;0.6;1.6)
P8	(1.8;0.6;1.6)

Table 7.3: List of logarithmically spaced frequencies, in MHz

800.00	1463.88
845.17	1546.54
892.90	1633.87
943.32	1726.13
996.58	1823.60
1052.86	1926.58
1112.31	2035.37
1175.12	2150.30
1241.48	2271.72
1311.58	2400.00
1385.64	2513.50

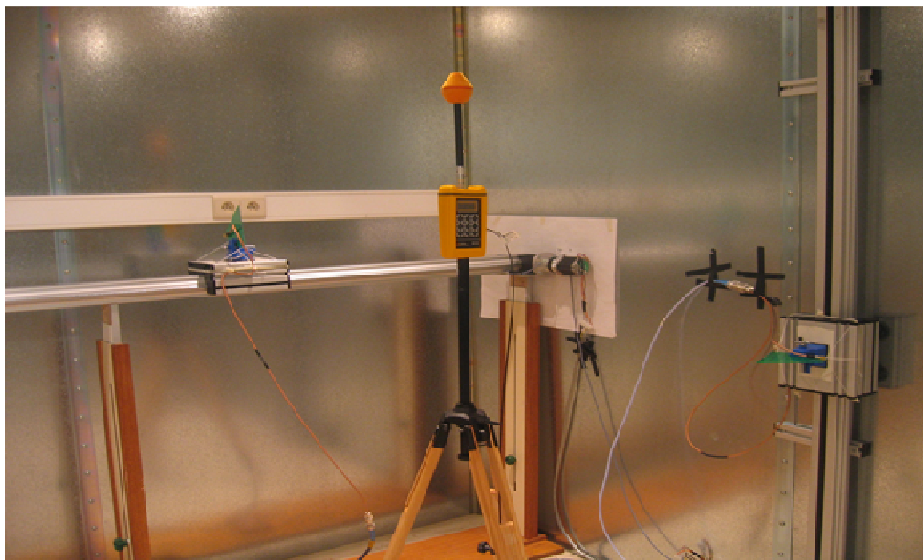


Fig. 7.3: Two orthogonal rails tuning method in RC.

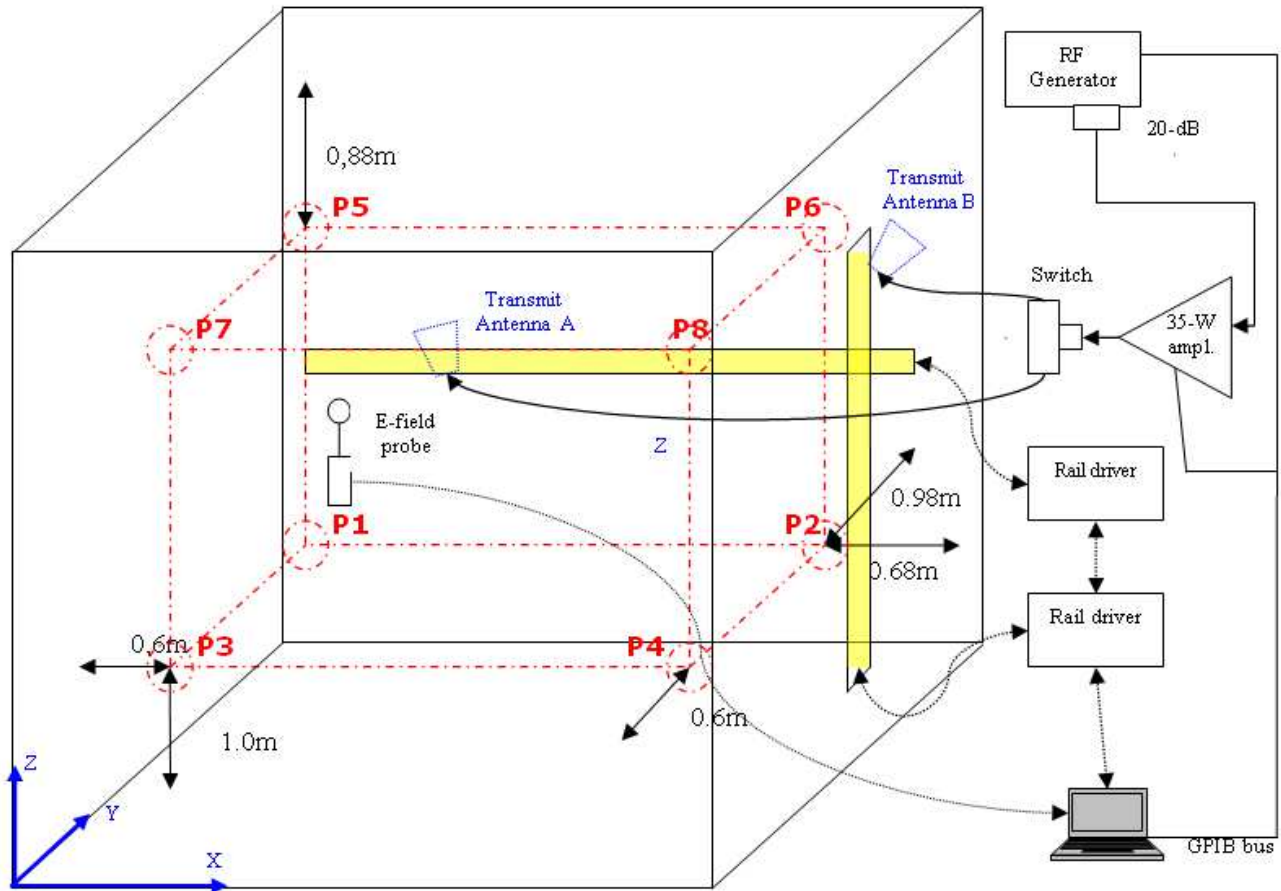


Fig. 7.4: Measurement set-up

7.4.2 Data acquisition of E-fields

A Narda EMR-300 meter with a (3 MHz -18 GHz) E-field probe type 9.2 has been used. It gives the three components of the E-field. The E-Field probe is placed, successively, on eight spatial points (P1 to P8), delimiting the working volume. The separation distances between the surfaces bounding the working volume and any chamber surface are kept higher than $\lambda/4$ i.e. 9 cm at 800 MHz. Closer to the walls, the field meter would stand in the wall boundary layer, where the electric field orientation is rather dictated by the local boundary condition and thus more deterministic than

stochastic in terms of polarization. At each frequency a measurement is done of the three components (E_x , E_y , E_z) of the E-field for the N steps of the tuners. A PC running LabVIEW based software for controlling the instruments and the data acquisition is in the centre of the test system. The following elements are connected to it (see Fig. 7.4):

- 1) NARDA EMR-300 + E-field probe (3 MHz-18 GHz);
- 2) Signal generator;
- 3) 35 W amplifier;
- 4) Power meter;
- 5) Two rails controller.

7.4.3 Measurement results

After performing all measurements (8 points, 22 frequencies, and 150 tuner steps representing 150 time steps) the mean value of the electric field components (x , y , and z) and also the mean value of the total electric field (as defined in (7.20)) are calculated. First, this is done in each of the 8 spatial points taking the average over time (tuner steps). Then, it is done for each of the 150 tuner steps (time) taking the average over the 8 points. It is important to realize that the 8 time averages can be compared with 150 spatial averages. This can be represented in matrix form. The resulting matrix (8 columns, corresponding to the 8 spatial points and 150 rows, corresponding to the 150 tuner-time steps) for the total electric field E_{rms} and the first frequency f_1 is the following:

$$\left(\begin{array}{ccc} \frac{E_{rmss_1 f_1}}{E_{rmst_1 f_1}} & \frac{E_{rmss_1 f_1}}{E_{rmst_2 f_1}} & \dots & \frac{E_{rmss_1 f_1}}{E_{rmst_p f_1}} \\ \frac{E_{rmss_2 f_1}}{E_{rmst_1 f_1}} & \frac{E_{rmss_2 f_1}}{E_{rmst_2 f_1}} & \dots & \frac{E_{rmss_2 f_1}}{E_{rmst_p f_1}} \\ \dots & \dots & \frac{E_{rmss_i f_1}}{E_{rmst_k f_1}} & \dots \\ \frac{E_{rmss_n f_1}}{E_{rmst_1 f_1}} & \frac{E_{rmss_n f_1}}{E_{rmst_2 f_1}} & \dots & \frac{E_{rmss_n f_1}}{E_{rmst_p f_1}} \end{array} \right)$$

Where $E_{rms\ s_i\ f_1}$ is the spatial average of the total electric field over the 8 spatial points for the i_{th} tuner (time) step at frequency f_1 and $E_{rms\ t_k\ f_1}$ is the time average of the total electric field over the 150 tuner (time) steps for the k_{th} spatial point at frequency.

The same type of matrix can be calculated for each of the 22 frequencies, and for each of the three separate components Ex, Ey and Ez. This means that in total $22 \times 4 = 88$ matrices are available. The total electric field is presented in Fig. 7.5 to Fig. 7.7.

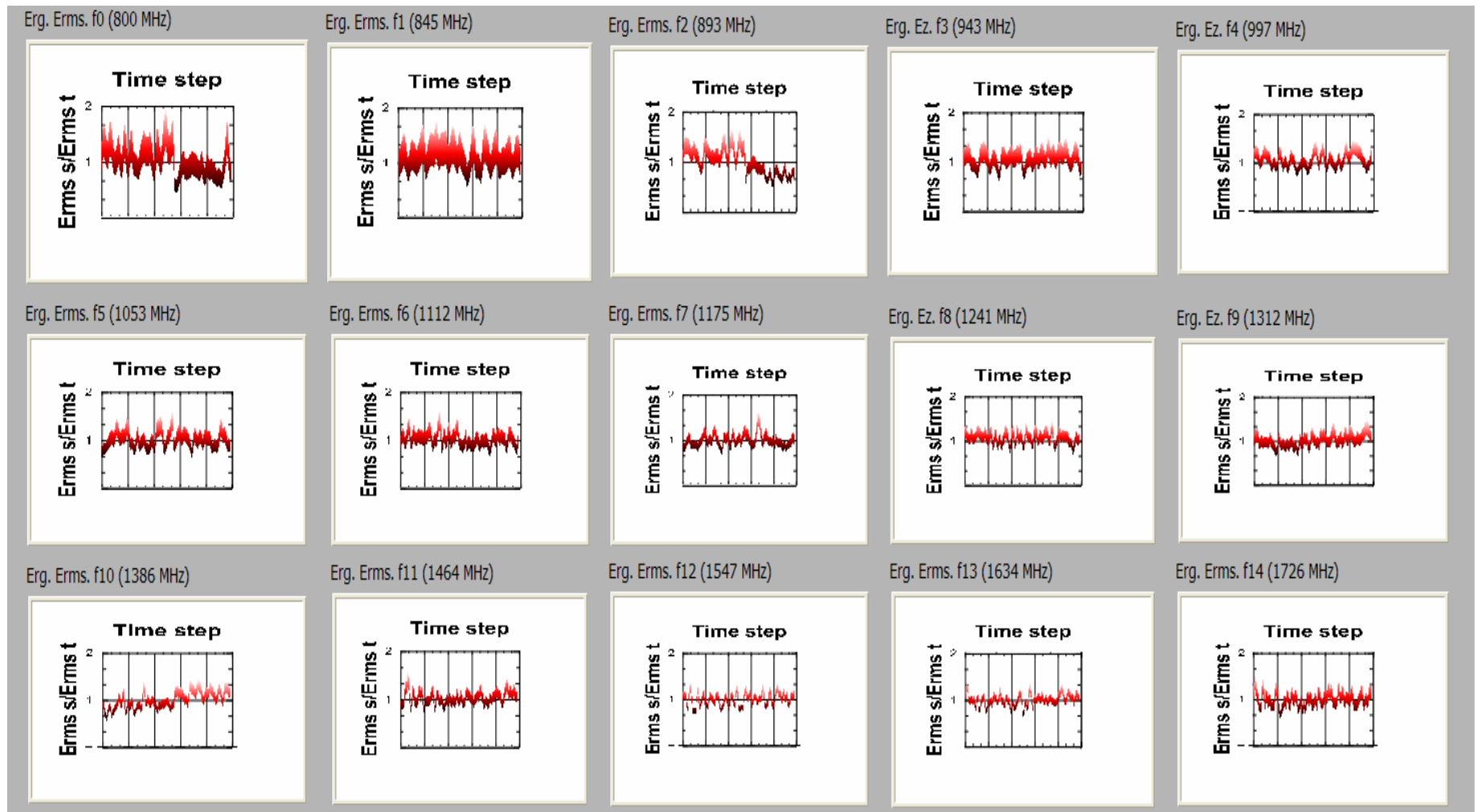
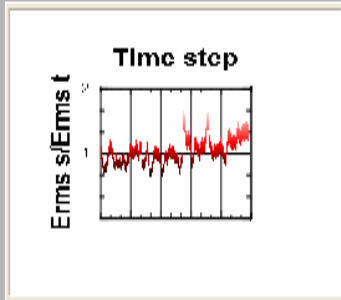
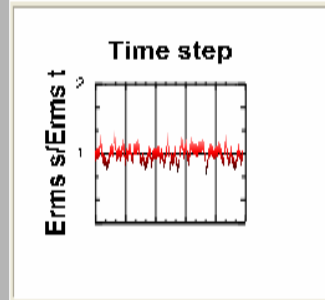


Fig. 7.5: Ergodicity measurement results for Erms. Each plot represents a different frequency. The indication “samples” refereeing to the abscissa corresponds to the row of the matrix (there are 150 “sample” points, each representing a time step). All values on a row of the matrix have been depicted in the plots, yielding a red zone rather than a single red line, see also Fig. 7.7 top left plot for details.

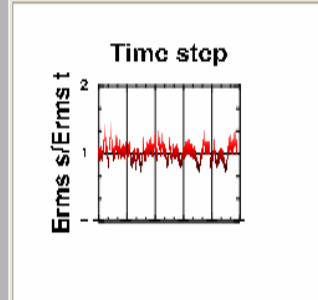
Erg. Erms. f15 (1824 MHz)



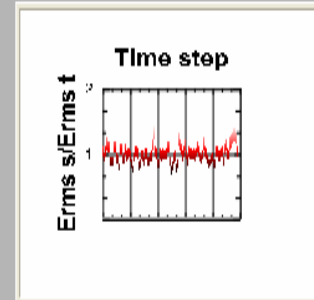
Erg. Erms. f16 (1927 MHz)



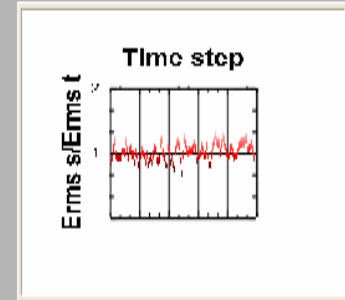
Erg. Erms. f17 (2035 MHz)



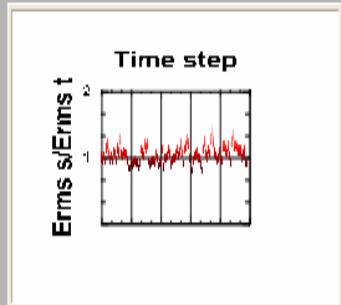
Erg. Erms. f18 (2150 MHz)



Erg. Erms. f19 (2272 MHz)



Erg. Erms. f20 (2400 MHz)



Erg. Erms. f21 (2514 MHz)

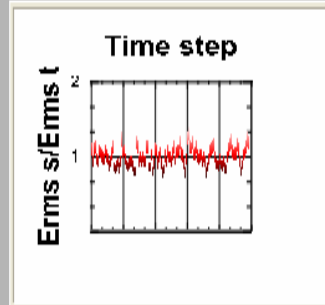


Fig. 7.6: Ergodicity measurement results for Erms (continuation of Fig. 7.5).

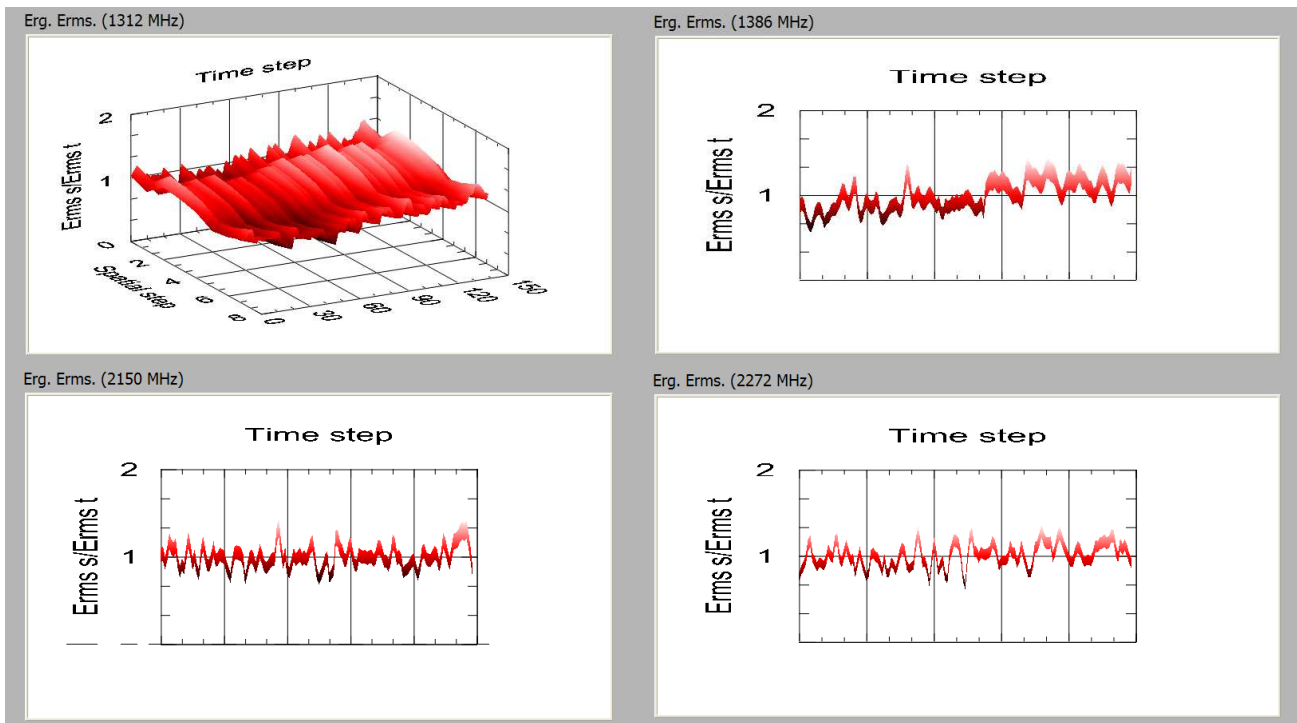


Fig. 7.7: Ergodicity measurement results for Erms, details.

The matrix can be further processed in order to derive standard deviations as a function of frequency. This is done in the following way. First, for each column of the matrix (i.e. for each of the 8 spatial points), the standard deviation over the 150 time steps (the rows) is calculated. Then, the mean over the 8 columns is calculated. This is done for all matrices as a function of frequency. The result is depicted in Fig. 7.8.

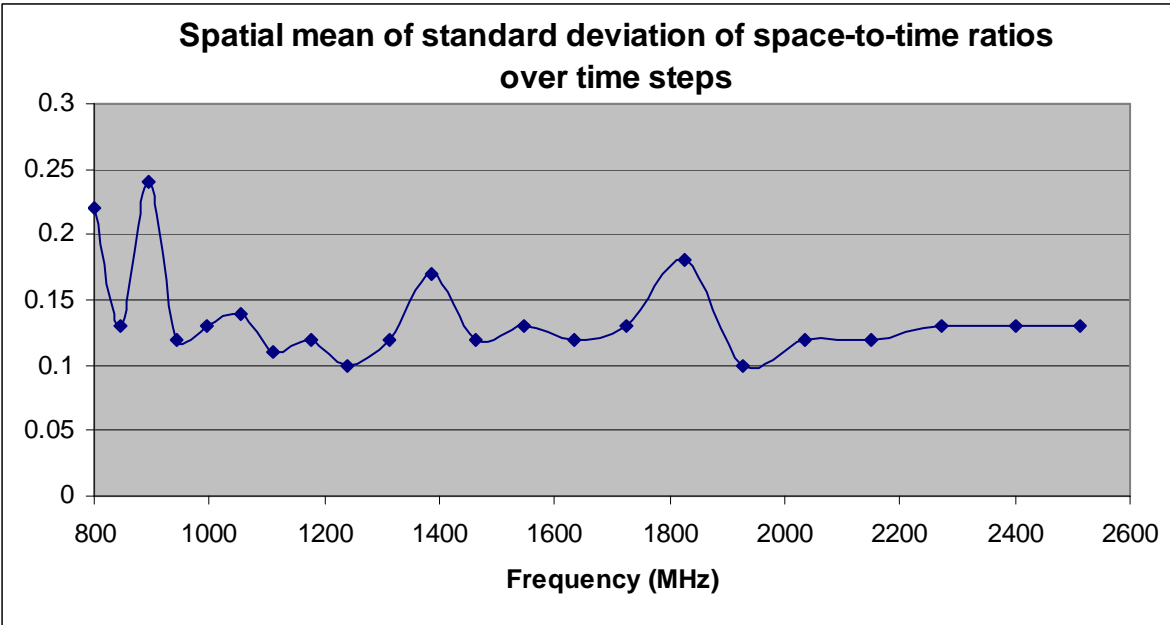


Fig. 7. 8: Standard deviation of space-to-time ratios as a function of frequency

We found that the standard deviation σ lies between 0.10 and 0.15 for 18 of the 22 frequencies. If we take $2\sigma = 0.33$, we are at a 95% confidence level. This explains why the threshold level applied in the Pass/Fail criterion for ergodicity behavior acceptance is set at 33 %. The accuracy of the measurements is maximum about 14%, mainly due to the field probe limitations.

From Fig. 7.5 to Fig. 7.7, , it can be seen that E_{rms} for nearly all frequencies above 1200 MHz fulfills the ergodic hypothesis, as the ratio of the spatial mean to the time mean of the total electric field is within $1 \pm 33\%$. Only at 1824 MHz, there is a larger deviation, as shown in Fig. 7.8. A possible explanation is that, as the shape of our RC is cubic, the number of modes at this specific frequency is not enough to assure full ergodicity, although it is sufficient to satisfy to the uniformity requirements of the standard IEC 61000-4-21.

7.5 Conclusion

In the literature the ergodicity of the electric field in a reverberation chamber in many papers is assumed. However, up to now, very few experimental data were available that support this hypothesis. By processing and interpreting the results of an extensive measurement campaign this paper has shown that the electric field generated in a Reverberation Chamber (RC) within the band of interest indeed can be considered as a mean-ergodic process. More specifically, for our RC with a LUF of 800 MHz, the ergodicity is verified from 1200 MHz (1.5 times the LUF) up to the maximum frequency usable with the instrumentation available (about 2.5 GHz), except for 1824 MHz, where there is a larger deviation. Ergodicity is important because it links the time and the spatial average of a random value (the electric field for example). In an RC the ergodicity property makes it possible to estimate the spatial average of the Electric field in the complete volume of the RC at a fixed time by measuring this random value in a fixed point in the RC volume but for a given length in time. This considerably reduces measuring time.

8. General conclusions

Starting from the theory of resonances of time harmonic fields in cavities, we have presented the principle of operation of the reverberation chamber.

This type of test facility can be used as an alternative to the conventional semi-anechoic room (SAR) for testing the immunity of electronic equipment to high intensity radiofrequency fields. This electrically large highly conductive cavity aims to generate electromagnetic waves with a direction of incidence, a polarization and a time of arrival on the EUT that are varying randomly in time.

Such characteristics are generally obtained by installing into the chamber a fixed radiating source and a large (cumbersome) rotating conductive paddle. The rotation makes the boundaries time dependent. Although there are international standards describing how to conduct an immunity test in a RC, this type of facility has been less popular than the SAR up to now. One of the reasons is perhaps that there is still some doubt about the fact whether SAR and RC testing are equally severe for the EUT and the question rises in what way a correct equivalence between them can be obtained.

In fact, the presented research had two objectives: the first objective is to conceive, design and evaluate the efficiency of innovative and less cumbersome tuning systems and the second is to compare the severity level of RC and SAR for immunity testing by using both facilities available at RMA.

The statistics of the random field components and the total field existing in RC have been thoroughly studied in Chapter 1, as that of power received at the terminals of the antenna used to monitor the fields. Mean value and standard deviation are of course

relevant features describing time variation and spatial distribution of the fields. But the probability density function (PDF) and its integral, the cumulative density function (CDF) have also been analysed, since they characterize globally the whole range of values the field strength can take over one tuner period. Moreover, it is then possible to compare the experimental PDF and CDF obtained with our innovative tuning systems with the theoretical ones expected in an ideal RC, by using an hypothesis test approach based on statistical criteria like that of Kolmogorov-Smirnov (KS).

The first innovative tuning method (RAIL) we have conceived, designed and assessed in the RC at RMA is a dynamic source-mode tuning based on a translation movement of two broadband antennas on two orthogonal rails. The system and its validation over the frequency band of interest (800-2500MHz) according to the IEC 61000-4-21 standard has been described in Chapter 2. From its efficiency analysis turns out that it complies with the field uniformity requirement of the IEC 61000-4-21 in a large part of the chamber working volume. Mean Electric field strengths of the order of 10 to 20 V/m are easily obtained from only 1.5 W power input. Statistical treatment has shown that the experimental PDF is close to the theoretical one. KS tests applied to the experimental and theoretical CDF's have demonstrated that the equal hypothesis passes.

The second innovative tuning method (STATIC) we have conceived and investigated in the same RC is based on a fixed network of sixteen static antennas where a limited subset of eight antennas is randomly activated by means of fast electronic switches. Tuning is obtained without any movement in the RC. But it is necessary to have more steps (37 compared to 24 for the RAIL) in order to obtain compliance with the field uniformity requirements

of the IEC 61000-4-21. Mean electric field strength is also lower (about 10 V/m for 1.5 W power input) due to losses in the cabling and the power divider. Statistical analysis shows that both experimental PDF and CDF are close to theory, as proved by the KS test. The great advantage is the testing time reduction (about seven hours) as the transition from one tuner step to another is quasi-instantaneous. But neither this tuner nor the first one succeeds in achieving a testing time equal to the one in a semi-anechoic chamber (SAR), in tuning mode, when it is necessary to stop at each step in order to verify the status (Pass or Fail) of the equipment under test.

After investigation of the two innovative tuning methods and evaluation of their respective merits, we have used one of them (RAIL method) to develop in Chapter 4 a new method for measuring the radiation efficiency of an antenna. Applied to different types of antennas (quarter-wave, horn available on the market, PIFAs and dual-band patch antenna) it has shown an accuracy of $\pm 20\%$, which is the same as the equivalent gain-directivity method performed in an anechoic environment. This method has the advantage to demonstrate the efficiency without needing a reference antenna. The relative method has also been applied. Its accuracy is estimated at 10 % and the measured reproducibility is 7.5 %. The accuracy can be improved by making a larger number of tuning steps but then the measurement time is increased. The relative method is described in the IEC 61000-4-21 standard using a conventional rotating mechanical tuner. As the antenna efficiency results are satisfactory this implicitly consolidates the pertinence of the new RAIL tuning method.

In order to perform a severity comparison of the immunity testing to Electric fields between a semi-anechoic

environment and a reverberating one, (Chapter 5) a Canonical Equipment Under Test (CEUT) has been designed, developed and manufactured at the Royal Military Academy. It is an original realization with no equivalent in the EMC community. It consists of a coupling part, a sensitive electronic part and a remote control part. The aim was to be able to measure in an objective and quantitative way whether the electronics inside have been disturbed or not and to determine its susceptibility level as a function of parameters like frequency, field strength and number of tuner steps. The external aspect of the CEUT is a shielded metallic box (24.5x20x25 cm³) powered by batteries and connected outside of the testing environment by optical fibres to a PC. Home-made driver software has been developed for remote controlling. An unexpected development of this initiative lies in the fact that it has been accepted, by ABLE (Association of accredited laboratories in Belgium) as reference material for interlaboratory testing, financed by the Ministry of Economy, in the field of radiated immunity testing to RF, according to IEC 61000-4-3. Moreover, EMC testing laboratories in Germany and Japan have shown interest and have participated in this campaign.

The comparison of radiated immunity testing performed both in a reverberation chamber and in a semi-anechoic room has produced several interesting results:

a) The frequency response of the CEUT does not change when modifying the tuner (STATIC or RAIL).

b) The severity of the radiated immunity testing to RF according MIL-STD-461F (50 V/m) in a reverberation chamber is dependent on the number of tuner steps. The severity increases with the number of tuner steps. In this way we can extend the same rationale to civil standards.

c) A radiated immunity testing to RF according to MIL-STD-461F in a semi-anechoic room (SAR) is only equivalent to a testing in a reverberation chamber (RC) when some conditions are respected (see Fig. 6. 12). Applied to test RS103 of the MIL-STD-461F, it means that with one aspect angle in a semi-anechoic room, it is recommended to use from 20 to 30 tuner steps in order to achieve equivalence of testing results. For the IEC 61000-4-3, testing with 4 aspect angles in a semi-anechoic room, from 40 to 60 tuner steps are recommended for equivalence.

d) Equal RF power is needed in a reverberation room to establish the necessary electric field according to MIL-STD-461F comparing to the RF power needed in a semi-anechoic room, this for the STATIC tuning method, and 2.5 times less power is needed for the RAIL tuning method. The power advantage of using a reverberation chamber is not an issue any more because the testing distance is 1 meter for MIL-STD-461F. For IEC 61000-4-3, where the testing distance is 3 meter, testing in a RC requires 9 times less power and becomes advantageous. Finally, we pointed out that 2 dB higher electric field can be obtained in a reverberation chamber when the number of tuner steps is increased from 24 to 150 (RAIL method). This, however, is at the expense of the testing time which becomes 3.5 times higher. One working method should then be to test at the lowest possible number of tuner steps. If high levels of electric field are needed, that are not achievable by increasing the output power of the amplifier, then the number of tuner steps should be increased to gain some dB.

e) Using 24 steps in the RAIL method or 37 steps in the STATIC one, the testing time in tuning mode is higher than the one in a semi-anechoic room. Around 30 minutes are needed, for IEC 61000-4-3, in a semi-anechoic room to scan from 800 to 2500 MHz

compared to around 1 h in a reverberation chamber. The testing time in a reverberation chamber will always be longer than in a semi-anechoic room, for the same dwell time, in a tuning mode when you stop at each step in order to verify the status of the equipment under test. What we gain by using an amplifier of relatively less power is lost by the relatively longer testing time. The technological breakthrough is that important testing time reduction can be achieved when using the STATIC tuner instead of using conventional mechanical tuners. For MIL-STD-461F, test RS103 from 30 MHz to 18 GHz, assuming that static tuner is 1 second quicker than the mechanical one, around 7.6 hours of testing time reduction are obtained for 12 tuner steps and around 23.3 hours of testing time reduction are obtained for 37 tuner steps.

Finally, we have shown experimentally (Chapter 7) that, in a reverberation chamber, spatial averages and time averages are equal; this is a characteristic of ergodic processes. This experimental demonstration of ergodicity establishes a scientific breakthrough since, as far as we know, there is no literature about this subject yet. From now on, we can say that the stochastic generation of an electric field in a reverberation chamber is a stationary process and that various statistical parameters in its volume can be estimated by measuring the time average in a fixed spatial point.

From the abovementioned results, we think that all the objectives that we had put forward for the present work have been reached.

In the future, it would be interesting to investigate the efficiency of the two innovative tuning methods in reverberation chambers of larger dimensions and in other frequency bands, for

example for frequencies lower than the 800 MHz minimum considered in our work. About the differences observed between theoretical and measured pdf and cdf, it would be interesting to analyse the phenomenon more deeply. Another issue could be to compare the values obtained in different RC's for the radiation efficiency of a set of antennas.

Fig. 6. 12 applies only to the tested device (CEUT, described in chapter 5), but it has been shown that comparison testing (SAR versus RC) of other types of devices also complies with this figure. So, it will be interesting to verify the compliance with many other testing results in such a way that the validity of Fig. 6. 12 can be extended to any type of device.

About the conditions of equivalence of testing results to radiated immunity to electric fields, the relation in Fig. 6. 12 is expected to give more confidence to the normalization committees on the use of reverberation chamber as an alternative to semi-anechoic rooms.

In Chapter 7, the experimental demonstration of ergodicity awaits for confirmation and comments from the scientific community. Finally, in Table 7.1 , the statistical physical models between the Kinetic Theory of Gases (KTG) and the ElectroMagnetic Theory of RC (EMTRC) is the starting point to a more deep and large comparison between Thermodynamics and the Maxwell's equations, for example, what becomes the entropy in EMTRC ? Can we derive an equivalent to the Boltzmann's formula of entropy in EMTRC ? Can we use an RC as a statistical model for the KTG, according to table 7.1, the pdf of the velocity (for KTG) and the electric field (for EMTRC) are the same ?

9. List of Publications

- a) C. Tsigros, M. Piette, "*Efficiency of electronic mode tuning with two orthogonal LPDA antennas scanning system in a reverberation chamber*" presented at 14ème Colloque International CEM08, Paris, May 2008.
- b) C. Tsigros, M. Piette, "*IEC 61000-4-21 testing: selective source-mode tuning with two orthogonal antennas scanning system*", Proc. of the 8th Int. Symposium on Electromagnetic Compatibility (EMC Europe 2008), Hamburg, Germany, September 8-12, 2008, pp 477-482.
- c) C. Tsigros, M. Piette, G.A.E. Vandenbosch, "*Static source-mode tuning using a constellation of LPDA antennas in a reverberation chamber*", Proc. of the 9th International Symposium on EMC joint with 20th International Wroclaw Symposium on EMC (EMC Europe 2010), September 13-17, 2010, Wroclaw, Poland.
- d) C. Tsigros, M. Piette, G.A.E. Vandenbosch and D. Van Troyen, "*Antenna efficiency in a reverberation chamber: from the relative to the E-Field method*", Proc. of the 10th Int. Symposium on Electromagnetic Compatibility (EMC Europe 2011), pp. 164-169, York, UK, September 26-30, 2011.
- e) C. Tsigros, M. Piette, G.A.E. Vandenbosch and D. Van Troyen, "*Radiated Immunity in Reverberation and Semi-anechoic Rooms: Conditions for Equivalence*", IEEE Trans. on Electromagnetic Compatibility, Vol. 55, Issue 2, pp 222-230, April 2013.

- f) C. Tsigros, M. Piette and G.A.E. Vandenbosch, "Ergodicity in Reverberation Chambers: Theory and Experimental Validation", submitted, on March 2014, to IEEE Trans. on Electromagnetic Compatibility.

Annex 1: Bibliography

- [1] B.E. Keyser "Principles of Electromagnetic compatibility", Artech House, 1979.
- [2] IEC 61000-4-21 (2003): Electromagnetic compatibility (EMC). Part 4-21: Testing and Measurements techniques – Reverberation Chamber methods.
- [3] MIL-STD-461F 10 December 2007: Department of Defense Interface Standard: Requirements for the control of the electromagnetic Interference characteristics of subsystems and equipment.
- [4] M.L. Crawford and G.H. Koepke, "Design, evaluation and use of a reverberation chamber for performing electromagnetic susceptibility/vulnerability measurements," U.S. Nat. Bur. Stand. Tech. Note 1506, 1998.
- [5] J. Ladbury, G. Koepke, and D. Camell, "Evaluation of the NASA Langley Research Center Mode-Stirred Chamber Facility," U.S. Nat. Inst. Stand. Technol. Tech. Note 1508, 1999.
- [6] Wu, Chang, "*The effect of an Electrically Large Stirrer in a Mode Stirred Chamber*" IEEE Trans. on EMC, Vol. 31, No.2, 164-169, 1989.
- [7] David A. Hill, "Electromagnetic Fields in Cavities, Deterministic and Statistical Theories", A John Wiley & Sons, Inc., Publication, ISBN:978-0-470-46590-5, 2009.
- [8] T.A. Loughry, "Frequency stirring: an alternate approach to mechanical mode-stirring for the conduct of electromagnetic

susceptibility testing," Phillips Laboratory, Kirtland Air Force Base, NM Technical Report 91-1036, 1991.

- [9] F. Leferink, "In-situ High Field Testing using a transportable Reverberation Chamber", Asia-Pacific Symposium on Electromagnetic Compatibility and 19th International Zurich Symposium on Electromagnetic Compatibility, 19-23 May 2008, 439-442.
- [10] J.S. Hong, "Multimode chamber excited by an array of antennas", Electronics letters 16th September 1993, vol. 29, n° 19.
- [11] J. Kunthong and C.F. Bunting, "Source-Stirring and Mechanical-Stirring Reverberation Chamber Measurement Comparison for 900 MHz and 1800 MHz", IEEE International Symposium on Electromagnetic Compatibility, 17-21 Aug 2009, pp 193-196.
- [12] C. Tsigros, M. Piette, "IEC 61000-4-21 testing: selective source-mode tuning with two orthogonal antennas scanning system", Proc. of the 8th Int. Symposium on Electromagnetic Compatibility (EMC Europe), Hamburg, Germany, September 8-12, 2008, pp 477-482.
- [13] P. Corona, G. Ferrara, M. Migliaccio, "Statistical Electromagnetic Field in Reverberating Chambers", EuroEM 1994, Bordeaux, pp.1285-1292.
- [14] P. Corona, G. Ferrara, M. Migliaccio, "Reverberating Chambers as Sources of Stochastic Electromagnetic Fields", IEEE Transactions of Electromagnetic Compatibility, Vol. 38, n° 3, August 1996.

- [15] Frederick Emmons Terman, "Radio Engineers' Handbook", McGraw-Hill Book Company, 1943, pages 135-172.
- [16] J.D. Kraus and K.R. Carver, Electromagnetics, 1973, pp.587-588.
- [17] A. Vander Vorst, Hyperfréquences, théorie, pratique et mesure. De Boek Université, 1988, pp.6.1-6.3.
- [18] T.H. Lehman, "A Statistical theory of electromagnetic fields in complex cavities", Interaction Notes, Note 494, May 1993.
- [19] P. Corona, G. Ferrara, M. Migliaccio, "Reverberating Chambers and absorbers", Symposium EMC 2001 Zürich, pp.631-634.
- [20] P. Corona, G. Ferrara, M. Migliaccio, "Reverberating Chamber Electromagnetic Field in Presence of an Unstirred Component", IEEE Transactions on Electromagnetic Compatibility vol. 42, n°2, May 2000, pp. 111-115.
- [21] M. PIETTE, "*From cubic Faraday Cage to HIRF Testing Reverberation Chamber*", IEEE & URSI Joint Symposium EuroElectromagnetics (EUROEM'04), 12-16 July 2004, Magdeburg, Germany, Paper HPEM 13-2.
- [22] M. PIETTE, K. MOESEN, S. MONTEZUMA, "*Experimental Field Statistics Validation in a Cubic Reverberation with Mechanical Mode Stirring & Bistatic Cross-Polarized Illumination*", Progress In Electromagnetic Research Symposium, 22-26 Aug 2005, Hangzhou, China. Proc. pp.424-427.
- [23] M. PIETTE, "*Complete Space-Time Validation of a Single Mode Stirrer Reverberation Chamber for Immunity Testing*", Fourth IEEE Asia-Pacific Conf. on Environmental Electromagnetics (CEEM'06), Dalian, China, Proc. pp.449a-d.

- [24] M. PIETTE, "Anisotropy & Polarization Analysis in a Cubic Mode Stirred Chamber", Fourth IEEE Asia-Pacific Conf. on Environmental Electromagnetics (CEEM'06), Dalian, China, Proc. pp.448a-e.
- [25] P. Corona, G. Ferrara, and M. Migliaccio, "Reverberating Chamber Electromagnetic Field in Presence of an Unstirred Component," IEEE Trans. Electromagn. Compat., vol.42, no.2, pp.111-115, May 2000.
- [26] V.E. Vickers and J. Silverman, "A technique for generating Specialized Gray Codes", IEEE Transactions on computers, vol. C-29, n° 4, April 1980.
- [27] IEC 61000-4-3 (2002) : Electromagnetic compatibility (EMC). Part 4-3: Testing and measurement techniques – Radiated, radio-frequency, electromagnetic field immunity test.
- [28] Harold A. Wheeler, "The radiansphere around a small antenna," Proc. IRE, pp.1325-1331, Aug. 1959.
- [29] Shawn D. Rogers, James T. Aberle, David T. Auckland, "Two-port model of an antenna for use in characterizing wireless communications systems, obtained using efficiency measurements," IEEE Antennas and Propagation Magazine, Vol. 45, No. 3, pp.115-118, June 2003.
- [30] Gert Frolund Pedersen, Kim Olesen, Steen Leth Larsen, "Antenna efficiency of Handheld phones," IEE, Savoy Place, London WC2R OBL, UK, pp.6/1-6/5, 1999.
- [31] Pawel Kabacik, Arkadiusz Byndas, Robert Hossa, Marek Bialkowski, "A measurement system for determining radiation efficiency of a small antenna," Antennas and Propagation, 2006. EuCAP 2006.

- [32] Ronald H Johnston, John G. McRory, "An improved small antenna radiation efficiency measurement method," IEEE Antennas and Propagation Magazine, Vol. 40, No. 5, pp.40-48, October 1998.
- [33] Gwenn Le Fur, Christophe Lemoine, Philippe Besnier, Ala Sharaiha, "Performances of UWB Wheeler Cap and reverberation chamber to carry out efficiency measurements of narrowband antennas," IEEE Antennas and Wireless Propagation Letters, Vol. 8, pp.332-335, 2009.
- [34] A.A.H. Azremi, H. Gharoufi Shiraz and Peter S. Hall, "A Comparative study of small antenna efficiency measurements," Asia-Pacific Conference on Applied Electromagnetics Proceedings, pp.74-78, December 2005.
- [35] K. Rosengren, P.S. Kildal, "Radiation efficiency, correlation, diversity gain and capacity of a six-monopole antenna array for a MIMO system: theory, simulation and measurement in reverberation chamber," IEE, Proc.-Microw. Antennas Propag. Vol. 152, No1, pp.7-16, February 2005.
- [36] M. Piette, "Antenna radiation efficiency measurements in a reverberation chamber," in Proc. Asia-Pacific Radio Science Conf., Qingdao, China, Aug. 2004, pp.19-22.
- [37] Amir Galehdar, David V. Thiel and Steven G. O'Keefe, "Antenna efficiency calculations for electrically small, RFID antennas", IEEE Antennas and Wireless Propagation Letters, Vol.6, pp.156-159, 2007.
- [38] Melvin M. Weiner, Stephen P. Cruze, Cho-Chou Li, Warren J. Wilson, "Monopole elements on circular ground planes" Artech House, 1987, pp. 66-67.

- [39] R.W.P.King, Tables of Antenna Characteristics, IFI Plenum, pp.143-149, 1971.
- [40] John M. Ladbury and Galen H. Koepke, "Reverberation chamber relationships: corrections and improvements or three wrongs can (almost) make a right", Proc. IEEE International Symposium on Electromagnetic Compatibility, Seattle, Washington, USA, pp.2-6, Aug. 1999.
- [41] Joseph G. Kostas and Bill Boverie, "Statistical model for a mode-stirred chamber", IEEE Transactions on Electromagnetic Compatibility, Vol. 33, No. 4, pp.366-370, November 1991.
- [42] Per-Simon Kildal, Charlie Carlsson, "Study of polarization stirring in reverberation chambers used for measuring antenna efficiencies", IEEE Antennas and Propagation Society International Symposium, pp.486-489, 2002.
- [43] Kent Rosengren, Per-Simon-Kildal, Charlie Carlsson, Jan Carlsson, "Characterization of antennas for mobile and wireless terminals by using reverberation chambers: improved accuracy by platform stirring", IEEE Antennas and Propagation Society International Symposium, pp. 350-353, 2001.
- [44] Andreas Wofgang, J. Carlsson, C.Orlenius and P-S. Kildal, "Improved procedure for efficiency of small antennas in reverberation chambers", IEEE Antennas and Propagation Society International Symposium, pp. 350-353, 2003.
- [45] T. D. Sudikila and T. E. Gilles, "Design and manufacturing of a Dual-Band, Dual Polarized and Dual fed Perforated Array Patch Antenna pair", PIERS, Moscow 2012.

- [46] M. Piette, cours "Antennes", TE 547, Edition 2003.
- [47] F.E. Terman, "Radio Engineers' Handbook", A McGraw-Hill book company, Inc, Publication, 1943, page 815.
- [48] R. J. Pirkl, J. M. Ladbury, and K. A. Remley, "The reverberation chamber's unstirred field: A validation of the image theory interpretation," in *Proc. IEEE Int. Symp. Electromagn. Compat.*, May 14–19, 2011, pp. 670–675.
- [49] C. Tsigros, M. Piette, and G. A. E. Vandenbosch, "Static source-mode tuning using a constellation of LPDA antennas in a reverberation chamber," in *Proc. 9th Int. Symp. Electromagn. Compat.*, Wroclaw, Poland, Sep. 13–17, 2010, pp. 445–450.
- [50] G. Freyer and M. Bäckström, "Comparison of anechoic and Reverberation Chamber Coupling Data as a Function of Directivity Pattern – Part II." In *Proc. IEEE International Symposium on Electromagnetic Compatibility*, Montréal, Canada. August 13-17, 2001, pp.286-291.
- [51] L.R. Arnaut, "Compromizing and optimizing the design of special-purpose reverberation chambers for HIRF testing," in *Proc. IEEE Symp. Electromagnetic Compatibility*, vol. 1, San Jose, CA, Aug. 2004, pp.237-240.
- [52] L. Musso, F. Canavero, B. Demoulin, V. Berat, "Radiated Immunity Testing of a Device with an External Wire: Repeatability of Reverberation Chamber Results and Correlation with anechoic Chamber Results," in *Proc. 2003 IEEE Int. Symp. Electromagnetic Compatibility*, Aug. 2003, pp. 828-833.
- [53] M. Petirsch, W. Kurner, I. Sottriffer, and A. Schwab, "Comparing different measurement approaches in a mode-

stirred chamber," in *Proc. IEEE Int. Symp. Electromagn. Compat.*, 1999, vol. 2, pp. 929–933.

- [54] G. Freyer, M. Bäckström, "Comparison of anechoic & Reverberation Chamber Coupling data as a Function of Directivity Pattern." In *Proc. IEEE International Symposium on EMC*, Washington DC, August 2000.
- [55] Mendes, H.A. "A new approach to electromagnetic field-strength measurements in shielded enclosures." Weston, Los Angeles, C.A., 1968.
- [56] D.A. Hill, "Electromagnetic theory of reverberation chambers." U.S. National Institute of Standards and Technology, Technical Note 1506, 1998.
- [57] D.A. Hill, "Electronic mode stirring." *IEEE Transactions on Electromagnetic Compatibility*, vol. 36, pp294-299, 1994.
- [58] J.G. Proakis, "Digital communications", New York, NY, Mac Graw-Hill, 1995.
- [59] D.A. Hill, M.T. Ma, A.R. Ondrejka, B.F. Riddle, M.L. Crawford and R.T. Johnk, "Aperture excitation of electrically large, lossy cavities." *IEEE Transactions on Electromagnetic Compatibility*, vol. 36, pp.169-178, 1994.
- [60] D.A. Hill, "Plane wave integral representation for fields in reverberation chambers." *IEEE Transactions on Electromagnetic Compatibility*, vol. 40, pp.209-217, 1998.
- [61] M.L. Crawford, T.A. Loughry, M.O. Hatfield and G.J. Freyer, "Band-limited, white Gaussian noise excitation for reverberation chambers and applications to radiated susceptibility testing." U.S. National Institute of Standards and Technology, Technical Note 1375, 1996.

- [62] K. Rosengren and P.-S. Kildal, "Radiation efficiency, correlation, diversity gain and capacity of a six monopole antenna array for a MIMO system: Theory, simulation and measurement in reverberation chamber." Proc. Inst. Elect. Eng. Microwave, Antennas, Propag., vol. 152, pp. 7-16, 2005.
- [63] K. Harima, "Determination of EMI antenna factor using reverberation chamber." Proc. IEEE Int. Symposium Electromagnetic Compatibility, Chicago, IL, pp.93-96, 2005.
- [64] L.R. Arnaut, "Effect of size, orientation and eccentricity of mode stirrers on their performance in reverberation chambers." IEEE Transactions on Electromagnetic Compatibility, vol. 48. pp600-602, 2006.
- [65] A.A.H. Azremi, "An investigation of Rayleigh distribution in reverberation chamber." RF and Microwave conference, pp. 71-74, 2006.
- [66] Athanasios Papoulis and S. Unnikrishna Pillai, "Probability, Random Variables and Stochastic Processes" Mc Graw-Hill, International edition, ISBN: 0-07-122661-3, 2002.
- [67] Jan von Plato, "Boltzmann's Ergodic Hypothesis", Archive for History of exact Sciences, Volume 42, Issue 1, 3.VI.1991, pp 71-89.
- [68] L. Boltzmann, "Lösung eines mechanischen Problems", as reprinted in "*Wissenschaftliche Abhandlungen*", vol. 1, 1868.
- [69] L. Boltzmann, "Lectures on Gas Theory", Dover publications, Inc, New York, ISBN 0-486-68455-5, 1995.
- [70] I.P. Cornfeld, S.V. Fomin, Y.G. Sinai, A.B. Sossinskii, "Ergodic Theory" Springer-Verlag New York, Inc, ISBN 978-14615-6929-9, 1982.

- [71] Ya.G. Sinai, "Ergodic Theory and Dynamical Systems", Selecta, Volume I, Springer, ISBN 978-0-387-87869-0, 2010.
- [72] N. Simanyi, D. Szasz, "The Boltzmann-Sinai ergodic hypothesis for hard ball systems", The Erwin Schrödinger International Institute for Mathematical Physics, Vienna, 1996.
- [73] Ya.G. Sinai, "On the Foundation of the Ergodic Hypothesis for a Dynamical System of Statistical Mechanics, Soviet Math. Dokl. 4, 1818-1822, 1963.
- [74] N. Simanyi, "Proof of the Ergodic Hypothesis for Typical hard Ball Systems", in Ann. Henri Poincaré, 203-233, Basel, 2004.
- [75] Ya.G. Sinai, "Dynamical Systems with Elastic Reflections", Russian Math. Surveys 25, 2, 137-189, 1970.
- [76] L.A. Bunimovich, Ya.G. Sinai, "The fundamental theorem of the theory of scattering billiards, Math, USSR-Sb. 19, 407-423, 1973.
- [77] Ya.G. Sinai, N.I. Chernov, "Ergodic properties of certain systems of 2D-discs and 3-D balls", Russian Math. Surveys 42, No. 3, 181-207, 1987.
- [78] Wm.B. Joyce, "Sabine's Reverberation Time in Ergodic Auditoriums", J. Acoust. Soc. Am. Vol. 58, No. 3, pp. 643-655, September 1975.
- [79] Joël L. Lebowitz and Oliver Penrose, "Modern ergodic theory", Physics today, February 1973.
- [80] F. Feil, S. Naumov, J. Michaelis, R. Valiullin, D. Enke, J. Karger and C. Braüchle, "Single-Particle and Ensemble Diffusivities – Test of Ergodicity", Angewandte. Chem. Int. Ed. 2012, 51, 1152-1155, 2012.

- [81] P. Corona, G. Ferrara and M. Migliaccio, "A Spectral approach for the determination of the Reverberating chamber quality factor", in IEEE transactions on EMC, Vol. 40, N° 2, May 1998.
- [82] L. R. Arnaut and G. Gradoni "Probability distribution of the quality factor of a mode-stirred reverberation chamber", in IEEE Transactions on EMC, Vol. 55, N° 1, February 2013.
- [83] L. R. Arnaut, P. D. West, "Evaluation of the NPL Untuned Stadium Reverberation Chamber using mechanical and electronic stirring techniques." National Physical laboratory (NPL) Report CEM11, August 1998.
- [84] P. Besnier and B. Démoulin, "Electromagnetic Reverberation Chambers", John Wiley & Sons, ISTE Ltd, ISBN 978-1-84821-293-0, 2011.
- [85] Karl Petersen, "Ergodic theory" Cambridge University Press, New-York, ISBN: 978-0-521-38-997-6, 1983
- [86] Walter Kauzmann, "Kinetic Theory of Gases", Dover Publications, Inc. Mineola, New York, 2012, ISBN-13:978-0-486-48833-2.
- [87] Richard Feynmann, "Lectures on Physics", Basic books, volume I, ISBN:978-0-465-02414-8, 2011.
- [88] Marcelo Alonso and Edward J. Finn, "Physics", Pearson Prentice Hall, ISBN 978-0-201-56518-8, 1992.
- [89] F. Mandl, "Statistical Physics", John Wiley & Sons, ISBN 978-0-471-91532-4, 1988.

Annex 2: List of Acronyms and Abbreviations

ABLE	Accredited Bodies and Laboratories in Electrotechnics
AUT	Antenna Under Test
CDF	Cumulative Distribution Function
CEUT	Canonical Equipment Under Test
CST	Computer Simulation Technology
EUT	Equipment Under Test
KUL	Katholieke Universiteit Leuven
LEMA	Laboratory of ElectroMagnetic Applications
LPDA	Log Periodic Dipole Array
PDF	Probability Density Function
PIFA	Planar Inverted-F Antenna
RAIL	Innovative tuner using two orthogonal rails
RC	Reverberation Chamber
RF	Radio Frequency
RFID	Radio-Frequency Identification
RMA	Royal Military Academy
SAR	Semi-Anechoic Room
SPDT	Single Pole Double Throw
STATIC	Innovative tuner using a static array of antennas

Annex 3: List of Symbols

\vec{D}	Electric flux density	(As/m ²)
\vec{E}	Electric field strength	(V/m)
\vec{B}	Magnetic flux density	(Vs/m ²)
\vec{H}	Magnetic field strength	(A/m)
ϵ	Electric permittivity	(F/m or As/Vm)
μ	Magnetic permeability	(H/m or Vs/Am)
\vec{J}	Current density	(A/m ²)
ω	Angular frequency	(rad/s)
ρ	Electric charge density	(Cb/m ³)

Annex 4: Mathematical Notations

(In rectangular coordinates)

$$\nabla f = \vec{i}_x \frac{\partial f}{\partial x} + \vec{i}_y \frac{\partial f}{\partial y} + \vec{i}_z \frac{\partial f}{\partial z} \quad \text{Gradient of } f$$

$$\nabla^2 f = \frac{\partial^2 f}{\partial x^2} + \frac{\partial^2 f}{\partial y^2} + \frac{\partial^2 f}{\partial z^2} \quad \text{Laplacian of } f$$

$$\nabla \cdot \vec{A} = \frac{\partial A_x}{\partial x} + \frac{\partial A_y}{\partial y} + \frac{\partial A_z}{\partial z} \quad \text{Divergence of vector } A$$

$$\nabla \times \vec{A} = \begin{vmatrix} \vec{i}_x & \vec{i}_y & \vec{i}_z \\ \frac{\partial}{\partial x} & \frac{\partial}{\partial y} & \frac{\partial}{\partial z} \\ A_x & A_y & A_z \end{vmatrix} \quad \text{Curl of vector } A$$

Annex 5: Interlaboratory Testing in Belgium and Japan



Parc scientifique Fleming
 Granbonpré 1
 B-1348 Louvain-la-Neuve
 T +32 10 47 52 11 - F +32 10 47 52 67
www.anpi.be



Interlaboratory comparison report – 18/12/2012 Anonymous version of the report

Coordination:	Royal Military Academy (technical aspects) ANPI asbl (administrative aspects)
Participants:	<ul style="list-style-type: none"> - Laborelec - Lemcko - More@Mere (BGEMC) - Université de Liège (Laboratoire CEM) - BARCO - PHILIPS (EMC Test lab) (Netherlands) - Royal Military Academy - ANPI - Laboratoria De Nayer - Pioneer (Japan) - Fuji Xerox (Japan) - SGS Munchen (Germany)

Products submitted to the tests			
Nature	Manufacturer	Brand	Reference
Canonical equipment	Royal Military Academy	-	-

Standards and specifications
IEC61000-4-3:2006 + A1:2007 + A2:2010 Electromagnetic compatibility (EMC) – Part 4-3: Testing and measurement techniques - Radiated, radio-frequency, electromagnetic field immunity test

Test history	Date	Remarks
Start of the tests	8/05/2012	
End of the tests	23/08/2012	

This report contains 19 pages.



A. TABLE OF CONTENTS

B. CIRCULATION TABLE3

C. CEUT DESCRIPTION.....3

D. TEST PROCEDURE.....5

FIRST TEST: WHOLE TEST ACCORDING TO THE USUAL PROCEDURE5

SECOND TEST: CALIBRATION PROCEDURE.....5

E. TESTS RESULTS.....7

FIRST TEST 7

SECOND TEST 15

F. PROBLEMS DURING THE TESTS19

G. CONCLUSIONS19



B. CIRCULATION TABLE

Deleted to keep the results anonymous.

C. CEUT DESCRIPTION

CEUT = canonical equipment under test

The CEUT housing is a metallic box with the following dimensions:
L=25 cm; Height=24,5 cm; depth=20 cm



Fig. 1: CEUT closed



Fig. 2: CEUT open

It has been designed and fabricated in order to have a common reference for the immunity testing both in an anechoic and in a reverberating environment.

It is composed of three identical "Channels" (one channel by polarization). Each channel contains (see fig. 3) a square wave pulse generator, an envelope generator, a loop antenna, a counter and a comparator.

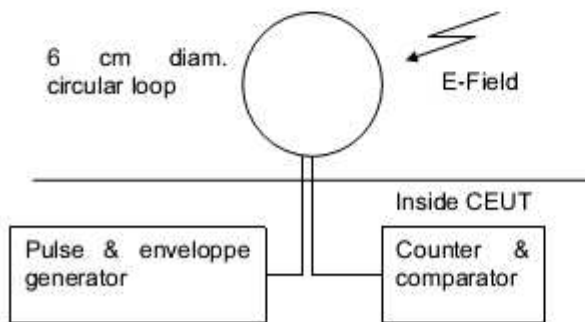


Fig. 3: Schematics of CEUT; single channel

The theory of operation is as follows. When the E-field is established into the room (AN or RC), a trigger produces a square wave of 100 pulses, during 2 seconds. These pulses pass through the loop antenna to the counter and to the comparator. The radio signal received by the loop will disturb the square signal and produce an error in the pulse count if the disturbance level is sufficiently high. The expected number of pulses is set by a dip-switch. A "greater" or "lower" indication is activated in case of mismatch.

The main characteristics of the CEUT are:

- Count 100 Pulses (adjustable) during 2 seconds (adjustable);
- Pulse duration: 20 ms; Duty cycle : 50%;
- Driver LabVIEW software developed for remote controlling;
- 20 m optic fiber link;
- Battery powered (24 VDC), about 7 hours autonomy.

D. TEST PROCEDURE

First test: whole test according to the usual procedure

Introduction

The aim of this test is to compare the reactions of the CEUT in the different laboratories when using their own procedures and calibration files. Each laboratory makes use of its usual calibration files and test distances. The CEUT is considered as stable in its reactions. Any difference in the reported reactions for a given conditioning is considered as a discrepancy in the conditioning itself.

CEUT configuration

The CEUT has to be considered as tabletop equipment.

The test has to be carried out in the following 4 orientations of the CEUT:

- Orientation 1: z-probe to the top and x-probe towards the antenna
- Orientation 2: z-probe to the top and y-probe towards the antenna
- Orientation 3: z-probe to the top and x-probe towards opposite of the antenna
- Orientation 4: z-probe to the top and y-probe towards opposite of the antenna

Test requirements

The test has to be carried out at a series of 17 frequencies: 85, 95, 150, 250, 350, 450, 550, 650, 750, 850, 950 MHz, 1.3, 1.6, 1.9, 2.2, 2.5, 2.9 GHz

Level:

85 – 950 MHz	1.3 GHz	1.6 GHz	1.9 GHz	2.2 GHz	2.5 GHz	2.9 GHz
10 V/m	27 V/m	35 V/m	43 V/m	50 V/m	57 V/m	68 V/m

Modulation: sinusoidal AM 80% 1 kHz

Orientation: all 4 orientations described in section 5.1.

Polarisation: V and H polarisations for each orientation

Dwell time: 6s

Test procedure

Apply the usual procedure and calibration data with the requirements given in section 5.3.

Report the CEUT reactions in the work document given in Annex 1.

Second test: calibration procedure

Introduction

The aim of this test is to compare the reactions of the CEUT in the different laboratories after a defined calibration requirement when using their own calibration procedures. The CEUT is considered as stable in its reactions. Any difference in the reported reactions for a given conditioning is considered as a discrepancy in the calibration itself.

Calibration

Calibration requirement

- Location: on 1 point localized at the central point of the CEUT
- Distance: at 1 m (between CEUT front face and antenna tip)
- Polarisation: V and H
- Frequencies: 85, 150, 550, 850 MHz, 1.6, 2.5 GHz
- Level:

85 – 850 MHz	1.6 GHz	2.5 GHz
20 V/m	50 V/m	70 V/m

Calibration procedure

Apply the usual procedure for field calibration with the requirements given in section 6.2.

Test

CEUT configuration

The CEUT has to be considered as tabletop equipment.

The test has to be carried out in the following orientation of the CEUT:

- Orientation 1: z-probe to the top and x-probe towards the antenna

The field probe used in open loop for the verification of the field existence around the CEUT has to be placed on a location considered as having no significant influence on the field level on the CEUT.

Test requirement

Frequencies: 85, 150, 550, 850 MHz, 1.6, 2.5 GHz

Modulation: sinusoidal AM 80% 1 kHz

Orientation: 1 orientation

Polarisation: V and H

Dwell time: 6s

Test procedure

At each frequency, apply the requirements given in section 6.3.2 and raise the level as given in Annex 2.

Report the CEUT reactions in the work document given in Annex 2.



E. TESTS RESULTS

First test

Orientation 1

Frequency	85	95	150	250	350	450	550	650	750	850	950	1.3	1.6	1.9	2.2	2.5	2.9	
Pol V	Pass	1 1b 2 3 4 5 6 7 8 9 10	1 1b 1b 3 4 5 6 8 9 10	1b 5 7	1 1b 2 3 4 5 6 7 9 10	2 8 9 10	8 9 10	8 9 10	8 10	8 10	8 10							
	Fail	4	7	1 1b 2 3 4 5 6 7 8 9	1 1b 2 3 4 5 6 8 9	8												



Orientation 1

Frequency	85	95	150	250	350	450	550	650	750	850	950	1.3	1.6	1.9	2.2	2.5	2.9	
Pol H	1	1			1	1	1	1	1	1	1							
	1b	1b	1b		1b	2		2	2									
	2	2	2		2	2	2	2	2	2	2							
	3	3			3	3	3	3	3	3	3							
	4	4			4	4	4	4	4	4	4							
	5	5			5	5	5	5	5	5	5							
	6	6			6	6	6	6	6	6	6							
	7	7		7	7	7	7	7	7	7	7							
	8	8			8	8	8	8	8	8	8	8	8	8	8	8	8	8
	9	9	9		9	9	9	9	9	9	9	9	9	9	9	9	9	9
10	10	10	10	10	10	10	10	10	10	10	10	10	10	10	10	10	10	
Fail		4		1														
				1b														
				2														
				3					3									
				4														
				5														
				6														
				7														
				8		8								8				
				9														
			10															



Orientation 2

Frequency	85	95	150	250	350	450	550	650	750	850	950	1.3	1.6	1.9	2.2	2.5	2.9	
Pol V	1	1	1		1	1	1	1	1	1	1							
	1b	1b	1b		1b													
	2	2			2	2	2	2	2	2	2	2	2	2				
	3				3	3	3	3	3	3	3							
	4	4			4	4	4	4	4	4	4							
	5	5			5	5	5	5	5	5	5							
	6	6			6	6	6	6	6	6	6							
	7	7			7	7	7	7	7	7	7							
	8	8			8	8	8	8	8	8	8	8	8	8	8	8	8	8
	9	9			9	9	9	9	9	9	9	9	9	9	9	9	9	9
10	10	10	10	10	10	10	10	10	10	10	10	10	10	10	10	10	10	
Fail	4																	
		3																
			2															
			3															
			4															
			5			5												
			6			6												
			7			7												
			8			8												
		9			9													

Orientation 2

Frequency	85	95	150	250	350	450	550	650	750	850	950	1.3	1.6	1.9	2.2	2.5	2.9
Pol H	1	1	1	1		1	1	1	1	1	1						
	1b	1b	1b	1b		1b	1b	1b	1b	1b	1b			2			
	2	2	2	2		2	2	2	2	2	2						
	3	3	3	3	3	3	3	3	3	3	3						
	4	4	4	4		4	4	4	4	4	4						
	5	5	5	5		5	5	5	5	5	5						
	6	6	6	6		6	6	6	6	6	6						
	8	8	8				8	8	8	8	8	8	8	8	8	8	8
	9	9	9		9	9	9	9	9	9	9	9	9	9	9	9	9
	10	10	10	10	10	10	10	10	10	10	10	10	10	10	10	10	10
Fail					1												
					1b												
					2												
					4												
				5													
				6													
			8	8	8												
			9														

Orientation 3

Frequency	85	95	150	250	350	450	550	650	750	850	950	1.3	1.6	1.9	2.2	2.5	2.9	
Pol V	1	1			1		1	1	1	1	1							
	1b	1b	1b		1b													
	2	2			2	2	2	2	2	2	2	2			2			
	3	3			3	3	3	3	3	3	3							
	4	4			4	4	4	4	4	4	4							
	5	5			5	5	5	5	5	5	5							
	6	6			6	6	6	6	6	6	6							
	7	7			7	7	7	7	7	7	7							
	8	8			8	8	8	8	8	8	8	8	8	8	8	8	8	8
	9	9		9		9	9	9	9	9	9	9	9	9	9	9	9	9
10	10		10		10	10	10	10	10	10	10	10	10	10	10	10	10	
Fail		4		1		1												
				1b														
				2														
				3														
				4														
				5		5												
				6														
				7														
				8														
				10														



Orientation 3

Frequency	85	95	150	250	350	450	550	650	750	850	950	1.3	1.6	1.9	2.2	2.5	2.9	
Pol H	1	1			1	1	1	1	1	1	1							
	1b	1b	1b		1b													
	2	2		2	2	2	2	2	2	2	2			2				
	3	3			3	3	3	3	3	3	3							
	4	4			4	4	4	4	4	4	4							
	5	5			5	5	5	5	5	5	5							
	6	6			6	6	6	6	6	6	6							
	7	7	7		7	7	7	7	7	7	7							
	8	8			8	8	8	8	8	8	8	8	8	8	8	8	8	8
	9	9	9		9	9	9	9	9	9	9	9	9	9	9	9	9	9
10	10	10		10	10	10	10	10	10	10	10	10	10	10	10	10	10	
Fail				1														
				1b														
	4		2															
			3															
			4	3														
			5	4		5												
			6	5														
			7	6														
			8	7														
			10	8														

Orientation 4

Frequency	85	95	150	250	350	450	550	650	750	850	950	1.3	1.6	1.9	2.2	2.5	2.9	
Pol V	1	1		1	1	1	1	1	1	1	1							
	1b	1b		1b														
	2	2			2	2	2	2	2	2	2	2	2	2				
	3	3			3	3	3	3	3	3	3							
	4	4			4	4	4	4	4	4	4							
	5	5			5	5	5	5	5	5	5							
	6	6			6	6	6	6	6	6	6							
	7	7			7	7	7	7	7	7	7							
	8	8		8	8	8	8	8	8	8	8	8	8	8	8	8	8	8
	9	9	9	9	9	9	9	9	9	9	9	9	9	9	9	9	9	9
	10	10	10	10	10	10	10	10	10	10	10	10	10	10	10	10	10	
Fail			1								2							
			1b															
			2	2		2												
			3	3														
			4	4														
			5	5		5												
			6	6														
			7	7		7												
			8	8														
			9	9														
	10	10	10															

Orientation 4

Frequency	85	95	150	250	350	450	550	650	750	850	950	1.3	1.6	1.9	2.2	2.5	2.9	
Pol H	1	1	1	1		1	1	1	1	1	1							
	1b	1b	1b	1b		1b	1b	1b	1b	1b	1b							
	2	2	2	2	2	2	2	2	2	2	2			2				
	3	3	3	3		3	3	3	3	3	3							
	4	4	4	4		4	4	4	4	4	4							
	5	5	5	5		5	5	5	5	5	5							
	6	6	6	6		6	6	6	6	6	6							
	7	7	7	7	7	7	7	7	7	7	7							
	8	8	8	8	8	8	8	8	8	8	8	8	8	8	8	8	8	8
	9	9	9	9	9	9	9	9	9	9	9	9	9	9	9	9	9	9
10	10	10	10	10	10	10	10	10	10	10	10	10	10	10	10	10	10	
Fail					1 1b													
					3													
		5			4													
					5													
					6													
				8														
				9														

Frequency 2 - 150 MHz

Level	V/m	1	4	7	10	13	16	19	
Pol V	Pass	1	1	1	1				
		1b	1b	1b					
		2	2	2	2				
		3	3						
		4	4	4					
		5	5	5			5	5	
		6	6	6					
		7	7	7	7	7			
		8	8	8	8				
		9	9	9	9				
	10	10	10	10					
	Fail				3	1b	1	1	1
						1b	1b	1b	1b
						2	2	2	2
						3	3	3	3
						4	4	4	4
						5	5		
						6	6	6	6
							7	7	7
						8	8	8	8
					9	9	9	9	
				10	10	10	10		
Pol H	Pass	1	1						
		2	2						
		3	3						
		4	4						
		5	5						
		6	6	6					
		7	7	7	7	7			
		8	8	8	8	8			
		9	9	9					
		10	10	10	10	10			
	Fail				1	1	1	1	1
					2	2	2	2	2
					3	3	3	3	3
					4	4	4	4	4
					5	5	5	5	5
					6	6	6	6	6
							7	7	7
							8	8	8
					9	9	9	9	9
							10	10	10



Frequency 3 - 550 MHz

Level	V/m	1	4	7	10	13	16	19	
Pol V	Pass	1	1	1	1	1	1	1	
		1b	1b	1b	1b	1b	1b	1b	
		2	2	2	2	2	2	2	
		3	3	3	3	3	3	3	
		4	4	4	4	4	4	4	
		5	5	5	5	5	5	5	
		6	6	6	6	6	6	6	
		7	7	7	7	7	7	7	
		8	8	8	8	8	8	8	
		9	9	9	9	9	9	9	
	10	10	10	10	10	10	10		
	Fail						7	1b	
					9		9	7	
	Pol H	Pass	1	1	1	1	1	1	1
			1b						
			2	2	2	2	2	2	2
			3	3	3	3	3	3	3
			4	4	4	4	4	4	4
5			5	5	5	5	5	5	
6			6	6	6	6	6	6	
7			7	7	7	7	7	7	
8			8	8	8	8	8	8	
9			9	9	9	9	9	9	
10		10	10	10	10	10	10		
Fail				9	9				



Frequency 4 - 850 MHz

Level	V/m	1	4	7	10	13	16	19
Pol V	Pass	1	1	1	1	1	1	1
		1b						
		2	2	2	2	2	2	2
		3	3	3	3	3	3	3
		4	4	4	4	4	4	4
		5	5	5	5	5	5	5
		6	6	6	6	6	6	6
		7	7	7	7	7	7	7
		8	8	8	8	8	8	8
		9	9	9	9	9	9	9
	10	10	10	10	10	10	10	
Pol H	Pass	1	1	1	1	1	1	1
		1b						
		2	2	2	2	2	2	2
		3	3	3	3	3	3	3
		4	4	4	4	4	4	4
		5	5	5	5	5	5	5
		6	6	6	6	6	6	6
		7	7	7	7	7	7	7
		8	8	8	8	8	8	8
		9	9	9	9	9	9	9
	10	10	10	10	10	10	10	
	Fail							7

Frequency 5 - 1.6 GHz

Level	V/m	20	25	30	35	40	45	50
Pol V	Pass	2	2	2	2	2	2	2
		6	6	6	6	6	6	6
		8	8	8	8	8	8	8
		9	9	9	9	9	9	9
		10	10	10	10	10	10	10
	Fail							
Pol H	Pass	2	2	2	2	6	6	6
		6	6	6	6	6	6	6
		8	8	8	8	8	8	8
		9	9	9	9	9	9	9
		10	10	10	10	10	10	10
	Fail							

Frequency 6 – 2.5 GHz

Level	V/m	40	45	50	55	60	65	70
Pol V	Pass	8 9 10	8 9 10	8 8 10	8 8 10	8 8 10	8 8 10	
	Fail							
Pol H	Pass	2 8 9 10	8 8 9 10	8 8 10				
	Fail							

F. PROBLEMS DURING THE TESTS

Remark from Lab 2: Software disconnection (2 times per sweep).

Remark from Lab 6: Periodically (about every half an hour to 1 hour) the CEUT seems to reset automatically and lights ON the "<0" fault indication for all 3 axes simultaneously.

Failure statement from Lab 12:

The CEUT was partly dismantled when arriving at our premises. This dismantling did occur at the custom between Japan and Germany.

G. CONCLUSIONS

The test program has been followed up to the end of August. 10 laboratories have been able to perform their tests. The CEUT has been sent back to RMA for fixing and is presently waiting for verification at RMA. It will be tested by the remaining 2 laboratories afterwards.

The CEUT has been tested by RMA at the start of the process and at the end of July, before leaving Europe to Japan. The aim of this verification is to assess the stability of the equipment after being tested in the 7 other laboratories. Differences in reaction between the initial (1) and intermediary (1b) tests can be found for the following configuration:

- orientation 1, Pol V, 150 MHz
- orientation 1, Pol H, 150 MHz
- orientation 3, Pol V, 150 MHz and 450 MHz
- orientation 3, Pol H, 150 MHz
- Test 2, 150 MHz, Pol V, 10 V/m
- Test 2, 550 MHz, Pol V, 19 V/m.

According to the very limited amount of discrepancies between the initial and intermediary tests, it can be stated that the CEUT did remain stable within this period. A slight instability can be considered at 150 MHz.

Each laboratory has to make its own interpretation with regard to these results.